

**FIRST STROKE PEAK CURRENT CHARACTERISTICS FOR THE UNITED
STATES**

A Dissertation

by

GARY RUSSELL HUFFINES

Submitted to the Office of Graduate Studies of
Texas A&M University
in partial fulfillment of the requirements for the degree of

DOCTOR OF PHILOSOPHY

December 1999

Major Subject: Meteorology

DTIC QUALITY INSPECTED 4

19991108 114

REPORT DOCUMENTATION PAGE			Form Approved OMB No. 0704-0188	
Public reporting burden for this collection of information is estimated to average 1 hour per response, including the time for reviewing instructions, searching existing data sources, gathering and maintaining the data needed, and completing and reviewing the collection of information. Send comments regarding this burden estimate or any other aspect of this collection of information, including suggestions for reducing this burden, to Washington Headquarters Services, Directorate for Information Operations and Reports, 1215 Jefferson Davis Highway, Suite 1204, Arlington, VA 22202-4302, and to the Office of Management and Budget, Paperwork Reduction Project (0704-0188), Washington, DC 20503.				
1. AGENCY USE ONLY (Leave blank)	2. REPORT DATE 6.Oct.99	3. REPORT TYPE AND DATES COVERED DISSERTATION		
4. TITLE AND SUBTITLE FIRST STROKE PEAK CURRENT CHARACTERISTICS FOR THE UNITED STATES		5. FUNDING NUMBERS		
6. AUTHOR(S) MAJ HUFFINES GARY R				
7. PERFORMING ORGANIZATION NAME(S) AND ADDRESS(ES) TEXAS A&M UNIVERSITY		8. PERFORMING ORGANIZATION REPORT NUMBER		
9. SPONSORING/MONITORING AGENCY NAME(S) AND ADDRESS(ES) THE DEPARTMENT OF THE AIR FORCE AFIT/CIA, BLDG 125 2950 P STREET WPAFB OH 45433		10. SPONSORING/MONITORING AGENCY REPORT NUMBER FY99-302		
11. SUPPLEMENTARY NOTES				
12a. DISTRIBUTION AVAILABILITY STATEMENT Unlimited distribution In Accordance With AFI 35-205/AFIT Sup 1			12b. DISTRIBUTION CODE	
13. ABSTRACT (Maximum 200 words)				
14. SUBJECT TERMS			15. NUMBER OF PAGES	
			16. PRICE CODE	
17. SECURITY CLASSIFICATION OF REPORT	18. SECURITY CLASSIFICATION OF THIS PAGE	19. SECURITY CLASSIFICATION OF ABSTRACT	20. LIMITATION OF ABSTRACT	

ABSTRACT

First Stroke Peak Current Characteristics for the United States. (December 1999)

Gary Russell Huffines, B.A., Ohio Northern University;

M.S., Utah State University

Chair of Advisory Committee: Dr. Richard E. Orville

The first stroke peak currents of over 105 million cloud-to-ground lightning flashes from 1995-1998 were analyzed over the continental United States (US) landmass. The peak currents exhibit a variation based on season and geography, but positive flashes have different features than negative flashes. Several factors are considered when examining the peak current variations including latitudinal dependence, sensor separation in the National Lightning Detection Network, flash density variations, the percentage of positive flashes, and surface elevation. Two possible explanations for the peak current variations are changes in the return stroke velocity based on the atmospheric pressure and that the peak currents are dependent on the length of the lightning channel. Negative lightning demonstrated an inverse relationship between peak currents and the surface elevation. Positive peak currents and the percentage of positive flashes were strongly correlated. Further examinations of individual storm cases indicated fluctuations in the peak currents within larger storm systems. In the cases studied, the peak currents of the more intense flashes, or those with higher peak currents, demonstrated a periodicity on the order of one hour which is comparable to the lifetime of individual thunderstorm cells in the larger systems. This variation within storm systems seems to negate the possibility that the variations in the return stroke velocity make up the only contribution to peak current

differences. The length of the lightning channel appears to have some influence on the strength of the peak currents.

DEDICATION

This work would not have been possible without the help of so many people. I am not able to even come close to mentioning all those who played a part in this work by providing expert advice, an encouraging word, or other motivational help. Since it is impractical to list all of them here, I will dedicate this to those who helped the most. This work is the result of hard work and sacrifice of the most important people in the world to me – my family. Specifically, I would like to dedicate this to my wife, Ann, my daughter, Robyn, my sons Jared, Jacob, David, and Tanner, and to my dad, John. I hope to be spending a lot more time with you from now on.

ACKNOWLEDGEMENTS

There are incredibly talented and bright people in the world and I am awed by their knowledge and humility. So many of them helped me through this. Please forgive me if I miss anyone.

I want to thank my office mates, Svetla Veleva and David Gold who were always there to help whenever I needed it. They even put up with my eccentricities. This work would not have been possible without the help of the United States Air Force who paid the bills and the rent and put enough faith in me to give me the chance to try. As was mentioned previously, my family helped so much with this that I cannot begin to list all that they gave when I did not have anything left. There were so many others who answered my endless questions: Rick Toracinta, Chris Lucas, Dan Cecil, and many others. I would also like to acknowledge Ron Lowther who kept me sane.

The faculty and staff of Texas A&M University are awesome! My committee members were always there for me with words of encouragement and guidance. I hope to be able to return the favor some day by helping others as well. The unsung heroes are the people who work behind the scenes. Jerry Guynes and Neil Smith who keep the computers and network running, Margaret Jones, Mary Gammon, and all the others who keep the office working and the students in line are all worth their weight in gold!

A special thanks goes to Dr. Richard E. Orville who took a chance on a student who was out of the ordinary in age and other ways. I hope you were not disappointed.

TABLE OF CONTENTS

	Page
ABSTRACT	iii
DEDICATION	v
ACKNOWLEDGEMENTS	vi
TABLE OF CONTENTS	vii
LIST OF TABLES	x
LIST OF FIGURES	xi
CHAPTER	
I INTRODUCTION.....	1
A. Nature and source of problem	1
B. Research objectives	4
II BACKGROUND INFORMATION AND LITERATURE REVIEW	6
A. Charge separation process	6
B. Measured thunderstorm charge structure	9
C. Cloud-to-ground lightning discharge process	11
D. Detection of a lightning flash	14
E. The National Lightning Detection Network.....	20
F. Observations of peak current variations	24
III DATA SOURCES	26
A. Lightning data	26
B. Upper air data	28
C. Satellite data	30
D. Surface elevation data	30

CHAPTER		Page
IV	METHOD OF INVESTIGATION.....	32
	A. Restriction of data to US boundaries.....	32
	B. Comparison of median peak currents for regional variations	32
	C. Flash density calculations.....	35
	D. Variations in the median of peak currents based on seasons	35
	E. Correlation between possible factors affecting peak currents.....	37
	F. Case studies for comparisons of individual storms.....	40
	G. Determination of CAPE and vertical wind shear	41
	H. Satellite imagery and lightning data plots	44
V	LARGE SCALE VARIATIONS IN PEAK CURRENT	47
	A. Peak current distributions for the US	47
	B. Regional peak current distributions.....	50
	C. Peak current variations based on latitude.....	56
	D. Peak current characteristics across the US.....	61
	E. The effect of IMPACT sensor locations on peak currents	65
	F. Influence of the distribution of all NLDN sensors on peak current strength	73
	G. Flash densities and the effect on peak currents	79
	H. Percentages of positive flashes and the effect on peak currents	85
	I. Surface elevation and the effect on peak currents.....	93
VI	SEASONAL AND SMALL-SCALE VARIATIONS IN PEAK CURRENT	101
	A. Seasonal variations in peak currents	101
	B. Small scale variations in peak currents	105
	C. Lightning in the Northern Plains.....	107
	D. Other case studies.....	113
VII	CONCLUSIONS AND RECOMMENDATIONS.....	122
	A. Conclusions	122
	B. Recommendations for further research	125
	REFERENCES.....	127
	APPENDIX A: SUMMARY OF DAYS WITH LIGHTNING IN THE NORTHERN PLAINS FROM 1995-1998.....	134

APPENDIX B: LIGHTNING AND VERTICAL WIND SHEAR FOR THE NORTHERN PLAINS CASES	146
APPENDIX C: APPROXIMATE HEIGHT OF THE MAIN NEGATIVE CHARGE REGION (-10°C HEIGHT)	181
APPENDIX D: CAPE VALUES FOR THE CASES STUDIED	187
APPENDIX E: TIME SERIES AND PERIODICITY OF PEAK CURRENTS FOR INDIVIDUAL CASES	192
APPENDIX F: CLOUD-TOP BRIGHTNESS TEMPERATURES AND LIGHTNING DATA FOR 15 MAY 1998	241
APPENDIX G: IDL PROGRAMS USED TO ANALYZE LIGHTNING DATA.....	264
VITA	277

LIST OF TABLES

TABLE		Page
1	Cloud-to-Ground (CG) lightning summaries for 1989 through 1998.....	29
2	Summary of lightning data for case studies.....	42
3	Peak current statistics for the continental US from 1995 – 98	49
4	Regional peak current descriptive statistics for nine regions of the US	54
5	Median of peak currents over the US in one degree latitude increments	58
6	Peak current characteristics based on the distance between IMPACT sensors .	72
7	Peak current characteristics based on the distance to required NLDN sensors .	78
8	Peak current characteristics based on flash densities.....	84
9	Peak current characteristics based on percent positive flashes.....	92
10	Peak current characteristics based on surface elevation	100
11	Monthly median peak currents for the US landmass	102
12	Periods of band-pass filters used for each case study.....	118

LIST OF FIGURES

FIGURE	Page
1 Inductive charge separation process	7
2 Measured charge density regions of MCSs	10
3 The cloud-to-ground lightning process.....	12
4 Electric field waveform of a lightning discharge.....	15
5 Geometry of the electromagnetic field calculations for a lightning discharge..	17
6 Method of locating return stroke with direction-finders (DFs)	19
7 Method of locating return stroke with time-of-arrival (TOA) sensors	21
8 National Lightning Detection Network (NLDN) sensor distribution.....	23
9 Map indicating upper air stations used in case studies	31
10 An example of the 0.2 degree latitude and longitude grid.....	33
11 Trapezoidal approximation to latitude and longitude grid box	36
12 Case where more than four NLDN sensors are required to detect a return stroke.....	39
13 Example of Skew-T diagram showing region of CAPE.....	45
14 Peak current distributions for the continental Unites States from 1995 – 98	48
15 Divisions of the US for regional peak current distributions	51
16 Negative peak current distributions for nine regions of the US	52
17 Positive peak current distributions for nine regions of the US	53
18 Median peak currents for lightning in one-degree latitude increments	57
19 Percent of flashes over 80 kA in each one-degree latitude increment.....	60
20 Contour of the median of positive peak currents from 1995 – 98	62

FIGURE		Page
21	Contour of the median of negative peak currents from 1995 – 98	63
22	Contour of distances between IMPACT sensors in the NLDN.....	66
23	Map of grid elements having at least 100 flashes from 1995 – 98	68
24	Scatter plot of median peak currents and IMPACT sensor separation.....	69
25	Direct comparison of median peak currents and IMPACT separations	71
26	Contour of distances to the minimum required NLDN sensors.....	74
27	Distance to the minimum required NLDN sensors and median peak currents..	75
28	Direct comparison of median peak currents and required NLDN sensors	77
29	Flash density contours for the US from 1995 – 98	80
30	Scatter plot of median peak currents and flash densities	82
31	Direct comparison of median peak currents and flash densities.....	83
32	Average flash density based on latitude	86
33	Contour of percent positive flashes from 1995 – 98.....	88
34	Scatter plot of median peak current and percent positive flashes.....	90
35	Direct comparison of median peak currents and percent positive flashes	91
36	Latitudinal dependence of percent positive flashes	96
37	Contours of median peak negative currents and surface elevations	97
38	Scatter plot of median peak currents and surface elevations	98
39	Direct comparison of median peak currents and surface elevations.....	99
40	Monthly median peak currents for the US landmass.....	104
41	Plot of the lightning data for the 15 May 98 case.....	106
42	The region used to select data for the Northern Plains study	108

FIGURE		Page
43	Peak current distribution for the Northern Plains region of the US.....	109
44	Diurnal flash rates for the Northern Plains region.....	110
45	Daily lightning summary for the Northern Plains (1995 – 98).....	111
46	Time series of positive peak currents for 15 May 1998 storm	115
47	Maximum peak currents and flash counts for the 15 May 1998 storm	116
48	Cloud top IR temperatures with lightning data from 15 May 1998 storm	121

CHAPTER I

INTRODUCTION

A. Nature and source of problem

Cloud-to-ground lightning data have been collected using the National Lightning Detection Network over the continental United States since 1989, yet little is understood concerning the variations in the peak currents associated with the first stroke of each lightning flash. Many studies have been made concerning other features of cloud-to-ground lightning such as flash densities (Orville 1991a, 1994; Orville and Silver 1997), positive lightning (Rust et al. 1981; Brook et al. 1982; Idone et al. 1987; Baral and Mackerras 1993; MacGorman and Burgess 1994), and the accuracy of the network (Mach et al. 1986; Cummins et al. 1998), but few explanations have been offered concerning peak current variations. As peak currents are intrinsic to the nature of lightning, further understanding of their characteristics should shed additional light on the microphysics involved in the lightning process.

Four general characteristics of peak currents have been reported. First, there are higher peak currents for positive lightning in the Northern and Great Plains than in other regions of the United States (Lopez et al. 1991; Lyons 1996; Lyons et al. 1998). Second, variations in the peak currents with altitude were reported (Robertson et al. 1942; Foust et al. 1953). Third, a connection between peak current and latitude was reported in a study of lightning along the East Coast of the United States and collaborated in Brazil (Pierce 1970; Orville 1990; Pinto et al. 1996). Fourth, peak currents vary with the time of year. Upward

This dissertation follows the style and format of the *Monthly Weather Review*.

discharges from the cloud to the ionosphere (sprites) have also been observed in connection with positive lightning having high peak currents within the Great and Northern Plains (Lyons 1996). While these characteristics have been observed, no explanation is offered as to the possible cause. Little is known concerning the factors affecting the peak currents.

It is apparent that peak currents vary based on the amount of charge transferred from the cloud to the ground but this explanation is incomplete. This is not in dispute as it is no doubt correct, but it is possibly incomplete. The remaining question is why there are consistent patterns over the United States and between seasons in the peak current variations. If the amount of charge transferred to ground on a flash was a random event, then there should not be a noticeable pattern, either spatially or temporally, yet these patterns exist year after year, denying the possibility that the variations are random. This implies that something is governing the amount of charge lowered to ground for each flash.

There are three possible explanations for the repetitive nature of the peak current variations. First, these differences could simply be an artifact of the detection network and have no meteorological cause. Second, the peak currents are simply a result of different amounts of charge being transferred to the Earth. The variations could be a result of varying amounts of charge buildup in the thunderstorm making more charged particles available for some flashes than for others. Third, it is also possible that the charge transferred to the ground is first deposited along the lightning channel and the length of the channel, in part, determines the peak current of the lightning flash. Each of these possibilities will be examined.

The theory that explains these peak current variations must help explain all of the observations. It must take into account the relationship between the sensors distribution and

the peak currents, the reversal of peak current strength between positive and negative flashes, the variation in peak currents with increased surface elevation, and the seasonal variations in peak current strength. There must be some aspect of the thunderstorm microphysics that would explain these variations, if they were not simply an artifact of the separation between the sensors or of the variation of the return stroke velocity.

One theory that would explain all of the variations reported thus far and those seen in this research would be if the peak currents were dependent upon the channel length of the lightning. Larger variations in peak currents are seen with positive lightning than with negative lightning. This is expected, if the peak currents are dependent upon the channel length, as positive lightning has been observed to originate in the upper portions of the cloud (Rust et al. 1981; Brook et al. 1982). Negative flashes probably originate in or near the cloud base in the lower negative charge region and should not show the same amplitude in peak current variations. There are still some differences attributable to the sensor separations, but these have nothing to do with the lightning microphysics.

The dependence of peak currents upon the channel length or on the return stroke velocity must be inferred. There is no way to measure the return stroke velocity for all of the cloud-to-ground flashes in the United States. Likewise, there is no way to determine the origination point of the lightning discharge or the tortuosity of the lightning channel. The apparent deviations from this relationship may be explained in terms of either the lightning detection network configuration or by orographic effects on the storm as it passes over higher terrain.

B. Research objectives

There are several goals in this research effort. The first is to identify the variation in the peak current associated with the first stroke in cloud-to-ground lightning flashes. These include both temporal and spatial aspects. The second is to explain the variations. The explanation is complicated and must be divided into parts.

The first step in explaining the variations must be an examination of the measurement system. Detection criteria and spatial distribution of sensors both play a part in estimating the peak currents associated with lightning. It is somewhat comforting to know that the effect of the network should be consistent throughout the data set, regardless of season.

Knowledge of the electrical structure of thunderstorms is critical to the understanding of peak currents. By examining what is known about the charge separation process and reports of charge structure in thunderstorms, it is possible to propose the mechanism involved in producing different peak currents. Since the peak current is an indication of the net charge lowered to ground, there are two possible causes for the variation in the amount of charge transferred. Either there is simply more charge lowered directly from the cloud to the ground repeatedly in the same areas but for different seasons, or the charge is deposited on the channel as the stepped leader moves toward the ground determining the peak current variations. The latter possibility is the most probable.

Once the proposed mechanism is developed, it will be tested using case studies of thunderstorm systems. These cases were selected to find storms that were isolated from other systems. This will reduce bias in the data.

To summarize the research objectives, a listing follows.

- 1) Identify the spatial variations in peak currents across the United States.
- 2) Identify the temporal variations in peak currents for the United States.
- 3) Consider the measurement network and its influence on the variations.
- 4) Consider how the channel length affects the peak current strength.
- 5) Attempt to verify this by using case studies of isolated storm systems.

CHAPTER II

BACKGROUND INFORMATION AND LITERATURE REVIEW

In order to understand the reasons for variations in lightning peak currents, it is necessary to have a general overview of the lightning process from the charge separation mechanisms to the combination of return strokes into a lightning flash. The method used to detect lightning is also important as it affects the peak current distributions. This information and an overview of the published peak current variations to-date will be provided here.

A. Charge separation process

In order for lightning to occur in a thunderstorm, there must be regions within the cloud having a net charge producing electric fields exceeding the breakdown potential. These regions are produced by the separation of charge within the thunderstorm. While this process is not completely understood, there are prevailing theories as to the charge separation mechanism. Saunders (1993) discusses these theories in detail.

One of the prevailing theories involves an induced dipole charge on both supercooled liquid water droplets and on the larger ice particles falling from the cloud (Jayaratne et al. 1983). Both the water droplets and the ice particles have an induced positive charge on the bottom and negative charge on the top in response to the environmental electric field (Fig. 1). As the larger ice particles fall through the cloud they collide with the water droplets which are lifted by the updrafts. During this collision, charge is transferred and the ice particle continues to fall, but with a net negative charge. The water droplet continues along its upward path, but it now has a net positive charge after the collision.

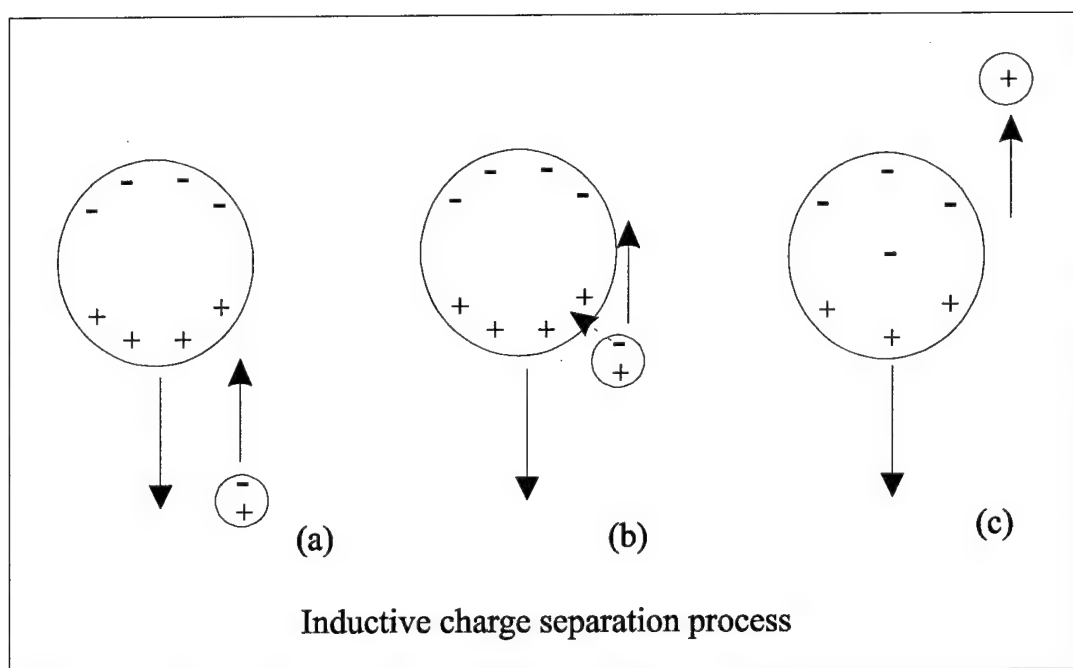


Figure 1. Inductive charge separation process. Upward moving supercooled liquid water droplet (small circle) and falling ice particle (large circle) approach in presence of downward directed electric field. Charge is induced to top and bottom of particles by electric field. Water droplet and ice approach (a) and then collide (b), transferring a negative charge from the water droplet to the ice particle leaving a net charge on each as they continue in their original directions (c).

As the ice particle falls through the cloud, it is warmed by the environment and starts to melt and evaporate. Either it will escape from the base of the cloud as precipitation or it will evaporate sufficiently to allow the updraft to suspend it within the cloud. The water droplet continues its upward motion until it has grown enough to maintain its position in the cloud or to fall back down. The result is a region of positive charge aloft and a negative charge region toward the base of the cloud.

Since the inductive charge separation process includes the presence of supercooled liquid water, it is most likely to occur in the lower portion of the cloud, but above the freezing level (Takahashi 1978; Keith and Saunders 1990). Observations support this (Stolzenburg et al. 1998) as the main negative charge region of the cloud is found between -10 and -20°C range. This also satisfies the basic charge structure indicated by the electric field measurements made from the ground which indicate a positively charge layer aloft and a negative charge region at the cloud's base (Krehbiel 1986).

The rather simplistic bipolar charge structure does not sufficiently describe the regions of net charge found within the cloud. There is also a region of weak net positive at the base of the cloud (Simpson and Scrase 1937). This has also been explained as a screening layer (Dye et al. 1989; Marshall and Rust 1991) where the negative charge region near the base of the cloud attracts positively charged ions to the cloud base. It may also be a result of a reversal in the inductive charge separation process due to the warmer temperature near the cloud's base (Gaskell and Illingworth 1980). As the temperatures warm and further collisions occur with the falling ice particles, there is a positive charge transferred to the ice and a negative charge to the water droplets. This not only helps to explain the positively

charged region at the cloud base, but also helps to increase the negative charge region just above it.

B. Measured thunderstorm charge structure

Recent measurements of the electric fields within thunderstorms using instrumented balloons (Stolzenburg et al. 1998) show a more complex structure than the bipolar or tripolar charge mentioned above. These measurements indicate at least four charge regions in the cloud (Fig. 2). While this adds to the complexity of the electrical structure within storm, the main negative charge region is still found near the base of the cloud with the main positive region aloft.

Stolzenburg et al. (1998) report measuring a weak positive charge region near the base of the cloud, a strong negative charge region above that, a strong positive charge layer aloft, and a weak negative layer near the top of the cloud (Fig. 2). The strengths of the electric fields and, therefore, the net charge in the layer is stronger outside the updraft region than within it. Also outside the updraft region, there were multiple charge layers. This is likely due to the positively charged ice particles beginning to fall without the sustained updrafts. This would allow the net charge to be stratified within the cloud as the ice particles are of varying size and mass, affecting the highest level they can obtain within the cloud before falling. The updraft region does not have this difficulty, as the stronger vertical motion would allow the particles to be elevated to approximately the same height.

It is important to remember that the majority of measurements taken in a thunderstorm are made during the mature phase of the storm. Little is known about the electrical structure of a storm in the growth phase or of the extent of the regions of net charge. Also, regardless of how much is known concerning the charge structure of a

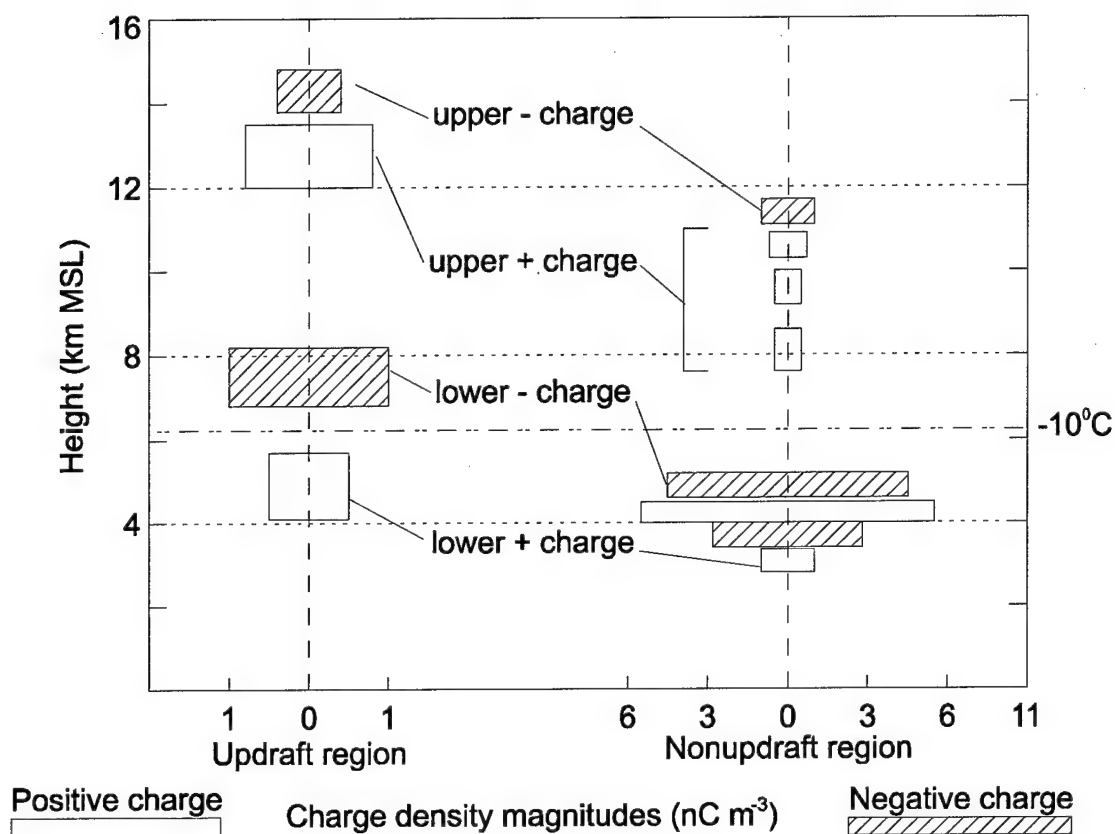


Figure 2. Measured charge density regions of MCSs. Compilation of charge regions in MCSs based on balloon soundings as reported by Stolzenburg et al. (1998). In the MCS updraft, four charge regions are found while, outside the updrafts, two additional charge regions are present. The general structure of the charge remains the same, a lower positive and negative charge and another positive and negative charge region aloft. The approximate location of the -10°C temperature line is also indicated.

thunderstorm, it is next to impossible to predict which charge region will generate an electrical discharge.

C. Cloud-to-ground lightning discharge process

As the charge separation continues, additional net charge builds up in the different regions (Fig. 2) of the cloud (Stolzenburg et al. 1998) increasing the charge density. As the charge density increases, so does the electrical field surrounding the charge region. If this process continues, the potential difference between the charge region and its surroundings will exceed a breakdown field strength of about $150 - 250 \text{ kV m}^{-1}$ (Griffiths and Phelps 1976). This starts the coronal discharge that may lead to a cloud-to-ground lightning discharge (Fig. 3).

The discharge from the cloud, called a leader, causes an ionized path to form in the atmosphere. Additional charge can move along this path from the charge region of the cloud. As the path is narrow, $0.1 - 0.5 \text{ m}$ (Orville 1968), the potential at the tip of the leader becomes large and an additional coronal discharge follows. This new discharge may follow the same path as its predecessor or it may take a new direction. This process forms a stepped leader (Fig. 3) and each step in the process is only approximately 50 m long (Idone and Orville 1982). There can be two discharges from the same segment, or step, of the leader, which will form a new branch and these may form additional leaders. As the stepped leader travels through the atmosphere, it may make many twists and turns before reaching its destination. The more crooked the path, the higher the channel's tortuosity.

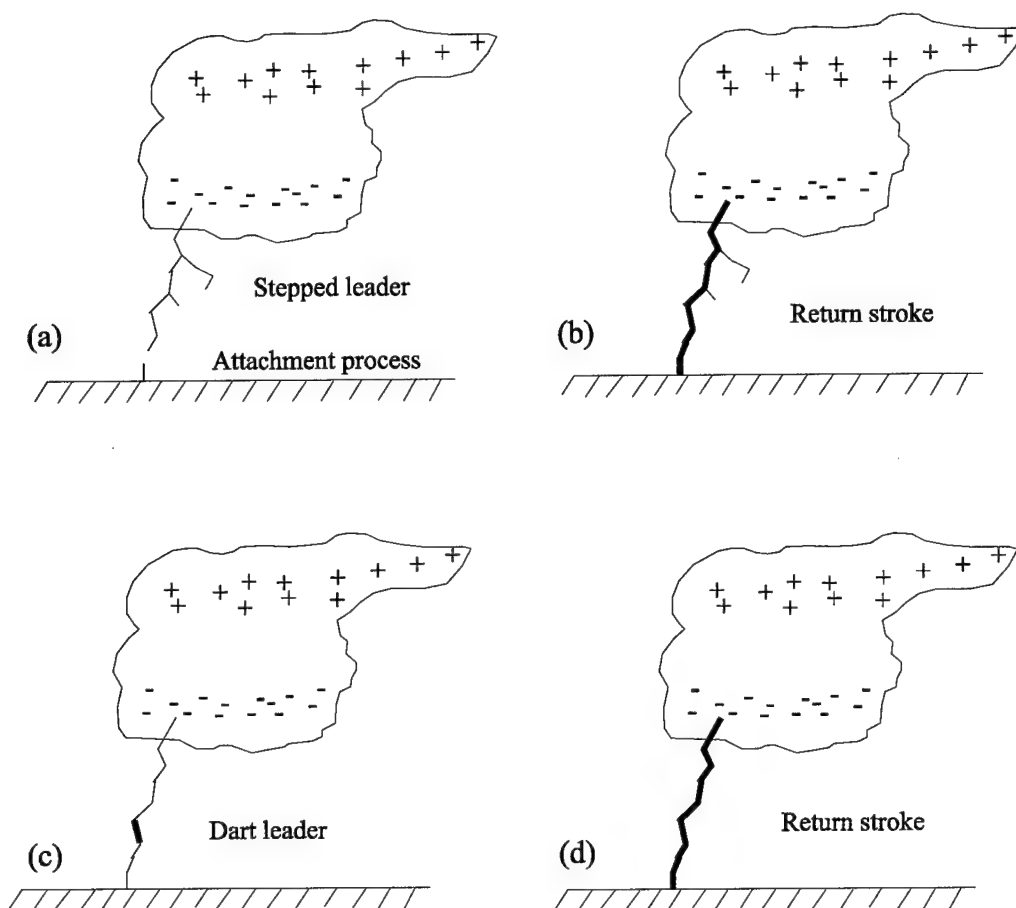


Figure 3. The cloud-to-ground lightning process. In (a), the stepped leader is propagating away from the cloud toward the ground. Branches have formed in the stepped leader. As it approaches the ground, the attachment process takes place and an upward directed discharge occurs from the ground which will complete the channel from the cloud. After this happens, a return stroke occurs in (b), moving charge rapidly from the ground back to the cloud along the main channel. In (c), a dart leader travels from the cloud to the ground along the main channel followed by another return stroke (d). (After Uman 1987, p. 9)

For cloud-to-ground lightning, the stepped leader must eventually approach the ground. As this happens, the potential between the leader and the Earth is high, causing an upward discharge to occur (Golde 1967, 1977). This is the attachment process and it occurs when the leader is within about 30 m of the ground (Fig. 3). Once the circuit from the cloud to the ground is complete, charge moves rapidly from the other branches down this main channel. This happens from the base of the channel forming a wave that moves up toward the cloud otherwise known as a return stroke. The return stroke travels at approximately $2 \times 10^8 \text{ m sec}^{-1}$ (Idone and Orville 1982) and is the brightest feature of the lightning flash.

For some lightning flashes, the process ends after the stepped leader and the subsequent return stroke. In other cases, additional discharges from the cloud follow the main channel formed by the first stroke. These are dart leaders and travel at extremely high speeds along the ionized channel. As with the stepped leader, a return stroke follows the dart leader. This dart leader and return stroke combination may happen several times during a lightning flash and appears as a flicker to the eye. The number of return strokes in a flash is the multiplicity. The time from the initial coronal discharge to the last return stroke usually takes a second or less (Cummins et al. 1998).

There is an additional distinction between the types of lightning. While there are cloud-to-ground and intracloud lightning, there are also different types of cloud-to-ground lightning. Only one distinction is important here and that is the polarity of the lightning flash. Either a net positive charge or a net negative charge may be lowered to the ground in a lightning discharge. If a net positive charge is lowered to the ground in the first stroke, the flash is defined as a positive flash. A negative flash lowers a net negative charge to the ground in the first stroke. While bipolar lightning does exist (Brook et al. 1982 and Pinto et

al. 1996) where a flash may lower a net positive or negative charge to ground in the different strokes, these are not considered here. By convention, the polarity of the flash is determined by the first stroke.

D. Detection of a lightning flash

In the lightning process (Fig. 3), net charge is lowered from the cloud to the ground. This change in the charge structure of the cloud manifests itself as a change in the environmental electric field (Krider et al. 1976) which can be measured at the Earth's surface. Based on the signal generated by this electric field change (Fig. 4), a cloud discharge can be categorized as either a cloud-to-ground flash or an intracloud flash. Included in the criteria are the rise time of the electric field change, the overshoot of the electric field compared with the peak signal strength received, and the length of time the signal remains above the background electric field strength.

There are two methods currently used to detect the return strokes in a cloud-to-ground lightning flash. The first involves measuring the electric and magnetic radiation field generated by the return stroke, from which one can determine the peak current and location of the return stroke (Krider et al. 1976). The second method involves measuring the change in the electric field at several locations with extremely accurate timing (Lyons et al. 1989). From this, one can also determine the peak current and location of the return stroke. Both methods are described in more detail below.

The return stroke generates a magnetic field by the rapid movement of the charge along the channel following the attachment process. There is also an electric field from the

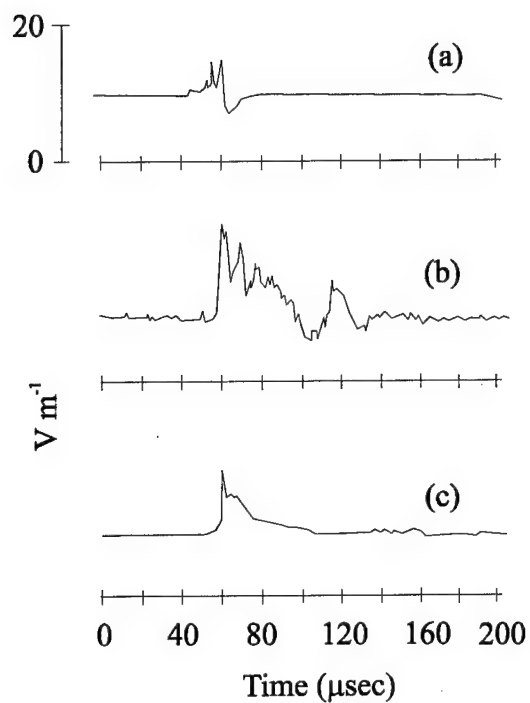


Figure 4. Electric field waveform of a lightning discharge. The top chart (a) depicts a cloud discharge while the center chart (b) is that of a return stroke. A subsequent return stroke is depicted in (c). The first return stroke (b) shows the rapid rise time at 50 μsec and the overshoot at approximately 103 μsec . (From Krider et al. 1980)

charge moving along the channel (Fig. 5), which can be used to detect the return stroke in a flash. The relationships that describes the electric and magnetic fields are given by (Uman 1987, p. 137)

$$\left| \vec{E}(r, \phi, 0, t) \right| = \frac{1}{2\pi\epsilon_0} \left[\int_{H_b}^{H_T} \frac{2z'^2 - r^2}{R^5} \int_0^t i\left(z', \tau - \frac{R}{c}\right) d\tau dz' + \int_{H_b}^{H_T} \frac{2z' - r^2}{cR^4} i\left(z', t - \frac{R}{c}\right) dz' - \int_{H_b}^{H_T} \frac{r^2}{c^2 R^3} \frac{\partial i\left(z', t - \frac{R}{c}\right)}{\partial t} dz' \right] \quad (1)$$

and

$$\left| \vec{B}(r, \phi, 0, t) \right| = \frac{\mu_0}{2\pi} \left[\int_{H_b}^{H_T} \frac{r}{R^3} i\left(z', t - \frac{R}{c}\right) dz' + \int_{H_b}^{H_T} \frac{r}{cR^2} \frac{\partial i\left(z', t - \frac{R}{c}\right)}{\partial t} dz' \right] \quad (2)$$

In these equations, ϵ_0 is the permittivity of free space, μ_0 is the permeability of free space, and c is the speed of light. For the electric field (1), the first term is the electrostatic term and is not present in (2), as the magnetic field does not have a static term. The second term in (1) and the first term in (2) are the induction terms. The last term in (1) and (2) represents the radiation component. The electrostatic term falls off as $1/r^3$ and the inductive terms decrease as $1/r^2$. The radiation term is attenuated as $1/r$. At distances greater than a few tens of kilometers, the radiation component dominates.

Lin et al. (1980) proposed using a transmission line model (TLM) that approximates the return stroke current as a vertical line where the return stroke velocity is constant along

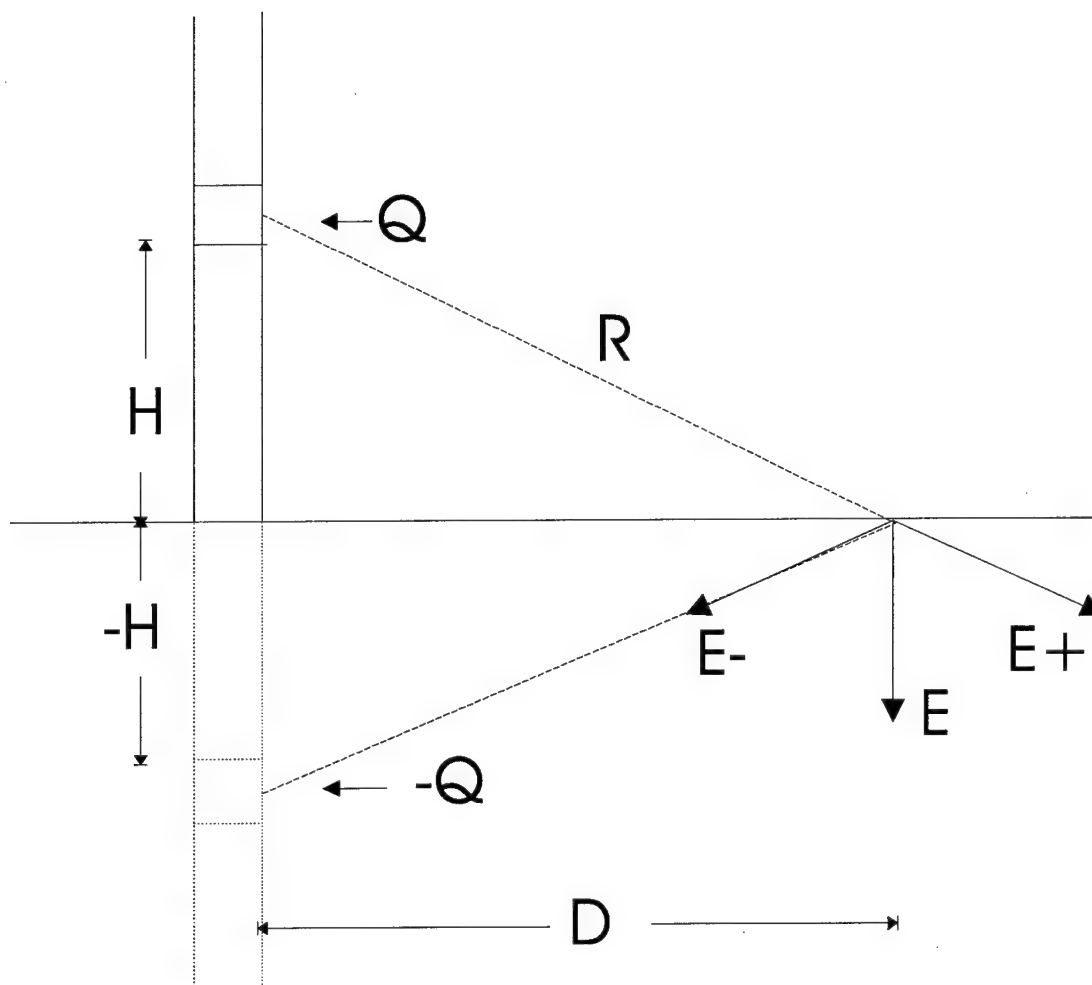


Figure 5. Geometry of the electromagnetic field calculations for a lightning discharge. The charge, Q , is traveling in a vertical path above the ground at a distance, R , from the measurement location (horizontal distance is D). The negative values indicate a mirror charge used to represent the induced or mirror charge at the ground. (From Uman 1987, p. 317.)

the length of the channel. If the distance from the channel is far enough that the radiation terms of (1) and (2) dominate, then peak current may be found using

$$I_{pk}(t) = -\frac{2\pi\epsilon_0 c^2 R}{v} E_{pk}\left(t + \frac{R}{c}\right) \quad (3)$$

where $I_{pk}(t)$ is the peak current at time t , v is the return stroke velocity, and $E_{pk}\left(t + \frac{R}{c}\right)$ is

the peak in the electric field associated with the peak current at time t . A similar relationship may be found for the magnetic field.

If a wire loop passes through a magnetic field, or a stationary loop is in the presence of a changing magnetic field, there will be a current induced in the wire loop. This is the basis for lightning detectors using a direction finding capability. The magnetic radiation field from the return stroke is treated as if it originated from a vertical transmission line which would produce a magnetic field oriented in the horizontal plane and whose field strength is only dependent on the distance from the source. As this changing magnetic field passes through a wire loop oriented in the vertical plane, a current is induced in the wire. The amount of current is dependent on the strength of the magnetic field and the angle between the field and the wire loop.

Two wire loops oriented in the vertical plane but perpendicular to one another allow the angle of incidence to be determined for the magnetic field. The tangents of the currents induced in each wire loop provides this angle. As the tangents of an angle and 180 degrees plus the angle are the same, it is impossible to determine the direction to the return stroke from one sensor (Fig. 6). It is also impossible to determine the range to the source of the magnetic field as the field strengths vary dependent upon the amount of charge lowered to

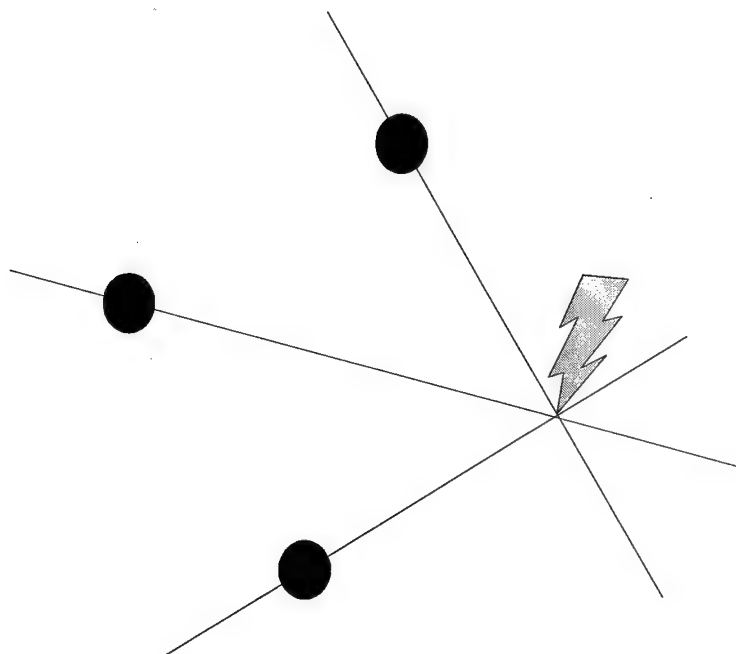


Figure 6. Method of locating return stroke with direction-finders (DFs). The circles represent the DFs. The lines through the DFs intersect at the ground location of the return stroke. Should only one DF detect the stroke, it would be impossible to determine the direction along the line to the proper location. Two DFs can find a location, unless the return stroke occurs very close to one of them. The use of three DFs allows all flashes within range to be located.

ground. If two or more sensors detect the same return stroke, then a location may be determined using triangulation methods. To accurately determine the location of a return stroke, a system of at least three direction finders must be used (Orville et al. 1987).

The time-of-arrival sensors do not depend on the magnetic radiation field to identify and locate a return stroke associated with a lightning flash. These sensors measure the change in the electric field and report those changes that meet the criteria for a cloud-to-ground discharge (Krider et al. 1976) with extremely accurate timing (Lyons et al. 1989). These time-of-arrival (TOA) sensors are time synchronized using the signals from the Global Positioning System (GPS) atomic clocks. Locations for the return strokes are determined by finding the difference in arrival times between multiple sensors. From these time differences, hyperbolas may be found. If two (TOA) sensors detect the return stroke, then the source of the electric field could have been anywhere along a hyperbola defined by the time difference in the detection of the stroke (Fig. 7). Traditionally, four sensors are required to accurately determine the location of a return stroke using the TOA sensors (MacGorman and Rust 1998, p. 161).

E. The National Lightning Detection Network

The National Lightning Detection Network (NLDN) incorporates both the direction finding (DF) and time-of-arrival (TOA) methods in locating lightning flashes (Cummins et al. 1998). The NLDN is operated by Global Atmospheric, Inc. in Tucson, Arizona and consists of 106 sensors, 43 of which use both the TOA and DF technology. These are called IMPACT (IMproved Accuracy from Combined Technology) sensors. The other 63 sensors use only the TOA method of detecting cloud-to-ground lightning (Fig. 8). The NLDN was formed from three separate networks in 1987. The State University of New

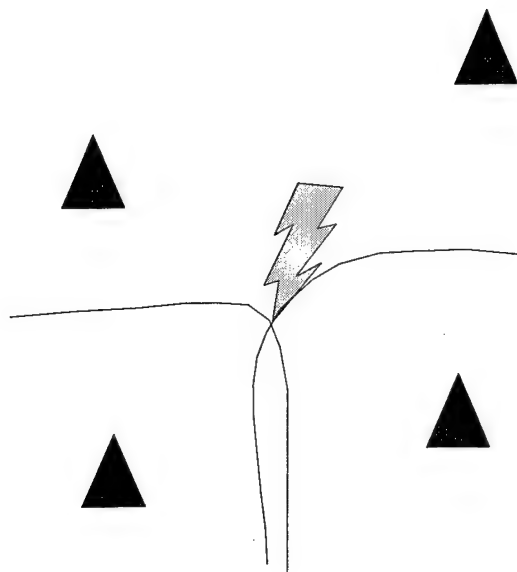


Figure 7. Method of locating return stroke with time-of-arrival (TOA) sensors. The triangles represent the TOA sensors. When a return stroke is detected by two of these sensors, the time difference is translated into a difference in distances, which define a hyperbola. This return stroke can be at any angle from the sensors. In order to determine the location of the return stroke, another hyperbola must be found which requires another sensor. The intersection of the hyperbola defines the position of the return stroke. Four sensors are required for adequate coverage as the return stroke may be too close to one of the sensors to define a hyperbola.

York (SUNY) at Albany network covered the east coast (Orville et al. 1983). The National Severe Storms Laboratory (NSSL) network covered the Great Plains (Mach et al. 1986). The Bureau of Land Management (BLM) network covered the Intermountain West and the West Coast (Krider et al. 1980).

A major upgrade in the network occurred in 1994 that both increased the effective range of each sensor to about 600 km (Cummins et al. 1998) and modified the criteria for acceptance of a cloud-to-ground stroke (Cummins personal conversation 1998). This modification affected the data collection enough that the data set used for this study was limited to the period after the upgrade for reasons to be presented later. One of the effects of the upgrade was a change in the distributions of peak signal strengths throughout the United States. This was a result of the increase in detection range and the change in selection criteria for cloud-to-ground lightning (Wacker and Orville 1999).

The peak current for a lightning flash is calculated from the peak range normalized signal strength (RNSS) reported by the NLDN. The signal received by the sensors varies depending on the actual strength of the return stroke and the distance from the sensor to the return stroke. The range normalization attempts to eliminate the effect of attenuation due to distance. In order to accomplish this, the signal strength at each sensor is adjusted according to the $1/r$ relationship to a distance of 100 km from the return stroke to the sensor (Cummins et al. 1998).

Field measurements of the peak currents in triggered lightning were compared with the reported RNSS giving an empirical relationship between the RNSS and the peak current (Orville 1991b; Idone et al. 1993). In order to trigger the lightning flash, a rocket, trailing a

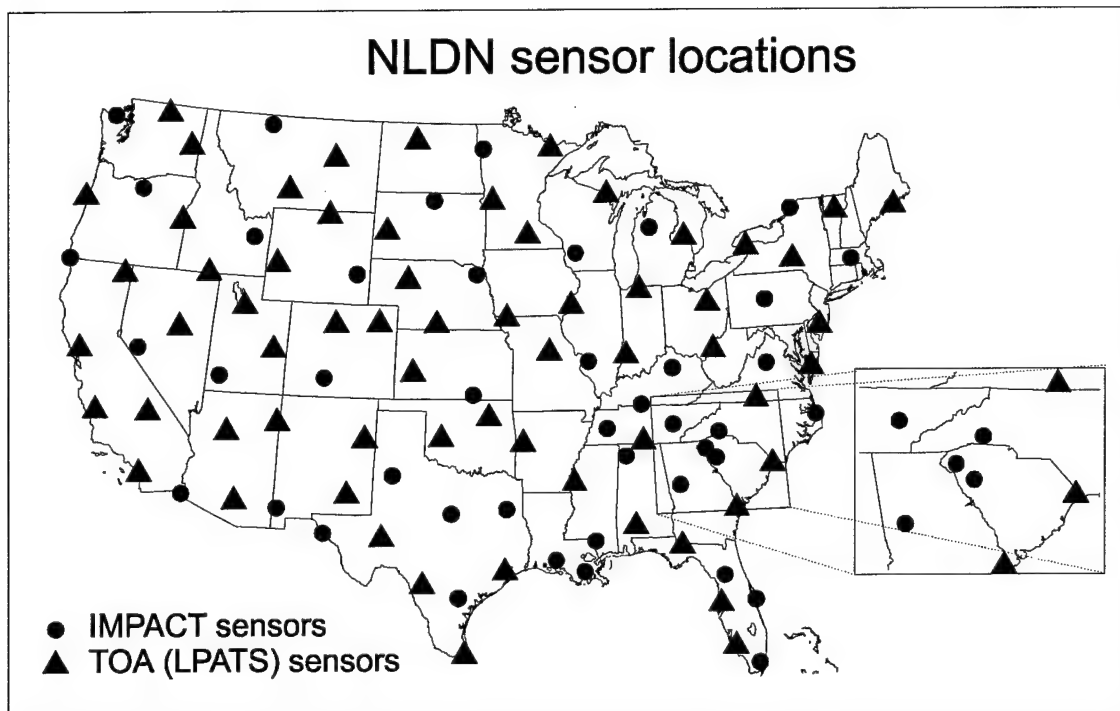


Figure 8. National Lightning Detection Network (NLDN) sensor distribution. This depicts the NLDN configuration as of 1997. The IMPROVED Accuracy with Combined Technology (IMPACT) sensors, having both Time-Of-Arrival (TOA) and Direction-Finding (DF) capabilities are indicated as filled circles. The sensors with only TOA capability are shown as triangles. The insert shows the sensors placed closer to one another.

thin wire, is launched into the thunderstorm when the conditions appear right for a lightning discharge to occur. Since these were empirical relationships, some variation is expected arising from the data set used in the study. There was actually very close agreement between the studies on the conversion between the peak signal strength and the peak current. The conversion from peak signal strength to peak current used in this study was (Cummins et al. 1998)

$$Peak_Current = \frac{0.185kA}{LLP}(RNSS). \quad (4)$$

Here the RNSS is in LLP units and the peak current is in kiloamps (kA). It should be noted that no triggered lightning with a peak current over 60 kA has been recorded.

F. Observations of peak current variations

Recent studies of upward electrical discharges, sprites and blue jets, have indicated that the majority of these events are related to positive cloud-to-ground lightning with high peak currents (Lyons et al. 1998). Another study indicates that the maximum in peak currents for positive flashes occur in the Northern and Great Plains (Orville and Huffines 1999). This area of the US has the highest median peak currents for positive lightning for each year from 1989 – 98. This is not true for negative lightning as the median peak current for negative flashes have a maximum in Florida and along the Gulf and East Coasts. Positive lightning has different regional variations in the peak currents than negative flashes.

Studies of variations in lightning with altitude indicate a connection between the peak currents and surface elevation. Robertson et al. (1942) performed a study of peak currents in Colorado using the excess voltage of electrical transmission lines due to the lightning discharge. They found that the peak current decreased as the surface elevation

rose from 650 to 4300 m above sea level. Others (Golde, 1968) found the same relationship between peak currents and surface elevations in the former USSR (Union of Soviet Socialist Republics) with surface elevations ranging from 250 to 1140 m above sea level. Foust et al. (1953) found the opposite trend in the Andes Mountains where the surface elevation ranged from 1800 to 4100 m above sea level. The latter study also mentioned that the reverse tendency for the peak currents could have been due to variable surface resistance beneath the towers used in the study. It should also be noted that none of these studies made a distinction between positive and negative flashes.

Reports of lightning in the Eastern United States indicate a relationship between the peak currents and latitude (Pierce 1970; Orville 1990). These works show that the peak currents for negative flashes increase with decreasing latitude. Other studies, such as that of Pinto et al. (1996) support this relationship. From the published literature, it is clear that much remains unknown concerning the nature of or causes for peak current variations.

CHAPTER III

DATA SOURCES

A. Lightning data

The lightning data used in this study are a product of the National Lightning Detection Network (NLDN) which was described in Chapter II. In order to provide a better understanding of the spatial and temporal extent of the data set, some additional information about the network is provided. A summary of the annual lightning data is also included.

The NLDN records about 80 – 90 percent of all cloud-to-ground lightning flashes (Cummins et al. 1998, Idone et al. 1998). Once the stroke data are received at Global Atmospheric, Inc. they are processed into flashes on a real-time basis. These data are provided to their subscribers. The data set used in this study includes only lightning flashes that have been quality controlled via post-processing by Global Atmospheric, Inc. This post-processing corrects the data for site errors, but there are other errors that may be included and must be accounted for.

Only the information for the first stroke in each flash is used in this study. This is a result of the reporting method of Global Atmospheric, Inc. The return strokes are combined into flashes using the locations and peak signal strength of the first stroke. No subsequent stroke information is available, although the number of strokes in each flash, or the multiplicity, is reported.

Cummins et al. (1998) report that the changes in the waveform acceptance criteria made in the NLDN upgrade of 1994 may allow intracloud flashes with weaker signal strengths to enter the data set as positive cloud-to-ground flashes. These intracloud flashes would be identified as lowering a net positive charge toward the ground either from a

discharge from the upper positive region to the lower negative layer or visa versa. All positive flashes having a peak current less than 10 kA are eliminated from any calculations unless otherwise noted.

Other considerations must be made when dealing with the NLDN data. As was previously stated, at least three direction-finding or four time-of-arrival sensors must detect a return stroke in order to provide an accurate location. An additional restraint is placed on data from the NLDN. In order for a return stroke to be reported, at one IMPACT sensor must detect the return stroke signal. This helps eliminate possible errors or misreported data by combining the capabilities of the DF and TOA sensors. The constraint requires additional consideration when examining the effect of the spacing of network sensors. Sensors that have a larger separation will not detect flashes with weaker signals as the electromagnetic pulse will be reduced to levels below the detection threshold.

All peak currents have been calculated using the empirical relationship found in Equation 3. This converts the range normalized signal strength (RNSS) to a peak current. It is worth repeating that this conversion is based on triggered lightning and no measurements of triggered lightning over 60 kA have been recorded. Peak currents over 60 kA must be taken as an approximation, since they are determined by extrapolating the studies beyond the data used to drive the formula.

For this study, all lightning data have been limited to within the borders of the continental United States (hereinafter referred to as the US). This is done in order to eliminate any effects of lightning near the fringe of the network's coverage area, which would tend to only report return strokes and flashes with high peak currents. The signal from return strokes with lower peak currents would be weakened before they reached the

required number of sensors to be reported, thus skewing the data set toward higher peak current values. The lightning data over the Great Lakes have also been eliminated from the data set. This allows comparisons between peak currents and surface elevation data, which will be explained later.

The last restriction of the lightning data is a temporal one. Since the 1994 upgrade of the NLDN (Cummins et al. 1995 and 1998), there was a shift in the peak current distribution for both positive and negative flashes (Wacker and Orville 1999). In order to avoid the additional factor of comparing pre-upgrade and post-upgrade peak current distributions and flash counts, this study is limited to data from 1995 through 1998.

A summary of lightning flashes for the years since 1989 is in Table 1. This lists the number of flashes and percent positive flashes for the entire data set and for the US only. The restriction of only using positive flashes with peak currents of 10 kA or greater was placed on data after 1994. The median peak currents for the entire data set and the US are also listed. It can be seen that the peak currents drop off in magnitude after the upgrade, even with the exclusion of positive flashes with peak currents less than 10 kA.

B. Upper air data

The upper air data were provided by the Air Force Combat Climatology Center (AFCCC) in Asheville, North Carolina. The data are originally from the National Oceanic and Atmospheric Administration (NOAA) stations, which perform balloon launches for upper atmospheric measurements every 12 hours. Each balloon launch, or sounding, provides the temperature, pressure, and dew-point depression at predefined intervals during the ascent. Data at standard pressure levels are reported along with data at other significant levels in the atmosphere, dependent upon the atmospheric conditions for that sounding.

Table 1. Cloud-to-Ground (CG) lightning summaries for 1989 through 1998.

Cloud-to-ground flash characteristics without peak current restrictions								
All measured flashes					US boundary only			
			Median peak current (kA)				Median peak current (kA)	
Year	Flashes (x 10 ⁶)	% Positive	Positive	Negative	Flashes (x 10 ⁶)	% Positive	Positive	Negative
1989	13.422	3.07	54.3	-29.7	10.957	3.22	52.1	-28.0
1990	15.929	3.83	44.0	-30.1	12.601	4.21	42.4	-27.9
1991	16.903	3.98	43.8	-29.2	13.206	4.31	41.8	-27.3
1992	16.260	4.18	40.3	-27.8	13.203	4.37	38.2	-26.4
1993	24.234	4.56	37.2	-27.8	20.191	4.80	34.6	-26.3
1994	24.218	4.93	32.9	-26.4	19.884	5.24	31.0	-25.0
1995	22.721	9.27	19.6	-22.7	17.474	9.91	17.8	-21.0
1996	26.173	10.17	17.6	-21.5	19.680	11.10	16.3	-19.8
1997	26.943	10.15	16.5	-21.6	18.697	11.48	15.1	-19.4
1998	29.179	11.38	16.7	-20.0	20.276	12.67	15.7	-18.3
Cloud-to-ground flash characteristics (1995 – 98) without positive flashes < 10 kA								
Measured flashes					US boundary only			
			Median peak current (kA)				Median peak current (kA)	
Year	Flashes (x 10 ⁶)	% Positive	Positive	Negative	Flashes (x 10 ⁶)	% Positive	Positive	Negative
1995	22.353	7.78	23.9	-22.7	17.129	8.09	22.2	-21.0
1996	25.619	8.22	22.2	-21.5	19.174	8.75	20.9	-19.8
1997	26.288	7.91	21.4	-21.6	18.113	8.62	20.4	-19.4
1998	28.375	8.87	22.2	-20.0	19.588	9.60	21.9	-18.3

Upper air data are used in this study to determine the vertical wind shear and the Convective Available Potential Energy (CAPE) near the thunderstorm environment. They are only used for the case studies as it would be too time consuming to attempt calculations and comparisons for all thunderstorms during the 4-year period-of-study. A map showing the upper air data stations is included (Fig. 9).

C. Satellite data

Satellite data are used for the case studies in order to find the approximate height of the cloud tops. This requires the use of infrared (IR) satellite imagery. The Geostationary Operational Environmental Satellite (GOES) positioned over the East Coast (GOES EAST) provides data covering the regions of the case studies. The images are archived at Texas A&M University.

D. Surface elevation data

In order to compare the peak current variations with the surface elevations, it was necessary to have accurate topography data for the US. NOAA provides their data on-line at <http://ingrid.ldgo.columbia.edu/SOURCES/USTOPO/.topo/>. This covers the US and provides surface elevation data every 1/120 of a degree latitude and longitude. While this resolution is too fine for any statistical work with the lightning data, a mean surface elevation at every 0.2 degrees latitude and longitude matches the grids used in calculating general features for the lightning data. All surface data calculations are done with this mean elevation on a grid size of 0.2 degrees.

Upper air stations used in study

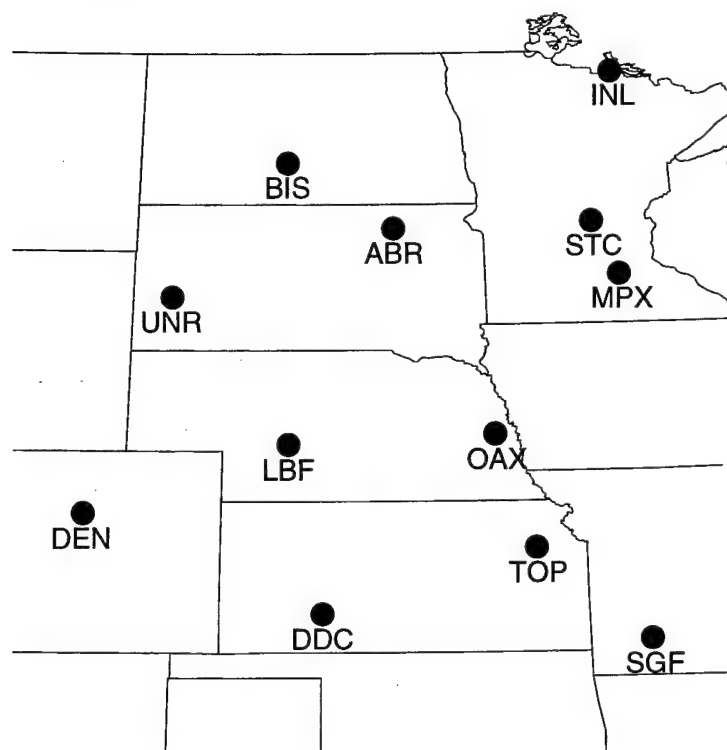


Figure 9. Map indicating upper air stations used in case studies. The letters indicate the International Civil Aviation Organization (ICAO) designators for the sites.

CHAPTER IV

METHODS OF INVESTIGATION

A. Restriction of data to US boundaries

In order to eliminate the influence of data at the extreme edge of the NLDN detection range, the comparisons of peak currents and other parameters were limited to the boundaries of the continental United States. The region of the Great Lakes was not included in the analysis as the peak currents can be influenced by the propagation of electromagnetic waves over water instead of land as the conductivity varies between land and water, although this difference may be negligible (Tyahla and Lopez 1994). The elimination of data over the Great Lakes makes comparisons with surface elevations much simpler as the elevation data are given for the Earth's surface and not for the water levels.

In order to restrict the data to the US boundaries, all locations with surface elevations less than zero MSL were ignored. This also eliminates regions of the US over land where the surface elevation is below sea level, such as Death Valley, but this is a small area of the US with little lightning activity.

B. Comparison of median peak currents for regional variations

All regional analyses were accomplished for lightning data within areas defined by a 0.2 by 0.2 degree latitude and longitude increments across the US. While this grid (Fig. 10) changes in size from 448 km² at 25 degrees north latitude to 325 km² at 49 degrees north, this provided the simplest method of analysis.

In order to calculate the median peak currents for each of the grid locations (Fig. 10), it was necessary to form a three dimensional array. The first dimension represented the longitude location in the grid and the second represented the latitude. The third dimension

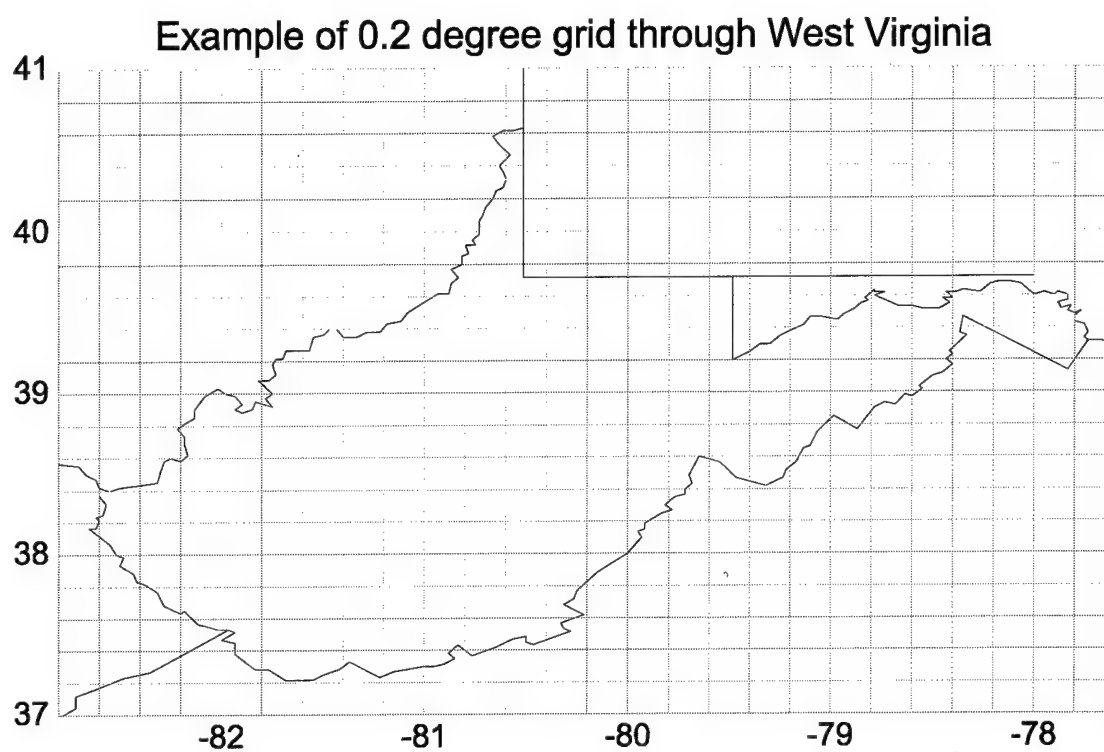


Figure 10. An example of the 0.2 degree latitude and longitude grid. The grid is placed over the West Virginia region to show the relative size of the individual elements or grid boxes. Latitude and longitude lines are labeled every degree for reference.

was used for the peak current distribution for flashes in the grid. For each flash in the region of study, the latitude and longitude grid position was found and the appropriate peak current bin was incremented by one.

Memory limitations required the restriction of the peak current bins to range from 0 – 100 kA using 1 kA increments, which was the best option using the memory available. All lightning data, except positive flashes with peak currents less than 10 kA (Cummings et al. 1998) must be included in the analysis. In order for this to happen, all flashes with a peak current greater than 100 kA were treated as if the peak current was 100 kA. This had no effect on the median calculations, as the median peak currents in each grid were less than 100 kA. The median peak current was then found by locating the bin where the cumulative total flash count from zero was at least half of the total number of flashes in that bin. This calculation was performed for positive and negative flashes separately. Only grids with at least two flashes were included when calculating the median peak currents. While this does not represent a valid sample size to form a median, the elimination of these grid locations is also misleading. Setting these median values for these grids to zero implies that there was no lightning in that region. The grid locations with low flash counts were filtered out of some of the comparisons in order avoid misrepresentative values.

The median peak current values have a precision of 1 kA, as the peak current increment in the calculations was only 1 kA. For example, if the true median value was 12.9 kA, it would be reported as 12 kA since all flashes from 12.0 through 12.9 kA were included in the bin representing the 12 kA flashes.

C. Flash density calculations

In order to determine the flash density, the same latitude and longitude grid was used as for the median peak current calculations (Fig. 10). Here, the array was only two dimensional as the flashes in each grid box were counted regardless of the amplitude of the peak currents. For the flash density, there was a separate calculation for all measured lightning and for all positive flashes with peak currents greater than or equal to 10 kA.

Once the number of flashes in each grid location was found, the flash count was divided by the area of each grid box. As mentioned above, this area changes with latitude. The density calculation must account for these differences. In order to find the area of a grid element, a trapezoidal approximation was made (Fig. 11). Although the sides of the area element are not actually straight lines but arcs, the approximation introduces very little error in the calculation for distances this small.

No attempt was made to adjust the flash counts for the network detection efficiency, as in other studies. (Orville 1991a, 1994, Orville and Silver 1997, and Orville and Huffines 1999). If an estimate of the actual flash counts is needed, note that the reported detection efficiency of the network was 84 percent after the 1994 upgrade (Idone et al. 1998). All flash counts and flash density values are based on the measured cloud-to-ground lightning reported by the NLDN without adjustment for detection efficiency.

D. Variations in the median of peak currents based on seasons

The calculation of the median peak current is very similar to the calculations performed for the grid based median peak currents. The main exception is the size of the region. For the grid based analysis, the United States was divided into very small grid boxes. In the seasonal study, the median peak current is calculated for larger portions

Trapezoidal area for grid based studies with formulas

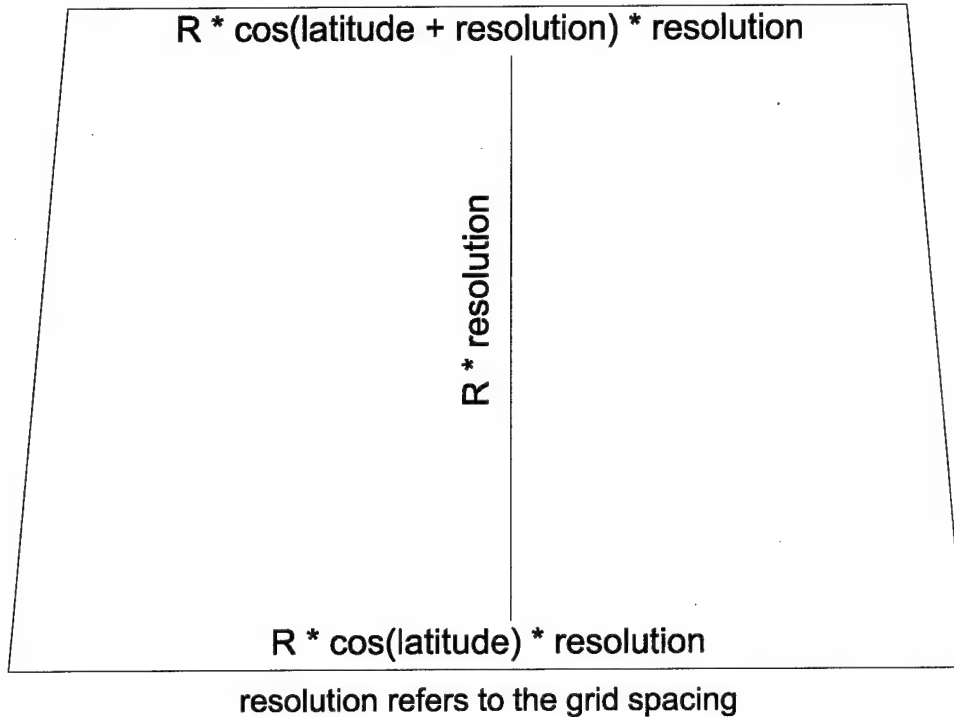


Figure 11. Trapezoidal approximation to latitude and longitude grid box. Since the top and bottom of the grid have slightly different lengths which exaggerated in this diagram to illustrate the point, a trapezoidal shape was selected for each grid element. The area of the grid was found using the equations listed for the top, bottom and height of the trapezoid. In the figure, R refers to the Earth's radius. All calculations were accomplished after converting the latitude and resolution values to radians.

of the country or for the entire country. As this calculation did not have the large memory requirement of the grid based analysis, the peak current increments could be reduced to 0.1 kA.

To find the median peak currents in various regions of the United States, the data were first limited to that region. Measured flashes were then grouped according to polarity and counts were made of flashes having the different peak current magnitudes. Once all the flashes were processed, the array holding the counts of peak current magnitudes was analyzed to find the median value.

Regions of the United States were selected to represent the median peak current distributions found in the grid based analysis and to facilitate the comparison of peak current characteristics based on longitude and latitude. Nine divisions were used in order to allow meaningful comparisons.

E. Correlation between possible factors affecting peak currents

A natural starting point for a correlation study of peak currents in a comparison of the peak currents with the spatial distribution of the sensors in the NLDN. Since the electromagnetic field strength from a return stroke is attenuated as it moves away from its origin, it is apparent that this could affect the detection of weaker signals. If the return stroke generated a weak signal and the network sensors were far away from it, then the return stroke may not even be detected. If this were to happen repeatedly, the median peak current for that region would be inflated, as the flashes with lower peak current values would not be included.

To determine the affect of sensor separation on peak currents two studies were accomplished. The NLDN requires that at least one IMPACT sensor detect a return stroke

before it is reported. Comparisons were done for the distance between the NLDN sensors and the peak currents, then for the distance from the center of each grid to the furthest of the minimum number of sensors required to detect a return stroke.

Distances between the IMPACT sensors were calculated by finding the arc along the latitude and longitude differences in the locations. These distances along the arcs were treated as sides of a right triangle and the distance between the two points found as if it were the hypotenuse of the triangle. This approximation is within 1 percent of the true spherical geometry, and provides accurate values for the distances. Although the separation between IMPACT sensors does not change as the return stroke positions do, there is still merit in performing this comparison.

Another comparison concerns the distance from the return stroke to the furthest sensor required to report the event. This calculation was not performed for each flash but used the center of the grid element for the distance calculations (Fig. 10). The distance to the nearest required sensors was found in the same manner as in the separation between IMPACT sensors. The requirements are either two IMPACT sensors or one IMPACT sensor and two TOA sensors. The common factor is the inclusion of an IMPACT sensor to determine the return stroke position (Fig. 12). The furthest distance between the grid center and the included sensors was used. Median peak currents from these grid locations were then compared to the calculated distances to determine the dependence on the sensor separation in the NLDN.

To determine if a relationship exists between the surface elevation and the peak currents from lightning flashes (Robertson et al. 1942 and Foust et al. 1953), the mean

Region requiring more than 4 NLDN sensors to report a return stroke

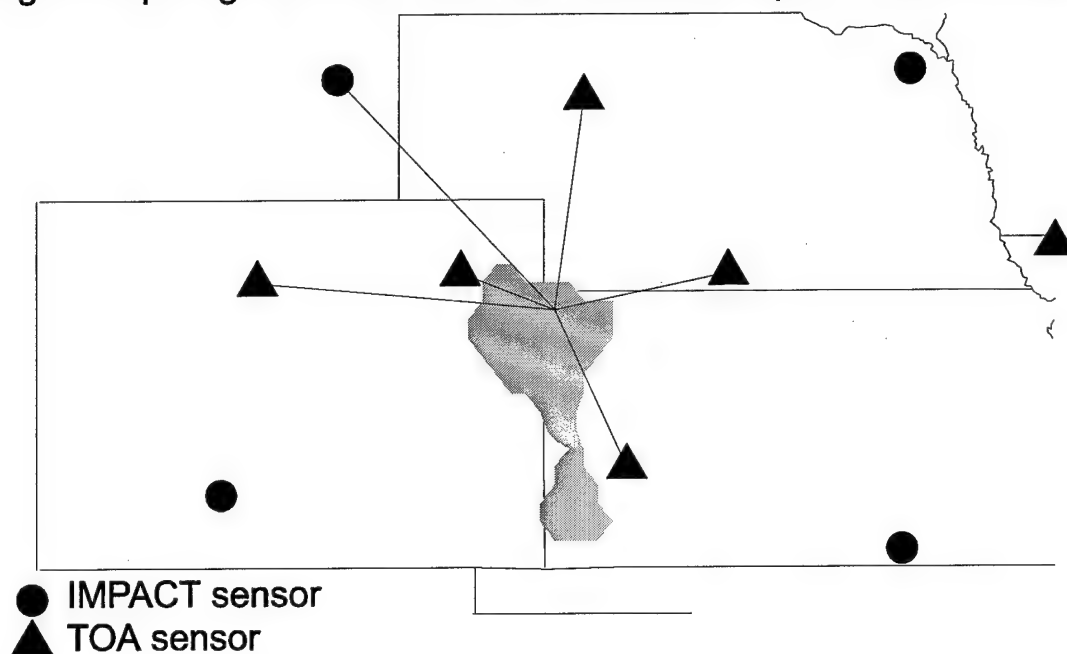


Figure 12. Case where more than four NLDN sensors are required to detect a return stroke.

The gray shaded area represents a region along the Colorado and Kansas borders where more than four NLDN sensors are required to detect a return stroke before it can be included in the data set. In this case, the six sensors required have lines drawn to them from a representative grid location in the shaded area. The additional sensors, beyond those normally required, are necessary in order to include an IMPACT sensor with direction finding capability. Other sensors may also detect the return stroke. This is just the minimum configuration required for that location.

surface elevation within each of the grid locations was found. Mean surface elevations were determined using data reported at 0.5 second latitude and longitude intervals over the US as described in Section 3D. The median peak currents were then compared with this mean elevation..

F. Case studies for comparisons of individual storms

Lightning's true nature can only be determined by moving from the summary information provided by mean and median values of multiple months without regard to region or condition to case studies for individual storms. During these individual storms there are smaller fluctuations in the environmental conditions than for summary data that covers the continental United States over several months or years.

Proper selection of storm data is critical to making meaningful comparisons. Random selection of storm days may yield inconclusive results since storm systems may have a mixture of characteristics. For this study, storms were selected that were easily separated from nearby systems and where the median peak currents were either high or low overall. Regional considerations were made to ensure a mixture of air mass types into the study. This avoids having storms which arise only from a continental or maritime airmass.

A listing of the storm cases (Table 2) shows the dates and times, regions of the US, flash counts, and median peak currents for each storm. Most of the storms were selected with a median peak current over 30 kA for positive flashes or 19 kA for negative flashes. These predominately occurred in the Northern Plains but were also found in the South Central US during the fall, winter, and early spring. These storms were fairly isolated from other nearby systems when viewing the lightning data even though many were quite large

and long lived. Every attempt was made to follow the storm track from beginning to end without including other storms that developed behind the storm or along a nearby track.

In order to isolate the thunderstorms, lightning data were plotted at regular intervals, often on an hourly basis after the storm days were identified. Lightning flashes were isolated at these small time intervals from the beginning of the storm until the apparent storm track ended. When multiple cells formed into a larger complex, all the cells that made up the complex were included from their start.

After the lightning data were isolated, time series analysis was performed on the peak currents. Using the median peak current over shorter periods proved uninformative as there were many more of the weaker peak currents than stronger ones. An examination of only the maximum peak current in a time window may be misleading as a single data value may be in error. To ensure representation of the changes in the peak currents the three flashes with the largest magnitude of peak current, positive and negative separately, are used to form a top three mean peak current. These mean values were then analyzed using time series methods to find any patterns that may be present (Lu et al. 1984).

G. Determination of CAPE and vertical wind shear

The Convective Available Potential Energy (CAPE) indicates the amount of potential energy available to a parcel of air given the environmental conditions. It is calculated by comparing the atmospheric temperatures for the sounding from the Level of Free Convection (LFC) to the Equilibrium Level (EL) with the saturated adiabatic (Fig. 13). The LFC is the point at which a parcel of air would continue to rise in the atmosphere if it were lifted to that level from the Earth's surface. The moist adiabat represents the temperature a parcel of air would have at a particular pressure level based on its temperature

Table 2. Summary of lightning data for case studies.

Date and time of first flash	Date and time of last flash	Minimum latitude	Minimum longitude	Maximum latitude	Maximum longitude	Number of flashes	Median peak positive current	Median peak negative current
02/27/95 21:00:15	02/28/95 11:58:36	31.0	-96.4	37.1	-82.9	5943	35.1	-17.0
03/25/95 01:03:38	03/25/95 14:59:26	38.5	-103.3	45.8	-91.8	6851	33.2	-22.8
05/21/95 12:06:36	05/22/95 11:59:00	43.7	-107.4	48.7	-93.1	2251	34.4	-17.6
06/06/95 12:02:54	06/07/95 11:59:58	39.5	-105.9	46.3	-93.8	12601	37.6	-16.8
07/02/95 12:00:06	07/03/95 05:59:58	45.4	-98.9	47.4	-91.6	2267	37.9	-17.7
07/08/95 03:00:27	07/08/95 16:38:48	44.1	-101.9	49.5	-93.8	5975	31.0	-20.6
07/11/95 15:00:17	07/12/95 21:57:15	34.1	-114.4	48.9	-82.6	41633	40.4	-20.1
07/14/95 00:00:02	07/14/95 15:41:26	42.3	-104.5	49.0	-86.9	19487	29.6	-20.8
07/18/95 22:00:07	07/19/95 19:59:47	41.8	-107.2	49.9	-91.4	18380	31.9	-19.8
07/24/95 22:01:07	07/25/95 14:58:54	44.5	-110.5	49.0	-96.6	3922	29.4	-23.3
07/26/95 19:32:10	07/28/95 04:59:56	38.9	-108.4	49.9	-82.9	61545	23.8	-21.7
08/02/95 18:27:17	08/03/95 11:17:51	42.3	-103.7	49.9	-93.8	5012	44.8	-18.1
08/04/95 00:00:06	08/04/95 18:59:56	39.6	-106.4	45.8	-90.5	7297	36.3	-18.7
09/18/95 06:00:06	09/18/95 19:59:41	40.1	-102.0	44.0	-92.5	10622	29.3	-22.3
01/18/96 00:00:02	01/18/96 09:59:42	30.2	-99.5	45.0	-83.3	13102	31.2	-17.3
05/09/96 00:51:08	05/09/96 19:59:58	38.0	-100.5	43.4	-78.1	53049	23.4	-22.6
05/15/96 19:29:10	05/16/96 19:59:46	39.5	-110.9	45.5	-90.7	16599	44.6	-19.3
05/18/96 21:23:50	05/19/96 14:58:12	41.0	-102.7	48.4	-79.7	23155	40.8	-22.4
06/19/96 04:22:17	06/20/96 12:57:27	40.4	-105.5	46.4	-93.0	15997	50.6	-18.4
07/15/96 15:09:58	07/16/96 11:07:04	38.6	-106.3	43.2	-97.1	8774	35.4	-17.1
07/27/96 20:00:36	07/28/96 13:59:27	38.0	-110.2	44.9	-96.0	7531	38.3	-17.6
08/02/96 12:00:10	08/03/96 23:42:39	28.8	-103.8	43.2	-84.5	88492	17.5	-20.8
08/06/96 21:24:48	08/07/96 13:59:54	36.5	-105.4	49.7	-80.9	65247	43.3	-18.0
08/21/96 23:00:02	08/22/96 17:59:55	41.1	-97.9	49.9	-79.6	35229	35.9	-19.3
10/24/96 13:33:17	10/25/96 04:59:48	25.0	-100.9	32.9	-88.3	14821	23.3	-23.3
11/23/96 21:23:33	11/25/96 10:56:54	25.0	-108.0	37.7	-86.4	77992	25.3	-18.5
02/03/97 17:30:01	02/04/97 11:50:34	33.2	-96.2	38.9	-83.6	3513	35.8	-19.0
03/09/97 20:00:09	03/10/97 11:00:44	25.6	-106.9	38.7	-86.2	9847	28.4	-18.3
03/24/97 22:42:00	03/26/97 01:59:55	25.9	-103.8	43.1	-83.9	41697	31.5	-17.8
06/11/97 20:01:08	06/13/97 02:17:22	30.3	-103.3	41.3	-90.2	31550	29.0	-16.9
06/14/97 16:52:44	06/15/97 11:55:04	45.0	-113.7	49.8	-93.1	11674	30.8	-19.1
06/20/97 18:00:18	06/21/97 17:20:19	36.1	-112.5	45.8	-83.0	88663	36.3	-20.5
06/22/97 00:00:37	06/23/97 09:18:41	40.6	-107.7	46.9	-89.6	15149	41.6	-17.6

Table 2 (continued)

Date and time of first flash	Date and time of last flash	Minimum latitude	Minimum longitude	Maximum latitude	Maximum longitude	Number of flashes	Median peak positive current	Median peak negative current
06/24/97 18:04:47	06/25/97 13:42:04	36.5	-111.6	44.8	-83.6	36200	32.6	-19.2
06/28/97 00:00:01	06/28/97 19:55:16	43.0	-100.5	49.8	-87.3	11647	51.2	-20.0
07/08/97 21:40:10	07/09/97 11:31:03	39.5	-104.7	42.9	-97.9	2535	31.5	-16.9
07/16/97 23:00:47	07/17/97 16:59:34	41.4	-102.5	46.3	-82.7	28938	48.2	-17.7
07/17/97 17:01:08	07/18/97 16:17:24	44.4	-112.8	49.8	-95.1	29447	37.8	-20.4
08/13/97 19:51:28	08/14/97 11:58:24	38.9	-103.7	41.6	-95.8	2986	40.0	-16.0
08/26/97 12:00:34	08/27/97 17:54:12	40.5	-105.8	46.5	-92.1	20879	43.2	-17.5
08/29/97 12:00:08	08/30/97 18:56:58	39.2	-104.2	49.8	-86.5	44124	31.9	-20.8
08/31/97 21:00:10	09/01/97 16:59:55	44.6	-105.0	48.0	-92.4	15575	50.1	-18.8
09/05/97 00:00:12	09/05/97 14:57:39	42.1	-101.5	46.3	-94.1	8402	37.1	-19.9
09/05/97 00:00:28	09/05/97 15:15:59	37.1	-101.6	40.9	-95.7	5289	31.4	-19.2
09/08/97 20:00:23	09/09/97 15:56:21	33.8	-102.2	43.6	-94.4	12316	34.9	-17.1
10/21/97 04:24:35	10/22/97 04:51:14	28.6	-102.7	38.6	-83.9	26200	30.8	-17.9
12/20/97 15:00:24	12/21/97 10:50:54	26.7	-100.8	34.0	-89.7	7942	30.3	-19.1
05/15/98 04:18:54	05/16/98 04:59:26	30.8	-102.7	50.0	-85.2	50932	35.6	-15.8

at the LFC. In other words, the saturated adiabatic temperature is the temperature a saturated parcel would have if it rose adiabatically from the LFC. The EL is the point at which the environmental temperature becomes warmer than the temperature of the parcel (saturation adiabat). The CAPE is not completely converted into vertical velocity, so the potential energy found in this method can not be directly converted to updraft speed. It is an indicator of the potential for stronger updrafts and larger storm development.

Vertical wind shear was found as a requirement for the occurrence of positive lightning in Japanese wintertime thunderstorms (Brook et al. 1982). The increased vertical wind shear is thought to tilt the vertical structure of the storm allowing positive charge to be lowered to ground from the upper positive charge region (Fig. 2). While the connection between vertical wind shear and positive lightning exists for these smaller scale wintertime storms, the connection may be more difficult for the larger scale storms in the US. In this study, the vertical wind shear is found by comparing the winds at the surface and the winds at various pressure levels. While these levels do not represent the base and top of the cloud, they should provide a good approximation to the wind shear experienced by the storm.

H. Satellite imagery and lightning data plots

Relative positioning of lightning data to the storm location can provide valuable information on the connection between storm development and peak current strength. To display this relationship, lightning data were plotted over infrared (IR) satellite data. Infrared satellite data provides approximate cloud top heights which indicate the development of the storm. The interval between satellite images is one hour in most cases

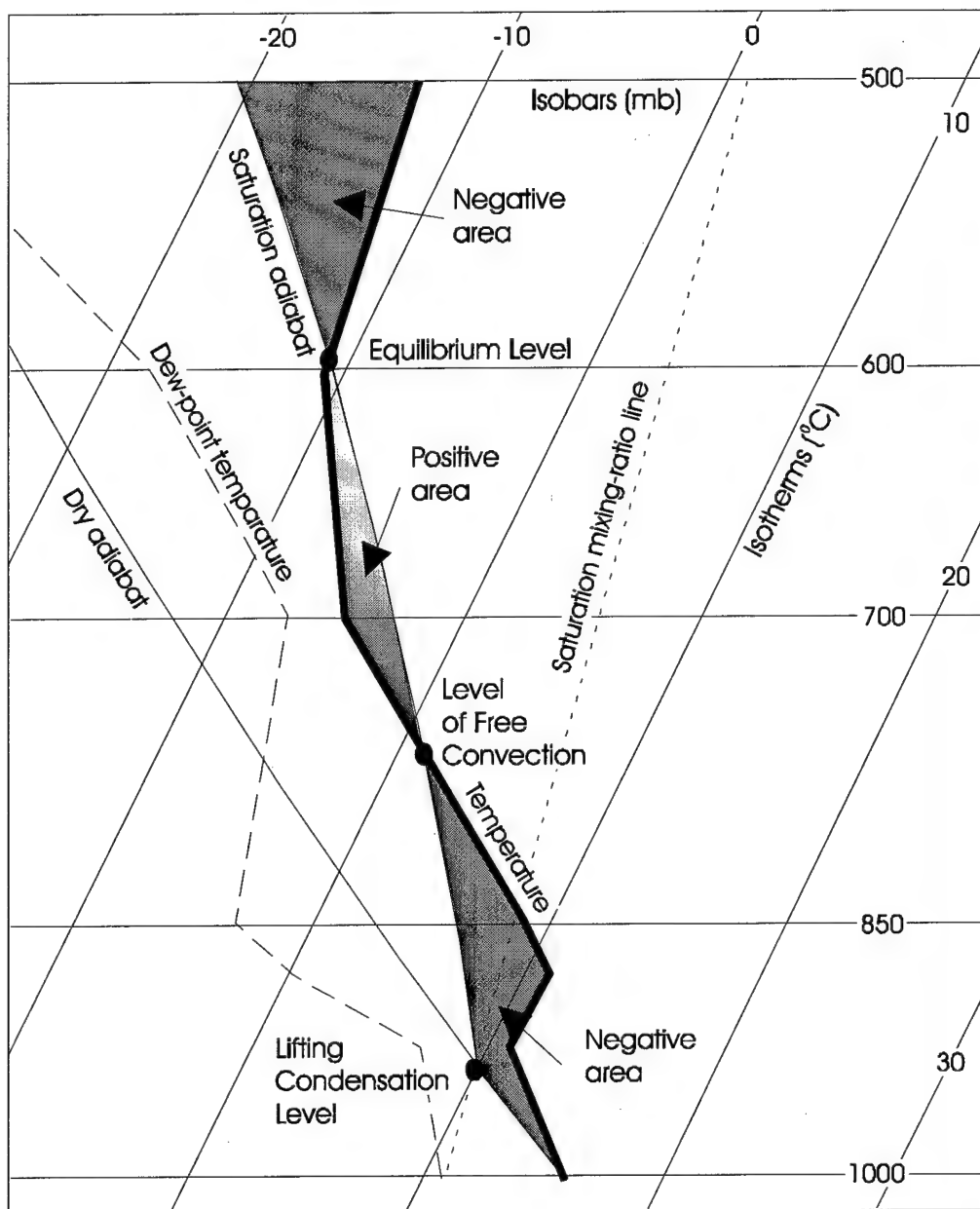


Figure 13. Example of Skew-T diagram showing region of CAPE. The temperature profile is shown as the bold line while the dew-point temperatures are plotted as a dashed line. The saturation adiabat passing through the Lifting Condensation Level is compared with the temperature profile to determine if the potential energy is positive or negative.

and this is too long to determine the shorter time scale variations in the lightning characteristics. Even so, it is still possible to determine if the larger peak currents are associated with the increase in storm intensity, as determined by the cloud top heights and the growth of the storm.

The satellite data were archived at Texas A&M University and were processed using the Man computer Interactive Data Access System (McIDAS). The IR imagery were limited to regions that included the lightning data from the storm cases. Once displayed, a legend was added to the satellite image to aid in the interpretation of gray scale shades into cloud top temperatures. State outlines were also added to enable the location of the clouds.

Once the images were built using McIDAS, they were further processed using the Interactive Data Language (IDL). The satellite image was read into memory and a map overlay fitted to the state outlines. This allowed a pixel-by-pixel analysis of the cloud top temperatures and lightning data to be displayed accurately on the image. The lightning data could be identified by polarity or by peak current strength and the satellite data could be enhanced to point out features of interest.

CHAPTER V

LARGE SCALE VARIATIONS IN PEAK CURRENT

A. Peak current distributions for the US

The distribution of peak current for the first stroke of each lightning flash over the continental United States (US) from 1995 through 1998 is shown in Figure 14. All measured cloud-to-ground lightning that occurred over the US are included, with the exception of those data over the Great Lakes, totaling over 76 million out of the 105 million lightning flashes reported in total by the NLDN. In order to show the details, only those flashes with a peak current less than 60 kA were shown. For the positive flashes, the region below 10 kA is shaded indicating the flashes that will not be included in later calculations based on the possibility of contamination by intracloud flashes (Cummins et al. 1998).

The peak current distributions for each year (Fig. 14) are skewed to the right with the mode for negative flashes being greater than that of positive flashes. This would be expected, since the change in selection criteria for cloud-to-ground flashes with the 1994 NLDN upgrade allowed weaker positive flashes to be detected (Cummins et al. 1998). For both positive and negative flashes the peak of each distribution increased monotonically from 1995 through 1998. Comparing the statistics of these peak current distributions (Table 3), the median for positive currents over 10 kA in strength was higher than for negative flashes in each year of the study. If weaker peak current flashes below 10 kA were included for the positive lightning, then the reverse trend would be seen in each year. It appears that either the network is reporting many questionable flashes or the peak current characteristics for the US are different than previously thought (Lopez et al. 1991).

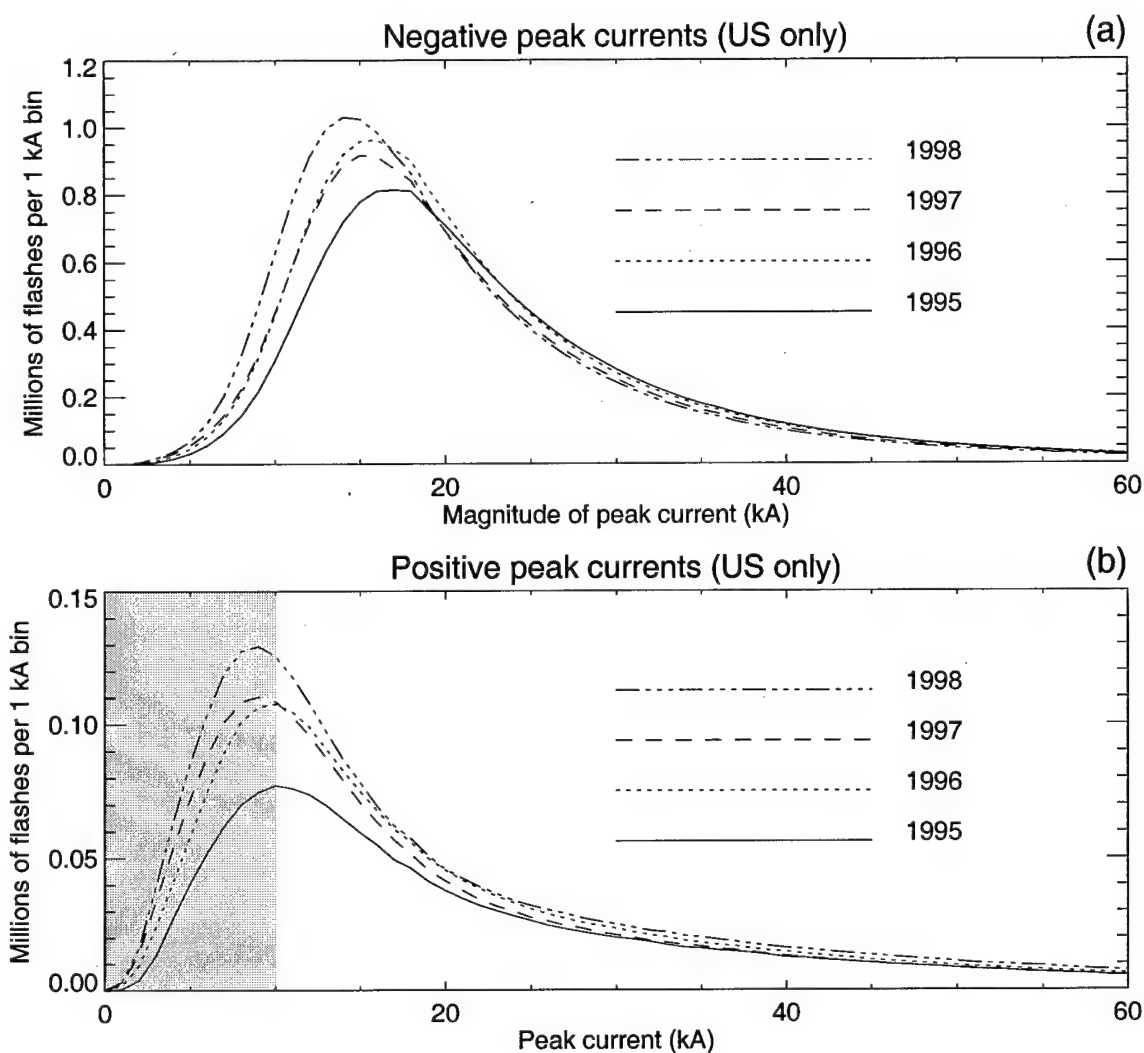


Figure 14. Peak current distributions for the continental United States from 1995 – 98. The peak currents for each 1 kA increment are displayed separated by negative (a) and positive (b) flashes through 60 kA. Each year is plotted separately for each polarity of cloud-to-ground flash. The gray shaded area for the positive flashes (b) indicated the flashes below 10 kA which were not used in many of the calculations as they may be intracloud lightning (Cummings et al. 1998).

Table 3. Peak current statistics for the continental US from 1995 – 98.

Year	Negative peak currents			Positive peak currents			Positive peak currents ≥ 10 kA		
	Mode	Median	Mean	Mode	Median	Mean	Mode	Median	Mean
1995	-17	-21	-24	10	17	26	11	31	30
1996	-16	-19	-23	10	16	24	11	29	28
1997	-15	-19	-23	9	15	22	10	29	27
1998	-14	-18	-21	9	15	23	10	29	29

B. Regional peak current distributions

In order to determine the peak current variation within the US, it is necessary to look beyond the distribution of all flashes in the country. To examine these regional variations, the US was divided into 9 regions (Fig. 15) and the peak current distribution for each region was found. The data were limited to the US land area. Distributions of the negative peak currents are found in Figure 16 and positive peak currents in Figure 17 with a summary of the peak current statistics in Table 4. With this large-scale breakout in the lightning data, variations are already noticeable.

Peak current distributions for negative flashes vary from one region to the next (Fig. 16). While the number of flashes in each region cannot be compared due to the different size of each region (Fig. 15), the patterns of the distributions may be compared. For the northern regions (1, 2, and 3) and those including Texas and the Southeastern US (8 and 9), the peak current distributions indicate a shift toward the right, or higher values than are found in the rest of the country. This is also evident in Table 4 in the median of the peak currents for negative flashes.

Variation between years is more evident in the regional analysis than was seen for the entire US (Fig. 14). When all of the lightning for the US was examined the maximum in the peak current distributions increased monotonically over time. The regional analysis does not show the same trend as not all regions have the monotonic increase. For example, Region 5 had a higher peak in 1996 (Fig. 16) than for the other three years in the study period. Since the location and intensity of thunderstorms vary on an annual basis, the changes in the regional peak current distributions would be expected.

The peak current distributions for positive lightning (Fig. 17) show a greater

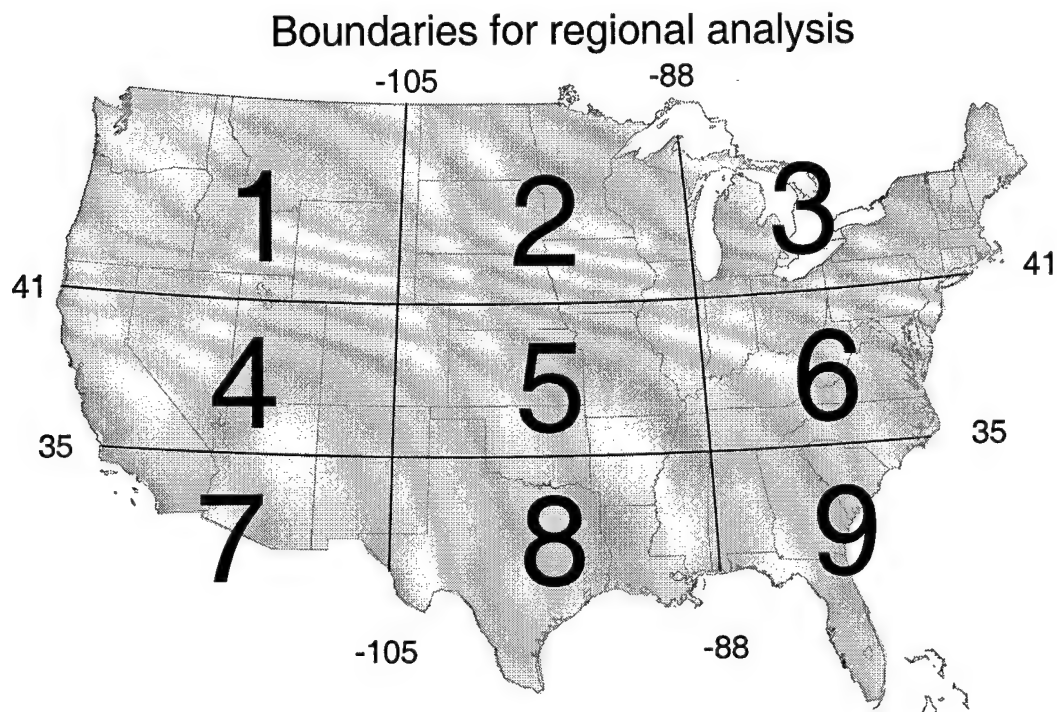


Figure 15. Divisions of the US for regional peak current distributions. The regions used to determine the peak current distributions for different parts of the country are shown and the latitude and longitude lines used to divide the country into sections. The land region of the US is shaded to indicate the limitation applied to the lightning data. Each region is numbered to allow comparisons with the peak current distributions and descriptive statistics.

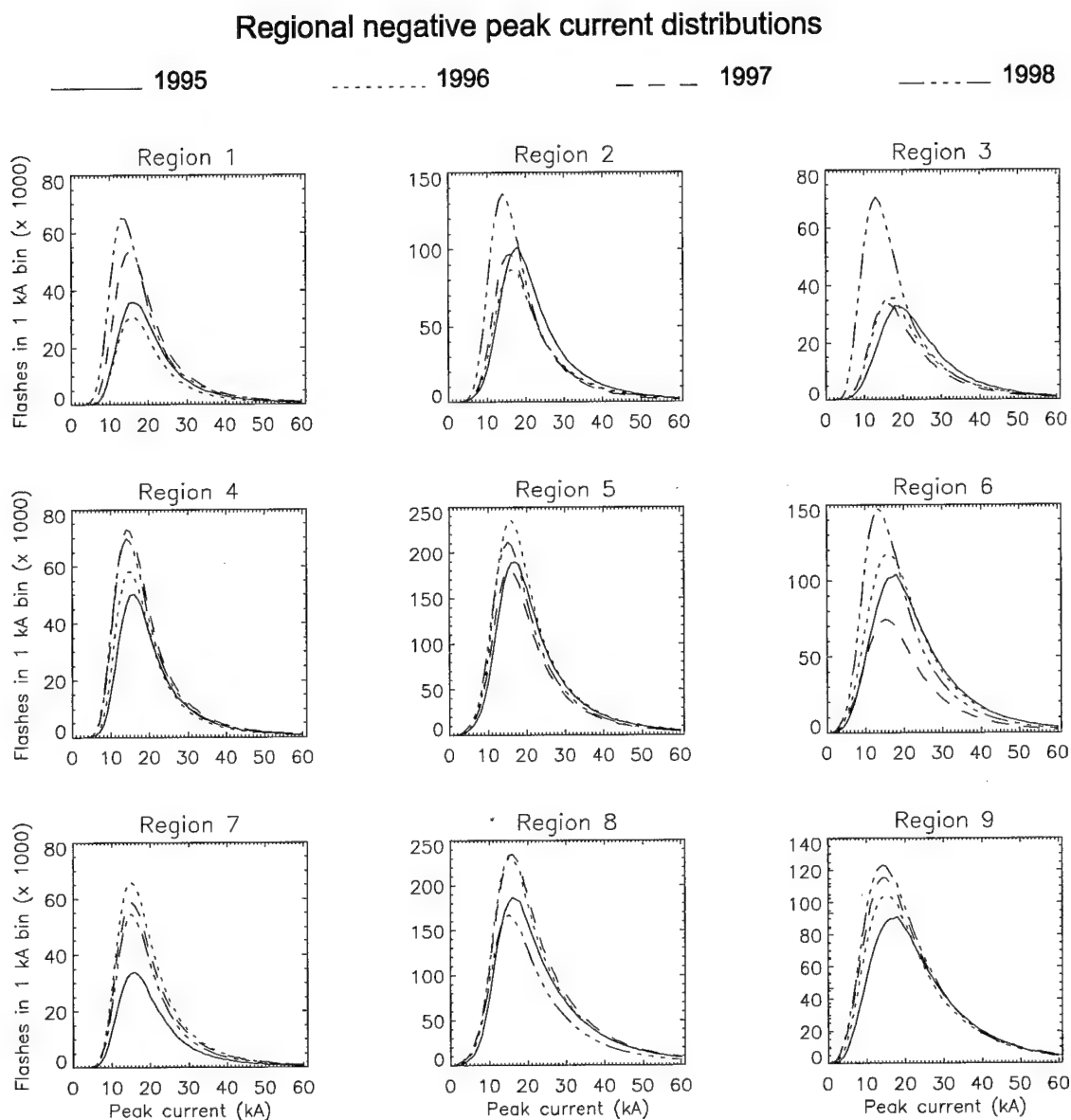


Figure 16. Negative peak current distributions for nine regions of the US. The number of negative cloud-to-ground lightning flashes in each 1 kA increment of peak current from 1995 – 98 are shown. A separate distribution for each year is plotted for each of the nine regions shown in Figure 16. Peak current increments above 60 kA are not shown.

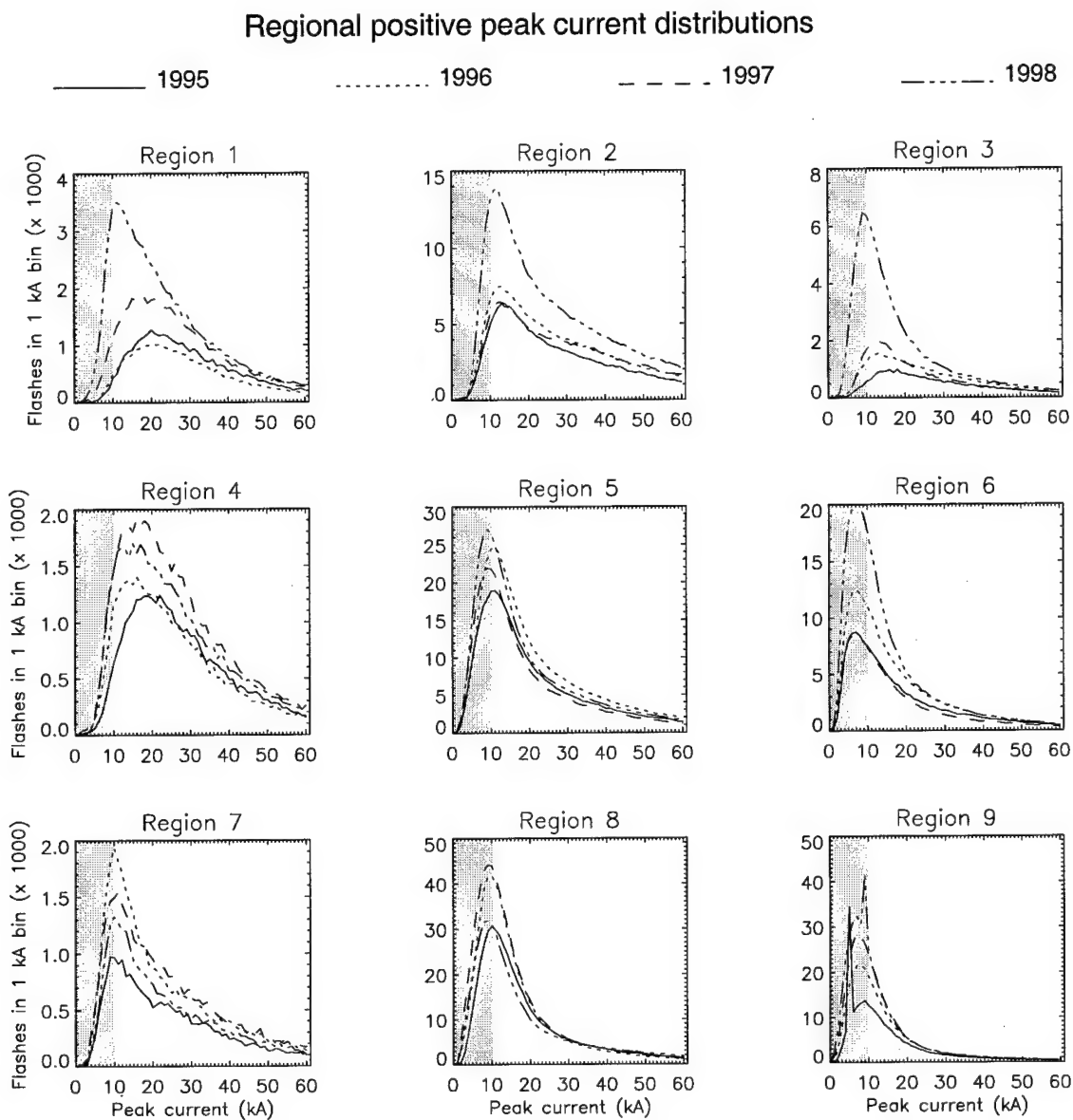


Figure 17. Positive peak current distributions for nine regions of the US. The number of positive cloud-to-ground lightning flashes in each 1 kA increment of peak current from 1995 – 98 are shown. A separate distribution for each year is plotted for each of the nine regions shown in Figure 16. Peak current increments above 60 kA are not shown. Gray regions indicate flashes with peak currents less than 10 kA.

Table 4. Regional peak current descriptive statistics for nine regions of the US.

Year/ Region	Negative peak currents				Positive peak currents				Positive peak currents ≥ 10 kA			
	Mode (kA)	Median (kA)	Mean (kA)	Flash count (million)	Mode (kA)	Median (kA)	Mean (kA)	Flash count (million)	Mode (kA)	Median (kA)	Mean (kA)	Flash count (million)
1995												
1	16	19	22.8	0.576	20	29	34.9	0.041	20	39	35.3	0.041
2	18	21	24.2	1.708	13	28	35.4	0.204	13	40	37.1	0.204
3	18	23	25.9	0.658	18	27	34.2	0.031	18	38	35.3	0.031
4	16	19	22.4	0.754	22	27	33.2	0.041	22	38	34.0	0.041
5	17	20	23.7	3.305	11	18	25.8	0.432	11	32	30.2	0.432
6	18	21	24.2	2.182	7	15	22.5	0.173	10	32	29.7	0.173
7	16	19	21.8	0.535	9	22	28.8	0.026	10	36	32.1	0.026
8	16	21	26.2	3.835	10	16	23.5	0.567	10	29	27.8	0.567
9	18	22	25.9	2.189	5	11	17.4	0.242	10	27	24.8	0.242
1996												
1	16	19	21.9	0.475	20	28	34.3	0.034	20	39	35.0	0.034
2	16	20	23.9	1.487	13	28	35.9	0.255	13	41	37.8	0.255
3	16	20	24.4	0.652	13	25	32.6	0.048	16	37	34.4	0.048
4	15	18	20.7	0.815	16	24	30.2	0.042	16	35	31.7	0.042
5	16	19	22.9	3.859	11	18	26.1	0.547	11	32	30.0	0.547
6	16	20	23.3	2.408	7	14	21.4	0.237	10	30	28.5	0.237
7	15	18	21.0	0.985	10	20	27.4	0.041	10	34	31.0	0.041
8	15	20	24.7	4.435	10	13	19.2	0.663	10	27	23.9	0.663
9	15	20	24.6	2.380	8	11	16.8	0.315	10	26	23.7	0.315
1997												
1	15	18	21.7	0.822	18	26	32.0	0.061	18	37	33.1	0.061
2	16	19	21.6	1.512	31	31	37.4	0.239	12	43	39.2	0.239
3	16	20	23.0	0.594	13	21	29.2	0.046	13	33	31.1	0.046
4	14	17	20.7	1.044	16	25	30.8	0.061	16	36	32.3	0.061
5	16	19	22.5	3.008	9	15	23.0	0.427	10	30	28.4	0.427
6	15	19	22.0	1.464	6	13	20.6	0.158	10	30	28.3	0.158
7	15	18	21.4	0.890	11	22	28.7	0.041	11	35	32.2	0.041
8	16	20	24.9	4.611	9	13	19.1	0.735	10	27	24.7	0.735
9	15	20	24.1	2.606	7	10	15.1	0.378	10	25	22.2	0.378
1998												
1	13	16	20.3	0.920	11	21	28.4	0.088	11	33	30.6	0.088
2	14	17	20.5	1.980	12	26	33.6	0.389	12	38	35.9	0.389
3	13	16	19.5	1.073	9	15	22.2	0.106	10	29	26.5	0.106
4	14	17	20.5	0.998	15	25	31.7	0.055	15	36	33.3	0.055
5	15	18	21.8	3.433	9	16	24.2	0.531	10	31	29.7	0.531
6	13	17	20.4	2.541	7	12	18.0	0.320	10	28	25.6	0.320
7	15	18	21.1	0.799	10	21	28.8	0.032	10	35	32.1	0.032
8	15	19	24.1	3.269	9	14	23.4	0.591	10	30	29.9	0.591
9	14	19	22.9	2.693	9	10	14.4	0.424	10	26	22.6	0.424

variation than the negative flashes (Fig. 16). For the positive flashes the distributions appear jagged while those for negative flashes were smoother. This is likely due to the lower flash counts for positive lightning. Indeed, further examination of the distributions indicates a jagged appearance when the flash counts are low and a smoother appearance for the regions with more lightning.

For the Southeastern US (Region 9), there are spikes in the peak current distributions (Fig. 17). These spikes occur below the 10 kA threshold suggested by Cummins et al. (1998) and are likely caused by the inclusion of intracloud flashes. Approximately half of all positive lightning flashes for the Southeastern US (Region 9) have a return stroke peak current of 10 kA or less (Table 4). The NLDN sensor locations in this region include a sensor group in the Carolinas (Fig. 8) where the distance between sensors is less than 70 km. When the sensors are closer together, there is less attenuation of the electromagnetic signal generated by the return stroke, allowing the flashes with weaker peak current strength to be detected. It is likely that the peak current spikes seen in this region are an artifact of the NLDN sensor locations.

Peak current distributions for positive flashes (Fig. 18) show a shift toward higher values when comparing the southern regions and those further to the north. This shift is also evident in the median peak current values (Table 4) regardless of the inclusion of flashes below 10 kA. Latitude dependence on lightning characteristics have been previously noted (Pierce 1970; Orville 1990; Pinto et al. 1996), but those observations have been for all lightning flashes and not restricted to any polarity. This latitudinal dependence is not as evident for negative flashes (Fig. 16) and bears further examination.

C. Peak current variations based on latitude

Regional analysis of peak current distributions indicates a latitudinal dependence in the median peak currents for positive flashes. This dependence of lightning parameters on latitude has been observed in other cases (Pierce 1970; Orville 1990; Pinto et al. 1996). To further examine this relationship, the median of peak currents over the US was found for each one degree increment of latitude. The results are plotted in Figure 18 with summary information listed in Table 5. All positive flashes with peak currents less than 10 kA were eliminated from the calculations (Cummins et al. 1998).

The median peak currents in the US from 1995 – 98 based on latitude (Fig. 18a) increase with latitude for positive flashes while the negative flashes show the opposite trend. The relationship for positive flashes was implied in the regional analysis (Table 4), but the trend for negative flashes was not as obvious. Negative flashes vary less with latitude than do the positive peak currents and have median peak currents less than positive flashes except south of 30 degrees north latitude. Equations for the trends of positive (4) and negative flashes (5) describe this in more detail. Med_Neg is the median of negative peak currents, Med_Pos is the median of positive peak currents, and Lat is the latitude in degrees north. The correlation coefficients are 0.954 and 0.576 for positive and negative flashes, respectively.

$$Med_Pos = 20.8kA + \frac{20.6kA}{deg}(Lat) \quad (4)$$

$$|Med_Neg| = 26.7kA - \frac{0.24kA}{deg}(Lat) \quad (5)$$

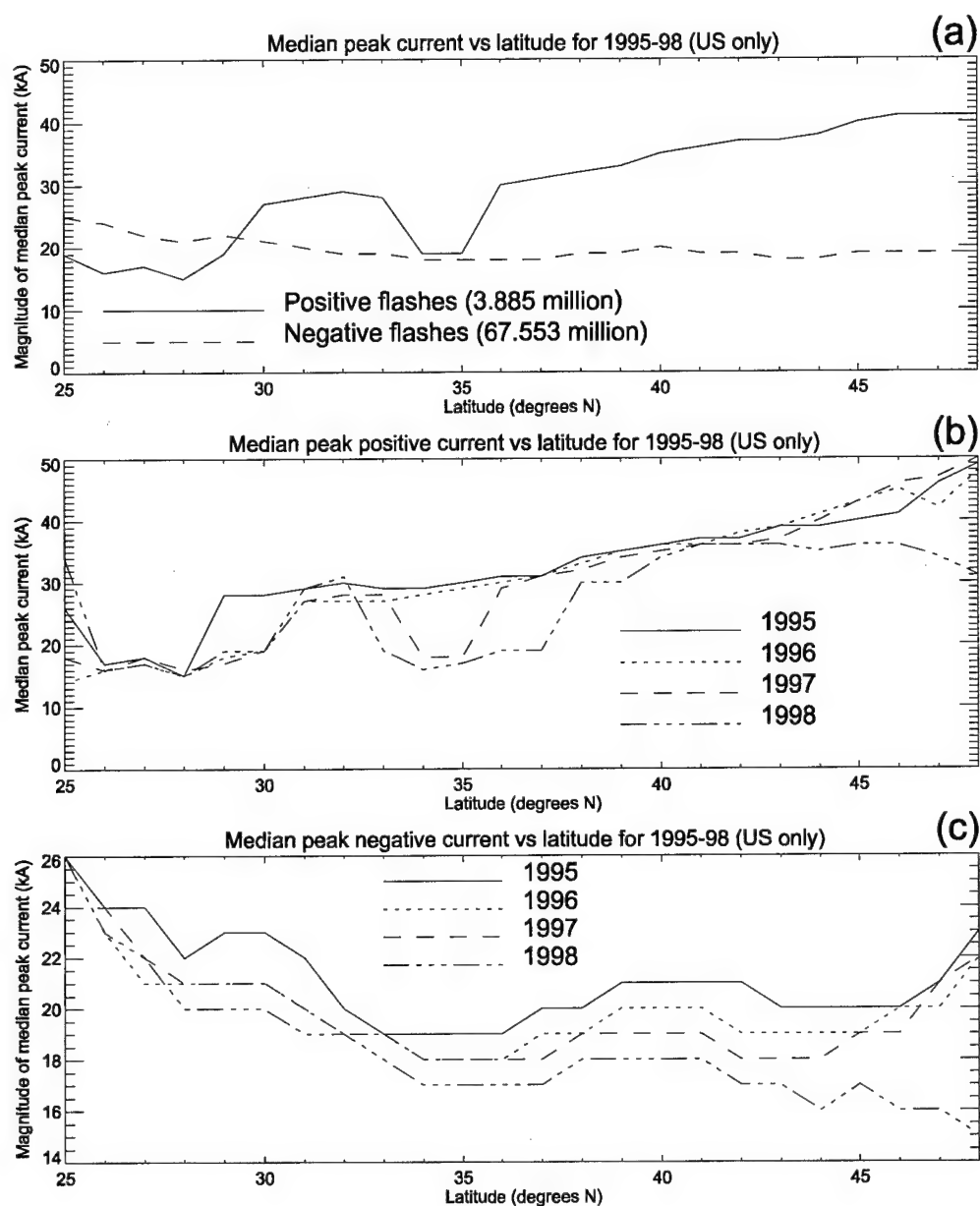


Figure 18. Median peak currents for lightning in one-degree latitude increments. The median of peak currents for positive and negative lightning over the US from 1995 – 98 (a) and yearly breakouts of median peak currents for positive (b) and negative (c) flashes. No positive flashes with peak currents less than 10 kA were included.

Table 5. Median of peak currents over the US in one degree latitude increments. No positive flashes with peak currents less than 10 kA were used.

Latitude (deg N)	Negative peak currents				Positive peak currents			
	Mode (kA)	Median (kA)	Mean (kA)	Flashes (millions)	Mode (kA)	Median (kA)	Mean (kA)	Flashes (millions)
25	-15	-25	-30.9	0.250	15	19	23.7	0.018
26	-18	-24	-27.4	0.838	10	16	20.6	0.061
27	-18	-22	-25.9	0.969	10	17	25.6	0.069
28	-17	-21	-25.2	1.088	10	15	24.1	0.073
29	-17	-22	-26.5	2.244	10	19	24.6	0.226
30	-16	-21	-26.1	4.377	10	27	24.9	0.455
31	-15	-20	-24.8	4.425	10	28	27.6	0.460
32	-15	-19	-23.7	4.726	10	29	28.2	0.460
33	-15	-19	-22.8	5.125	10	28	26.9	0.465
34	-15	-18	-22.3	5.246	10	19	27.0	0.467
35	-15	-18	-21.8	4.980	10	19	27.9	0.447
36	-15	-18	-21.7	4.645	10	30	28.7	0.419
37	-15	-18	-22.0	4.267	10	31	29.3	0.399
38	-15	-19	-22.8	4.335	10	32	30.8	0.397
39	-16	-19	-23.1	4.107	12	33	32.1	0.327
40	-16	-20	-23.1	3.475	14	35	33.8	0.308
41	-16	-19	-23.0	3.077	12	36	34.8	0.299
42	-15	-19	-22.2	2.427	12	37	35.3	0.253
43	-15	-18	-21.7	1.855	12	37	36.3	0.209
44	-15	-18	-21.6	1.590	13	38	37.1	0.195
45	-15	-19	-22.2	1.269	14	40	38.5	0.159
46	-15	-19	-22.3	0.982	13	41	39.5	0.142
47	-16	-19	-22.7	0.721	10	41	38.8	0.095
48	-17	-19	-22.7	0.535	10	41	39.1	0.071

Comparisons of the annual variations in the median peak currents at each latitude show the same trends for positive (Fig. 18b) and negative (Fig. 18c) flashes. There are differences in the values from year-to-year, but that is to be expected. One noticeable deviation that carries over from the four year summary (Fig. 18a) into the annual breakout is the decreased median peak current for positive flashes between 33 and 36 degrees north for 1997 and 1998. These decreases are large enough that they affect the overall values for the four years.

Examination of the distribution of NLDN sensors in the 33 – 36 degree latitude band (Fig. 8) shows the sensors in the region of the Carolinas to be more closely spaced than for the rest of the country. If the network sensors are closer together, there is less attenuation of the signal generated by the return stroke for lightning in that region. Less attenuation would mean that lightning flashes with a weaker peak current would be detected while they may be undetected if the sensors were further apart. This natural filtering of the weaker peak current flashes would cause larger median peak current values for the rest of the country. It is not obvious that the peak currents for positive flashes would be affected while the negative flashes are not. The intracloud lightning contamination for positive flashes with weaker peak currents (Cummins et al. 1998) was not expected to play a role in flashes with peak currents greater than 10 kA, as weaker flashes were eliminated for these calculations.

In order to examine the relationship between latitude and peak currents, the percentage of measured cloud-to-ground flashes within each degree of latitude having peak currents greater than 80 kA were found (Fig. 19). This technique follows a study of the same values in Brazil (Pinto et al. 1996). In this case, the percentage of all positive flashes

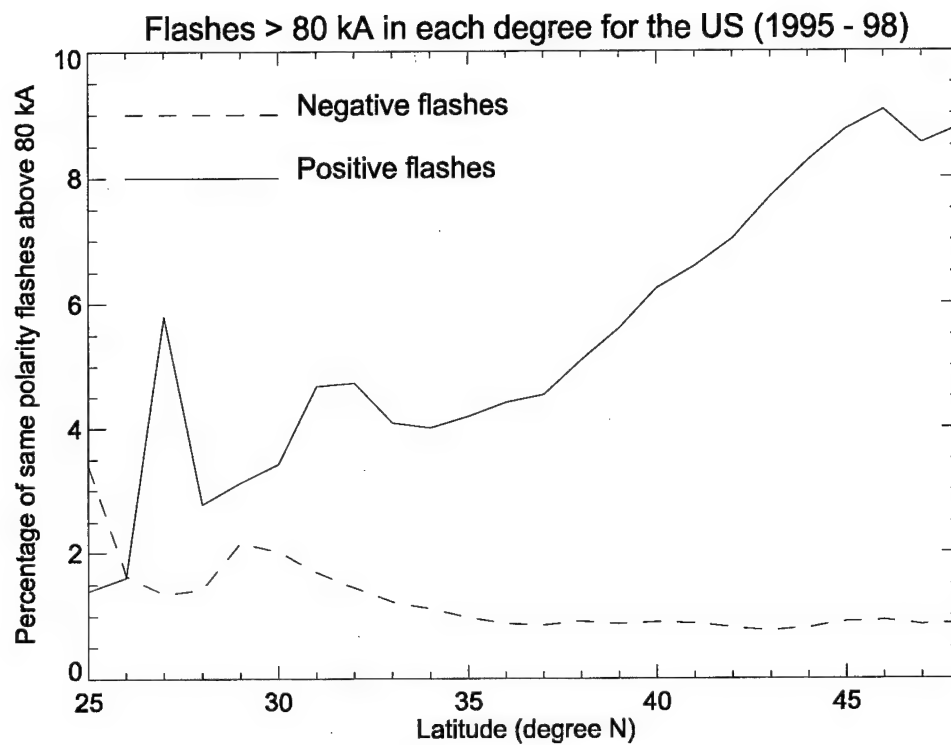


Figure 19. Percent of flashes over 80 kA in each one-degree latitude increment. The percentages are in comparison to the number of flashes in the latitude band with the same polarity.

within a latitude increment having peak currents greater than 80 kA increased almost linearly with increasing latitude. The main exception was for positive flashes between 27 and 28 degrees north. Negative flashes did not follow this trend as there was an initial decrease in the percentage of negative flashes over 80 kA in strength from 25 – 37 degrees north. The negative flash values stayed essentially the same north of 37 degrees latitude.

D. Peak current characteristics across the US

To examine the peak current characteristics across the US, median values of peak currents within each 0.2 by 0.2 degree latitude and longitude grid were found and contoured for positive (Fig. 20) and negative lightning (Fig. 21). The mean peak currents for each year from 1995 – 98 were found for each year and then the same calculations were made for the entire time period. A listing of the number of flashes used in the calculations is included for each polarity of lightning. No positive flashes with peak currents less than 10 kA were used in these calculations in an attempt to avoid the inclusion of intracloud lightning (Cummins et al. 1998). Also, each grid with fewer than two flashes was assigned a median peak current of zero. While this number is not sufficient to accurately determine the median of peak currents, it allows many regions of the country to be analyzed that would not be shown had more flashes in each grid been required.

For positive flashes (Fig. 20), a minimum in the median of peak currents (< 15 kA) was found in Florida, the Carolinas, Northern Georgia, Alabama, and in the extreme Western US. Maximums (> 30 kA) were found in Western Pennsylvania, West Virginia, the West Coast, and the Northern Plains extending from the Eastern Dakotas into Colorado. These patterns were consistent in each year of the study. In 1998 (Fig. 20d), there was also a maximum in the median peak positive currents (> 30 kA) which extended from Central

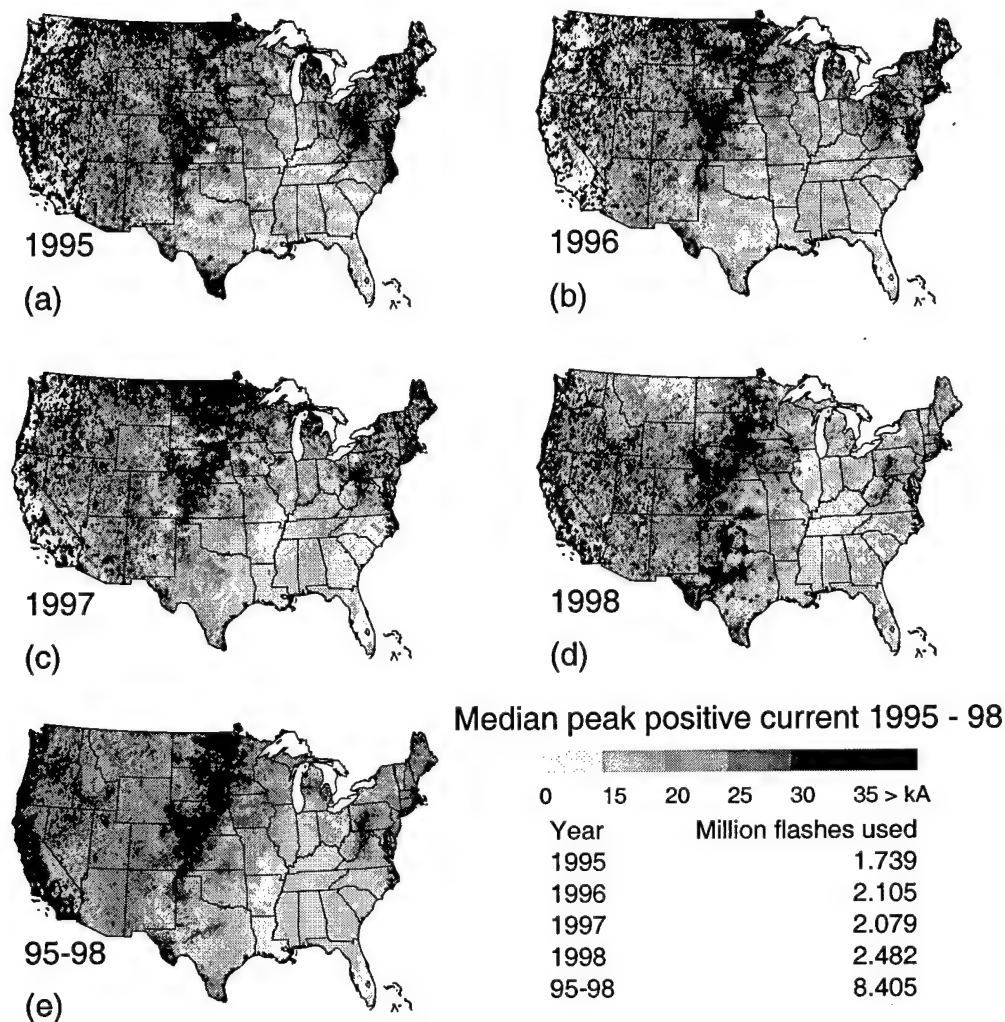


Figure 20. Contour of the median of positive peak currents from 1995 – 98. The median of peak currents were found for a 0.2 by 0.2 degree latitude and longitude grid for the United States on an annual basis (a – d) and for the 4 years as a whole (e). The positive cloud-to-ground flash counts for each year are listed as well. Positive lightning with peak currents less than 10 kA were not used in these calculations in an attempt to avoid the inclusion of intracloud lightning (Cummins et al. 1998).

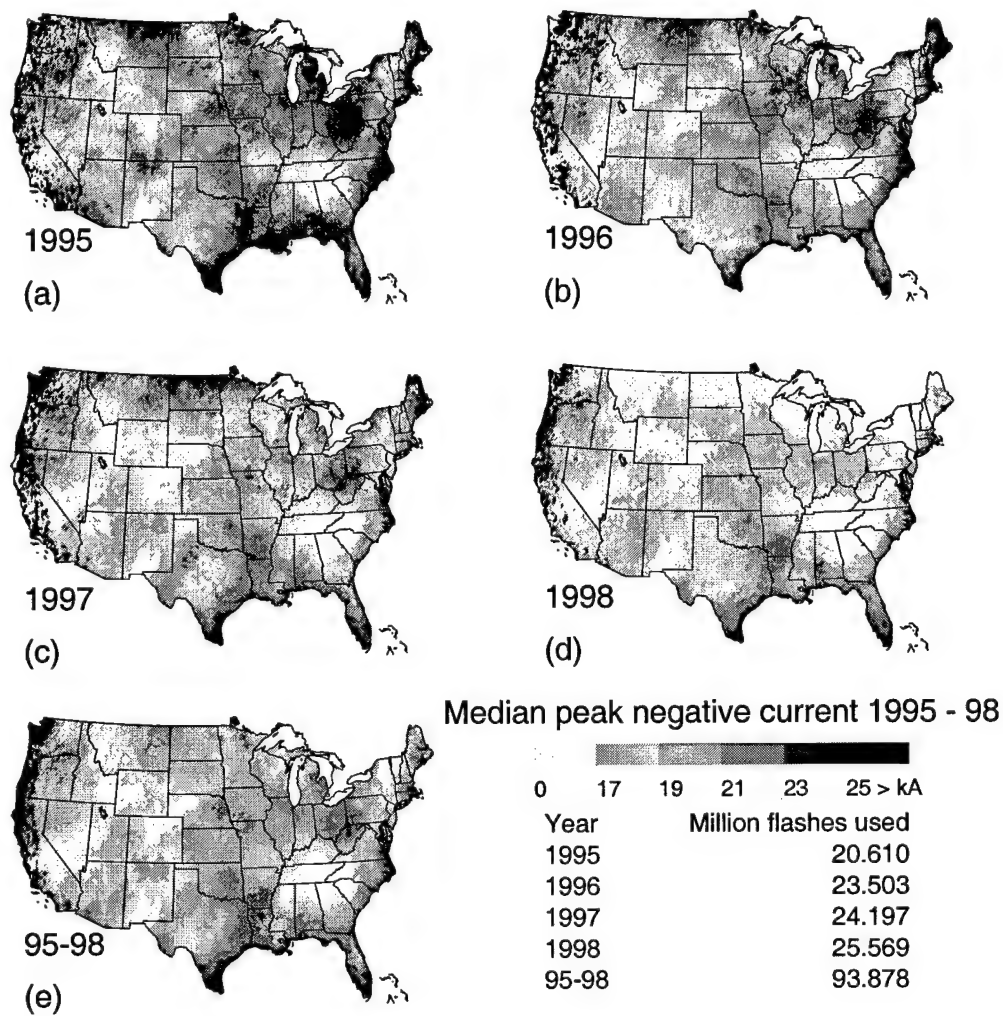


Figure 21. Contour of the median of negative peak currents from 1995 – 98. As in Figure 20 except all negative flashes were included, regardless of the peak current strengths.

Texas through the Plains States. The largest number of positive flashes also occurred in 1998.

The low median values in the West Coast States for the individual years are replaced by high values in the 4-year summary chart (Fig. 20e). The 4-year summary actually has a maximum in this region. This dramatic change from a minimum to a maximum median peak current is indicative of a low flash count. The minimum values are actually zero until there are sufficient flashes to determine a median of peak currents using the two flash criteria stated above, then a maximum occurs. The change from low to high values also implies that the few flashes occurring in these grid elements have high peak currents. For these data sparse regions, it is more useful to examine the summary information than the data for individual years.

For negative flashes (Fig. 21), a somewhat different pattern emerges. Each year has an absolute minimum in the median peak currents (< 17 kA) over the Carolinas, Northern Georgia, Alabama, and Eastern Tennessee similar to that seen in positive lightning (Fig. 20). There is a maximum (> 25 kA) along the West Coast that is patchy on an annual basis, but is well defined in the 4-year summary (Fig. 21e). A maximum (> 21 kA) is also found in Western Pennsylvania and West Virginia, as was found in the positive flashes. Beyond this, the similarities between positive and negative peak currents end.

The medians of peak currents for negative flashes (Fig. 21) have a maximum (> 21 kA) along the Gulf and East Coasts. In each year, this maximum extends north into Arkansas along the Mississippi and Missouri River valleys. This region of maximum median peak currents also includes Oklahoma, Kansas, Missouri, and Iowa, but the values in these states are less than the median peak currents along the coasts.

The regions of the US where the medians of both positive (Fig. 20) and negative (Fig. 21) peak currents have a minimum coincide with regions of tightly spaced NLDN sensors (Fig. 8). This is also the same latitude band where the median of peak positive currents in each degree of latitude drops below the line of best fit for the data (Fig. 18). Further examination of this feature is warranted.

E. The effect of IMPACT sensor locations on peak currents

In the Carolinas, Georgia, and Eastern Tennessee, NLDN sensors are more tightly spaced than anywhere else in the US (Fig. 8). This is the same region where the minimum in both positive (Fig. 20) and negative (Fig. 21) median peak currents occur. When the median peak currents of flashes in a one-degree latitude band are found (Fig. 18), there are lower values for positive flashes in this latitude band than would be expected based on the rest of the country. This relationship implies a connection between the sensor separation and the median peak currents. As the NLDN sensors in this region are mainly IMPACT sensors with direction-finding capability, the examination will begin with IMPACT sensors.

To begin quantifying the variations in sensor separation and the effect on peak currents, the distances between nearest IMPACT sensors were found across the US (Fig. 22). As at least one IMPACT sensor must detect a return stroke before it is reported by the NLDN. The separation between IMPACT sensors represent twice the maximum distance the electromagnetic wave from a return stroke must travel in order to be detected. Therefore, by halving the separations (Fig. 22) one knows the furthest distance a return stroke signal must travel to be detected by an IMPACT sensor.

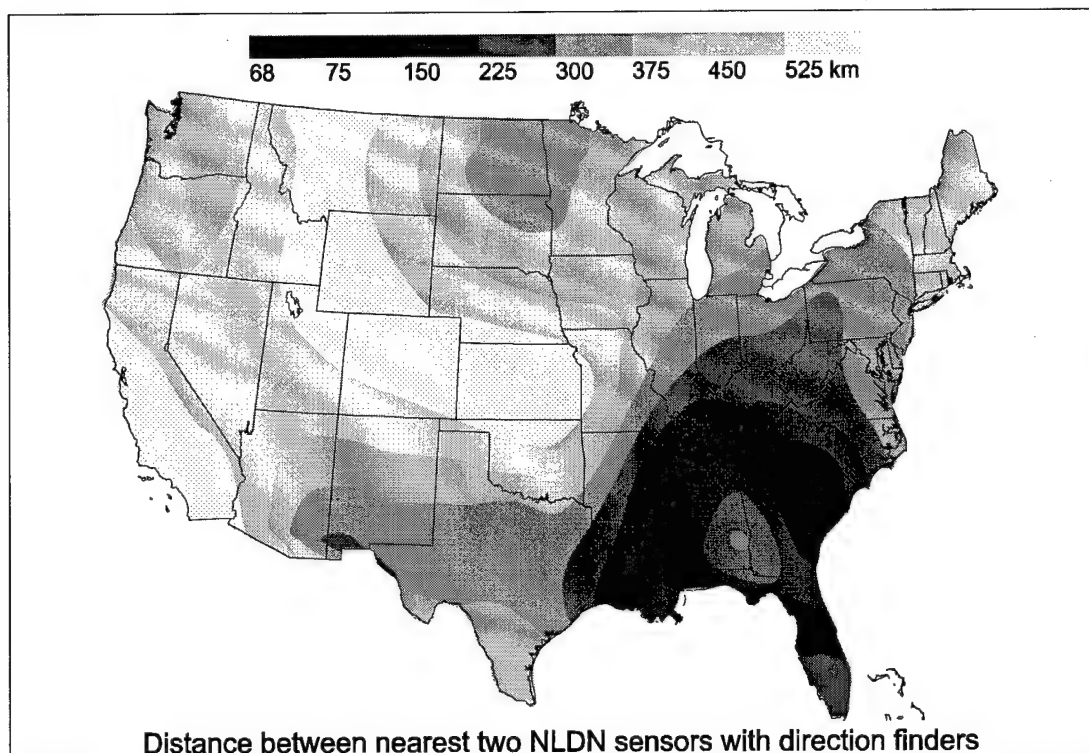


Figure 22. Contour of distances between IMPACT sensors in the NLDN. The distances between nearest NLDN sensors with direction finding capability are contoured for the US. The minimum distance is 68 km and is located in the Carolinas. Taking half the distance between IMPACT sensors provides the maximum distance a return stroke signal must travel before being detected. At least one IMPACT sensor must detect a return stroke before it is reported.

As one would expect from the plot of NLDN sensor locations (Fig. 8), the shortest distance between IMPACT sensors is found in the Carolinas, Georgia and Eastern Tennessee (< 200 km). This corresponds exactly with the minimum in median peak currents for both positive (Fig. 22) and negative (Fig. 21) flashes. There is also a relative minimum in the IMPACT separation (< 200 km) that extends from Southern Louisiana into Kentucky along the Mississippi River Valley. Contrary to the connection between sensor separation in the Carolinas, the median peak negative currents have a maximum in this region.

A purely qualitative examination, such as that above, only indicates a connection between the closely spaced IMPACT sensors in the Carolinas and the minimum in the median of positive and negative peak currents. A more rigorous examination is required to describe the connection between IMPACT sensor separation and the median peak currents for the entire country. A scatter plot of the two parameters should show any connection. This comparison was accomplished by interpolating the IMPACT sensor separation to match the same grid elements used in the median peak current calculations. To avoid adding errors from median values found using only a few flashes in a grid element, only grid elements with at least 100 flashes (Fig. 23) were included in the scatter plot and subsequent calculations.

Direct comparison of IMPACT sensor separation and median peak currents (Fig. 24) indicates a trend for negative flashes and sensor separations less than 250 km. Positive flashes do not appear to show any significant change in the peak currents for the same range of sensor separations. The lack of variability for positive flashes is odd as a large range of median peak currents exist for all sensor separations greater than 250 km. This implies that

Grid elements with at least 100 flashes (1995 - 98)

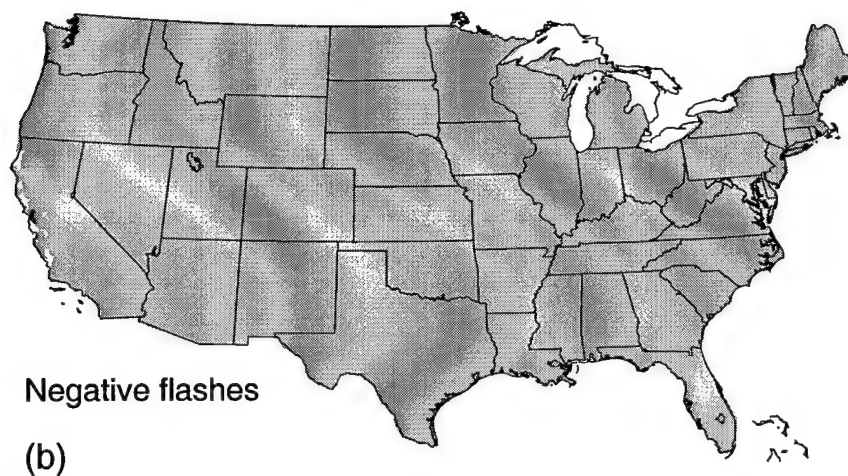
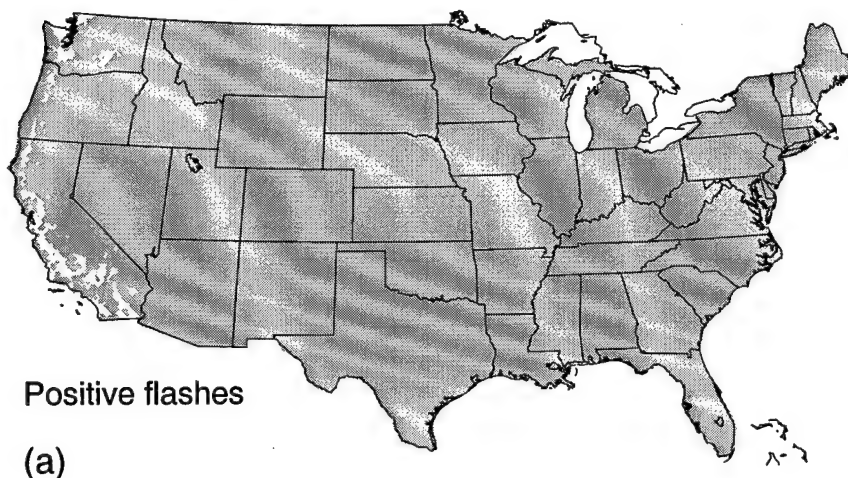


Figure 23. Map of grid elements having at least 100 flashes from 1995 – 98. The 0.2 by 0.2 grid elements used to calculate the lightning characteristics over the US having at least 100 flashes in the period of study are shown for positive (a) and negative (b) flashes. No attempt to correct for the area of each grid elements was made.

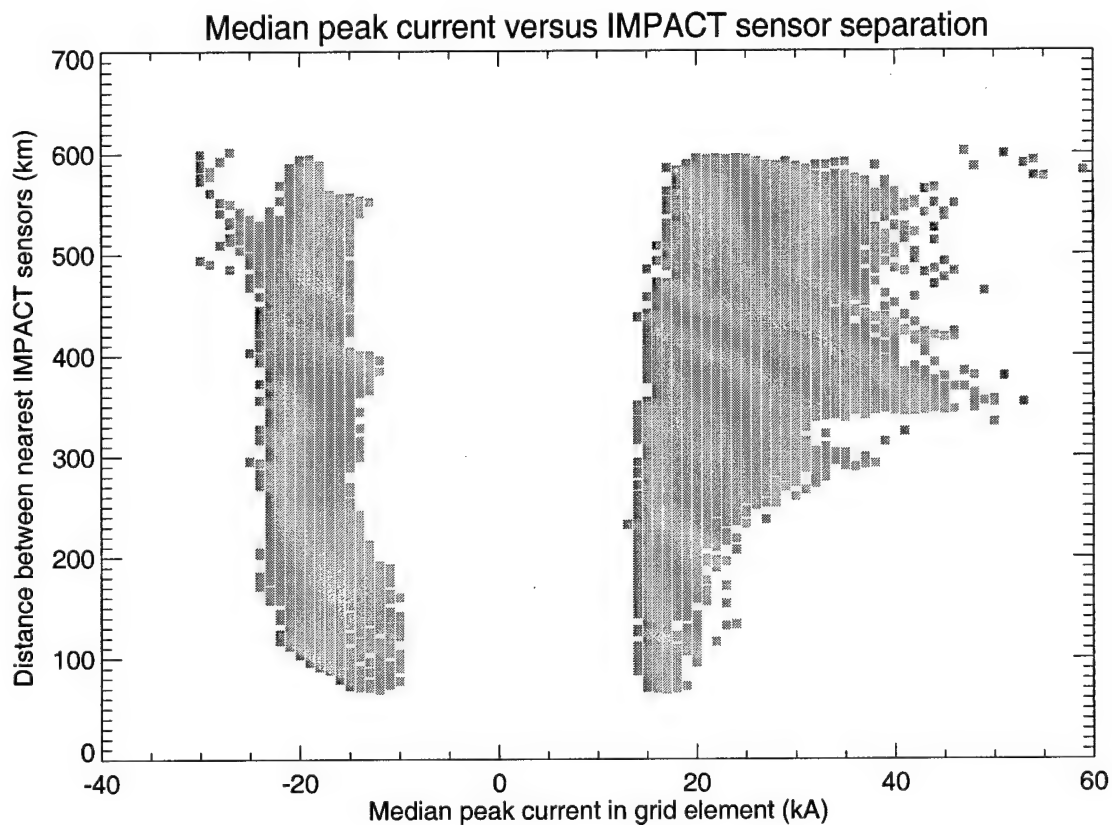


Figure 24. Scatter plot of median peak currents and IMPACT sensor separation. The median of peak currents for each 0.2 by 0.2 degree latitude and longitude grid element is plotted in relation to the distance between IMPACT sensors in the NLDN. This is done separately for positive flashes (where the median peak currents are positive) and for negative flashes (with negative median peak currents).

a predominance of weak positive flashes are measured within this region, reducing the effect of stronger positive flashes on the median values.

To quantify the effect of sensor separation on peak currents, direct calculation were made using the peak currents for flashes from 1995 – 98 and the grid distances described above. The distances were divided into 10 km increments. Each flash was assigned to the sensor separation value in the grid element containing the flash. The appropriate peak current bin counter was advanced by one. After all the flashes were counted into the proper distance increment and peak current bin, the medians of the peak currents were found for each distance increment. The results are shown in Figure 25 and are summarized in Table 6.

It is easier to see the dependence of peak currents on the IMPACT sensor separation distances by examining the median of each distance increment over the US (Fig. 25). There is a tendency for the median of peak currents to increase with increasing sensor separations. Using a least-squares approximation to describe the relationship between peak currents and IMPACT sensor separation provides the following equations,

$$Med_Pos = 30.1kA - \frac{1482.64kA \cdot km}{IMPACT(km)} \quad (6)$$

and

$$Med_Neg = -20.0kA + \frac{380.80kA \cdot km}{IMPACT(km)}, \quad (7)$$

where Med_Pos and Med_Neg are the median of peak currents for positive and negative flashes, respectively and IMPACT is the distance between impact sensors in kilometers.

The correlation coefficients were 0.554 and 0.606 for positive and negative flashes,

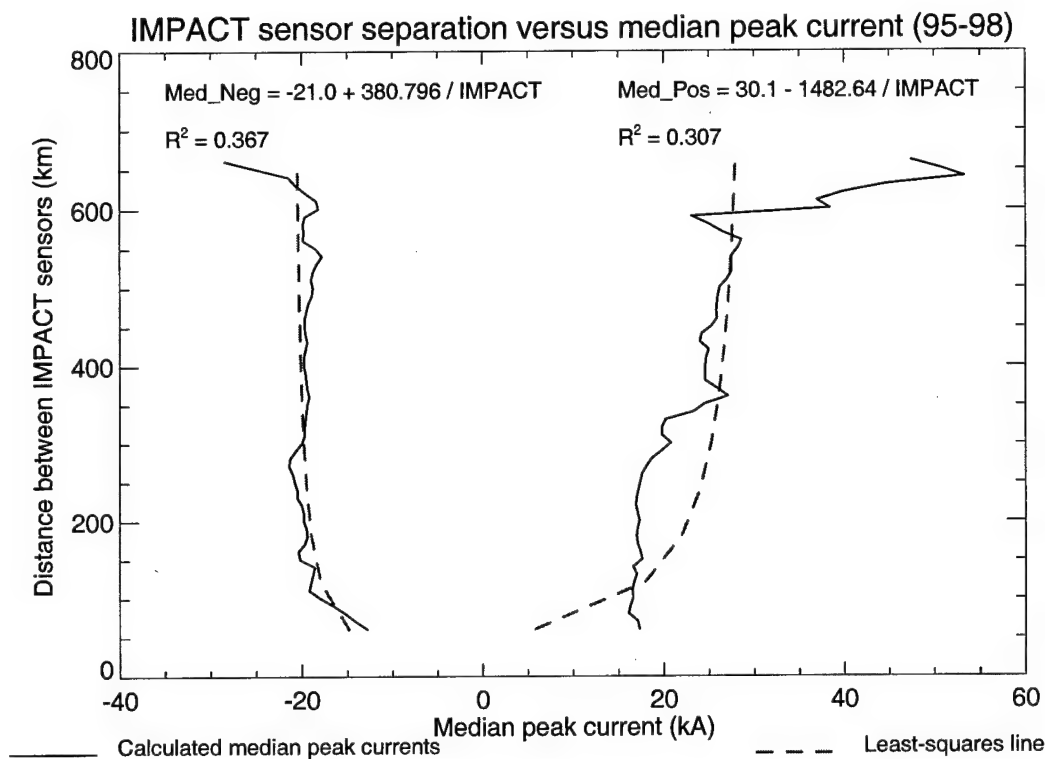


Figure 25. Direct comparison of median peak currents and IMPACT separations. The median peak currents for each 10 km increment in IMPACT sensor separation for 1995 – 98 are shown for both positive and negative flashes. Least squared lines-of-best-fit for positive and negative flashes are also shown with the line equations and the proportions of total variability (R^2) accounted for by the relationships.

Table 6. Peak current characteristics based on the distance between IMPACT sensors.

Minimum in IMPACT sensor separation increment (km)	Median of negative peak currents (kA)	Median of positive peak currents (kA)	Minimum in IMPACT sensor separation increment (km)	Median of negative peak currents (kA)	Median of positive peak currents (kA)
61.0	-12.8	17.3	361.0	-19.2	27.1
71.0	-14.1	17.1	371.0	-19.4	25.9
81.0	-15.2	16.1	381.0	-19.5	24.6
91.0	-16.5	16.3	391.0	-19.6	24.6
101.0	-18.0	16.6	401.0	-19.8	24.6
111.0	-19.2	16.5	411.0	-19.8	24.7
121.0	-19.0	16.7	421.0	-19.6	25.0
131.0	-18.8	17.0	431.0	-19.4	24.0
141.0	-18.6	16.6	441.0	-19.6	24.2
151.0	-20.2	17.6	451.0	-19.7	25.3
161.0	-20.4	17.4	461.0	-19.7	25.9
171.0	-19.7	17.1	471.0	-19.5	25.8
181.0	-19.4	17.0	481.0	-19.3	25.9
191.0	-19.5	17.1	491.0	-18.9	26.0
201.0	-19.8	17.3	501.0	-18.8	26.2
211.0	-19.8	17.1	511.0	-19.0	27.0
221.0	-20.0	16.9	521.0	-18.8	27.5
231.0	-20.5	17.0	531.0	-18.4	27.5
241.0	-20.5	17.2	541.0	-17.8	27.5
251.0	-20.8	17.4	551.0	-18.5	28.2
261.0	-21.0	17.6	561.0	-19.9	28.6
271.0	-21.4	18.1	571.0	-19.8	26.5
281.0	-21.3	18.7	581.0	-19.9	25.0
291.0	-20.7	19.8	591.0	-19.7	23.1
301.0	-20.0	20.8	601.0	-18.2	38.4
311.0	-19.7	19.8	611.0	-18.4	37.0
321.0	-19.7	19.8	621.0	-19.6	39.9
331.0	-19.6	20.2	631.0	-20.7	44.7
341.0	-19.5	23.3	641.0	-21.5	53.3
351.0	-19.4	24.5	651.0	-25.0	50.7

respectively. These relationships further support a connection between sensor separation and peak currents, but the connection between the parameters is weak.

F. Influence of the distribution of all NLDN sensors on peak current strength

The NLDN not only requires that a direction finder, or IMPACT, sensor detect a return stroke before it is reported, but there must also be sufficient sensors to determine the location of the return stroke. To determine the influence that this broader criterion has on the peak current distributions, the distance from the center of each grid element (Fig. 10) to the furthest of the minimum required sensors (Fig. 12) was calculated (Fig. 26).

There is a minimum distance (< 100 km) to the fewest required sensors over the Carolinas, and distances between 100 km and 200 km in Northern Georgia and Alabama, Tennessee, and Kentucky (Fig. 26). Most of this region matches well with the minimum median peak currents of both positive (Fig. 22) and negative flashes (Fig. 21). The minimum distances in Florida matches the minimum seen each year in the positive peak currents over Florida. The distances for the rest of the country do not provide much guidance as they have little variability. The exceptions are in Kansas, Montana, and Maine where the maximum distances are found (> 300 km).

The maximum in distances to the required NLDN sensors in Maine does not match any pattern in the median of peak currents with any consistency in the four years of this study. Montana however has a maximum in median of negative peak currents but not for positive flashes. The difference between the two regions is probably due to Montana having more lightning each year than Maine (Orville and Huffines 1999). More lightning flashes would provide a better representation of the true median peak currents than regions with fewer flashes.

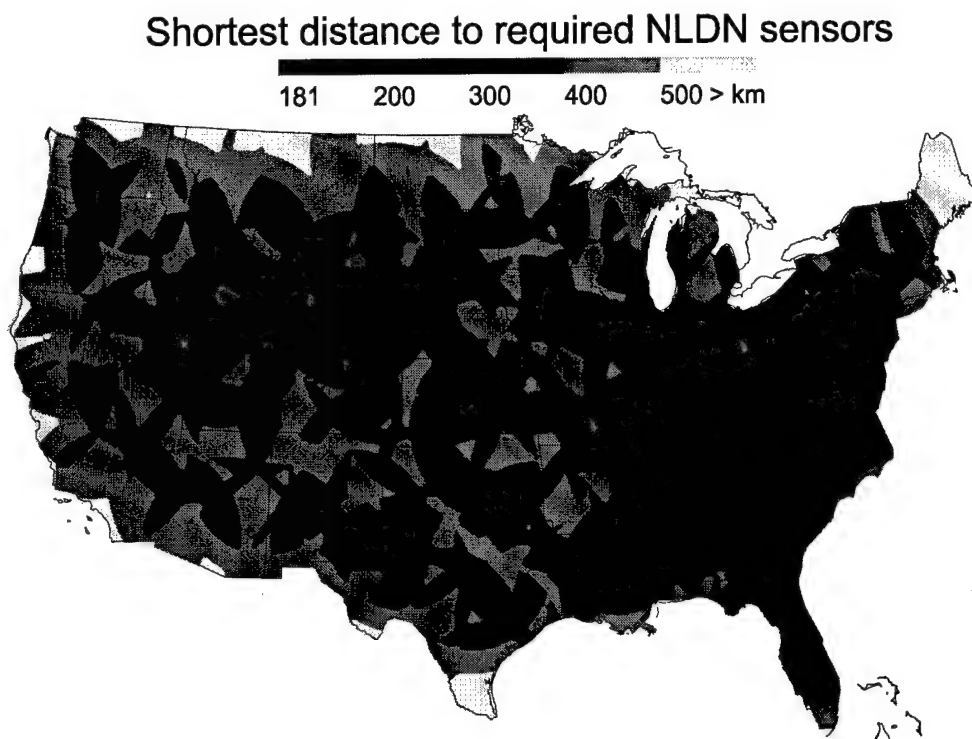


Figure 26. Contour of distances to the minimum required NLDN sensors. Distances from the center of each 0.2 by 0.2 degree latitude and longitude grid element to the furthest NLDN sensor that will meet the minimum criteria necessary to report a return stroke are contoured. Either two IMPACT sensors or two TOA sensors and an IMPACT sensor are required to accurately determine the position of a lightning stroke. The contours shown here are of the distances to the furthest of these required sensors.

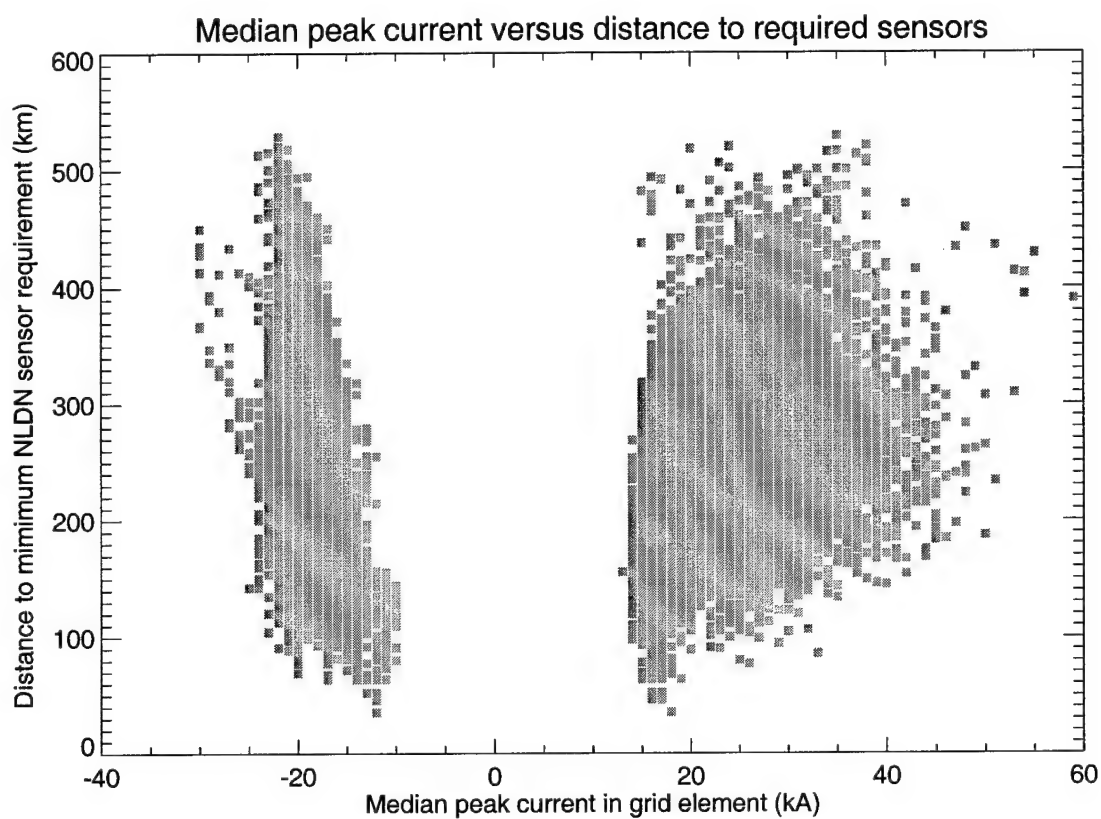


Figure 27. Distance to the minimum required NLDN sensors and median peak currents. As in Figure 24 except the distances are to the furthest of the minimum number of NLDN sensors required to detect a return stroke.

The shift from qualitative comparisons of features to a more quantitative analysis was accomplished by using a scatter plot of distances versus the median of peak currents in each grid element (Fig. 27). The restriction to elements having at least 100 flashes (Fig. 23) was applied in this comparison. For both positive and negative flashes, there is a trend toward increasing peak currents as the distance to the outermost required sensor increases.

Similar comparisons were made between the minimum required sensor distances and median peak currents as was accomplished for the IMPACT sensor separations. The results (Table 7) show a good agreement between the median positive peak currents and the minimum required sensor distances (Fig. 28). The same comparison for negative flashes shows less agreement between the two values. Mathematical descriptions of these trends are

$$Med_Pos = 5.7kA + 0.128 \frac{kA}{km} * Dist - \left(1.47 * 10^{-4} \frac{kA}{km^2} \right) * Dist^2 \quad (8)$$

and

$$Med_Neg = -13.1kA - 0.044 \frac{kA}{km} * Dist + 6.594 \frac{kA}{km^2} * Dist^2 \quad (9)$$

where Med_Pos and Med_Neg are the median of peak currents for positive and negative flashes, respectively and Dist represents the distance to the furthest minimum required sensor in kilometers. These relationships for positive flashes had a correlation coefficient of 0.872 while the calculations for negative flashes had a correlation coefficient of 0.653.

The equations describing the effect of sensor separation on positive (8) and negative (9) flashes use the inverse of the distance as was indicated by the equations for electric (1) and magnetic (2) field strengths. It appears that these descriptive equations do not fully explain the variability in peak currents, as the correlation coefficients are much less than the

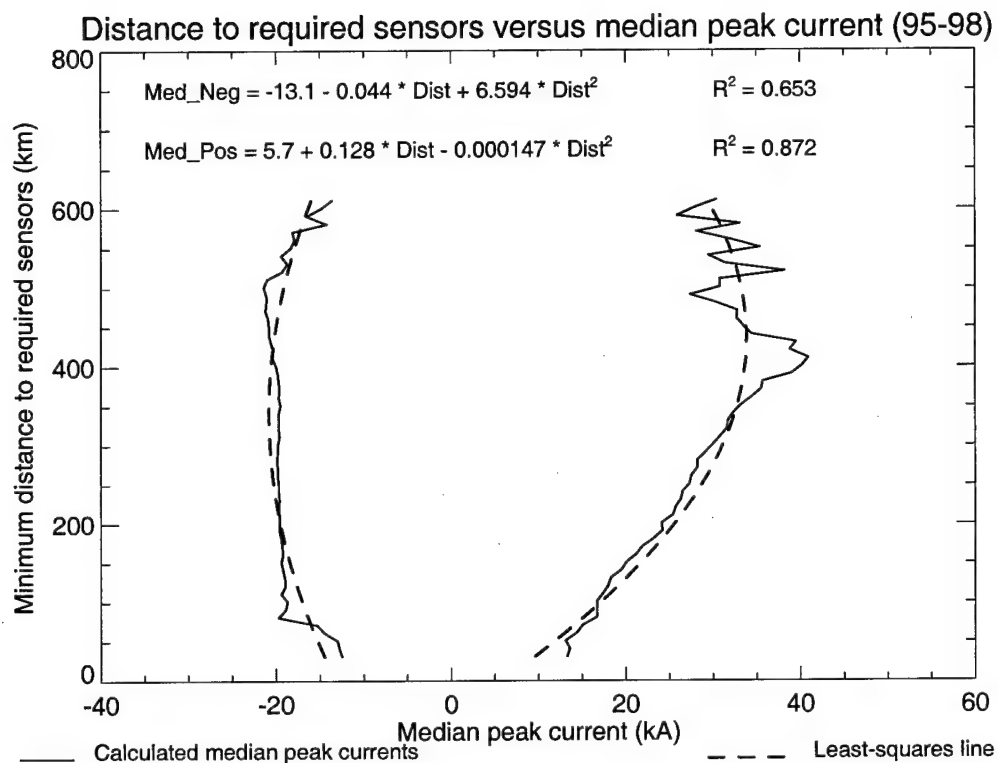


Figure 28. Direct comparison of median peak currents and required NLDN sensors. As in Figure 25 except the distances are from the center of each 0.2 by 0.2 degree latitude and longitude grid element to the furthest of the minimum required NLDN sensors required to report a return stroke

Table 7. Peak current characteristics based on the distance to required NLDN sensors.

Minimum of increment in distance to furthest required sensor for return stroke detection (km)	Median of negative peak currents (kA)	Median of positive peak currents (kA)	Minimum of increment in distance to furthest required sensor for return stroke detection (km)	Median of negative peak currents (kA)	Median of positive peak currents (kA)
31.0	-12.5	13.3	331.0	-19.7	31.7
41.0	-12.8	13.6	341.0	-19.7	32.3
51.0	-13.0	13.1	351.0	-19.5	33.2
61.0	-14.5	14.4	361.0	-19.7	34.4
71.0	-15.3	15.1	371.0	-19.6	35.5
81.0	-19.7	16.7	381.0	-19.7	35.7
91.0	-18.9	16.7	391.0	-19.8	39.0
101.0	-18.7	16.7	401.0	-20.0	40.2
111.0	-19.4	17.4	411.0	-20.4	40.9
121.0	-18.9	18.0	421.0	-20.3	38.8
131.0	-19.0	18.3	431.0	-20.6	39.5
141.0	-19.2	19.5	441.0	-20.8	34.4
151.0	-19.4	20.1	451.0	-20.8	33.5
161.0	-19.2	21.2	461.0	-20.9	32.7
171.0	-19.3	21.9	471.0	-21.2	32.8
181.0	-19.4	23.2	481.0	-21.1	30.4
191.0	-19.6	24.2	491.0	-21.1	27.4
201.0	-19.6	24.1	501.0	-21.4	30.8
211.0	-19.6	25.4	511.0	-21.0	30.8
221.0	-19.7	25.7	521.0	-19.3	38.2
231.0	-19.6	26.3	531.0	-18.7	31.4
241.0	-19.7	26.5	541.0	-19.4	29.5
251.0	-19.7	27.3	551.0	-18.3	35.4
261.0	-19.8	27.5	561.0	-17.9	32.0
271.0	-19.8	28.2	571.0	-18.1	28.1
281.0	-19.9	28.2	581.0	-14.2	33.1
291.0	-19.8	29.1	591.0	-16.5	25.9
301.0	-19.8	30.0	601.0	-14.8	27.9
311.0	-19.6	30.8	611.0	-13.6	30.4
321.0	-19.7	31.6			

desired value of one, especially for negative flashes. The large spread in peak currents, especially for positive flashes (Fig. 27), also indicates a lack of fit with the relationship to sensor separation. Other factors must be influencing the peak current strengths.

G. Flash densities and the effect on peak currents

The amount of lightning each year may play a part in the peak current distributions. If more lightning occurs in a particular location, the implication is that more thunderstorms occur. Air mass or convective types of thunderstorms occur more frequently than mesoscale convective systems (MCSs) or the frontal induced thunderstorms. With the exception of a large scale, long lived MCS producing a lot of lightning, such as occurred in 1993 (Orville and Silver 1997), larger flash densities imply a region consisting predominately of convective thunderstorms. A comparison of peak currents with flash densities may also be a comparison with the types of thunderstorms, either convective or larger scale. To examine this possibility, it was necessary to calculate the flash densities for the US. As before, all positive flashes with peak currents less than 10 kA are excluded from these calculations.

Flash density calculations have been reported in previous studies (Orville 1991a, 1994, Orville and Silver 1997, and Orville and Huffines 1999), but are repeated here (Fig. 29). The annual flash densities vary somewhat from year to year with major features being consistent over time. Florida consistently has the maximum flash density (> 9 flashes $\text{km}^{-2} \text{yr}^{-1}$) and there is a consistent minimum over the Appalachian Mountains (< 3 flashes $\text{km}^{-2} \text{yr}^{-1}$). There are also relative maximums in Southern Illinois and Eastern Tennessee (> 6 flashes $\text{km}^{-2} \text{yr}^{-1}$). In 1998 (Fig. 29d), the higher flash densities (> 3 flashes $\text{km}^{-2} \text{yr}^{-1}$) shifted away from Western Texas, Oklahoma, and Kansas. This year also had a maximum

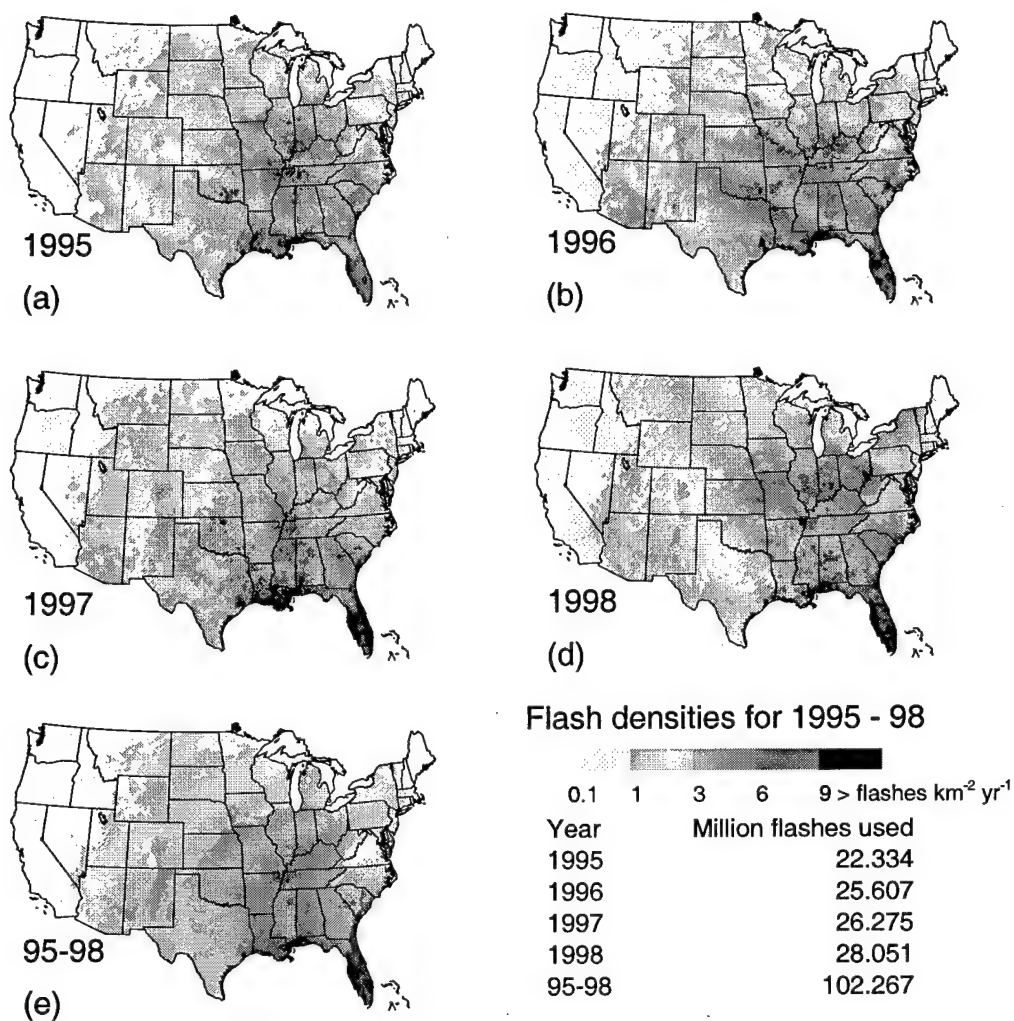


Figure 29. Flash density contour for the US from 1995 – 98. The flash densities were calculated for the US using a 0.2 by 0.2 degree latitude and longitude grid. The change in the size of grid elements with latitude was taken into account. No positive flashes with peak currents less than 10 kA were included in order to avoid contamination by intracloud flashes (Cummins et al. 1998).

(> 6 flashes $\text{km}^{-2} \text{yr}^{-1}$) at the corners of Ohio, Pennsylvania, and West Virginia and had the maximum number of flashes in the period of record.

Initial comparisons between the flash densities and the median of peak current for both positive (Fig. 20) and negative (Fig. 21) flashes do not reveal an obvious relationship. The only features that stand out are the high flash densities in Florida which correspond with the maximum in median peak negative currents and the minimum in median positive peak currents. Direct comparisons of these lightning characteristics are difficult using the contour scales available. To provide a more direct comparison, a scatter plot of median peak currents and flash densities (Fig. 30) in the same grid elements was built similar to those previously shown.

It is impossible by looking at the scatter plot (Fig. 30) to determine how many matching flash density and peak current combinations are plotted on top of one another. One may easily see, however, that the spread in median peak current values decreases with increasing flash densities. This narrowing effect is due to the number of grid elements having high flash densities being much fewer than those with the lower values. The upper limit of the spread in positive peak currents shows a parabolic decrease as the flash densities increase. Negative flashes have a curved tendency as well, but they tend to increase in magnitude for flash densities above 5 flashes $\text{km}^{-2} \text{yr}^{-1}$.

To overcome the problem of over plotting combinations of flash densities and median peak currents, the median peak currents were determined for each increment in flash density of 0.25 flashes $\text{km}^{-1} \text{yr}^{-1}$. These median values (Table 8) were then plotted for comparisons (Fig. 31). The effect of the spread in positive peak currents becomes evident

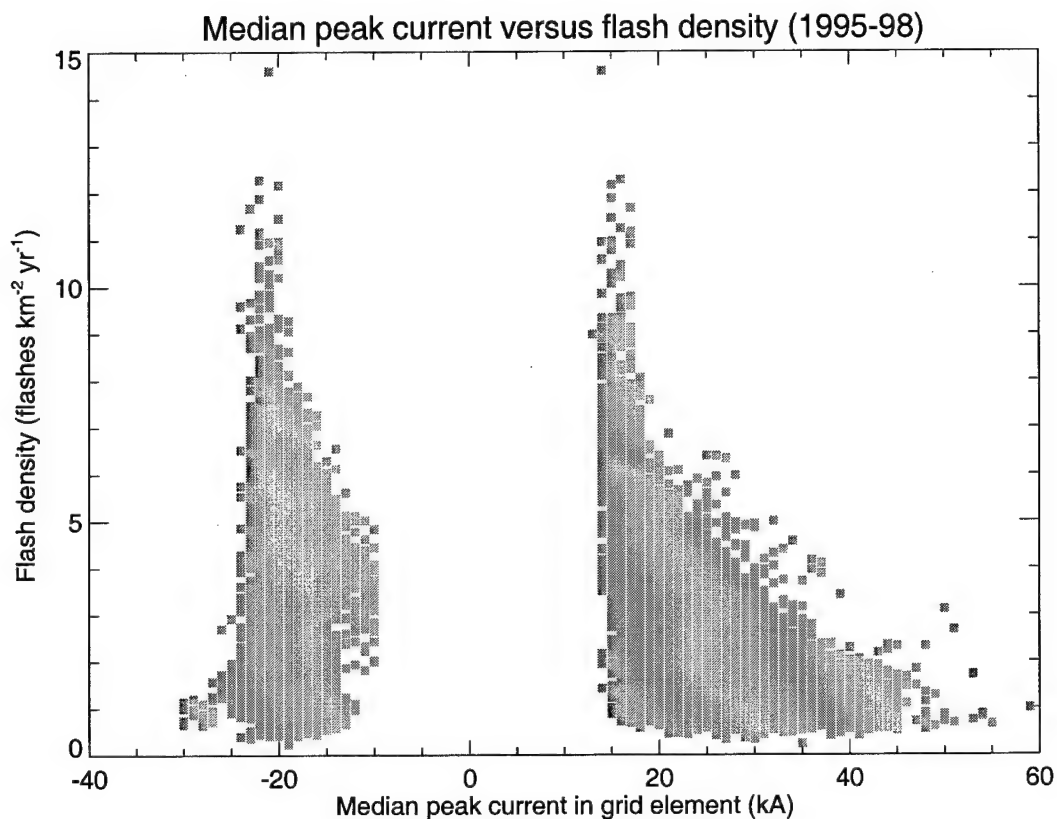


Figure 30. Scatter plot of median peak currents and flash densities. The median peak currents were plotted against the flash density values for each 0.2 by 0.2 degree grid element over the US. Points with positive median peak currents indicate positive flashes while negative flashes are those with negative peak currents. Positive flashes with peak currents less than 10 kA were not included. No restrictions were applied to the negative flashes.

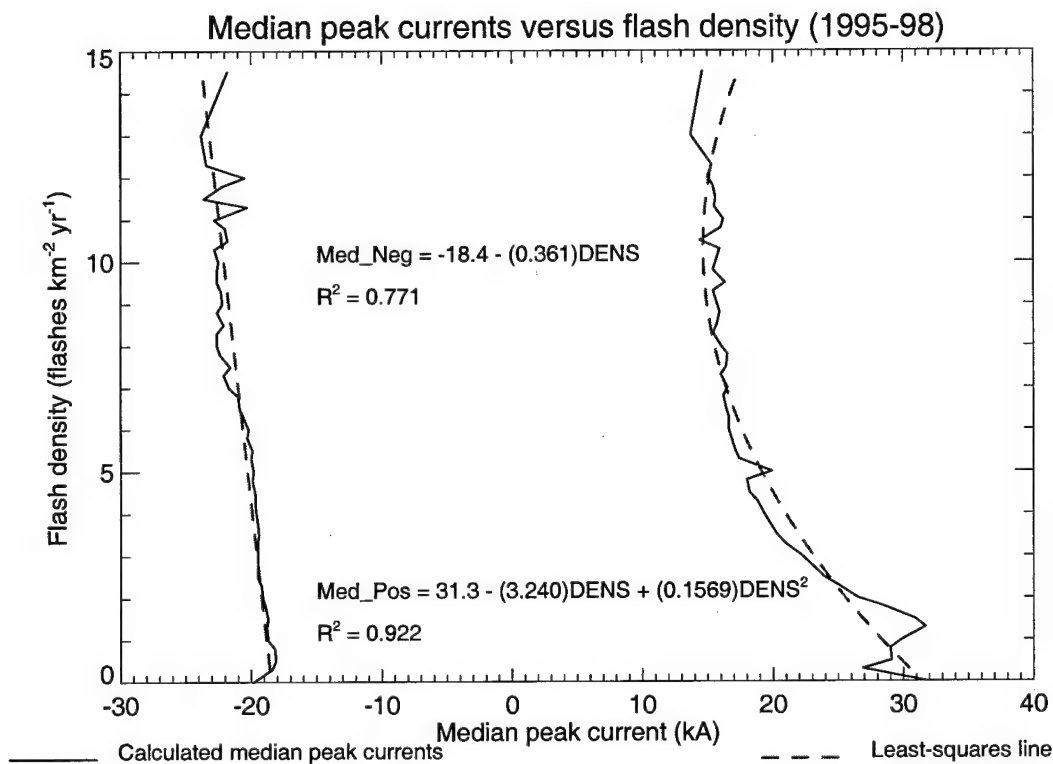


Figure 31. Direct comparisons of median peak currents and flash densities. The solid lines indicate the median peak currents calculated for each $0.25 \text{ flashes km}^{-2} \text{yr}^{-1}$ change in flash density. Dashed lines are the lines of best fit using least squared approximations. Equations for these lines are included with the portion of variability explained by them (R^2). No positive flashes with peak currents less than 10 kA were used in order to reduce the possibility of contaminating the data with intracloud flashes (Cummins et al. 1998).

Table 8. Peak current characteristics based on flash densities.

Minimum of increment in flash density (flashes km ⁻² yr ⁻¹)	Median of negative peak currents (kA)	Median of positive peak currents (kA)	Minimum of increment in flash density (flashes km ⁻² yr ⁻¹)	Median of negative peak currents (kA)	Median of positive peak currents (kA)
0.00	-19.80	31.80	6.25	-20.60	16.60
0.25	-18.40	26.90	6.50	-20.90	16.40
0.50	-18.10	29.10	6.75	-21.00	16.20
0.75	-18.20	29.00	7.00	-21.70	16.50
1.00	-18.70	29.90	7.25	-22.10	16.00
1.25	-18.80	31.70	7.50	-21.60	16.40
1.50	-18.70	30.90	7.75	-22.40	16.50
1.75	-18.90	28.50	8.00	-22.60	16.00
2.00	-19.10	26.50	8.25	-22.60	15.40
2.25	-19.20	25.00	8.50	-22.10	15.70
2.50	-19.50	23.90	8.75	-22.60	15.90
2.75	-19.50	22.90	9.00	-22.20	15.70
3.00	-19.50	22.20	9.25	-22.30	15.40
3.25	-19.50	20.90	9.50	-22.60	16.30
3.50	-19.40	20.30	9.75	-22.60	15.40
3.75	-19.50	19.70	10.00	-22.50	15.60
4.00	-19.60	19.30	10.25	-22.80	15.90
4.25	-19.70	18.80	10.50	-21.80	14.40
4.50	-19.70	18.20	10.75	-22.00	16.00
4.75	-19.90	18.00	11.00	-22.80	16.20
5.00	-19.80	19.90	11.25	-20.30	15.50
5.25	-20.00	17.40	11.50	-23.60	15.60
5.50	-19.90	17.10	11.75	-22.20	15.40
5.75	-20.30	16.80	12.00	-20.50	15.00
6.00	-20.20	16.60	12.25	-23.40	15.30

when the regions are combined. The second order changes in the positive peak currents based on flash densities is still present, but is absent for the negative flashes. The trend for negative flashes is the opposite to that in positive lightning since negative peak currents increase in magnitude with increasing flash density.

The reversal of trends between positive and negative lightning (Fig. 31) may be explained by examining the flash densities (Fig. 29). In general, the flash densities are greatest at lower latitudes and show an overall decrease with increasing latitude. This is shown in a plot of mean flash densities over the US for each 0.2 degree latitude increment (Fig. 32). One can see an almost linear decrease in the flash densities from 30 N to 49 N, where the values end. Comparing this decrease with the change in the median peak currents based on latitude (Fig. 18) shows this reversal in trends between positive and negative flashes.

Applying least squares regression analysis to the mean flash density based on latitude (Fig. 32) provides the equation

$$Dens = 50.0 \text{ flashes} \cdot \text{km}^{-2} \cdot \text{yr}^{-1} - 4.8 \text{ flashes} \cdot \text{km}^{-2} \cdot \text{yr}^{-1} \cdot \text{deg}^{-1} (Lat), \quad (10)$$

where Dens is the mean flash density and Lat is the latitude in degrees ranging from 30 N to 49 N. This latitude band includes the US from the Florida Panhandle to the northern US border. The correlation coefficient for this relationship is 0.99.

H. Percentages of positive flashes and the effect on peak currents

Positive flashes have been observed to originate in the upper levels of the thunderstorms (Brook et al. 1982; Rust et al. 1981) or in the stratiform precipitation regions (Rutledge and MacGorman 1988; Rutledge et al. 1994; Holle et al. 1994) trailing a

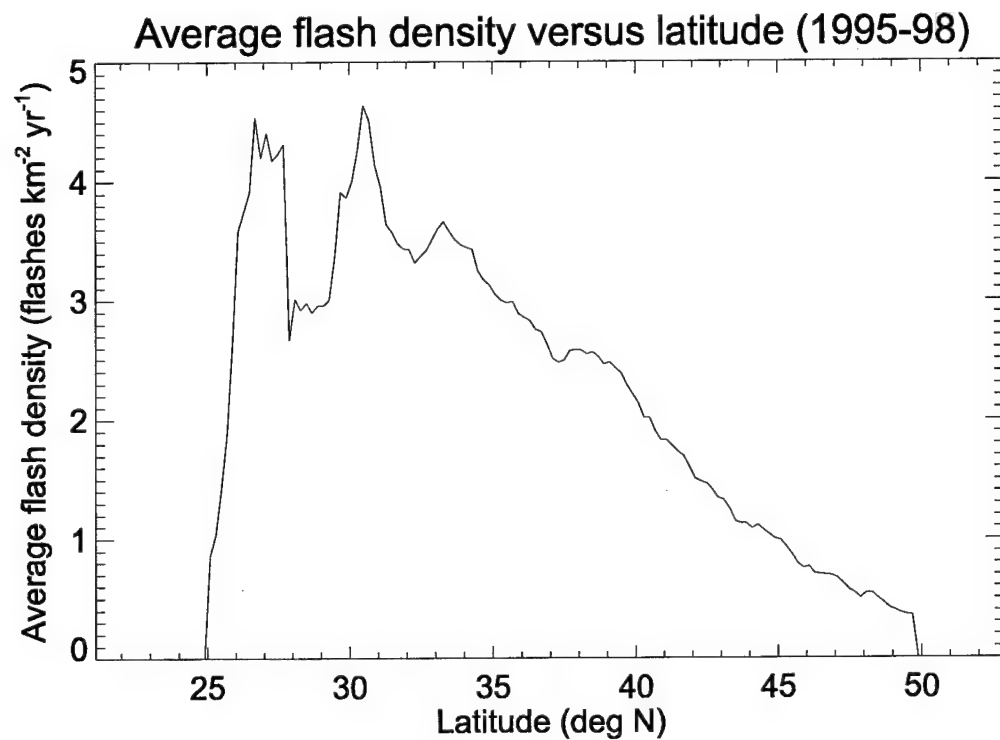


Figure 32. Average flash density based on latitude. The flash densities were averaged over the US land mass for each degree of latitude from 1995 – 98.

mesoscale convective complex (MCC) (Maddox 1980; Zipser 1982). The percentage of all flashes that lower a net positive charge to ground, hereafter referred to as percent positive flashes, varies with geographic region, time of the year, and between different storms. If the positive flashes do originate in the upper levels of the cloud or in the stratiform precipitation region of MCSs, then a higher percentage of positive flashes indicate increased electrical activity in the thunderstorm, an increased opportunity for the positive charge to travel to the ground, or both. Studies of positive lightning in thunderstorms have shown that an increased vertical tilt allows more positive discharges to reach the ground (Brook et al. 1982; Orville et al. 1988; Engholm et al. 1990; Curran and Rust 1992). Based on this observation, the regions with a higher percentage of positive flashes would also have thunderstorms that are vertically tilted.

The percent positive flashes for the US are shown in Figure 33 for each year of the study and for all years combined. Positive flashes with peak currents less than 10 kA were not included in order to avoid the inclusion of misidentified intracloud flashes (Cummins et al. 1998). Each year had a minimum of percent positive flashes ($<5\%$) in Florida, Western Pennsylvania, and West Virginia. The maximum ($>20\%$) is found in the Northern Plains during each year and as far south as Texas in 1998 (Fig. 33d).

Comparison with the median peak negative currents (Fig. 21) places the maximum peak currents (>19 kA) in the Southeastern US, extending well beyond the bounds of Florida where the minimum in percent positive flashes was found. There is another maximum for the negative currents (>21 kA) in Western Pennsylvania which is the same region as the minimum of percent positive flashes (Fig. 33e). A relative minimum in the negative peak currents was found in the Northern Plains in approximately the same region

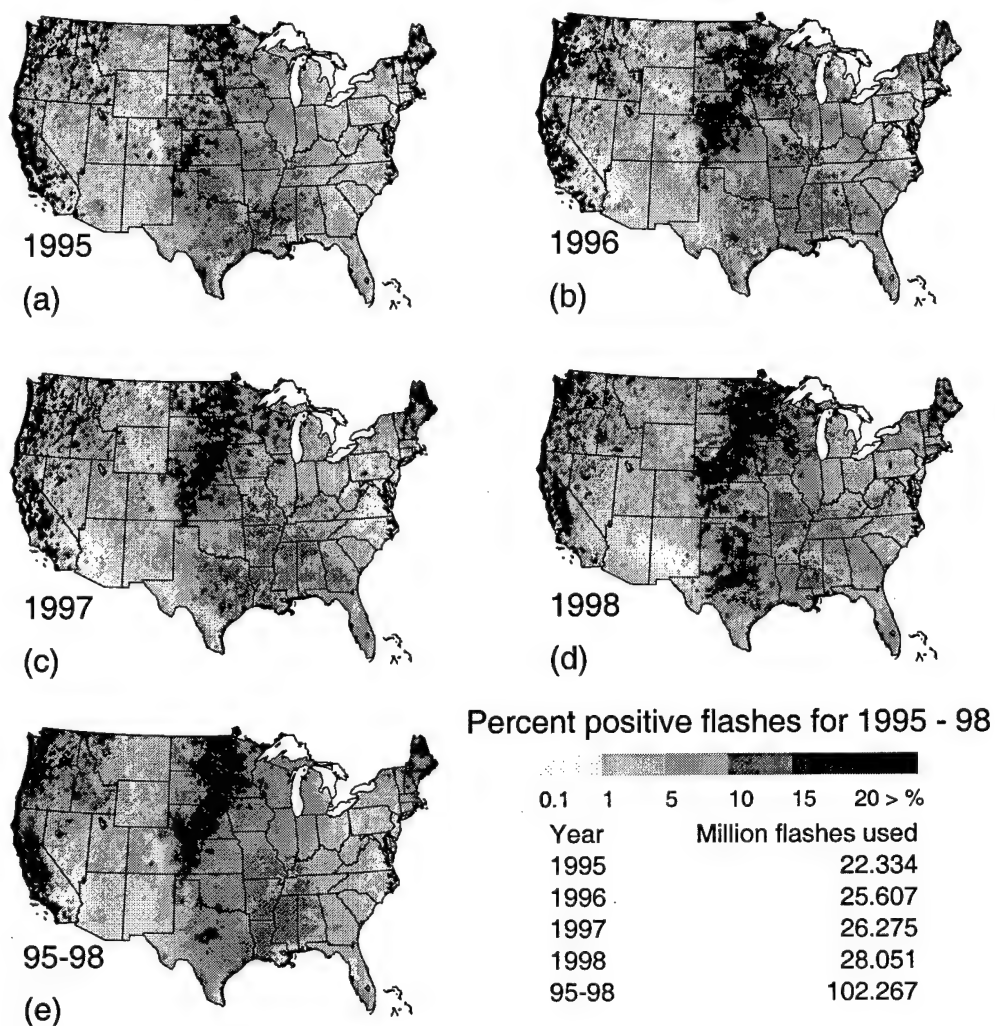


Figure 33. Contour of percent positive flashes from 1995 – 98. A presentation of the annual percentage of all cloud-to-ground flashes that are positive is shown for each year (a – d) and for the 4-year period studied. The flash counts are listed for all measured lightning, regardless of polarity. Positive flashes with peak currents less than 10 kA were not used in an effort to reduce the contamination by intracloud flashes (Cummins et al. 1998).

as the maximum in percent positive flashes. These characteristics imply an inverse relationship between the peak currents for negative flashes and the percentage of positive flashes, although the reasons for this are not obvious. A connection between the percent positive flashes and the median peak positive currents (Fig. 20) would be more likely to exist. Changes in the percentage of positive flashes should indicate changes in the storm that would affect the characteristics of positive lightning.

The most striking similarity between the percent positive flashes (Fig. 33) and the median peak positive currents (Fig. 20) is in the maximum for both quantities over the Northern Plains. These features are almost identical in location, even on an annual basis where more variability exists. For 1998, the maximum regions extend as far south as Texas. Although not as dramatic, there are relative minimums in the percent positive flashes and median peak positive currents in Florida and other regions of the Southeastern US.

A more direct comparison was made using a scatter plot of the peak currents and percent positive flashes for the 0.2 by 0.2 degree grid over the US (Fig. 34). The results appear to indicate little or no change in the median of peak currents for negative flashes with change in the percent positive flashes. The opposite is true for positive flashes, as there is a direct relationship between the two quantities. This verifies the tendencies seen in the contour plots.

As was done in previous parts of this study, median peak currents were calculated for incremental values in percent positive flashes, specifically for each percent change (Table 9). Linear regression analysis using the method of least squares (Fig. 35) provided the following relationships

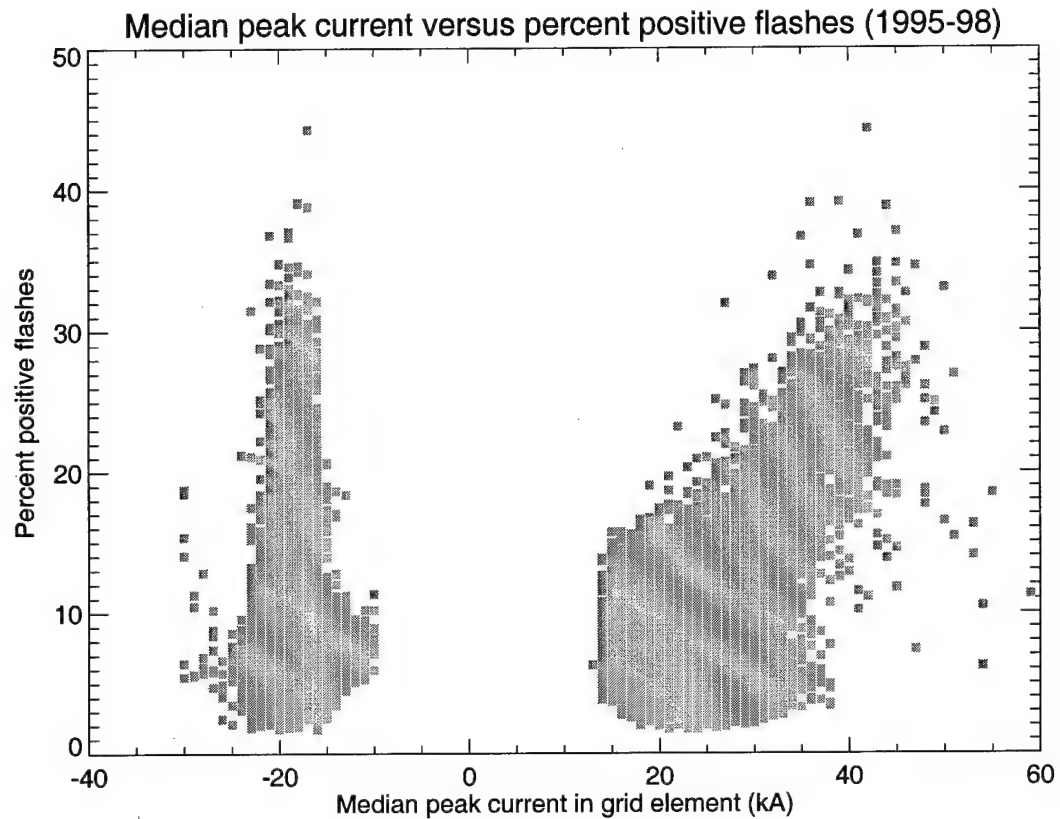


Figure 34. Scatter plot of median peak current and percent positive flashes. The median peak currents were plotted against the percentage of all measured flashes that lowered a net positive charge to ground for each 0.2 by 0.2 degree grid element over the US. Points with positive median peak currents indicate positive flashes while negative flashes are those with negative peak currents.

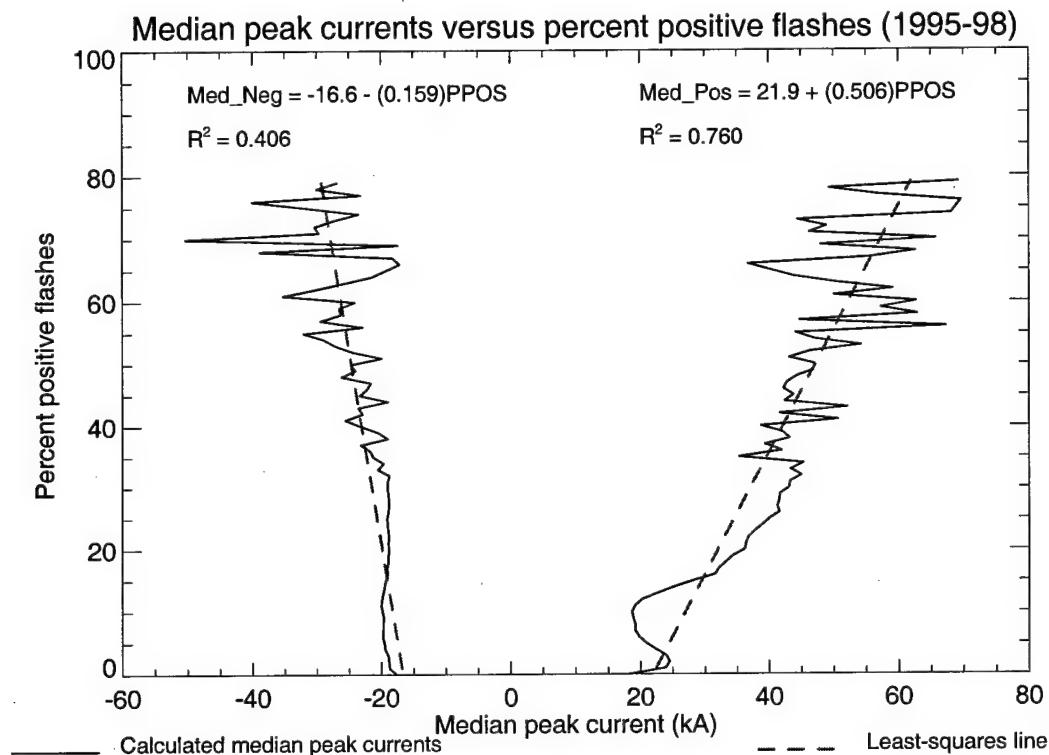


Figure 35. Direct comparison of median peak currents and percent positive flashes. The solid lines indicate the median peak currents calculated for each percentage change in the percent positive flashes. Dashed lines are the lines of best fit using least squared approximations. Equations for these lines are included with the portion of variability explained by them (R^2).

Table 9. Peak current characteristics based on percent positive flashes.

Minimum of increment in percent positive flashes	Median of negative peak currents (kA)	Median of positive peak currents (kA)	Minimum of increment in percent positive flashes	Median of negative peak currents (kA)	Median of positive peak currents (kA)
0.0	-17.60	18.20	40.0	-23.10	38.80
1.0	-18.70	23.90	41.0	-25.50	50.70
2.0	-18.80	24.50	42.0	-22.90	41.70
3.0	-18.90	24.00	43.0	-23.50	52.10
4.0	-19.40	22.40	44.0	-18.90	42.50
5.0	-19.50	20.90	45.0	-23.30	43.80
6.0	-19.80	19.80	46.0	-22.20	42.30
7.0	-19.70	19.20	47.0	-21.60	42.80
8.0	-19.70	19.20	48.0	-26.10	44.30
9.0	-19.60	18.90	49.0	-24.00	46.90
10.0	-19.80	18.70	50.0	-24.70	47.10
11.0	-20.00	19.20	51.0	-19.90	43.20
12.0	-19.90	20.30	52.0	-24.40	46.40
13.0	-19.70	22.70	53.0	-27.10	54.20
14.0	-19.50	25.30	54.0	-28.90	47.10
15.0	-19.30	28.30	55.0	-32.00	44.20
16.0	-19.00	31.60	56.0	-22.90	67.30
17.0	-19.10	32.20	57.0	-29.40	44.80
18.0	-18.90	33.30	58.0	-26.30	62.90
19.0	-18.90	34.40	59.0	-26.50	57.30
20.0	-18.80	36.20	60.0	-24.10	62.70
21.0	-18.90	36.40	61.0	-35.20	50.10
22.0	-18.80	36.80	62.0	-30.30	59.10
23.0	-18.90	37.80	63.0	-25.80	50.50
24.0	-19.00	39.00	64.0	-21.40	43.90
25.0	-19.10	40.10	65.0	-27.90	137.30
26.0	-18.90	41.60	66.0	-17.10	36.80
27.0	-18.80	41.30	67.0	-18.20	55.60
28.0	-18.80	41.60	68.0	-38.80	62.60
29.0	-18.90	41.70	69.0	-17.40	48.10
30.0	-19.00	43.10	70.0	-50.30	65.70
31.0	-19.00	43.30	71.0	-29.70	46.30
32.0	-18.70	45.00	72.0	-30.30	48.90
33.0	-20.50	43.40	73.0	-27.40	44.50
34.0	-19.60	45.30	74.0	-23.50	68.10
35.0	-21.20	35.40	75.0	0.00	60.50
36.0	-21.70	42.00	76.0	-40.00	69.60
37.0	-23.10	39.40	77.0	-23.20	56.80
38.0	-19.00	43.20	78.0	-30.00	49.40
39.0	-20.40	42.10	79.0	-26.90	69.20

$$Med_Neg = -16.6kA - 0.159kA \cdot percent^{-1}(PPOS) \quad (11)$$

$$\text{and} \quad Med_Pos = 21.9kA + 0.506kA \cdot percent^{-1}(PPOS) \quad (12)$$

where Med_Neg and Med_Pos are the median peak negative and positive currents, respectively and PPOS is the percentage of positive flashes. Correlation coefficients for these relationships are 0.637 and 0.872 for negative and positive flashes, respectively.

Comparing Equations (11) and (12), positive lightning is approximately four times as sensitive to changes in the percentage of positive flashes as are negative flashes. This may be because of the larger number of negative flashes that would tend to dampen out any changes in the median peak currents from the relatively small number of high peak negative currents. As stated before, it is not intuitively obvious why the median peak currents for negative flashes are affected by the percentage of positive flashes in a storm.

One possible explanation for the variations in negative peak currents with changes in the percentage of positive flashes can be found by examining at the latitudinal dependence of the percent positive flashes (Fig. 36). There is a positive relationship between the percent positive flashes and latitude while a negative relationship exists between the median peak negative currents and latitude (Fig. 19). The decrease in median peak negative currents with an increase in percent positive flashes could be a result of the decrease in negative peak current with increasing latitude.

1. Surface elevation and the effect on peak currents

The median peak negative currents (Fig. 21) tend to follow the terrain. For the most part, there are higher peak currents in the lower elevations and weaker peak currents in the

Appalachian Mountains, Eastern New York, Vermont, and New Hampshire. There does not seem to be a corresponding relationship for positive flashes (Fig. 20).

A further comparison of the median peak negative currents and the surface elevations (Fig. 37) shows an inverse relationship between the two quantities. Along the East Coast and through Florida, the negative peak currents are large (> 21 kA) while the surface elevations are low (< 100 m MSL). The same conditions extend along the Gulf Coast and north through Alabama, Mississippi, Louisiana, and Eastern Arkansas. This relationship may also be found along the West Coast of the US. The opposite is true in the Appalachians where, in general, the median peak currents for negative flashes are a minimum.

A scatter plot of the median peak currents and surface elevations using the values in the 0.2 by 0.2 degree grid elements for the US (Fig. 38) shows a decrease in negative peak currents with increasing surface elevation. Positive flashes actually increase in strength through the lowest 1000 m of elevation (Table 10) then remain unchanged until approximately 2.5 km where the peak currents decrease with altitude (Fig. 39).

Changes in peak currents, especially for negative flashes, may be a result of the changes in atmospheric pressure, which could affect the return stroke velocities (Griffiths and Phelps 1976). If this were the case, then there should be a more logarithmic tendency to the peak current changes and both negative and positive flashes should behave in the same manner. They do not. Another possibility is that the peak current strength is related to the length of the lightning channel. This would allow for the differences seen in the negative and positive flashes as the positive flashes are observed to originate in the upper regions of the cloud and the negative flashes are thought to originate in the lower negative charge

regions. This lower negative charge region tends to be found near the same temperature level in the cloud and would result in an overall shorter channel length as the surface elevation increases. This will be discussed further in the conclusions.

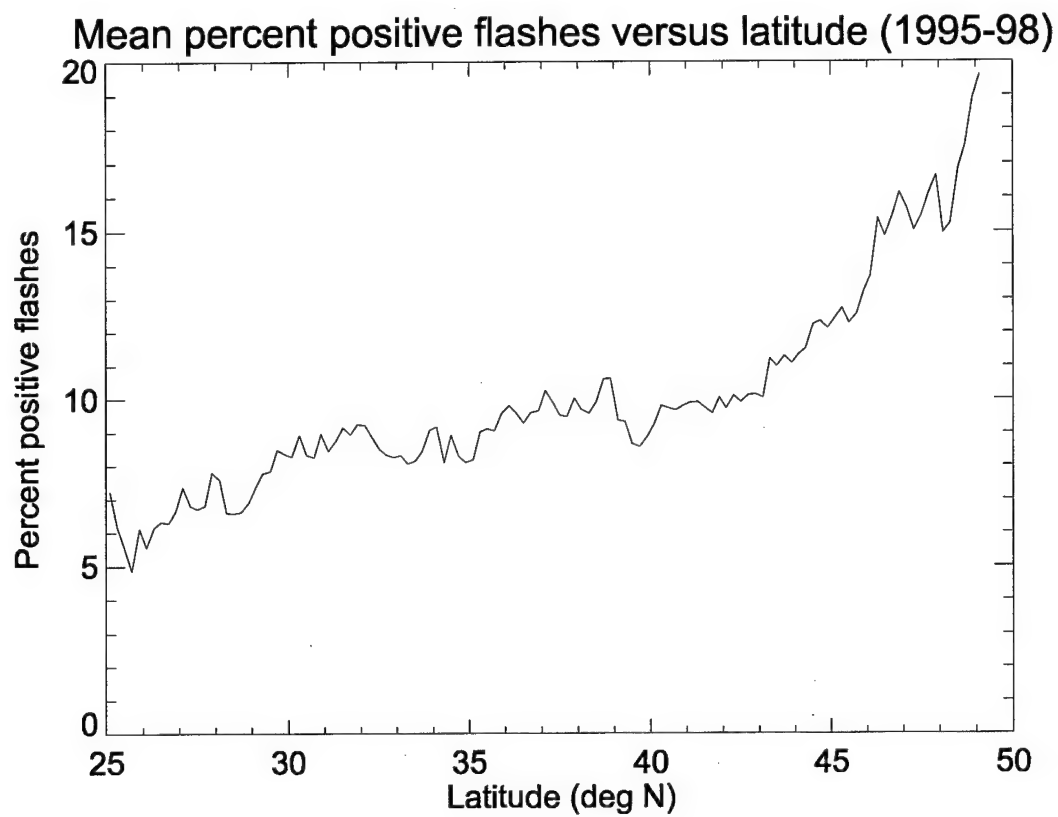


Figure 36. Latitudinal dependence of percent positive flashes. The percentage of all measured flashes from 1995 – 98 were found for each degree latitude.

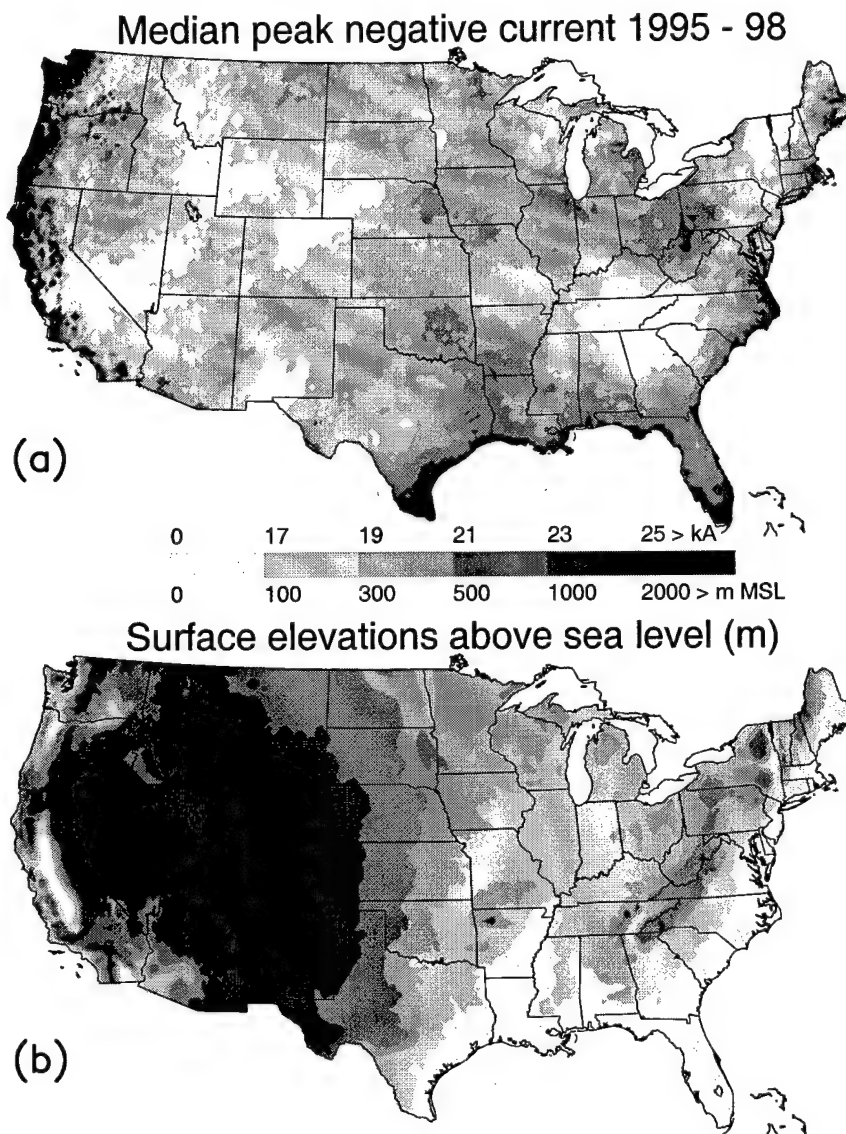


Figure 37. Contours of median peak negative currents and surface elevations. The median peak currents (a) are displayed from 1995 – 98 along with the surface elevations (b) above sea level (MSL). The values above the legend indicate the contour levels for the median peak negative currents, while the values below the legend are the surface elevations. Values were contoured for a 0.2 by 0.2 degree latitude and longitude grid over the US.

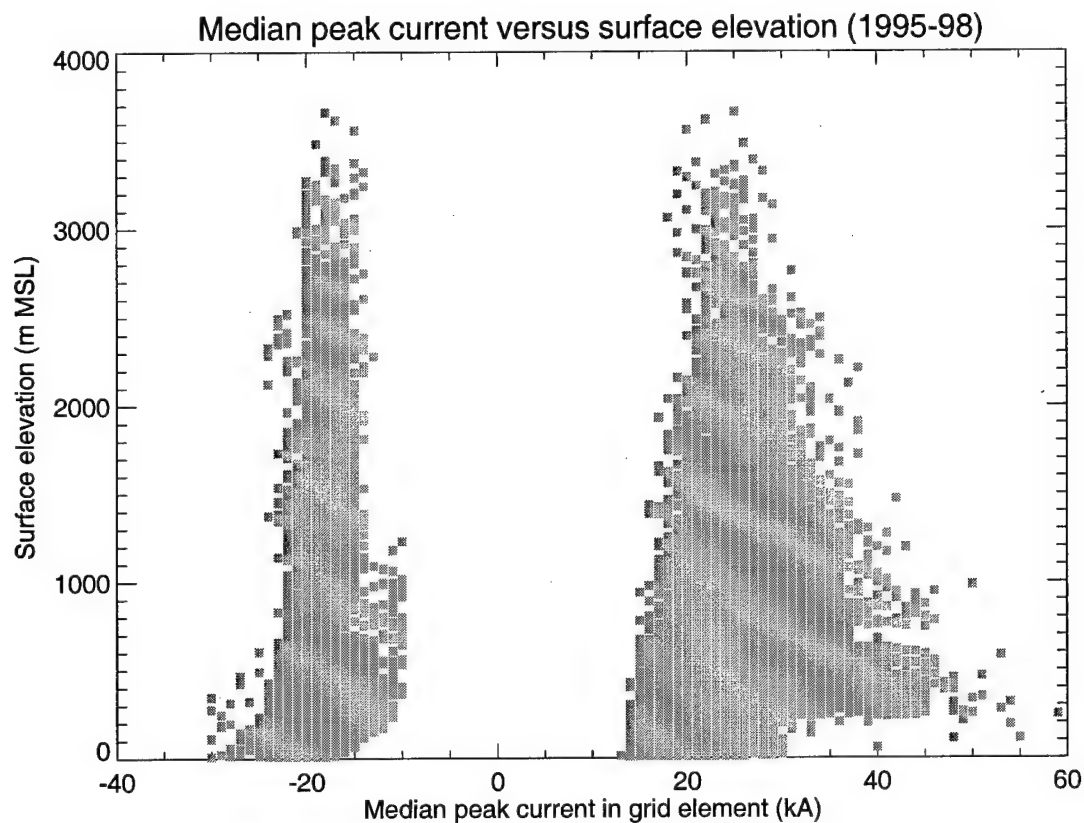


Figure 38. Scatter plot of median peak currents and surface elevations. The median peak currents and surface elevations found for a 0.2 by 0.2 degree latitude and longitude grid over the US are plotted. Points with positive median peak currents indicate positive flashes while negative flashes are those with negative peak currents.

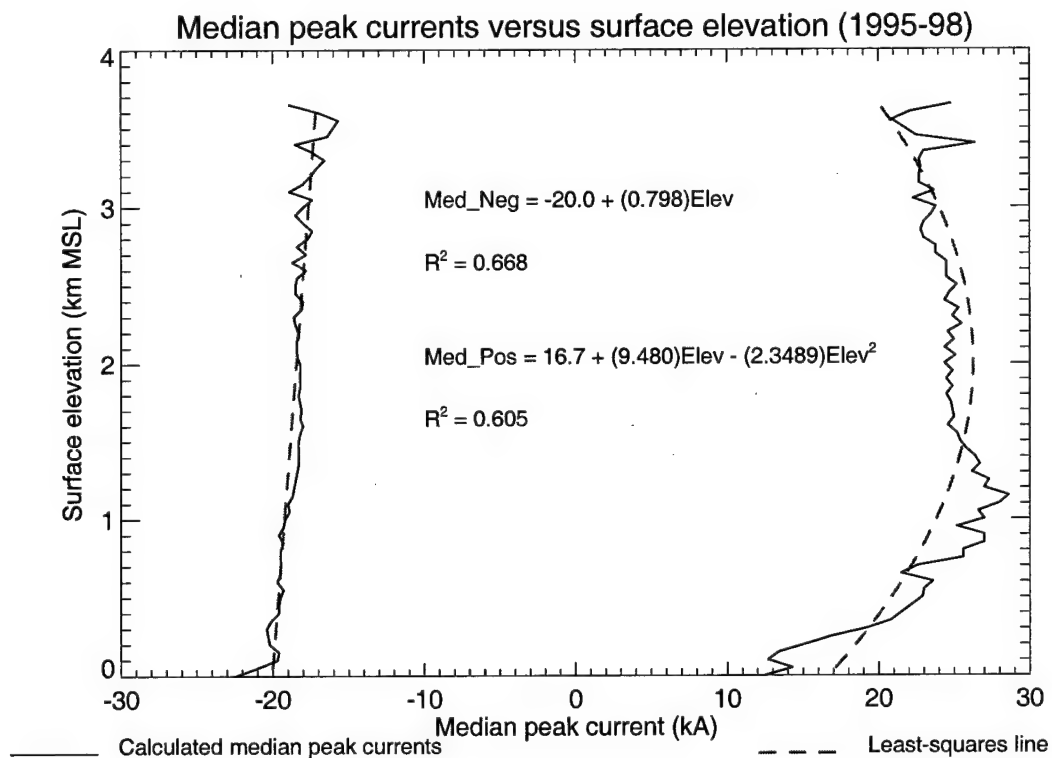


Figure 39. Direct comparison of median peak currents and surface elevations. The solid lines indicate the median peak currents for all 0.2 by 0.2 degree grid elements over the US within a 50 m surface elevation interval. Dashed lines are the lines of best fit using least squared approximations. Equations for these lines are included with the portion of variability explained by them (R^2).

Table 10. Peak current characteristics based on surface elevation.

Minimum of increment in surface elevation (m MSL)	Median of negative peak currents (kA)	Median of positive peak currents (kA)	Minimum of increment in surface elevation (m MSL)	Median of negative peak currents (kA)	Median of positive peak currents (kA)
1.0	-22.40	12.50	1751.0	-18.20	24.80
51.0	-21.00	14.30	1801.0	-18.30	24.50
101.0	-19.70	12.70	1851.0	-18.20	24.90
151.0	-19.60	13.40	1901.0	-18.20	24.50
201.0	-20.20	15.20	1951.0	-18.20	24.90
251.0	-20.30	16.90	2001.0	-18.20	24.40
301.0	-20.40	19.20	2051.0	-18.40	25.10
351.0	-20.10	20.80	2101.0	-18.40	24.40
401.0	-19.60	21.50	2151.0	-18.40	25.00
451.0	-19.60	22.20	2201.0	-18.30	24.60
501.0	-19.50	22.90	2251.0	-18.50	25.50
551.0	-19.30	23.00	2301.0	-18.60	24.90
601.0	-19.70	23.60	2351.0	-18.10	25.30
651.0	-19.50	21.50	2401.0	-18.00	24.40
701.0	-19.50	22.60	2451.0	-18.50	24.70
751.0	-19.50	25.60	2501.0	-18.50	25.20
801.0	-19.50	25.60	2551.0	-18.40	24.50
851.0	-19.30	27.00	2601.0	-17.80	24.50
901.0	-19.60	27.00	2651.0	-18.70	24.50
951.0	-19.30	25.20	2701.0	-17.80	23.80
1001.0	-19.20	27.00	2751.0	-18.40	23.80
1051.0	-18.90	26.60	2801.0	-17.70	23.00
1101.0	-19.00	28.00	2851.0	-17.40	22.80
1151.0	-18.70	28.60	2901.0	-18.00	23.00
1201.0	-18.60	27.00	2951.0	-18.50	23.50
1251.0	-18.50	27.30	3001.0	-18.00	23.80
1301.0	-18.40	26.20	3051.0	-17.40	22.30
1351.0	-18.30	26.70	3101.0	-18.90	23.70
1401.0	-18.30	26.40	3151.0	-18.00	22.70
1451.0	-18.30	25.80	3201.0	-17.50	22.70
1501.0	-18.30	25.40	3251.0	-17.10	22.80
1551.0	-18.20	25.20	3301.0	-16.60	22.70
1601.0	-18.00	24.60	3351.0	-17.40	23.00
1651.0	-18.20	25.00	3401.0	-18.50	26.40
1701.0	-18.10	24.90	3451.0	-16.40	22.50

CHAPTER VI

SEASONAL AND SMALL-SCALE VARIATIONS IN PEAK CURRENT

From the studies of the large scale variations in peak currents, a connection was found between peak current strength and latitude, sensor separation, flash density, the percentage of flashes lowering positive charge to ground, and the surface elevations. The number of variations adds enough complexity to the problem of determining the source of the variations that it becomes important to look at individual cases for additional insight. An additional factor that must be considered is the effect of seasonal variations. Smaller scale fluctuations in the peak currents will then be examined using case studies. As the sensor separation is a rather obvious contributor to the peak current variations, cases will be selected in regions without large variations in the distances to NLDN sensors.

A. Seasonal variations in peak currents

The median peak currents for the United States were calculated for each month of each year from 1995 – 98 and for each month of all the years combined (Table 11). As in the previous portion of this work, the lightning data were limited to the landmass of the United States and positive flashes were restricted to those with peak currents at or above 10 kA to reduce the chance of contamination by weaker intracloud flashes. No restriction to peak current strength was imposed on the negative cloud-to-ground flashes.

Positive lightning had larger peak currents than negative flashes for most of the year (Fig. 40). The exception to this was during July and August when the median peak currents for positive lightning become weaker than for negative flashes. There are other months during the summers when the median peak positive current was very close in magnitude to

Table 11. Monthly median peak currents for the US landmass.

Month	Flash counts	Negative flashes	Positive flashes	Percent positive	Median peak positive currents (kA)	Median peak negative currents (kA)
Jan 95	166866	134635	30404	18.2	28.1	-23.8
Feb 95	156846	138032	17631	11.2	27.2	-23.2
Mar 95	434007	371162	60067	13.8	26.7	-21.0
Apr 95	765783	643423	118096	15.4	23.0	-20.2
May 95	2221699	1944926	269592	12.1	21.4	-19.4
Jun 95	3291778	3065259	221605	6.7	21.8	-20.5
Jul 95	4397098	4147914	243922	5.5	20.3	-21.8
Aug 95	3401219	3211666	185683	5.5	18.9	-21.8
Sep 95	1602808	1501147	98072	6.1	22.4	-20.0
Oct 95	334870	295784	37657	11.2	23.5	-20.2
Nov 95	200374	165410	33161	16.5	21.4	-20.3
Dec 95	155897	123352	30395	19.5	24.5	-26.8
Jan 96	83741	60687	21659	25.9	28.1	-19.0
Feb 96	131828	104291	26367	20.0	25.3	-19.9
Mar 96	401046	334087	64144	16.0	25.2	-19.5
Apr 96	806481	687538	114927	14.3	23.1	-19.6
May 96	2550554	2237291	305930	12.0	20.5	-19.5
Jun 96	3867416	3591288	270339	7.0	20.6	-20.4
Jul 96	4692826	4381736	305668	6.5	19.1	-19.9
Aug 96	3784881	3559301	220644	5.8	19.7	-19.6
Sep 96	1948417	1770797	174525	9.0	18.6	-19.0
Oct 96	546012	473924	70549	12.9	19.0	-18.7
Nov 96	243679	200422	41739	17.1	25.3	-17.8
Dec 96	117325	95710	20430	17.4	24.9	-20.5
Jan 97	229140	189410	38107	16.6	22.3	-18.6
Feb 97	108954	81494	26041	23.9	27.0	-18.1
Mar 97	391691	323721	65527	16.7	23.5	-18.2
Apr 97	838927	724724	110604	13.2	21.9	-19.0
May 97	2018348	1798587	214983	10.7	19.0	-19.0
Jun 97	3720194	3390532	322984	8.7	19.8	-19.4
Jul 97	4956669	4631363	319391	6.4	18.2	-20.0
Aug 97	3398438	3186460	208457	6.1	19.1	-19.5
Sep 97	1679374	1566719	110180	6.6	22.3	-19.1
Oct 97	507193	441904	63482	12.5	20.6	-18.5
Nov 97	199352	166782	31329	15.7	22.6	-19.6
Dec 97	63902	49474	13534	21.2	27.5	-22.6

Table 11 (continued)

Month	Flash counts	Negative flashes	Positive flashes	Percent positive	Median peak positive currents (kA)	Median peak negative currents (kA)
Jan 98	297249	241749	53167	17.9	24.0	-21.5
Feb 98	252612	200579	49965	19.8	26.3	-17.7
Mar 98	512361	430897	79231	15.5	23.2	-17.3
Apr 98	647115	536811	105805	16.4	23.1	-15.7
May 98	2030641	1701812	315407	15.5	28.6	-16.5
Jun 98	4263731	3859453	395452	9.3	18.4	-17.8
Jul 98	5173013	4836748	329575	6.4	18.7	-19.0
Aug 98	4000963	3768585	229011	5.7	17.9	-19.1
Sep 98	1419458	1326039	91809	6.5	19.7	-17.5
Oct 98	794729	682741	109513	13.8	20.6	-19.7
Nov 98	130048	107655	21436	16.5	25.1	-19.2
Dec 98	20681	14538	5757	27.8	31.5	-19.0
Summary for the years 1995 – 98						
Jan	229164	189429	38114	16.6	22.3	-18.6
Feb	108949	81492	26038	23.9	27.1	-18.1
Mar	391710	323745	65522	16.7	23.5	-18.2
Apr	838880	724709	110571	13.2	21.9	-19.0
May	2018172	1798417	214977	10.7	19.0	-19.0
Jun	3719938	3390306	322951	8.7	19.8	-19.4
Jul	4956509	4631179	319411	6.4	18.2	-20.0
Aug	3396913	3184902	208326	6.1	19.1	-19.5
Sep	1679309	1566674	110162	6.6	22.3	-19.1
Oct	507240	441939	63493	12.5	20.6	-18.5
Nov	199401	166820	31340	15.7	22.6	-19.6
Dec	63912	49484	13534	21.2	27.5	-22.6

Monthly median peak currents for the US landmass

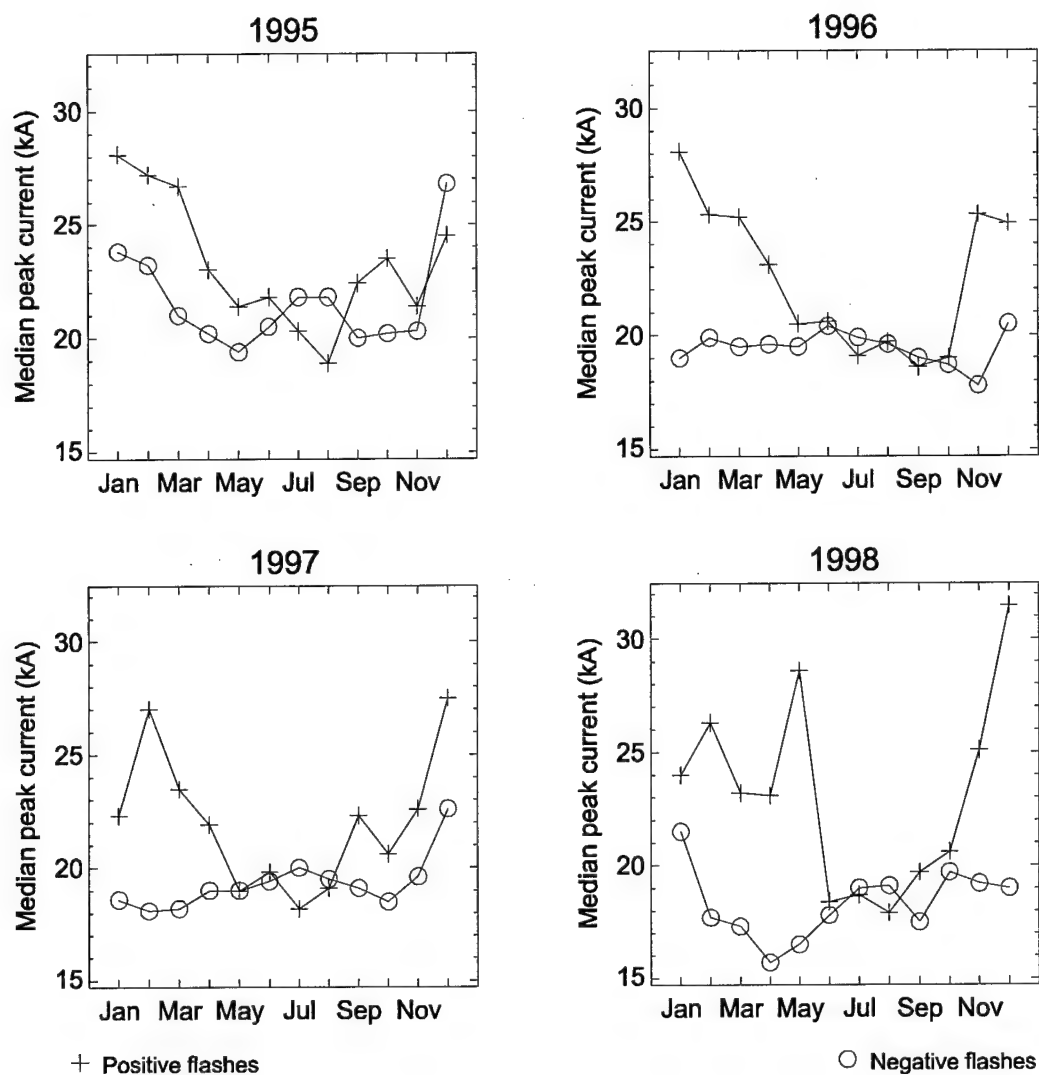


Figure 40. Monthly median peak currents for the US landmass. The median peak currents of all lightning over the US landmass for each month of each year from 1995 – 98 are shown. Positive flashes have larger median peak currents than do negative flashes except in the summer months and during December 1995. Positive lightning with peak currents less than 10 kA were not included in the calculations in an attempt to eliminate the contamination of the data by intracloud flashes.

that of negative flashes. This summertime switch in peak currents could be a result of more convective thunderstorms, such as those caused by sea breezes or differential heating of the surface, occurring in the summer months than during the rest of the year. In all the winter months, except December of 1995, the median peak positive currents were greater than for negative flashes, often by more than 4 kA.

B. Small scale variations in peak currents

The Northern Plains of the United States experience cloud-to-ground lightning with a high percentage of positive flashes and consistently high peak currents for positive flashes. As such, the lightning data for this region were separated from the national data set and the characteristics were studied in greater detail. In particular, the percentage of positive flashes and the median peak currents are examined for this region on a daily basis. Certain days are then examined with upper air data to determine any relationship between the lightning parameters and vertical wind shear or the height of the freezing level.

In an attempt to eliminate any bias that may exist in the data set from the Northern Plains, other storm cases were examined which extended into the Southern Plains states. For these cases, the peak currents were analyzed using time-series analysis techniques to determine if there is a pattern in the increasing and decreasing values of peak currents during storms. Also, a special case was included of a storm system that originated in western Texas and traveled through North Dakota in 24 hours (Fig. 41). The average ground speed of this storm was approximately 27 m sec^{-1} and the percentage of positive flashes exceeded 50 percent throughout its lifetime. This storm spawn several tornadoes that injured at least 47 people and caused over \$16 million in property damage in southeast Iowa and other wind damage throughout the Great Plains.

Plot of lightning for 15 May 98 storm
(15 May 98 0400 UTC - 16 May 98 0500 UTC)

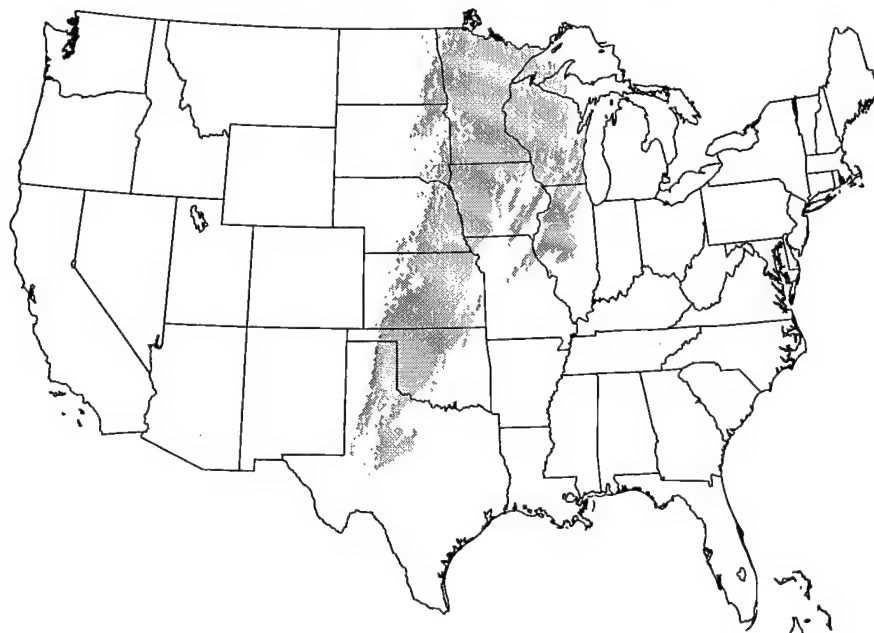


Figure 41. Plot of the lightning data for the 15 May 98 case. The lightning data from 15 May 98 0400 UTC – 16 May 98 0500 UTC are plotted to show the extent of the storm system.

C. Lightning in the Northern Plains

Lightning in the northern plains has a high percentage of positive flashes (Fig. 33) and higher peak currents for positive flashes than most other regions of the country (Fig. 20). To perform a more detailed analysis of this region, lightning data were isolated in the general area of increased percent positive flashes and positive peak currents (Fig. 42). The distributions of peak currents (Fig. 43) are similar to the distributions found in the Northern regions previously analyzed (Fig. 17). In this case, the mode of the positive peak currents is 13 kA, which is above the 10 kA threshold that is used to separate intracloud flashes from cloud-to-ground lightning (Cummins et al. 1998). Negative flashes have a mode at 15 kA.

The diurnal pattern of lightning in the Northern Plains (Fig. 44) shows a maximum in hourly flash counts at 0300 UTC with the minimum at 1700 UTC. This translates to a nocturnal maximum in the lightning activity (2100 Local time) and a minimum in the late morning (1000 Local time). Using the minimum in lightning activity at 1700 UTC as a starting point, daily lightning statistics were found for each 24 hour period with lightning (Appendix A). Each of these 24 hour periods will be hereafter referred to as a day, even though it begins at 1700 UTC.

A scatter plot of the percentage of all flashes lowering positive charge to ground (percent positive flashes) and the median peak currents for each 24 hour period shows a positive correlation for positive lightning, but no apparent connection for negative flashes (Fig. 45). Brook et al. (1982) state a requirement of vertical wind shear before positive lightning was found in wintertime thunderstorms in Japan; implying a need for tilt within the thunderstorm before positive charge may be transferred to the ground.

Data region for Northern Plains

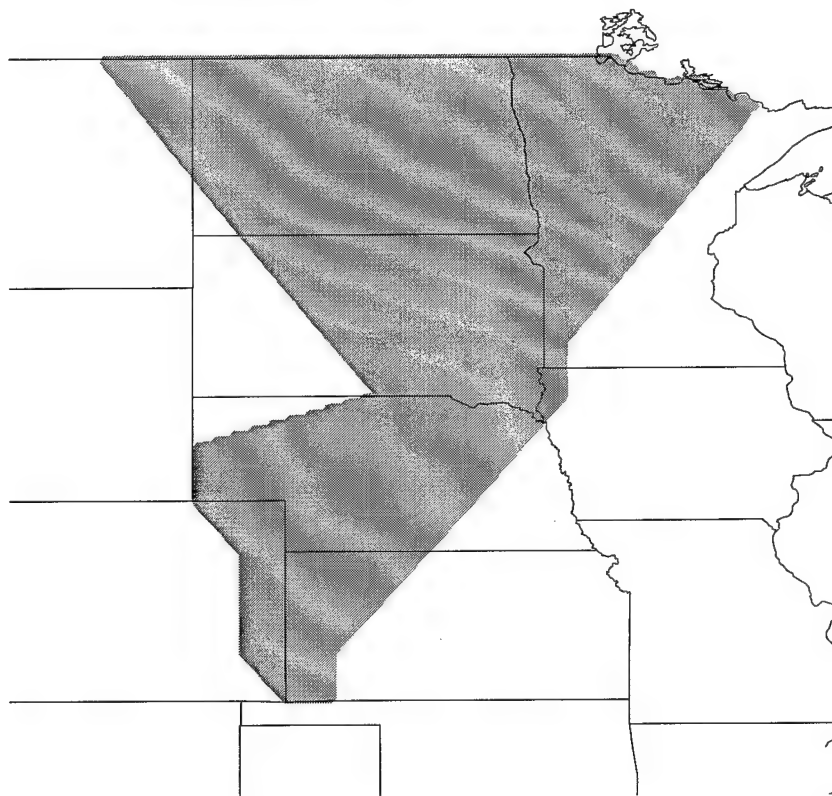


Figure 42. The region used to select data for the Northern Plains study. The data were restricted to this region of the US for a study of the peak currents. This region represents the general area of high peak positive currents and the high percentage of positive flashes in the US.

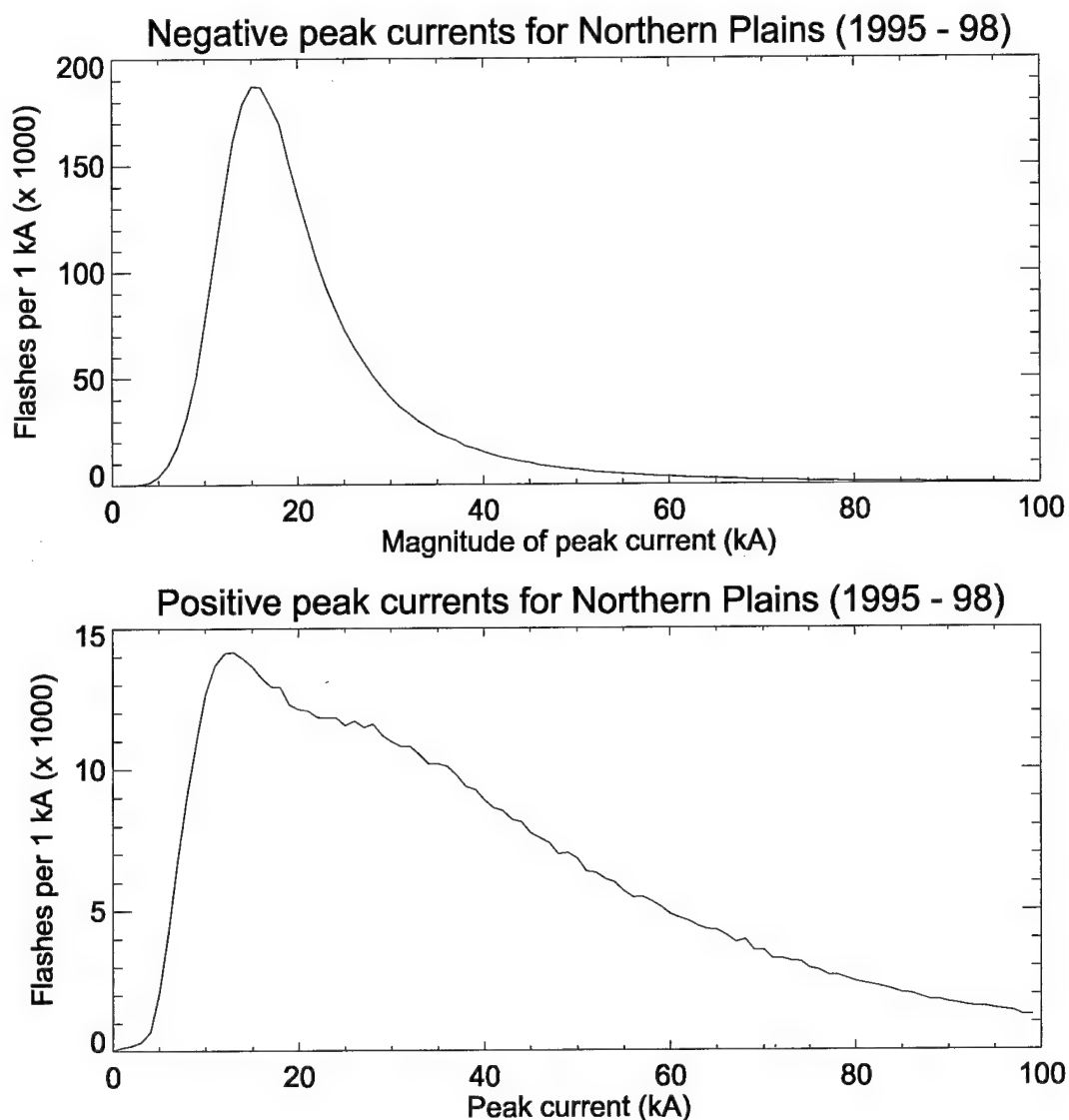


Figure 43. Peak current distribution for the Northern Plains region of the US. The peak currents for the Northern Plains region from 0 – 100 kA are shown. No restrictions were placed on these data, but positive flashes with peak currents less than 10 kA may be misidentified intracloud flashes.

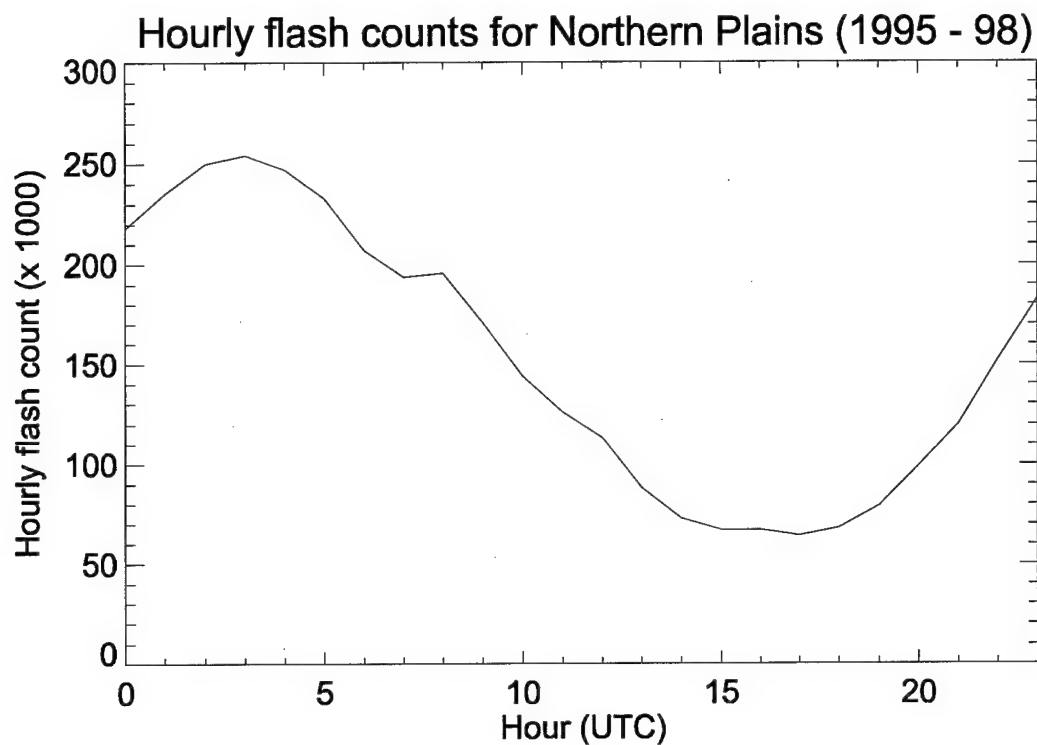


Figure 44. Diurnal flash rates for the Northern Plains region. The flash counts for each hour of the day using lightning data from the Northern Plains region from 1995 – 98. No positive flashes were included with peak currents less than 10 kA in order to exclude intracloud flashes that may contaminate the data set.

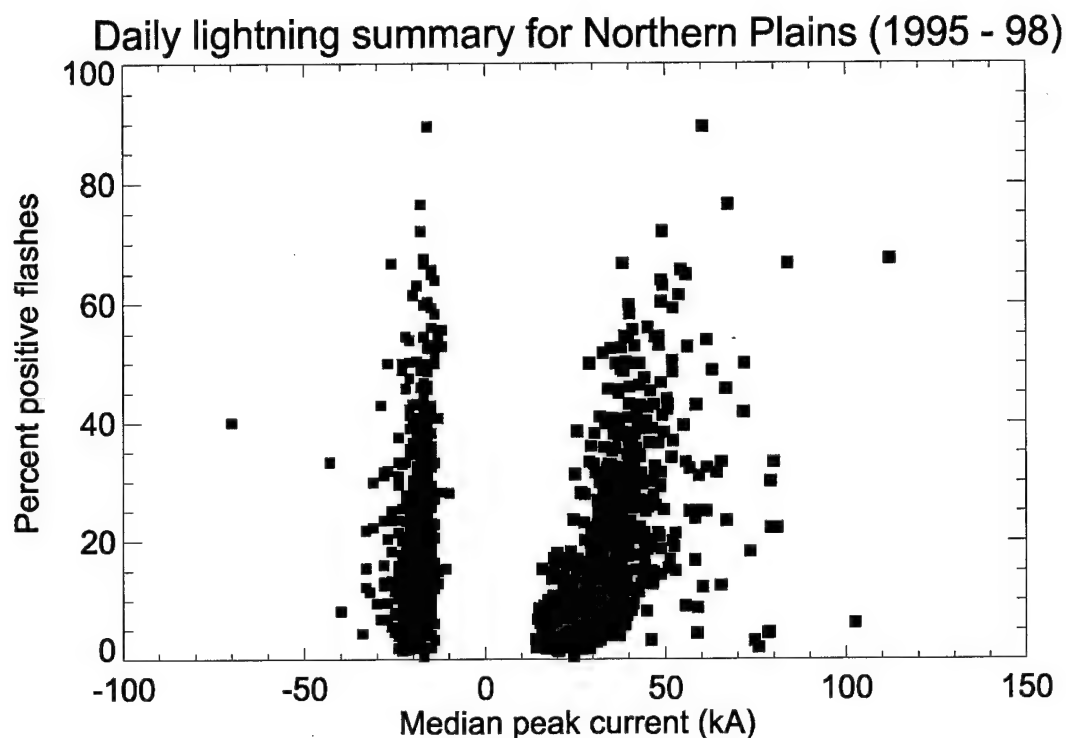


Figure 45. Daily lightning summary for the Northern Plains (1995 – 98). The medians of peak currents are compared with the percentages of positive flashes for each day having lightning in the Northern Plains. The patterns are similar to the results for the US (Fig. 34). Positive flashes having peak currents less than 10 kA were not included in the data as they may be misidentified intracloud flashes. No restriction was placed on negative flashes.

Select cases were examined in the Northern Plains to see if such a requirement exists in this region. These cases were limited to days when the percent positive flashes were either less than or equal to 5 percent or at least 50 percent resulting in 33 cases. Of these, 18 days had no more than 5 percent positive flashes and 15 days had at least 50 percent positive flashes. A summary can be found in Table 12.

As the lightning data used for these cases were from 1700 UTC and included the following 24 hours, upper air data from 0000 UTC during the cases were used. The wind shears were calculated from the surface to the 850, 500, 300, 250, and 200 mb levels. Wind shear is the geometric summation of the differences in speed in the east and west directions from the given pressure level and the surface divided by the distance between levels and has units of sec^{-1} . Plots of the lightning data and the vertical wind shears can be found in Appendix B.

No connection between vertical wind shear and any of the lightning parameters appear to exist. There are days when there is strong wind shear from the surface to 850 mb that have a low percentage of positive flashes and weak positive peak currents and others where the percent positive flashes are high along with the positive peak currents. This lack of any pattern exists for each level of vertical wind shear. It appears that the criteria used for positive lightning in wintertime storms in Japan do not apply to mid-latitude storms in the Northern Plains of the United States.

In order to test the theory that that channel length affects the peak current strength, the height of the -10°C temperature level was found for each of the soundings. The main negative charge region of the thunderstorm is typically found near this level (Stolzenburg et al. 1998). Using this temperature as an indication of the negative charge region, one should

see a connection between this height and the median peak negative currents, assuming the negative flashes originate in the main negative charge region of the cloud. The heights of the -10°C levels for all sounding locations in the cases studied are found in Appendix C.

No apparent connection was found between the -10°C level and the negative peak currents. This does not eliminate the possibility of a relationship between the peak current of a lightning stroke and the channel length. It does mean that there is not a connection between the median of all peak currents for negative flashes and the -10°C height. The height of the main negative charge region in the thunderstorm may be different than this temperature level. The larger variation in peak currents for negative flashes could also be a result of the discharge originating from the upper negative charge region of the storm. This would tend to happen more often during storms with a higher percentage of positive flashes, if the percentages of positive flashes are an indication of the tilt of the storms. It may be impossible to prove that assumption within this work.

The Convective Available Potential Energy (CAPE) was found for sounding in each of the cases studied. There was no connection between the CAPE and the peak currents for these cases. A summary of CAPE values may be found in Appendix D.

D. Other case studies

Additional storms were identified through the Plains states in the period from 1995 – 98. To avoid adding the influence of other storms and to make the isolation of lightning data simpler, storms were selected that were isolated from nearby systems. Each storm needed to have a beginning point and an end over land. As each storm was tracked, some merged with other storms to form a larger system. In these cases, every attempt was made

to include all the lightning for the whole system, from beginning to end. A summary of the storms selected can be found in Table 2.

These cases are used in an attempt to identify any characteristic pattern that may exist with the lightning throughout the life of the storms. Time series analysis techniques are used to determine the correlation of lightning parameters at different times in the storm. Specifically, once the data were isolated, the mean peak current of the three flashes in the 5 minute window having the largest magnitude in peak current was found. In other words, the three positive flashes with the strongest peak signal strength were found in each 5 minute window and the average peak current for those three flashes was calculated. The same procedure was followed for negative flashes. If there were less than 3 flashes in the time interval, then a value of zero was reported. The number of flashes in each 5 minute interval were also found for positive and negative flashes. To illustrate the point, the positive peak currents from Case 98051504 are plotted along with the mean of the 3 most intensive peak currents during each 5 minute interval (Fig. 46).

As the flash counts and means of the three extreme peak currents are equally spaced in time, time series analysis may be used to determine if there is a pattern in the peak currents. An example of the process is shown in Figure 47 for positive flashes in case 98051504. The averages of the top three positive peak currents are plotted in Figure 46a against time as thin gray lines. The peak currents seem to increase between 200 and 400 minutes into the storm file, or from the beginning of the lightning data. There appears to be a gradual decrease in the peak current values until the end of the positive lightning in the storm. A shorter cycle wave pattern seems to be superimposed on the overall rise and

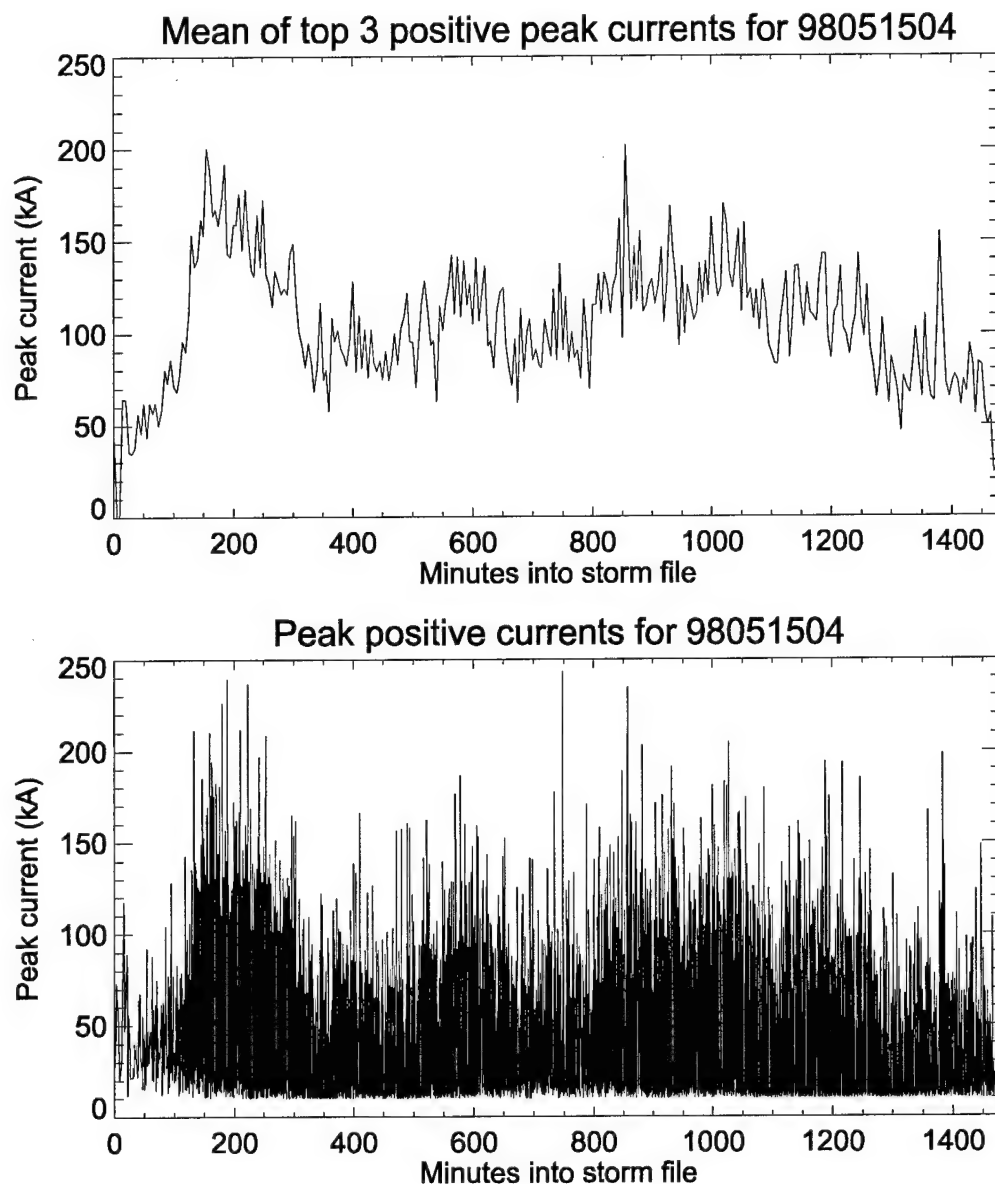


Figure 46. Time series of positive peak currents for 15 May 1998 storm. All peak currents are plotted for the 15 May 1998 storm and the average of the 3 highest peak currents within each 5 minutes of the storm are shown. No positive flashes with peak currents less than 10 kA were included, as they may be misidentified intracloud flashes.

Data summary for case 98051504

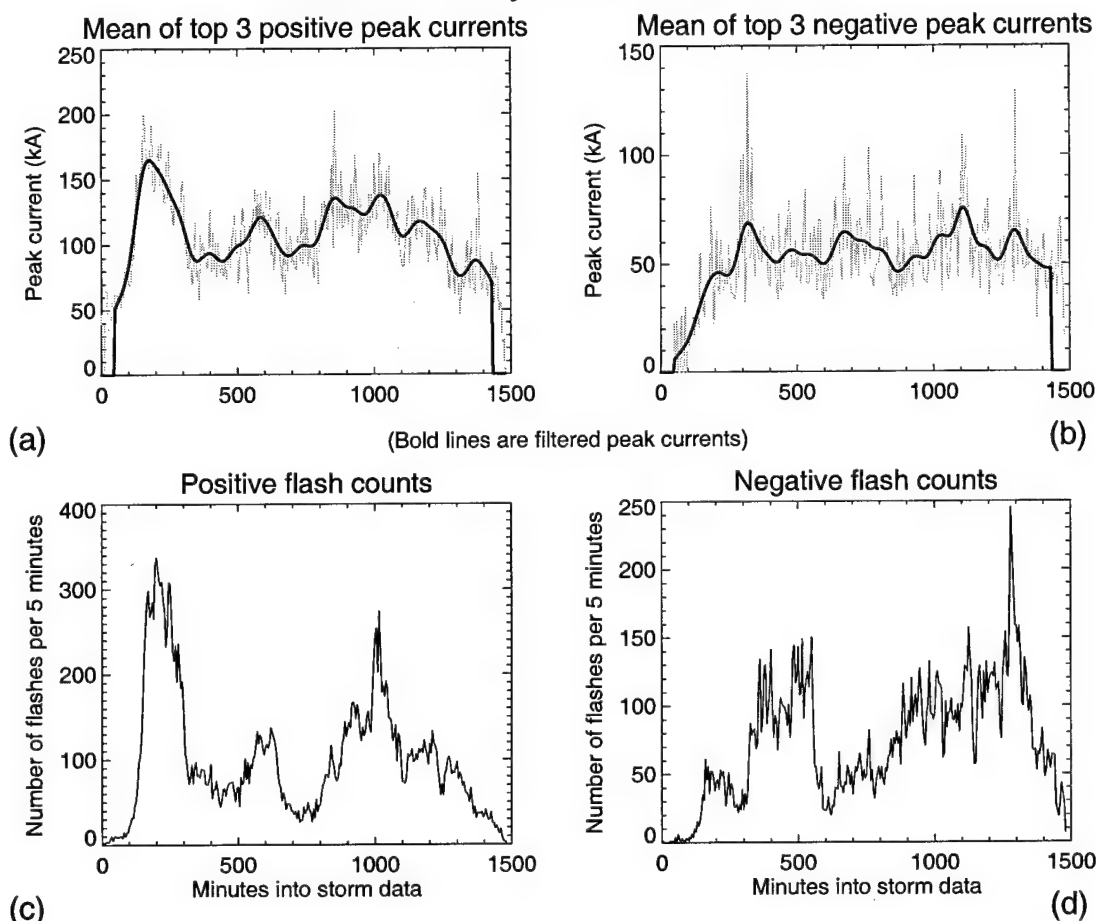


Figure 47. Maximum peak currents and flash counts for the 15 May 1998 storm. Data are plotted for every 5 minutes. The peak currents shown in the thin gray lines for positive (a) and negative flashes (b) are the averages of the 3 highest peak current values in the 5 minute interval. If there were less than 3 flashes in the 5 minute interval, then the values were set to zero. The time reference is from the first flash in the data file. It is possible that there were data that were not included in the files. For positive flash counts (c), no flashes with a peak current less than 10 kA were included. No such restriction was placed on the negative lightning (d).

decay of the peak currents. In order to examine this feature, band-pass filters were applied to the data until a central frequency was found yielding the smallest least squared residual error when compared with the original data. This frequency provided the best description of the overriding wave patterns and the periods of the waves. The bold line (Fig. 47a) indicates the data after a band-pass filter was applied. This filter represents waves having periods from 71 – 73 minutes. The negative flashes are displayed in the same fashion (Fig. 47b), but the periods used in this filter ranged from 72.5 – 74.5 minutes. The flash rates for each of the 5 minute increments are displayed for positive and negative flashes (Fig. 47c and 47d, respectively) with the times aligned below the peak current plots.

The positive flash rates (Fig. 47c) indicate growth and decay of the storms throughout the life of the system. There are similar variations in the average of the largest peak currents for the same 5 minute windows (Fig. 47a). There appears to be a direct correlation between the increase in the positive flash rates for this case and the increase in positive peak currents. The negative flashes also demonstrate growth and decay in the flash rates (Fig. 47d) during the period, but the strongest negative peak currents in the storm system (Fig. 47b) do not follow the same pattern.

All of the storms studied behave in a similar fashion (Appendix E). The periods of the band-pass filters used in identifying the waveform of the peak currents vary from storm to storm (Table 12), but the characteristic times for the waves in each storm vary no more than 5 minutes between positive lightning and negative lightning. If these waves were indicative of the growth and decay of storm cells, then the similarity of positive and negative peak current periodicity within each storm system would be expected. The time

Table 12. Periods of band-pass filters used for each case study. Case IDs are in the format YYMMDDHH for the start of the storm, where YY is the year, MM is the month, DD is the day, and HH is the hour.

Case	Date and time of first flash (UTC)	Date and time of last flash (UTC)	Periodicity of positive peak currents (min)	Periodicity of negative peak currents (min)
95022712	02/27/95 21:00:15	02/28/95 11:58:36	45.0	46.0
95032420	03/25/95 01:03:38	03/25/95 14:59:26	44.5	40.5
95052112	05/21/95 12:06:36	05/22/95 11:59:00	72.5	74.5
95060612	06/06/95 12:02:54	06/07/95 11:59:58	72.0	73.5
95070212	07/02/95 12:00:06	07/03/95 05:59:58	54.0	52.0
95070803	07/08/95 03:00:27	07/08/95 16:38:48	42.0	39.0
95071115	07/11/95 15:00:17	07/12/95 21:57:15	91.5	96.0
95071400	07/14/95 00:00:02	07/14/95 15:41:26	46.5	47.5
95071822	07/18/95 22:00:07	07/19/95 19:59:47	63.0	66.0
95072422	07/24/95 22:01:07	07/25/95 14:58:54	49.5	49.0
95072612	07/26/95 19:32:10	07/28/95 04:59:56	99.5	98.5
95080212	08/02/95 18:27:17	08/03/95 11:17:51	47.0	54.5
95080400	08/04/95 00:00:06	08/04/95 18:59:56	55.5	53.0
95091806	09/18/95 06:00:06	09/18/95 19:59:41	38.0	40.0
96011800	01/18/96 00:00:02	01/18/96 09:59:42	28.5	30.0
96050900	05/09/96 00:51:08	05/09/96 19:59:58	57.0	59.0
96051518	05/15/96 19:29:10	05/16/96 19:59:46	76.5	67.0
96051812	05/18/96 21:23:50	05/19/96 14:58:12	53.0	51.5
96061904	06/19/96 04:22:17	06/20/96 12:57:27	94.0	99.0
96071512	07/15/96 15:09:58	07/16/96 11:07:04	62.5	60.5
96072712	07/27/96 20:00:36	07/28/96 13:59:27	49.5	52.5
96080212	08/02/96 12:00:10	08/03/96 23:42:39	108.0	104.5
96080621	08/06/96 21:24:48	08/07/96 13:59:54	50.0	50.5
96082123	08/21/96 23:00:02	08/22/96 17:59:55	54.0	58.5
96102412	10/24/96 13:33:17	10/25/96 04:59:48	47.0	47.0
96112321	11/23/96 21:23:33	11/25/96 10:56:54	113.0	114.0
97020317	02/03/97 17:30:01	02/04/97 11:50:34	57.5	54.0
97030912	03/09/97 20:00:09	03/10/97 11:00:44	42.5	48.5
97032422	03/24/97 22:42:00	03/26/97 01:59:55	84.5	80.5
97061120	06/11/97 20:01:08	06/13/97 02:17:22	89.5	91.5
97061412	06/14/97 16:52:44	06/15/97 11:55:04	57.5	59.0
97062018	06/20/97 18:00:18	06/21/97 17:20:19	70.0	63.5

Table 12 (continued)

Case	Date and time of first flash (UTC)	Date and time of last flash (UTC)	Periodicity of positive peak currents (min)	Periodicity of negative peak currents (min)
97062200	06/22/97 00:00:37	06/23/97 09:18:41	102.0	99.0
97062418	06/24/97 18:04:47	06/25/97 13:42:04	60.0	60.5
97062800	06/28/97 00:00:01	06/28/97 19:55:16	57.5	61.5
97070817	07/08/97 21:40:10	07/09/97 11:31:03	42.0	44.0
97071623	07/16/97 23:00:47	07/17/97 16:59:34	52.0	52.0
97071717	07/17/97 17:01:08	07/18/97 16:17:24	68.5	72.5
97081312	08/13/97 19:51:28	08/14/97 11:58:24	47.5	49.0
97082612	08/26/97 12:00:34	08/27/97 17:54:12	85.5	90.5
97082912	08/29/97 12:00:08	08/30/97 18:56:58	93.0	91.0
97083121	08/31/97 21:00:10	09/01/97 16:59:55	57.5	59.0
97090500	09/05/97 00:00:12	09/05/97 14:57:39	44.5	43.0
97090501	09/05/97 00:00:28	09/05/97 15:15:59	46.0	42.5
97090820	09/08/97 20:00:23	09/09/97 15:56:21	59.5	59.5
97102020	10/21/97 04:24:35	10/22/97 04:51:14	75.5	72.5
97122015	12/20/97 15:00:24	12/21/97 10:50:54	59.5	59.5
98051504	05/15/98 04:18:54	05/16/98 04:59:26	72.0	73.5

between each maximum in the peak currents is on the order of an hour with the extreme periods being no more than 30 minutes on either side of the hour. This time period matches the reported growth and decay rates of thunderstorm cells (Lu et al. 1984).

Satellite data were compared with the lightning flash locations and peak current strengths (Fig. 48), but the time resolution of the satellite data (1 hour) reduced its usefulness to the point where it did not provide any additional information. Similar plots for the rest of this storm are included in Appendix F.

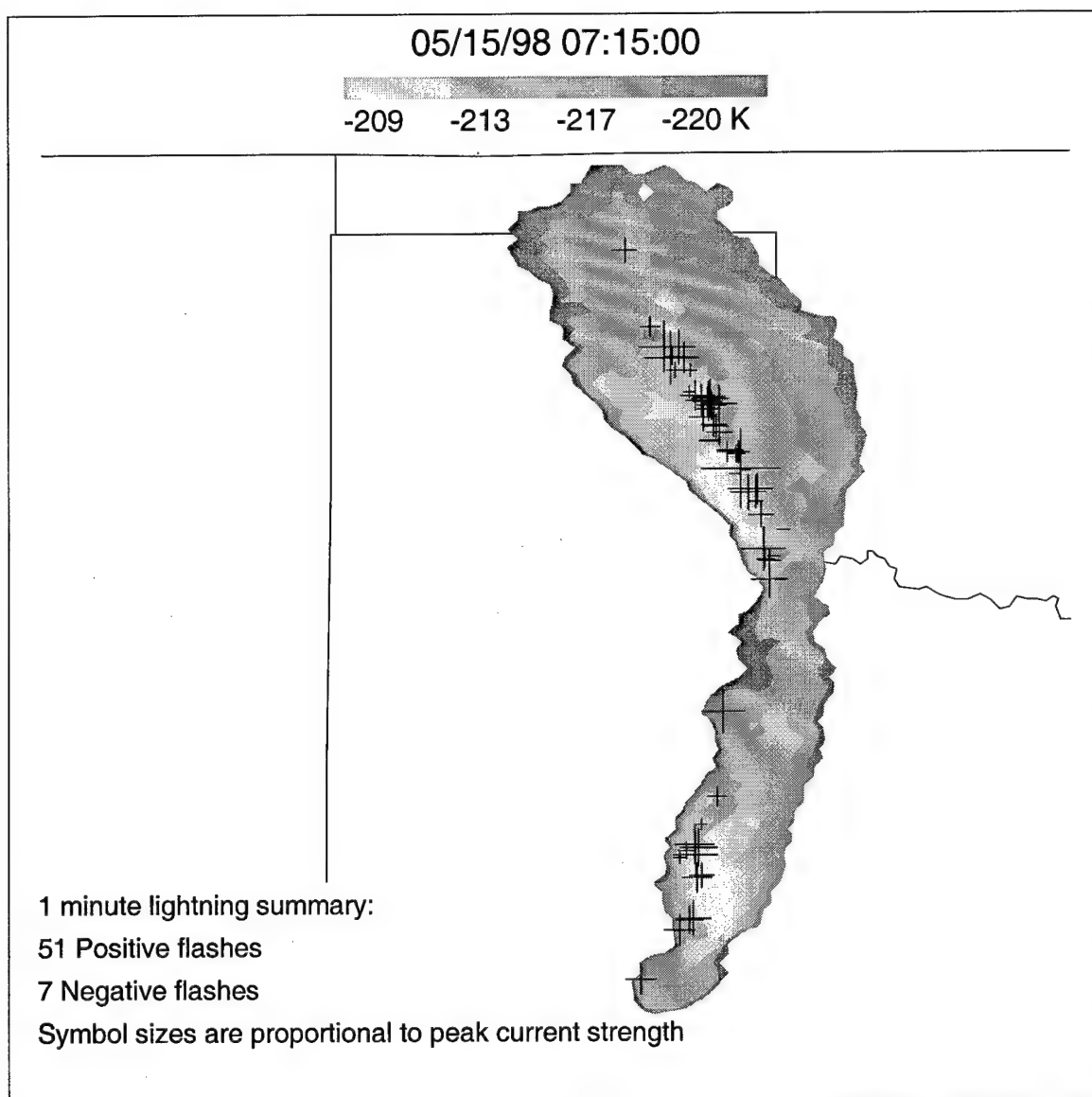


Figure 48. Cloud top IR temperatures with lightning data from 15 May 1998 storm.

Satellite based cloud top brightness temperatures are contoured. Lightning data for 1 minute prior to the reported satellite data time are included and are plotted with positive flashes having a plus sign and negative flashes plotted with a dash. The sizes of the plotting symbols are proportional to the peak currents.

CHAPTER VII

CONCLUSIONS AND RECOMMENDATIONS

A. Conclusions

Lightning data from 1995 – 98 for the United States landmass were studied in order to determine the characteristics of the peak currents. The peak current strengths varied based on time of year and the regions of the US, but these variations were consistent over the 4 years in this study. There were many factors that affected the peak currents including the distribution of sensors within the NLDN, latitude, the percentage of positive lightning, surface elevation, and the season of the year. The distribution of NLDN sensors is the only factor that may be modified and, while its effects are important, will not be considered further. It is the natural influences that are of interest.

After considering the factors listed above, it appears that the first stroke peak currents in cloud-to-ground lightning are determined, to a great extent by the length of the lightning channel. This is the only explanation that fits with each of the results when comparing the peak currents with the various factors affecting them. The channel length theory explains the variations found due to latitude, percentage of positive lightning, season, and surface elevation. Case studies of individual storms support this theory. The differences in the response of positive lightning and negative peak currents negates other possibilities such as the effect of surface conductivity or variations in the amount of charge within the cloud. If either of these alternative explanations were valid, they would apply equally as well for positive and negative flashes. The results of this research show that this is not the case.

There are certain assumptions that must be made in order to accept that peak currents are dependent upon the channel length. First, one must assume that the cloud-to-ground stroke originated in a charge region within the cloud that has the same polarity of charge as the lightning stroke. Second, that the positive lightning originate, for the most part, in the upper positive charge region (Fig. 2) while negative discharges primarily originate in the main negative charge region in the lower portion of the cloud. The latter assumption is necessary in order to explain the differences in the response of positive and negative lightning to the factors listed above.

When the length of the lightning channel is considered, it cannot be determined exactly with the present day measuring system. It is currently impossible to determine where the lightning discharge originates for such a large scale of distance and time. Tortuosity has a large effect on the channel length and could not be included in this study. The best that could be done is to consider the differences in the peak currents and compare these differences with changes in the factors that might influence the peak currents. A large number of flashes were always used in the comparisons in hopes of overcoming the absence of channel length information. The assumption was made that the channel lengths would, on the whole, either be similar enough within a time frame and region to ignore or their influence would be averaged out with the large number of flashes used.

For negative lightning, all indications point to the conclusion that the peak currents are directly connected to the length of the lightning channel. The annual medians of peak currents are a maximum at the southernmost extent of the US and decrease to the north until approximately 32 degrees latitude where they level off (Fig. 18c). The surface temperature in the US also decreases in a similar fashion, especially in the summer months when the

lightning activity is a maximum. This temperature variation with latitude would cause the altitude of the main negative charge region in the thunderstorm to vary similarly to the peak currents. The connection between the negative peak currents and surface elevation is apparent along the Gulf and Atlantic Coasts (Fig. 37). The surface elevations are at a minimum in these regions and the negative peak currents are a maximum. While the area in the Carolinas, Georgia, and Tennessee show a minimum in the negative peak currents, this also corresponds with the tightly spaced NLDN sensors (Fig. 26), biasing the peak currents toward lower values. In other areas, it can be seen that the negative peak currents decrease as the surface elevation rise, supporting the connection between peak current strength and the length of the lightning channel.

Positive lightning did not behave in the same fashion as negative flashes. There is no connection between the surface elevation and the positive peak currents. This does not negate the theory of peak current dependence on the channel length, as the positive lightning has a different origin in the cloud than negative lightning (Rust et al. 1991; Brook et al. 1982). The direct connection between the percentage of positive flashes and positive peak currents (Fig. 35) coupled with the observation of positive flashes originating from the upper regions of the clouds (Rust et al. 1981; Brook et al. 1982), support the theory of the peak currents depending upon the channel length. As the storm tilts, the discharges from the upper positive charge region are able to travel to the ground without being as likely to terminate in the negative charge region below. In addition, as a thunderstorm cell develops, the height of the cloud top increases and the height of the upper charge region should also increase. Examination of individual storms showed the positive peak currents to rise and fall with a period of approximately an hour. This time frame agrees with other reports of the

growth and decay cycles in thunderstorms (Lu et al. 1984). This is exactly in line with the theory of the peak current dependence on the channel length.

Other possibilities for the variations in the peak currents, namely that the amount of charge in the cloud or the surface conductivity effects, were not supported by the results found here. Particularly, the difference between the behavior of positive and negative lightning sheds considerably doubt upon these options. If the amount of charge that is separated in the cloud determined the peak current, then the amplitude of the variations within a storm system should be similar for positive and negative lightning. They are not. Positive flashes demonstrate a larger variation in the peak current strengths than do negative flashes (Fig. 47). If the amount of charge separated was the only consideration, then positive peak currents should have the same amplitude in variation as for negative flashes. Instead, the flash rates varied with the lifetime of the storm cells, which should be dependent upon the amount of charge separated in the cloud. As for the effect of the surface conductivity determining the peak currents, positive flashes should show similar variations between regions of the country as do negative flashes. They do not (Figs. 20 and 21). In fact, positive currents show the opposite trend as negative flashes, for the most part.

B. Recommendations for further research

Radar analysis of the vertical nature of the storm would help to better understand the influence of storm tilt on the percentage of positive flashes and the positive peak currents. The time resolutions of radar data are better suited to the study of thunderstorm features than satellite data. Radar data would also provide a depiction of the storm with features such as storm tops and internal structures. The addition of dual-Doppler analysis of vertical winds

would add the capability of examining the updraft velocities and their effect on the flash rates and peak currents.

The use of Lightning Detection And Ranging (LDAR) data, which is currently available at the Kennedy Space Center in Florida, would add the capability of mapping the lightning discharge from the cloud to the ground. Acoustical mapping techniques would provide similar information. The unknown influence of tortuosity could be studied using this approach. As the lightning flash densities are a maximum in Florida (Fig. 29), there should be sufficient data to analyze.

REFERENCES

- Baral, K. N. and D. Mackerras, 1993: Positive cloud-to-ground lightning discharges in Katmandu thunderstorms. *J. Geophys. Res.*, **98**, 10 331 – 10 340.
- Brook, M., M. Nakano, P. Krehbiel, and T. Takeuti, 1982: The electrical structure of the Hokuriku winter thunderstorms. *J. Geophys. Res.*, **87**, 1 207 – 1 215.
- Cummins, K. L., E. A. Bardo, W. L. Hiscox, R. B. Pyle, and A. E. Pifer, 1995: NLDN95: A combined technology of the U. S. national lightning network. *Proceedings Int. Aerospace & Ground Conf. on Lightning and Static Electricity*, Williamsburg, VA, USA, Sept. 26 – 28, 1995.
- _____, M. J. Murphy, E. A. Bardo, W. L. Hiscox, R. B. Pyle, and A. E. Pifer, 1998: A combined TOA/MDF technology of the U. S. national lightning detection network. *J. Geophys. Res.*, **103**, 9 035 – 9 044.
- Curran, E. B. and W. D. Rust, 1992: Positive ground flashes produced by low-precipitation thunderstorms in Oklahoma on 26 April 1984. *Mon. Wea. Rev.*, **120**, 544 – 553.
- Dye, J. E., W. P. Winn, J. J. Jones, and D. W. Breed, 1989: The electrification of New Mexico thunderstorms, 1, Relationship between precipitation development and the onset of electrification. *J. Geophys. Res.*, **94**, 8 643 – 8 656.
- Engholm, C. D., E. R. Williams, and R. M. Dole, 1990: Meteorological and electrical conditions associated with positive cloud-to-ground lightning. *Mon. Wea. Rev.*, **118**, 470 – 487.
- Foust, C. M., Maine, B. C. and Lee, C., 1953: Lightning stroke protection at high altitude in Peru. *Trans. Am. Inst. Elect. Engrs. Part III.*, **6**, 383 – 393.

- Gaskell, W. and A. J. I. Illingworth, 1980: Charge transfer accompanying individual collisions between ice particles and its role in thunderstorm electrification. *Quart. J. Roy. Meteor. Soc.*, **106**, 841 – 854.
- Golde, R. H., 1967: The lightning conductor. *J. Franklin, Inst.*, **283**, 451 – 477.
- _____, 1977: The lightning conductor, in *Lightning, Vol. II, Lightning Protection* R. H. Golde, ed., pp. 545 – 576. Academic Press, NY.
- Griffiths, R. F. and C. T. Phelps, 1976: The effects of air pressure and water vapor content on the propagation of positive corona streamers and their implications to lightning initiation. *Q. J. Roy. Meteorol. Soc.*, **102**, 419 – 426.
- Holle, R. L., A. I. Watson, R. E. López, D. R. MacGorman, R. Ortiz, and W. D. Otto, 1994: The life cycle of lightning and severe weather in a 3 – 4 June 1995 PRE-STORM mesoscale convective system. *Mon. Wea. Rev.*, **122**, 1 798 – 1 808.
- Idone, V. P. and R. E. Orville, 1982: Lightning return stroke velocities in the Thunderstorm Research International Program (TRIP). *J. Geophys. Res.*, **87**, 4 903 – 4 915.
- _____, _____, D. M. Mach, and W. D. Rust, 1987: The propagation speed of a positive lightning return stroke. *Geophys. Res. Lett.*, **14**, 1 150 – 1 153.
- _____, A. B. Saljoughy, R. W. Henderson, P. K. Moore, and R. Pyle, 1993: A reexamination of the peak current calibration of the National Lightning Detection Network. *J. Geophys. Res.*, **98**, 18 323 – 18 332.
- _____, D. A. Davis, P. K. Moore, Y. Wang, R. W. Henderson, M. Ries, and P. F. Jamason, 1998: Performance evaluation of the U. S. National Lightning Detection Network in eastern New York, 1. Detection efficiency. *J. Geophys. Res.*, **103**, 9 045 – 9 055.

- Jayaratne, E. R. C. P. R. Saunders, and J. Hallett, 1983: Laboratory studies of the charging of soft-hail during ice-crystal interactions. *Quart. J. Roy. Meteor. Soc.*, **109**, 609 – 630.
- Keith, W. D. and C. P. R. Saunders, 1990: Further laboratory studies of the charging of graupel during ice crystal interactions. *Atmos. Res.*, **25**, 445 – 464.
- Krehbiel, P. R., 1986: The electrification of storms, in *The Earth's Electrical Environment* E. P. Krider and R. G. Roble, eds., pp. 90 – 113, Natl. Acad. Press, Washington, DC
- Krider, E. P., R. C. Noggle, and M. A. Uman, 1976: A gated, wide-band magnetic direction finder for lightning return strokes. *J. Appl. Meteor.*, **15**, 301 – 306.
- _____, A. E. Pifer, and D. L. Vance, 1980: Lightning direction finding systems for forest fire detection. *Bull. Amer. Meteor. Soc.*, **61**, 980 – 986.
- Lin, Y. T., M. A. Uman, and R. B. Standler, 1980: Lightning return stroke models. *J. Geophys. Res.*, **85**, 1 571 – 1 583.
- López, R. E., M. W. Maier, R. L. Holle, 1991: Comparison of the signal strength of positive and negative cloud-to-ground lightning flashes in northeastern Colorado. *J. Geophys. Res.*, **96**, 22 307 – 22 318.
- Lu, D., T. E. VanZandt, and W. L. Clark, 1984: VHF doppler radar observations of buoyancy waves associated with thunderstorms. *J. Atmos. Sci.*, **41**, 272 – 282.
- Lyons, W. A., D. A. Moon, J. S. Schuh, N. J. Petit, and J. R. Eastman, 1989: The design and operation of a national lightning detections network using time-of-arrival technology. *1989 Intl. Conf. on Lightning and Static Elec.*, University of Bath, Bath, U. K., Ministry of Defense Procurement Executive, Sept. 26 – 28, 1989.

- _____, 1996: Sprite observations above the U.S. high plains in relation to their parent thunderstorm systems. *J. Geophys. Res.*, **101**, 29 641 – 29 652.
- _____, M. Uliasz, and T. E. Nelson, 1998: Large peak current cloud-to-ground flashes during the summer months in the contiguous United States. *Mon. Wea. Rev.*, **126**, 2 217 – 2 233.
- MacGorman, D. R. and K.E. Nielsen, 1991: Cloud-to-ground lightning in a tornadic storm on 8 May 1986. *Mon. Wea. Rev.*, **119**, 1 557 – 1 574.
- _____ and D. W. Burgess, 1994: Positive cloud-to-ground lightning in tornadic storms and hailstorms. *Mon. Wea. Rev.*, **122**, 1 671 – 1 697.
- _____ and W. D. Rust, 1998: *The Electrical Nature of Storms*, Oxford University Press, New York.
- Mach, D. M., D. R. MacGorman, W. D. Rust, and R. T. Arnold, 1986: Site errors and detection efficiency in a magnetic direction-finder network for locating lightning strikes to ground. *J. Atmos. Ocean. Tech.*, **3**, 67 – 74.
- Maddox, R. A., 1980: Mesoscale convective complexes. *Bull. Amer. Meteor. Soc.*, **61**, 1 374 – 1 387.
- _____, 1983: Large-scale meteorological conditions associated with midlatitude, mesoscale convective complexes. *Mon. Wea. Rev.*, **111**, 1 475 – 1 493.
- Marshall, T. C. and W. D. Rust, 1991: Electric field sounding through thunderstorms. *J. Geophys. Res.*, **96**, 22 297 – 22 306.
- Orville, R. E., 1968: Spectrum of the lightning stepped leader. *J. Geophys. Res.*, **87**, 11 177 – 11 192.

- _____, R. W. Hendersen, and L. F. Bosart, 1983: An east coast lightning detection network. *Bull. Amer. Meteor. Soc.*, **64**, 1 029 – 1 037.
- _____, R. A. Weisman, R. B. Pyle, R. W. Henderson, and R. E. Orville, Jr., 1987: Cloud-to-ground lightning flash characteristics from June 1984 through May 1985. *J. Geophys. Res.*, **92**, 5 640 – 5 644.
- _____, R. W. Henderson, and L. F. Bosart, 1988: Bipole patterns revealed by lightning locations in mesoscale storm systems. *Geophys. Res. Lett.*, **15**, 129 – 132.
- _____, 1990: Peak current variations of lightning return strokes as a function of latitude. *Nature*, **343**, 149 – 151.
- _____, 1991a, Lightning ground flash density in the contiguous United States – 1989. *Mon. Wea. Rev.*, **119**, 573 – 577.
- _____, 1991b, Calibration of a magnetic direction finding network using measured triggered lightning return stroke peak currents. *J. Geophys. Res.*, **96**, 17 135 – 17 142.
- _____, 1994: Cloud-to-ground lightning flash characteristics in the contiguous United States: 1989 – 1991. *J. Geophys. Res.*, **99**, 10 833 – 10 841.
- _____ and A. C. Silver, 1997: Lightning ground flash density in the contiguous United States: 1992 – 95. *Mon. Wea. Rev.*, **125**, 631 – 638.
- _____ and G. R. Huffines, 1999: Lightning ground flash measurements over the contiguous United States: 1995 – 1997. *Mon. Wea. Rev.*, accepted Nov. 1998.
- Pierce, E. T., 1970: Latitudinal variations in lightning parameters. *J. Appl. Meteor.*, **9**, 194 – 195.

- Pinto, O., Jr., R. B. B. Gin, I. R. C. A. Pinto, O. Mendes, Jr., J. H. Diniz, and A. M. Carcalho, 1996: Cloud-to-ground lightning flash characteristics in southeastern Brazil for the 1992 – 1993 summer season. *J. Geophys. Res.*, **101**, 29 627 – 29 635.
- Robertson, L. M., Lewis, W. W., and Foust, C. M., 1942: Lightning investigations at high altitude in Colorado. *Trans. Am. Inst. Elect. Engrs.*, **61**, 201 – 208.
- Rust, W. D., D. R. MacGorman, and R. T. Arnold, 1981: Positive cloud-to-ground lightning flashes in severe storms. *Geophys. Res. Lett.*, **8**, 791 – 794.
- _____, and _____, 1988: Cloud-to-ground lightning activity in the 10 – 11 June 1985 mesoscale convective system observed during the Oklahoma – Kansas PRE-STORM project. *Mon. Wea. Rev.*, **116**, 1 393 – 1 408.
- Rutledge, S. A. and W. A. Petersen, 1994: Vertical radar reflectivity structure and cloud-to-ground lightning in the stratiform region of MCSs: Further evidence for in situ charging in the stratiform region. *Mon. Wea. Rev.*, **122**, 1 760 – 1 776.
- Saunders, C. P. R., 1993: A review of thunderstorm electrification processes. *J. Appl. Meteor.*, **32**, 642 – 655.
- Simpson, Sir G. and F. J. Scrase, 1937: The distribution of electricity in thunderclouds. *Proc. Roy. Soc. Lond., A*, **161**, 309 – 352.
- Stolzenburg, M., 1994: Observations of high ground flash density of positive lightning in summertime thunderstorms. *Mon. Wea. Rev.*, **122**, 1 740 – 1 750.
- _____, W. D. Rust, B. F. Smull, and T. C. Marshall, 1998: Electrical structure in thunderstorm convective regions, 3, mesoscale convective systems. *J. Geophys. Res.*, **103**, 14 059 – 14 078.

- Takahashi, T., 1978: Riming electrification as a charge generation mechanism in thunderstorms. *J. Atmos. Sci.*, **35**, 1 536 – 1 548.
- Tyahla, L. J. and R. E. López, 1994: Effect of surface conductivity on the peak magnetic field radiated by first return strokes in cloud-to-ground lightning. *J. Geophys. Res.*, **99**, 10 517 – 10 525.
- Uman, M. A., 1987. *The Lightning Discharge*, Academic Press, Orlando, FL.
- Wacker, R. S. and R. E. Orville, 1999: Changes in measured lightning flash count and return stroke peak current after the 1994 U. S. national lightning detection network upgrade, 1. Observations. *J. Geophys. Res.*, **104**, 2 151 – 2 157.
- Zipser, E. J., 1982: Use of a conceptual model of the life-cycle of mesoscale convective systems to improve very-short-range forecasts. *Nowcasting*, K. A. Browning, ed., Academic Press, London, pp. 191 – 204.

APPENDIX A

SUMMARY OF DAYS WITH LIGHTNING IN THE NORTHERN PLAINS FROM 1995 – 1998

Each day with lightning for the area of the Northern Plains of the US described by Figure 42 is listed here. The days begin at 1700 UTC on the date listed and continue for 24 hours. The table includes a summary of the lightning activity including the number of measured flashes, the percentage of positive lightning, and the peak currents for both positive and negative flashes. In order to avoid the inclusion of intracloud flashes that may have been interpreted as cloud-to-ground lightning (Cummins et al. 1998), positive flashes with peak currents less than 10 kA were excluded from this summary. The median peak currents are only reported if there were at least 2 flashes of that polarity during the 24 hours.

Table A-1. Summary of days with lightning in the Northern Plains of the US.

Date for start of 24 hours (start at 1700 UTC)	Cloud-to-ground flashes	Percent positive flashes	Median peak positive current (kA)	Median peak negative current (kA)	Date for start of 24 hours (start at 1700 UTC)	Cloud-to-ground flashes	Percent positive flashes	Median peak positive current (kA)	Median peak negative current (kA)
03/04/95	9	22.2	80.9	-21.0	05/08/95	1873	11.6	31.4	-18.0
03/12/95	28	42.9	43.0	-15.0	05/09/95	24	12.5	65.3	-28.0
03/16/95	12	8.3	0.0	-14.0	05/10/95	3	33.3	0.0	-16.0
03/17/95	942	19.3	32.7	-18.0	05/11/95	3088	7.1	34.3	-22.0
03/19/95	252	11.5	37.7	-19.0	05/12/95	3685	10.5	37.1	-22.0
03/21/95	62	1.6	0.0	-17.0	05/13/95	77	39.0	46.3	-21.0
03/22/95	1644	7.3	32.4	-23.0	05/14/95	10	30.0	79.1	-19.0
03/23/95	1	0.0	0.0	0.0	05/15/95	3869	32.7	40.0	-19.0
03/24/95	4333	26.1	34.7	-22.0	05/16/95	1954	22.9	40.0	-20.0
03/25/95	911	25.8	37.6	-20.0	05/17/95	1114	24.0	33.7	-21.0
03/26/95	235	27.2	41.4	-21.0	05/18/95	738	7.9	36.1	-22.0
04/02/95	10	20.0	51.9	-20.0	05/19/95	876	25.3	49.6	-17.0
04/05/95	1	100.0	0.0	0.0	05/20/95	100	8.0	36.7	-25.0
04/06/95	492	53.9	61.5	-21.0	05/21/95	8199	13.1	35.2	-20.0
04/07/95	43	67.4	112.1	-17.0	05/22/95	6519	13.5	35.0	-20.0
04/08/95	570	34.6	42.8	-20.0	05/23/95	438	15.8	44.4	-24.0
04/09/95	115	12.2	29.9	-33.0	05/24/95	129	14.7	38.5	-19.0
04/14/95	1861	23.8	58.2	-20.0	05/25/95	1071	10.1	32.0	-23.0
04/15/95	245	19.2	33.2	-20.0	05/26/95	2298	27.5	35.6	-17.0
04/16/95	146	16.4	33.8	-22.0	05/27/95	1640	28.7	35.3	-19.0
04/17/95	582	29.6	43.7	-24.0	05/28/95	12	58.3	40.1	-14.0
04/19/95	12	50.0	29.0	-14.0	05/30/95	121	29.8	31.8	-16.0
04/20/95	47	25.5	40.7	-23.0	05/31/95	312	13.8	36.0	-20.0
04/22/95	48	16.7	58.3	-19.0	06/01/95	4283	9.2	34.9	-19.0
04/23/95	386	20.2	46.0	-21.0	06/02/95	3153	31.3	37.7	-19.0
04/24/95	65	16.9	44.3	-21.0	06/03/95	3867	17.5	36.6	-20.0
04/25/95	103	36.9	52.1	-16.0	06/04/95	2464	11.5	32.7	-19.0
04/28/95	1115	19.4	29.4	-18.0	06/05/95	2484	9.2	39.2	-16.0
04/29/95	82	15.9	28.3	-28.0	06/06/95	10769	25.5	40.1	-18.0
04/30/95	89	21.3	52.8	-18.0	06/07/95	3112	26.7	36.4	-19.0
05/02/95	616	12.0	41.7	-19.0	06/08/95	2459	8.5	24.8	-21.0
05/03/95	9	66.7	83.9	-17.0	06/09/95	631	12.5	25.4	-22.0
05/04/95	11	18.2	73.4	-26.0	06/10/95	15	33.3	29.1	-22.0
05/05/95	200	33.0	34.2	-23.0	06/12/95	407	9.3	37.9	-17.0
05/06/95	4909	30.3	33.4	-20.0	06/13/95	1263	4.4	34.2	-22.0
05/07/95	1165	28.8	38.3	-19.0	06/14/95	1682	54.5	48.2	-17.0

Table A-1 (continued)

Date for start of 24 hours (start at 1700 UTC)	Cloud-to-ground flashes	Percent positive flashes	Median peak positive current (kA)	Median peak negative current (kA)	Date for start of 24 hours (start at 1700 UTC)	Cloud-to-ground flashes	Percent positive flashes	Median peak positive current (kA)	Median peak negative current (kA)
06/15/95	1919	7.3	35.0	-21.0	07/23/95	2148	26.1	36.9	-18.0
06/16/95	112	1.8	17.1	-23.0	07/24/95	8133	11.2	36.9	-21.0
06/17/95	15	0.0	0.0	-21.0	07/25/95	1134	11.3	35.4	-18.0
06/18/95	4984	4.0	17.8	-17.0	07/26/95	12086	20.3	37.7	-20.0
06/19/95	1833	14.0	33.4	-21.0	07/27/95	333	3.3	25.0	-22.0
06/20/95	15646	20.3	37.0	-18.0	07/28/95	8	50.0	42.8	-23.0
06/21/95	11263	21.6	36.4	-19.0	07/29/95	4830	1.9	29.1	-24.0
06/22/95	25162	14.6	32.0	-19.0	07/30/95	24976	6.2	26.8	-19.0
06/23/95	4932	14.9	38.4	-20.0	07/31/95	1533	5.2	24.3	-18.0
06/24/95	471	15.3	37.5	-17.0	08/02/95	4768	42.6	45.1	-17.0
06/25/95	285	26.7	42.0	-22.0	08/03/95	5767	39.2	37.0	-17.0
06/26/95	658	8.2	31.5	-22.0	08/04/95	12349	24.8	36.6	-17.0
06/27/95	3640	35.3	41.6	-19.0	08/05/95	7195	16.1	32.6	-18.0
06/28/95	3613	9.6	36.7	-27.0	08/06/95	1322	11.3	24.6	-19.0
07/01/95	2337	25.8	31.9	-19.0	08/07/95	2608	5.9	30.8	-22.0
07/02/95	10205	14.6	37.2	-20.0	08/08/95	27088	4.2	16.3	-20.0
07/03/95	23752	43.0	46.8	-19.0	08/09/95	1325	17.3	29.4	-21.0
07/04/95	1331	20.7	39.3	-20.0	08/10/95	23576	10.6	24.2	-18.0
07/05/95	65	15.4	50.7	-33.0	08/11/95	4826	5.5	24.3	-20.0
07/06/95	547	2.6	15.9	-18.0	08/12/95	23116	6.0	20.9	-21.0
07/07/95	10158	13.0	33.6	-20.0	08/13/95	19073	11.3	25.7	-19.0
07/08/95	88	6.8	23.1	-21.0	08/14/95	312	17.0	32.8	-20.0
07/09/95	5790	11.4	26.3	-20.0	08/15/95	2	100.0	37.5	0.0
07/10/95	10943	4.5	28.5	-21.0	08/16/95	205	0.5	0.0	-25.0
07/11/95	21149	18.9	45.6	-20.0	08/17/95	10490	18.6	48.8	-20.0
07/12/95	24349	13.5	38.8	-22.0	08/18/95	22018	13.0	46.0	-21.0
07/13/95	17328	13.1	32.8	-20.0	08/19/95	44	9.1	55.6	-20.0
07/14/95	9272	12.4	31.9	-20.0	08/20/95	9339	5.1	16.8	-19.0
07/15/95	8700	5.3	29.4	-20.0	08/21/95	31856	7.4	24.5	-21.0
07/16/95	4534	11.6	40.1	-21.0	08/22/95	11601	8.2	44.8	-23.0
07/17/95	1802	30.1	40.4	-20.0	08/23/95	33877	6.4	23.5	-22.0
07/18/95	11125	11.0	28.5	-18.0	08/24/95	27501	7.3	22.1	-21.0
07/19/95	1255	15.6	37.8	-19.0	08/25/95	11408	5.0	24.3	-21.0
07/20/95	4704	10.1	34.1	-19.0	08/26/95	5041	5.6	30.7	-23.0
07/21/95	7161	20.4	38.3	-18.0	08/27/95	15770	8.9	37.6	-23.0
07/22/95	4911	8.3	31.7	-19.0	08/28/95	14097	13.1	46.6	-21.0

Table A-1 (continued)

Date for start of 24 hours (start at 1700 UTC)	Cloud-to-ground flashes	Percent positive flashes	Median peak positive current (kA)	Median peak negative current (kA)	Date for start of 24 hours (start at 1700 UTC)	Cloud-to-ground flashes	Percent positive flashes	Median peak positive current (kA)	Median peak negative current (kA)
08/29/95	4327	2.4	25.7	-23.0	10/26/95	40	25.0	56.6	-26.0
08/30/95	10992	1.9	19.4	-22.0	10/31/95	536	15.5	37.2	-24.0
08/31/95	959	4.0	37.2	-21.0	11/09/95	2	0.0	0.0	-15.0
09/01/95	10359	9.1	16.4	-18.0	12/04/95	76	14.5	44.1	-24.0
09/02/95	1032	4.5	31.5	-19.0	01/17/96	1	100.0	0.0	0.0
09/03/95	7329	2.0	21.2	-20.0	02/01/96	1	100.0	0.0	0.0
09/04/95	32684	4.3	22.4	-20.0	02/02/96	1	0.0	0.0	0.0
09/05/95	41973	6.3	22.5	-19.0	02/03/96	1	100.0	0.0	0.0
09/06/95	205	4.4	58.7	-19.0	02/14/96	1	0.0	0.0	0.0
09/08/95	141	18.4	34.4	-20.0	02/18/96	12	0.0	0.0	-14.0
09/09/95	6	83.3	60.0	0.0	02/19/96	15	13.3	31.0	-26.0
09/10/95	5874	3.9	25.3	-23.0	02/22/96	15	6.7	0.0	-42.0
09/11/95	5625	13.5	34.0	-19.0	02/26/96	7	14.3	0.0	-47.0
09/13/95	6	50.0	71.8	-27.0	03/04/96	1	100.0	0.0	0.0
09/14/95	3585	6.8	29.1	-20.0	03/13/96	41	46.3	42.8	-16.0
09/15/95	4991	8.3	40.5	-21.0	03/14/96	348	10.3	38.2	-24.0
09/17/95	5867	19.4	31.0	-21.0	03/15/96	26	3.8	0.0	-22.0
09/18/95	4117	19.3	33.0	-19.0	03/17/96	3	0.0	0.0	-75.0
09/19/95	4	25.0	0.0	-17.0	03/18/96	2	50.0	0.0	0.0
09/20/95	260	43.1	39.9	-20.0	03/23/96	1067	61.4	53.8	-20.0
09/23/95	42	31.0	36.4	-28.0	03/24/96	45	4.4	78.3	-34.0
09/27/95	1536	15.0	46.2	-19.0	03/29/96	77	23.4	66.9	-26.0
09/28/95	17721	6.0	30.0	-20.0	04/09/96	107	13.1	28.7	-25.0
09/29/95	7211	13.6	33.2	-20.0	04/10/96	139	48.9	63.0	-18.0
09/30/95	382	34.6	39.4	-21.0	04/11/96	14	21.4	44.3	-16.0
10/01/95	1387	11.6	37.6	-18.0	04/12/96	21	14.3	48.7	-15.0
10/02/95	64	42.2	50.5	-21.0	04/13/96	71	36.6	45.5	-20.0
10/03/95	1643	8.4	31.0	-20.0	04/14/96	17	23.5	24.6	-24.0
10/04/95	1763	7.8	32.1	-23.0	04/17/96	477	20.8	42.8	-19.0
10/07/95	987	3.2	46.0	-22.0	04/18/96	82	12.2	60.3	-20.0
10/08/95	85	29.4	48.6	-24.0	04/20/96	1	0.0	0.0	0.0
10/09/95	137	48.9	51.9	-23.0	04/22/96	10	40.0	37.3	-20.0
10/12/95	20	5.0	0.0	-17.0	04/23/96	88	4.5	78.9	-25.0
10/18/95	6	0.0	0.0	-13.0	04/24/96	99	20.2	35.4	-15.0
10/22/95	2708	10.5	31.4	-24.0	04/26/96	46	21.7	39.5	-33.0
10/23/95	197	23.4	36.0	-28.0	04/27/96	113	19.5	35.2	-19.0

Table A-1 (continued)

Date for start of 24 hours (start at 1700 UTC)	Cloud-to-ground flashes	Percent positive flashes	Median peak positive current (kA)	Median peak negative current (kA)	Date for start of 24 hours (start at 1700 UTC)	Cloud-to-ground flashes	Percent positive flashes	Median peak positive current (kA)	Median peak negative current (kA)
04/28/96	2	0.0	0.0	-11.0	06/03/96	1000	20.9	38.5	-18.0
04/29/96	2	0.0	0.0	-29.0	06/04/96	5380	12.6	29.5	-20.0
04/30/96	231	27.7	46.7	-22.0	06/05/96	7001	43.2	40.0	-19.0
05/01/96	305	10.8	28.5	-20.0	06/06/96	454	21.4	42.2	-18.0
05/02/96	1704	4.4	23.1	-22.0	06/08/96	5	20.0	0.0	-17.0
05/03/96	472	21.4	32.4	-24.0	06/09/96	3677	10.4	33.6	-23.0
05/04/96	279	35.1	35.3	-20.0	06/10/96	850	59.8	39.9	-17.0
05/05/96	74	6.8	14.6	-27.0	06/11/96	11617	13.4	30.5	-20.0
05/06/96	1794	20.1	27.7	-21.0	06/12/96	873	31.4	40.2	-19.0
05/07/96	4246	14.1	25.5	-22.0	06/13/96	5029	22.7	34.8	-19.0
05/08/96	3518	25.9	33.9	-16.0	06/14/96	12626	15.8	32.9	-19.0
05/09/96	2246	20.8	35.3	-23.0	06/15/96	4223	19.0	33.9	-18.0
05/10/96	32	6.2	102.4	-19.0	06/16/96	254	8.3	38.1	-20.0
05/11/96	253	7.5	39.4	-24.0	06/17/96	2263	29.1	34.9	-17.0
05/12/96	313	18.2	23.8	-22.0	06/18/96	10484	17.7	35.1	-20.0
05/13/96	420	24.3	37.2	-21.0	06/19/96	6266	64.8	55.7	-15.0
05/14/96	3772	16.3	35.2	-18.0	06/20/96	22137	19.4	39.1	-19.0
05/15/96	6145	53.1	48.2	-15.0	06/21/96	10920	16.3	33.6	-19.0
05/16/96	17887	31.5	43.3	-19.0	06/22/96	13885	19.9	35.9	-18.0
05/17/96	12378	46.7	48.7	-17.0	06/23/96	2053	12.1	29.7	-22.0
05/18/96	5747	63.0	49.3	-19.0	06/24/96	13041	16.1	34.2	-19.0
05/19/96	73	35.6	36.2	-21.0	06/25/96	12341	9.8	29.7	-22.0
05/20/96	504	20.0	46.0	-23.0	06/26/96	2431	3.9	28.2	-24.0
05/21/96	712	25.7	45.3	-19.0	06/27/96	2514	6.1	32.7	-19.0
05/22/96	7143	17.8	31.2	-20.0	06/28/96	8275	5.1	24.6	-21.0
05/23/96	7505	15.8	22.6	-20.0	06/29/96	731	7.9	31.5	-20.0
05/24/96	7339	17.1	23.0	-19.0	06/30/96	7409	9.0	29.5	-17.0
05/25/96	8825	27.8	27.7	-18.0	07/01/96	2155	32.3	61.5	-17.0
05/26/96	2834	39.8	33.5	-19.0	07/02/96	7263	17.3	31.6	-19.0
05/27/96	36	66.7	38.2	-26.0	07/03/96	6173	5.0	27.0	-19.0
05/28/96	55	9.1	23.4	-20.0	07/04/96	8116	8.6	30.2	-22.0
05/29/96	284	12.7	46.4	-22.0	07/05/96	33905	10.6	20.4	-18.0
05/30/96	20397	16.4	28.6	-20.0	07/06/96	11503	10.8	20.4	-18.0
05/31/96	9770	36.2	40.8	-17.0	07/07/96	13269	34.2	42.9	-17.0
06/01/96	1314	27.9	41.6	-17.0	07/08/96	108	10.2	25.2	-20.0
06/02/96	1085	21.4	48.0	-24.0	07/09/96	762	10.6	34.9	-20.0

Table A-1 (continued)

Date for start of 24 hours (start at 1700 UTC)	Cloud-to-ground flashes	Percent positive flashes	Median peak positive current (kA)	Median peak negative current (kA)	Date for start of 24 hours (start at 1700 UTC)	Cloud-to-ground flashes	Percent positive flashes	Median peak positive current (kA)	Median peak negative current (kA)
07/10/96	13258	10.8	23.8	-18.0	08/15/96	15030	15.5	32.1	-18.0
07/11/96	1622	19.2	39.3	-19.0	08/16/96	339	47.5	44.2	-21.0
07/12/96	2995	28.4	34.5	-18.0	08/17/96	1740	1.5	20.6	-22.0
07/13/96	9432	27.1	37.1	-18.0	08/18/96	24552	11.4	29.3	-19.0
07/14/96	6096	5.5	30.7	-26.0	08/19/96	1309	25.2	32.7	-20.0
07/15/96	7319	32.5	35.4	-17.0	08/20/96	13733	4.2	26.4	-21.0
07/16/96	11600	9.8	20.3	-20.0	08/21/96	19326	25.0	44.5	-18.0
07/17/96	17502	18.5	45.1	-19.0	08/22/96	527	19.2	39.8	-18.0
07/18/96	9322	11.6	37.1	-18.0	08/23/96	34	20.6	38.9	-19.0
07/19/96	18461	10.2	31.1	-20.0	08/24/96	1086	1.4	20.4	-23.0
07/20/96	8193	22.1	37.7	-18.0	08/25/96	3598	17.6	42.6	-23.0
07/21/96	9573	23.7	38.0	-18.0	08/26/96	49	32.7	47.1	-17.0
07/22/96	7885	7.0	28.1	-20.0	08/27/96	211	15.2	15.9	-24.0
07/23/96	9957	16.8	31.3	-18.0	08/28/96	2906	21.3	33.8	-17.0
07/24/96	1119	16.0	33.1	-19.0	08/29/96	6802	18.8	35.7	-15.0
07/25/96	9661	27.0	34.2	-18.0	08/30/96	1235	10.5	30.0	-20.0
07/26/96	9873	10.5	27.8	-18.0	08/31/96	2563	4.7	33.1	-22.0
07/27/96	3626	31.1	42.5	-17.0	09/01/96	20378	8.5	20.4	-17.0
07/28/96	17331	18.1	37.2	-18.0	09/02/96	15371	16.7	25.8	-19.0
07/29/96	823	22.4	43.0	-20.0	09/03/96	985	13.6	33.2	-19.0
07/30/96	5118	9.9	28.3	-17.0	09/04/96	9343	41.2	49.1	-21.0
07/31/96	15648	17.7	37.1	-18.0	09/05/96	4627	6.1	24.6	-17.0
08/01/96	5681	8.0	24.4	-18.0	09/06/96	8395	14.0	27.7	-17.0
08/02/96	29820	13.3	36.2	-19.0	09/08/96	32	9.4	41.1	-18.0
08/03/96	42553	11.1	27.4	-19.0	09/09/96	1988	34.8	41.9	-16.0
08/04/96	32422	11.3	32.2	-20.0	09/10/96	1499	3.8	19.9	-20.0
08/05/96	29	3.4	0.0	-20.0	09/11/96	27	0.0	0.0	-18.0
08/06/96	23947	48.6	51.9	-16.0	09/12/96	11	9.1	0.0	-18.0
08/07/96	6	33.3	65.5	-24.0	09/14/96	505	11.3	34.9	-20.0
08/08/96	157	29.9	35.0	-17.0	09/15/96	2	0.0	0.0	-15.0
08/09/96	7114	11.6	30.7	-18.0	09/16/96	1	0.0	0.0	0.0
08/10/96	2505	25.7	32.5	-15.0	09/17/96	9650	21.5	35.7	-18.0
08/11/96	134	20.9	31.4	-18.0	09/18/96	2366	35.8	33.2	-18.0
08/12/96	1661	13.2	32.6	-25.0	09/19/96	287	46.0	40.1	-18.0
08/13/96	5326	12.8	32.5	-18.0	09/20/96	141	20.6	38.6	-16.0
08/14/96	7494	16.0	31.0	-19.0	09/21/96	229	8.7	58.9	-17.0

Table A-1 (continued)

Date for start of 24 hours (start at 1700 UTC)	Cloud-to-ground flashes	Percent positive flashes	Median peak positive current (kA)	Median peak negative current (kA)	Date for start of 24 hours (start at 1700 UTC)	Cloud-to-ground flashes	Percent positive flashes	Median peak positive current (kA)	Median peak negative current (kA)
09/22/96	1178	29.1	48.6	-20.0	03/24/97	7	0.0	0.0	-44.0
09/23/96	133	20.3	42.6	-27.0	04/01/97	374	45.7	66.7	-22.0
09/24/96	4287	8.0	33.4	-19.0	04/02/97	6	0.0	0.0	-24.0
09/25/96	386	28.8	38.8	-18.0	04/03/97	19	89.5	60.4	-16.0
09/26/96	23	0.0	0.0	-16.0	04/04/97	352	18.2	34.4	-15.0
09/28/96	16	31.2	25.0	-17.0	04/05/97	16	25.0	58.1	-17.0
09/30/96	11	0.0	0.0	-22.0	04/07/97	166	7.8	30.0	-22.0
10/01/96	12	41.7	71.6	-17.0	04/09/97	97	8.2	18.9	-40.0
10/03/96	140	2.9	16.6	-20.0	04/10/97	60	15.0	52.8	-19.0
10/06/96	2434	6.4	29.2	-22.0	04/18/97	127	22.8	31.2	-14.0
10/07/96	1	0.0	0.0	0.0	04/19/97	367	39.5	55.0	-16.0
10/08/96	275	14.5	45.9	-18.0	04/20/97	80	15.0	32.6	-18.0
10/13/96	5	40.0	37.0	-70.0	04/21/97	1	100.0	0.0	0.0
10/14/96	909	17.3	39.7	-23.0	04/25/97	36	50.0	36.3	-18.0
10/15/96	9	0.0	0.0	-13.0	04/26/97	267	32.2	56.7	-18.0
10/16/96	5555	28.6	39.8	-18.0	04/28/97	39	12.8	43.3	-13.0
10/17/96	18	22.2	79.3	-31.0	04/29/97	1003	15.9	36.4	-16.0
10/19/96	39	0.0	0.0	-16.0	04/30/97	358	11.5	42.0	-25.0
10/20/96	29	31.0	59.3	-18.0	05/01/97	753	49.0	37.6	-16.0
10/25/96	1788	14.8	32.5	-16.0	05/04/97	537	45.3	45.8	-17.0
10/26/96	2756	13.0	36.9	-20.0	05/05/97	62	1.6	0.0	-23.0
10/28/96	818	11.7	28.4	-25.0	05/06/97	3354	23.3	40.4	-18.0
10/29/96	1205	13.4	36.6	-24.0	05/07/97	647	30.0	46.5	-20.0
11/03/96	1535	5.1	36.0	-24.0	05/10/97	184	6.0	37.1	-17.0
11/05/96	2	0.0	0.0	-18.0	05/12/97	1	0.0	0.0	0.0
11/06/96	1	100.0	0.0	0.0	05/14/97	1	0.0	0.0	0.0
11/14/96	352	11.9	35.4	-25.0	05/15/97	214	7.9	28.5	-19.0
11/15/96	1261	30.0	36.5	-19.0	05/16/97	210	11.9	30.5	-14.0
11/22/96	12	33.3	80.0	-43.0	05/17/97	3031	50.0	41.1	-16.0
11/23/96	79	11.4	42.7	-32.0	05/18/97	874	19.6	29.3	-15.0
12/14/96	3	0.0	0.0	-18.0	05/20/97	269	5.9	27.2	-22.0
01/03/97	9	11.1	0.0	-22.0	05/21/97	958	8.6	32.9	-15.0
03/03/97	24	37.5	39.8	-24.0	05/22/97	2005	20.7	32.1	-18.0
03/08/97	209	59.3	52.1	-15.0	05/23/97	3	66.7	51.5	0.0
03/12/97	8	12.5	0.0	-23.0	05/24/97	2656	27.0	42.7	-14.0
03/23/97	75	26.7	46.5	-16.0	05/25/97	386	25.6	44.1	-18.0

Table A-1 (continued)

Date for start of 24 hours (start at 1700 UTC)	Cloud-to-ground flashes	Percent positive flashes	Median peak positive current (kA)	Median peak negative current (kA)	Date for start of 24 hours (start at 1700 UTC)	Cloud-to-ground flashes	Percent positive flashes	Median peak positive current (kA)	Median peak negative current (kA)
05/26/97	473	22.2	33.0	-18.0	07/04/97	1026	16.8	35.7	-21.0
05/27/97	244	20.5	35.4	-14.0	07/05/97	3229	45.6	34.2	-16.0
05/28/97	294	24.8	31.4	-16.0	07/06/97	5733	22.7	33.4	-20.0
05/29/97	290	24.8	35.0	-16.0	07/07/97	3898	43.0	50.6	-17.0
05/31/97	193	7.8	28.7	-23.0	07/08/97	5092	45.5	37.0	-17.0
06/01/97	17300	10.4	27.7	-18.0	07/09/97	2589	6.1	15.3	-20.0
06/02/97	9344	11.7	28.4	-16.0	07/10/97	20096	11.7	32.1	-21.0
06/03/97	121	54.5	47.0	-22.0	07/11/97	32609	6.1	26.5	-19.0
06/04/97	583	14.8	37.9	-21.0	07/12/97	15821	8.1	28.2	-17.0
06/06/97	67	17.9	20.1	-20.0	07/13/97	11145	14.3	37.4	-19.0
06/07/97	820	4.1	16.3	-16.0	07/14/97	576	1.6	20.1	-21.0
06/08/97	1449	5.7	36.8	-21.0	07/15/97	3436	8.3	32.0	-21.0
06/09/97	188	5.3	29.8	-22.0	07/16/97	10013	65.6	54.3	-15.0
06/10/97	1828	10.9	29.1	-18.0	07/17/97	12566	28.9	38.8	-20.0
06/11/97	4642	20.2	36.8	-16.0	07/18/97	5975	9.3	18.2	-19.0
06/12/97	1704	35.7	36.0	-17.0	07/19/97	16852	17.4	35.6	-18.0
06/13/97	404	10.1	34.0	-18.0	07/20/97	3902	6.4	20.0	-18.0
06/14/97	11209	13.4	36.2	-17.0	07/21/97	4131	16.8	31.5	-17.0
06/15/97	1658	22.2	29.4	-15.0	07/22/97	8062	16.1	37.1	-20.0
06/16/97	3317	10.6	31.7	-19.0	07/23/97	18109	14.1	35.3	-21.0
06/17/97	186	11.8	39.1	-15.0	07/24/97	25358	13.3	24.1	-20.0
06/18/97	5121	15.0	38.4	-17.0	07/25/97	17817	20.8	48.5	-18.0
06/19/97	14284	17.0	34.1	-16.0	07/26/97	8226	34.1	51.7	-16.0
06/20/97	13132	60.3	48.9	-16.0	07/27/97	9091	13.5	38.6	-18.0
06/21/97	3685	23.1	37.5	-19.0	07/28/97	3044	14.7	26.0	-18.0
06/22/97	16525	29.8	43.3	-19.0	07/29/97	2004	12.0	27.5	-18.0
06/23/97	11753	19.2	37.6	-20.0	07/30/97	3357	9.5	34.9	-17.0
06/24/97	4115	48.7	38.4	-16.0	07/31/97	8494	4.3	16.9	-17.0
06/25/97	3739	33.0	34.9	-15.0	08/01/97	6202	4.8	31.7	-19.0
06/26/97	15	6.7	0.0	-17.0	08/02/97	12338	26.8	43.1	-17.0
06/27/97	13647	50.4	52.0	-19.0	08/03/97	5648	6.6	27.9	-17.0
06/28/97	20252	19.1	34.3	-18.0	08/04/97	1289	12.0	30.0	-20.0
06/29/97	14578	13.6	35.4	-20.0	08/05/97	1971	24.2	34.7	-19.0
06/30/97	17285	30.1	37.7	-19.0	08/06/97	426	6.8	17.1	-16.0
07/01/97	22540	13.1	27.4	-19.0	08/07/97	21	4.8	0.0	-19.0
07/02/97	98	8.2	17.6	-23.0	08/08/97	12530	4.8	22.7	-18.0

Table A-1 (continued)

Date for start of 24 hours (start at 1700 UTC)	Cloud-to-ground flashes	Percent positive flashes	Median peak positive current (kA)	Median peak negative current (kA)	Date for start of 24 hours (start at 1700 UTC)	Cloud-to-ground flashes	Percent positive flashes	Median peak positive current (kA)	Median peak negative current (kA)
08/09/97	4350	7.1	23.0	-18.0	09/16/97	53	17.0	25.8	-15.0
08/10/97	1076	23.1	31.5	-18.0	09/18/97	1203	33.3	55.6	-16.0
08/11/97	1813	20.7	30.4	-18.0	09/19/97	1052	3.7	22.8	-18.0
08/12/97	265	33.2	41.5	-14.0	09/20/97	6	33.3	65.3	-23.0
08/13/97	7069	21.0	36.0	-16.0	09/21/97	1	0.0	0.0	0.0
08/14/97	5103	14.6	32.7	-17.0	09/22/97	45	17.8	36.4	-20.0
08/15/97	386	11.4	30.7	-16.0	09/26/97	52	13.5	31.7	-20.0
08/16/97	2338	25.4	34.8	-18.0	09/27/97	242	13.6	39.4	-17.0
08/17/97	3061	8.9	26.4	-16.0	10/02/97	64	0.0	0.0	-19.0
08/18/97	7326	8.1	22.6	-20.0	10/03/97	13	0.0	0.0	-21.0
08/19/97	2330	8.6	36.1	-18.0	10/04/97	460	19.8	34.1	-17.0
08/20/97	968	23.0	27.5	-15.0	10/05/97	1581	4.3	25.6	-17.0
08/21/97	3209	38.0	41.6	-17.0	10/06/97	515	7.6	39.2	-21.0
08/22/97	756	15.1	27.8	-18.0	10/07/97	1265	12.3	33.6	-19.0
08/23/97	833	9.7	30.7	-15.0	10/08/97	1772	16.1	33.2	-16.0
08/24/97	9371	6.2	22.0	-18.0	10/10/97	6866	10.4	33.1	-21.0
08/25/97	1253	1.8	27.0	-19.0	10/11/97	10057	29.1	35.0	-16.0
08/26/97	13971	14.8	43.8	-17.0	10/12/97	1	0.0	0.0	0.0
08/27/97	11732	10.2	34.2	-19.0	10/13/97	5	20.0	0.0	-18.0
08/28/97	19759	3.7	31.1	-22.0	10/19/97	9	0.0	0.0	-52.0
08/29/97	17023	26.0	47.4	-18.0	10/23/97	623	11.6	38.5	-23.0
08/30/97	2288	15.6	35.2	-19.0	10/24/97	29	31.0	37.8	-24.0
08/31/97	17157	38.3	49.6	-19.0	10/25/97	21	9.5	40.6	-30.0
09/01/97	12210	10.0	17.6	-17.0	10/30/97	18	55.6	40.9	-12.0
09/03/97	1283	2.9	30.9	-23.0	10/31/97	1	0.0	0.0	0.0
09/04/97	3551	5.4	28.9	-17.0	11/01/97	2	0.0	0.0	-16.0
09/05/97	470	4.0	35.3	-16.0	11/27/97	23	13.0	29.9	-28.0
09/06/97	16900	16.5	33.7	-17.0	11/28/97	19	5.3	0.0	-39.0
09/07/97	5811	14.7	46.8	-17.0	12/08/97	8	25.0	61.3	-18.0
09/08/97	5605	34.6	42.3	-15.0	01/02/98	1	0.0	0.0	0.0
09/09/97	13	38.5	25.7	-17.0	01/03/98	1	0.0	0.0	0.0
09/11/97	4991	7.2	32.0	-21.0	01/17/98	12	0.0	0.0	-15.0
09/12/97	2504	6.7	32.4	-27.0	01/31/98	2	0.0	0.0	-11.0
09/13/97	5927	4.2	25.8	-18.0	02/24/98	391	23.3	36.2	-22.0
09/14/97	13187	16.1	38.0	-20.0	02/25/98	984	54.4	39.7	-17.0
09/15/97	16536	5.8	38.9	-21.0	03/06/98	24	4.2	0.0	-36.0

Table A-1 (continued)

Date for start of 24 hours (start at 1700 UTC)	Cloud-to-ground flashes	Percent positive flashes	Median peak positive current (kA)	Median peak negative current (kA)	Date for start of 24 hours (start at 1700 UTC)	Cloud-to-ground flashes	Percent positive flashes	Median peak positive current (kA)	Median peak negative current (kA)
03/24/98	132	54.5	38.7	-13.0	05/13/98	4892	40.7	35.4	-13.0
03/25/98	327	35.2	40.8	-17.0	05/14/98	9475	52.8	56.1	-12.0
03/26/98	3432	40.9	32.0	-15.0	05/15/98	6895	51.7	32.7	-14.0
03/27/98	181	38.1	30.5	-16.0	05/16/98	87	35.6	35.6	-15.0
03/28/98	1940	13.2	36.8	-16.0	05/17/98	3461	28.1	34.0	-10.0
03/29/98	426	20.0	44.0	-20.0	05/18/98	3968	32.3	33.8	-16.0
03/30/98	3	0.0	0.0	-37.0	05/19/98	7529	52.5	34.8	-15.0
03/31/98	9	0.0	0.0	-21.0	05/20/98	5165	38.7	36.2	-16.0
04/02/98	555	33.0	30.2	-18.0	05/21/98	7883	38.0	35.7	-17.0
04/05/98	140	26.4	31.9	-15.0	05/22/98	2118	52.6	37.7	-16.0
04/06/98	1180	40.3	35.9	-20.0	05/23/98	1159	23.1	35.9	-17.0
04/07/98	42	31.0	41.4	-19.0	05/24/98	1828	44.9	37.1	-17.0
04/09/98	72	15.3	35.9	-11.0	05/25/98	2	50.0	0.0	0.0
04/10/98	102	20.6	38.0	-14.0	05/26/98	3070	31.5	30.7	-17.0
04/11/98	1802	19.0	52.4	-17.0	05/27/98	10078	28.2	36.7	-12.0
04/12/98	793	28.5	41.0	-15.0	05/28/98	3356	56.0	45.2	-15.0
04/13/98	78	11.5	22.6	-15.0	05/29/98	9775	24.8	31.6	-16.0
04/14/98	624	30.3	35.8	-17.0	05/30/98	6092	63.9	48.9	-14.0
04/17/98	8	0.0	0.0	-15.0	05/31/98	731	20.1	35.5	-17.0
04/18/98	149	31.5	64.1	-17.0	06/01/98	3716	13.7	26.0	-14.0
04/19/98	512	36.5	48.0	-18.0	06/02/98	1802	40.6	36.8	-18.0
04/20/98	17	76.5	67.3	-18.0	06/03/98	98	3.1	74.7	-19.0
04/24/98	2856	25.5	37.5	-17.0	06/04/98	107	72.0	49.1	-18.0
04/25/98	1266	23.7	33.2	-20.0	06/05/98	3	33.3	0.0	-20.0
04/30/98	270	3.3	32.1	-14.0	06/06/98	214	18.7	44.3	-18.0
05/01/98	360	21.1	39.1	-15.0	06/07/98	9400	18.9	31.6	-18.0
05/03/98	155	52.9	41.4	-15.0	06/08/98	2250	14.7	28.6	-23.0
05/04/98	1514	38.9	43.1	-17.0	06/09/98	2002	19.7	31.9	-16.0
05/05/98	830	19.5	34.3	-18.0	06/10/98	8499	16.3	31.7	-14.0
05/06/98	1044	26.8	39.0	-17.0	06/11/98	3427	16.3	30.2	-15.0
05/07/98	338	31.1	37.3	-16.0	06/12/98	141	21.3	42.1	-16.0
05/08/98	1282	28.6	32.7	-17.0	06/13/98	11105	19.9	31.8	-17.0
05/09/98	286	23.4	31.6	-16.0	06/14/98	2869	15.3	29.2	-15.0
05/10/98	4571	29.4	36.4	-15.0	06/15/98	2451	16.4	19.5	-16.0
05/11/98	4273	36.0	40.0	-17.0	06/16/98	11610	12.8	27.9	-19.0
05/12/98	1603	15.5	30.7	-16.0	06/17/98	23889	31.4	33.0	-17.0

Table A-1 (continued)

Date for start of 24 hours (start at 1700 UTC)	Cloud-to-ground flashes	Percent positive flashes	Median peak positive current (kA)	Median peak negative current (kA)	Date for start of 24 hours (start at 1700 UTC)	Cloud-to-ground flashes	Percent positive flashes	Median peak positive current (kA)	Median peak negative current (kA)
06/18/98	5407	12.2	24.5	-16.0	07/24/98	9133	10.6	29.2	-19.0
06/19/98	506	36.0	29.5	-15.0	07/25/98	10015	11.5	31.5	-18.0
06/20/98	467	37.7	36.9	-17.0	07/26/98	306	17.6	37.3	-15.0
06/21/98	3157	29.9	34.3	-17.0	07/27/98	1241	9.8	20.8	-15.0
06/22/98	8765	28.7	34.1	-18.0	07/28/98	585	26.8	31.2	-19.0
06/23/98	14660	12.9	26.1	-16.0	07/29/98	9501	11.7	36.6	-18.0
06/24/98	16167	38.2	39.9	-15.0	07/30/98	1908	14.5	30.1	-18.0
06/25/98	6341	6.5	19.9	-17.0	07/31/98	416	0.5	24.7	-17.0
06/26/98	24390	32.4	37.5	-15.0	08/01/98	24751	10.2	25.5	-16.0
06/27/98	8872	10.9	21.4	-15.0	08/02/98	7564	10.9	29.7	-16.0
06/28/98	2419	6.5	17.5	-18.0	08/03/98	501	6.0	29.4	-17.0
06/29/98	2415	17.6	32.5	-19.0	08/04/98	1457	6.1	17.2	-14.0
06/30/98	5882	8.1	25.3	-16.0	08/05/98	754	4.1	15.8	-15.0
07/01/98	12274	18.2	31.0	-17.0	08/06/98	100	2.0	75.8	-21.0
07/02/98	17700	23.1	32.9	-16.0	08/07/98	44	13.6	18.6	-21.0
07/03/98	4932	6.8	23.7	-17.0	08/08/98	2311	16.8	33.8	-17.0
07/04/98	50173	10.6	19.1	-17.0	08/09/98	9638	12.1	31.2	-16.0
07/05/98	24105	14.1	21.9	-16.0	08/10/98	5187	9.5	20.5	-16.0
07/06/98	25556	25.6	42.9	-17.0	08/11/98	8349	13.1	30.1	-15.0
07/07/98	3051	18.6	32.3	-15.0	08/12/98	8166	12.4	21.8	-15.0
07/08/98	4596	13.2	30.3	-17.0	08/13/98	10242	7.0	17.6	-16.0
07/09/98	10647	12.0	29.9	-17.0	08/14/98	6397	15.3	31.5	-18.0
07/10/98	2897	5.7	22.3	-18.0	08/15/98	2456	10.2	22.0	-21.0
07/11/98	25271	9.9	19.2	-16.0	08/16/98	7585	35.7	41.9	-16.0
07/12/98	752	15.3	37.5	-17.0	08/17/98	6260	8.6	15.0	-16.0
07/13/98	11587	40.2	42.3	-16.0	08/18/98	29824	14.6	31.3	-15.0
07/14/98	24139	40.3	44.8	-16.0	08/19/98	17073	16.7	37.4	-15.0
07/15/98	1746	19.7	31.7	-18.0	08/20/98	4618	14.2	32.1	-19.0
07/16/98	952	8.1	19.2	-22.0	08/21/98	37722	14.6	19.1	-16.0
07/17/98	5578	17.1	19.1	-18.0	08/22/98	10375	11.4	25.5	-17.0
07/18/98	18511	44.0	50.3	-17.0	08/23/98	15981	7.0	23.2	-18.0
07/19/98	6995	10.8	19.0	-18.0	08/24/98	4055	10.2	28.8	-18.0
07/20/98	12750	26.7	44.8	-17.0	08/25/98	8525	5.0	21.7	-16.0
07/21/98	10389	21.6	35.0	-18.0	08/26/98	36868	8.4	19.9	-16.0
07/22/98	1207	13.0	25.8	-19.0	08/27/98	1167	16.1	33.2	-17.0
07/23/98	4623	14.6	33.9	-18.0	08/30/98	7673	17.6	38.8	-19.0

Table A-1 (continued)

Date for start of 24 hours (start at 1700 UTC)	Cloud-to-ground flashes	Percent positive flashes	Median peak positive current (kA)	Median peak negative current (kA)	Date for start of 24 hours (start at 1700 UTC)	Cloud-to-ground flashes	Percent positive flashes	Median peak positive current (kA)	Median peak negative current (kA)
08/31/98	10412	7.4	21.0	-15.0	10/02/98	3	33.3	0.0	-11.0
09/01/98	3	33.3	0.0	-9.0	10/03/98	15267	10.8	24.4	-24.0
09/05/98	1201	4.7	17.5	-18.0	10/04/98	12777	15.0	27.7	-21.0
09/07/98	125	8.8	20.7	-17.0	10/05/98	295	28.1	26.7	-19.0
09/08/98	2492	3.4	14.1	-18.0	10/10/98	8411	14.2	30.5	-18.0
09/09/98	768	2.0	14.3	-18.0	10/11/98	207	22.7	33.3	-18.0
09/10/98	2214	9.5	24.0	-15.0	10/13/98	147	6.8	23.1	-29.0
09/11/98	466	15.0	26.2	-13.0	10/14/98	8686	5.7	22.6	-20.0
09/12/98	2500	13.1	27.2	-16.0	10/15/98	16670	13.9	27.5	-18.0
09/13/98	6519	8.4	23.7	-16.0	10/16/98	5813	27.7	34.3	-17.0
09/14/98	85	8.2	26.2	-21.0	10/17/98	3	0.0	0.0	-12.0
09/15/98	4	25.0	0.0	-12.0	10/23/98	124	16.9	51.2	-19.0
09/17/98	300	2.0	23.8	-15.0	10/24/98	120	15.8	36.5	-21.0
09/18/98	9383	7.6	25.8	-15.0	10/25/98	442	11.3	27.1	-18.0
09/19/98	1240	6.5	19.1	-16.0	10/26/98	392	17.9	36.6	-22.0
09/20/98	741	14.8	34.4	-13.0	10/27/98	233	40.8	39.8	-20.0
09/21/98	17	41.2	42.1	-15.0	10/28/98	2511	25.6	34.9	-18.0
09/22/98	90	10.0	29.9	-17.0	10/29/98	176	21.6	39.6	-18.0
09/23/98	1433	3.6	22.2	-19.0	10/30/98	269	50.2	39.1	-21.0
09/24/98	280	7.9	31.0	-16.0	11/06/98	38	31.6	48.7	-28.0
09/25/98	9077	19.4	31.5	-16.0	11/09/98	359	31.8	47.0	-27.0
09/26/98	3	0.0	0.0	-22.0	11/10/98	3	0.0	0.0	-14.0
09/27/98	1	0.0	0.0	0.0	11/16/98	2	0.0	0.0	-17.0
09/28/98	1660	15.1	41.8	-17.0	11/17/98	107	29.9	38.7	-31.0
09/29/98	1710	10.0	32.4	-17.0	11/18/98	14	42.9	58.5	-29.0
09/30/98	345	38.3	38.1	-19.0	12/04/98	32	12.5	27.2	-19.0
10/01/98	28	14.3	37.6	-20.0					

APPENDIX B

LIGHTNING AND VERTICAL WIND SHEAR FOR THE NORTHERN PLAINS

CASES

The vertical wind shear was calculated from the surface to each of the following pressure levels: 850, 500, 300, 250, 200 mb. Overlays of the vertical wind shears for each case used in studying the connection between vertical wind shear and the percentage of positive flashes and peak currents in the Northern Plains follow. A listing of the sites used can be found in Table B-1.

No correlation was found between vertical wind shear and the percentage of positive flashes or the first stroke peak currents.

Table B-1. Summary of locations used in calculating vertical wind shear.

International Civil Aviation Organization (ICAO) designator	Latitude (deg N)	Longitude (deg W)	City
ABR	45.45	98.42	Aberdeen, SD
BIS	46.77	100.75	Bismark, ND
DDC	37.77	99.97	Dodge City, KS
DEN	39.77	104.88	Denver, CO
INL	48.57	93.38	International Falls, MN
LBF	41.13	100.68	North Platte, NE
MPX	44.83	93.55	Minneapolis, MN
OAX	41.32	96.37	Omaha, NE
SGF	37.23	93.40	Springfield, MO
STC	45.55	94.07	St. Cloud, MN
TOP	39.07	95.62	Topeka, KS
UNR	44.07	103.21	Rapid City SD

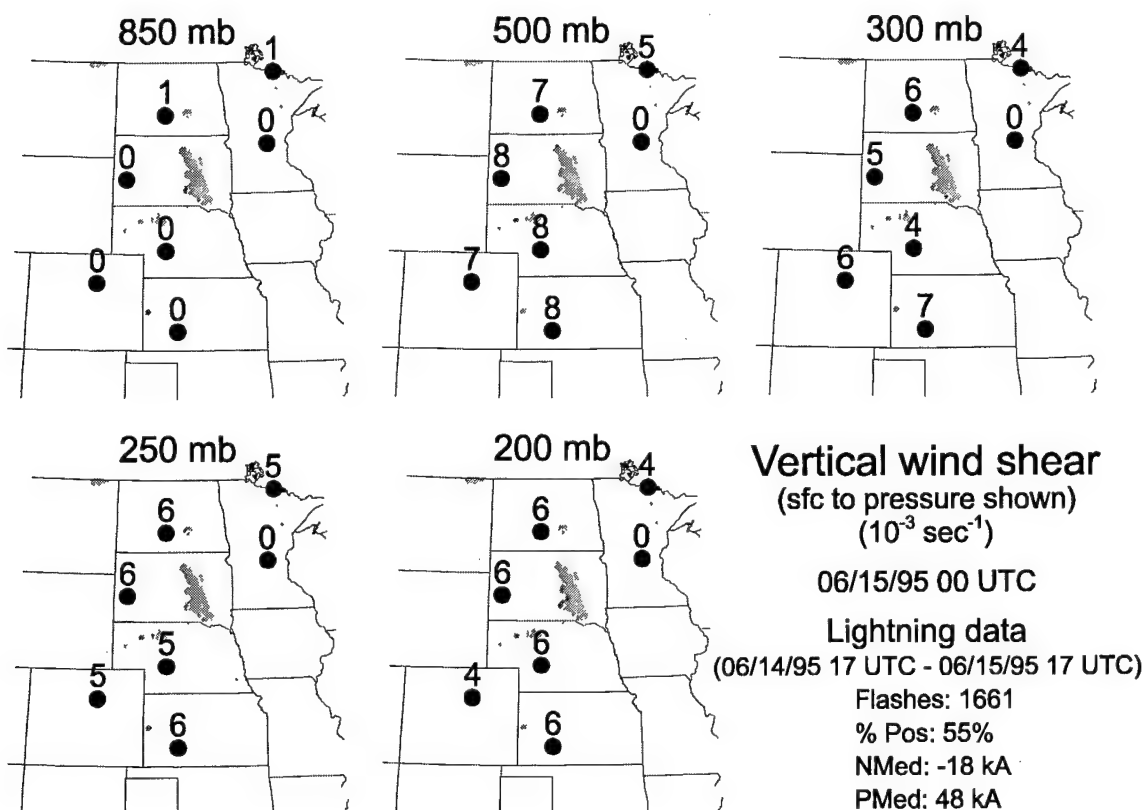


Figure B-1. Vertical wind shear and lightning locations for 15 Jun 95. Lightning locations are shown as gray shaded regions and the vertical wind shear is listed above the circle. Vertical wind shears are calculated from the surface to the pressure levels shown. Missing data are represented as zeroes. The lightning summary information is also provided to include the number of flashes, the percentage of positive flashes, and the median peak currents for negative and positive flashes. Only positive flashes of at least 10 kA were included.

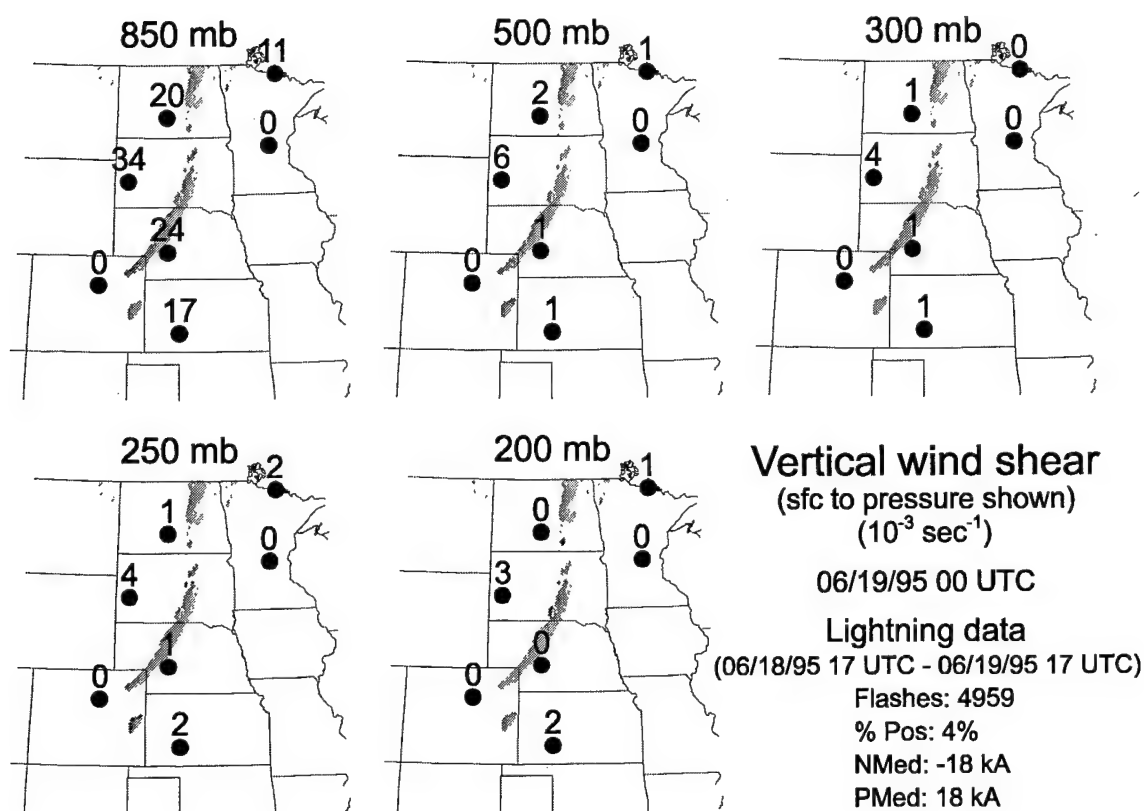


Figure B-2. Vertical wind shear and lightning locations for 19 Jun 95. Lightning locations are shown as gray shaded regions and the vertical wind shear is listed above the circle. Vertical wind shears are calculated from the surface to the pressure levels shown. Missing data are represented as zeroes. The lightning summary information is also provided to include the number of flashes, the percentage of positive flashes, and the median peak currents for negative and positive flashes. Only positive flashes of at least 10 kA were included.

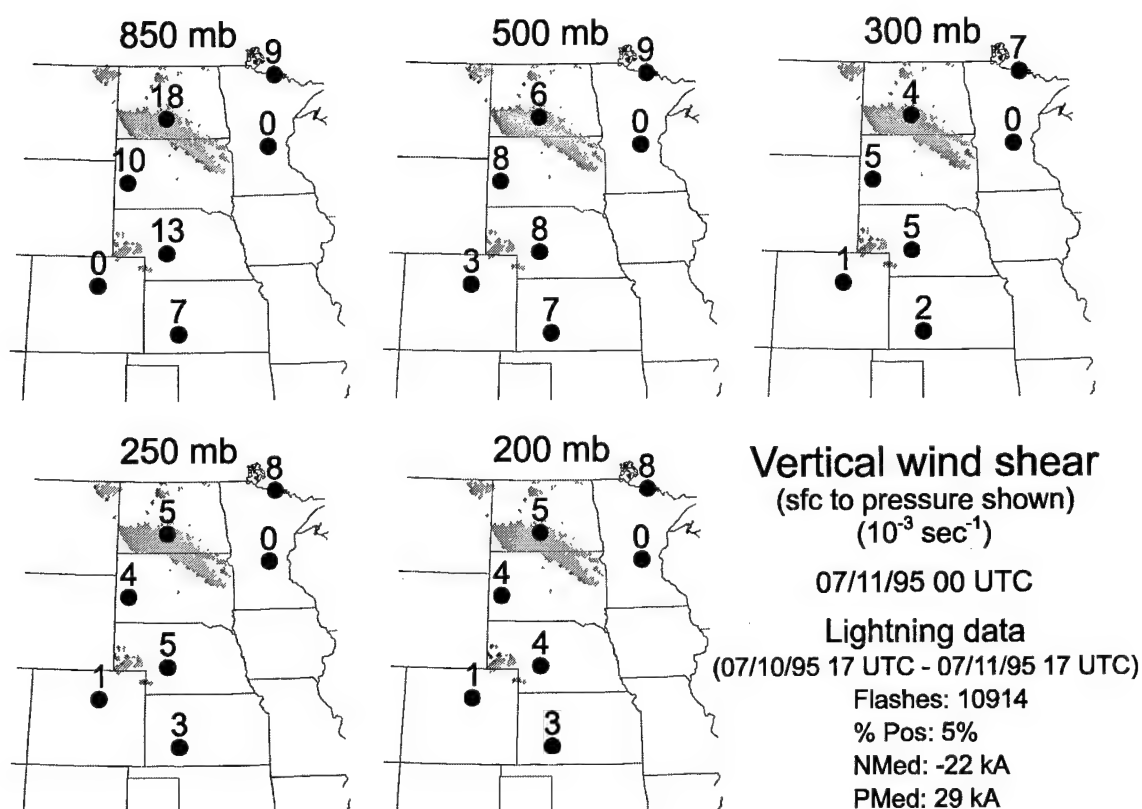


Figure B-3. Vertical wind shear and lightning locations for 11 Jul 95. Lightning locations are shown as gray shaded regions and the vertical wind shear is listed above the circle. Vertical wind shears are calculated from the surface to the pressure levels shown. Missing data are represented as zeroes. The lightning summary information is also provided to include the number of flashes, the percentage of positive flashes, and the median peak currents for negative and positive flashes. Only positive flashes of at least 10 kA were included.

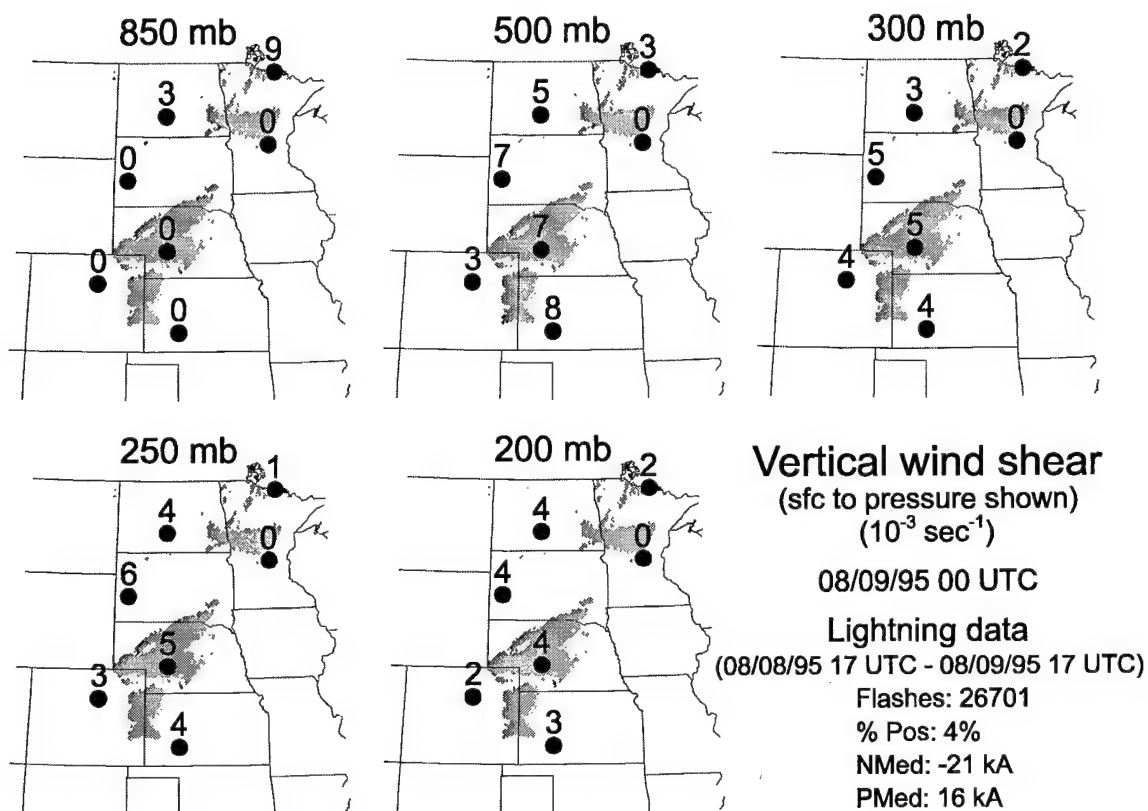


Figure B-4. Vertical wind shear and lightning locations for 9 Aug 95. Lightning locations are shown as gray shaded regions and the vertical wind shear is listed above the circle. Vertical wind shears are calculated from the surface to the pressure levels shown. Missing data are represented as zeroes. The lightning summary information is also provided to include the number of flashes, the percentage of positive flashes, and the median peak currents for negative and positive flashes. Only positive flashes of at least 10 kA were included.

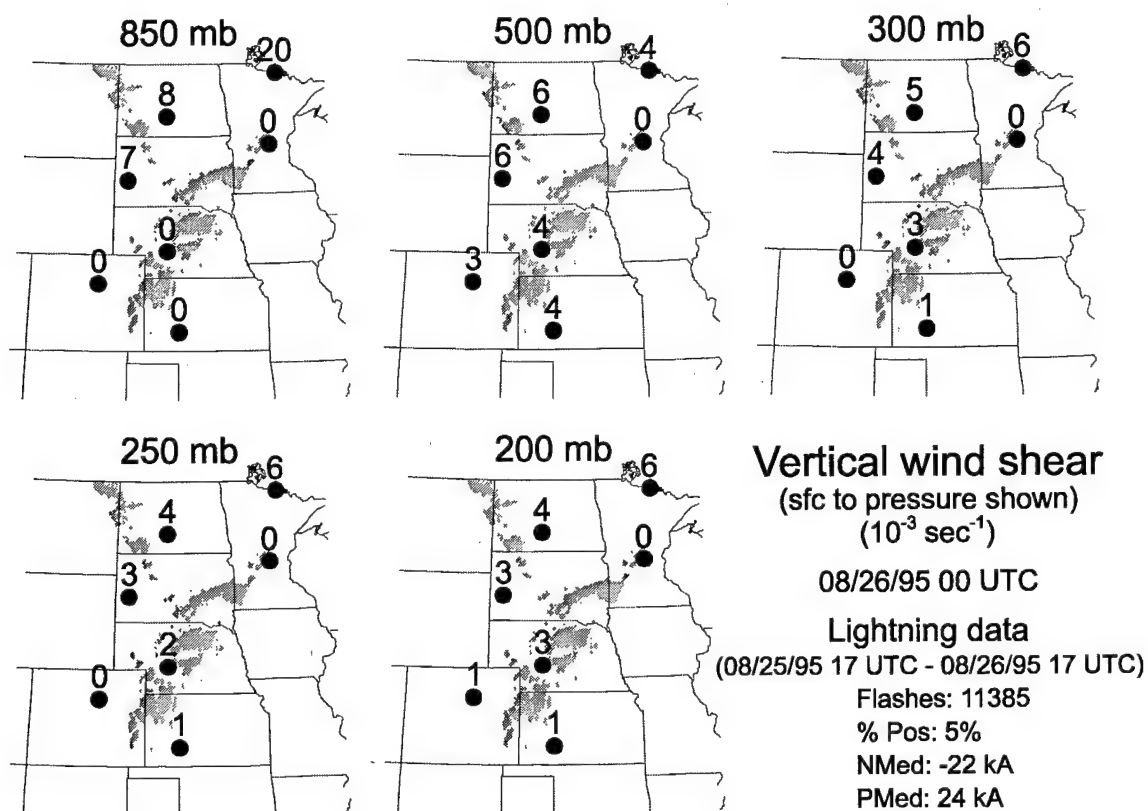


Figure B-5. Vertical wind shear and lightning locations for 26 Aug 95. Lightning locations are shown as gray shaded regions and the vertical wind shear is listed above the circle. Vertical wind shears are calculated from the surface to the pressure levels shown. Missing data are represented as zeroes. The lightning summary information is also provided to include the number of flashes, the percentage of positive flashes, and the median peak currents for negative and positive flashes. Only positive flashes of at least 10 kA were included.

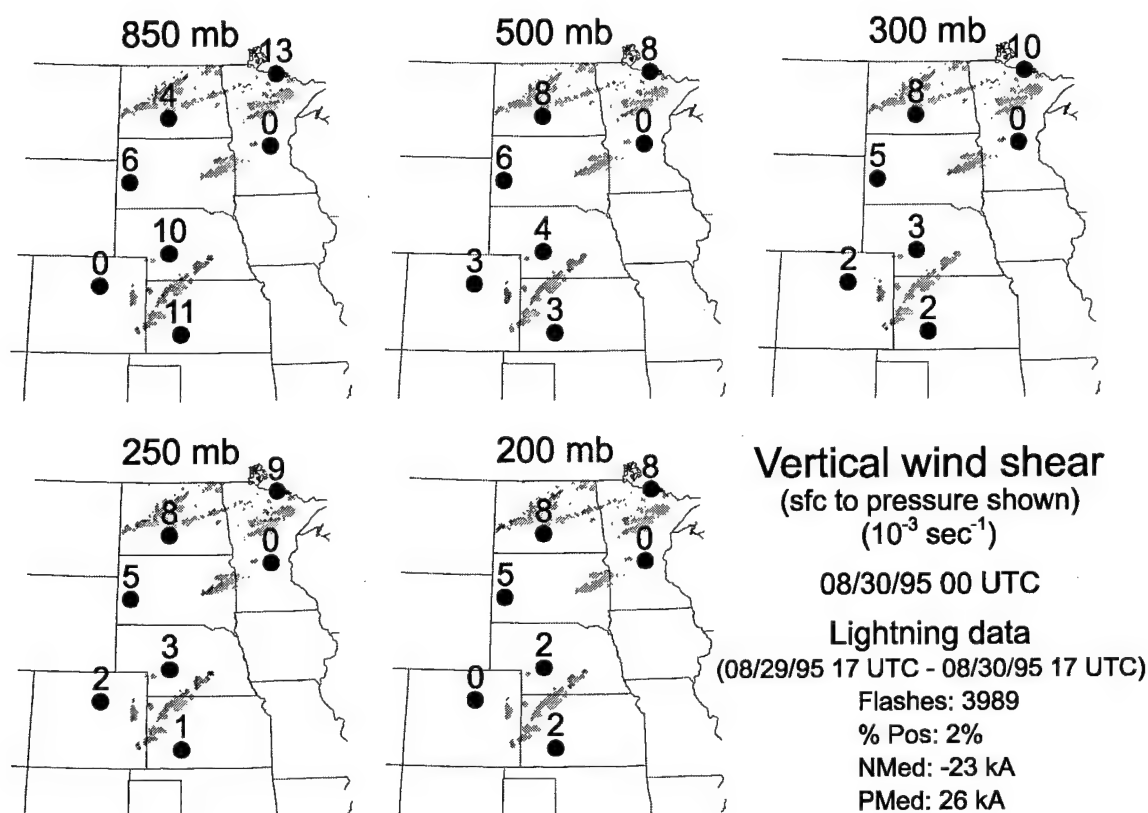


Figure B-6. Vertical wind shear and lightning locations for 30 Aug 95. Lightning locations are shown as gray shaded regions and the vertical wind shear is listed above the circle. Vertical wind shears are calculated from the surface to the pressure levels shown. Missing data are represented as zeroes. The lightning summary information is also provided to include the number of flashes, the percentage of positive flashes, and the median peak currents for negative and positive flashes. Only positive flashes of at least 10 kA were included.

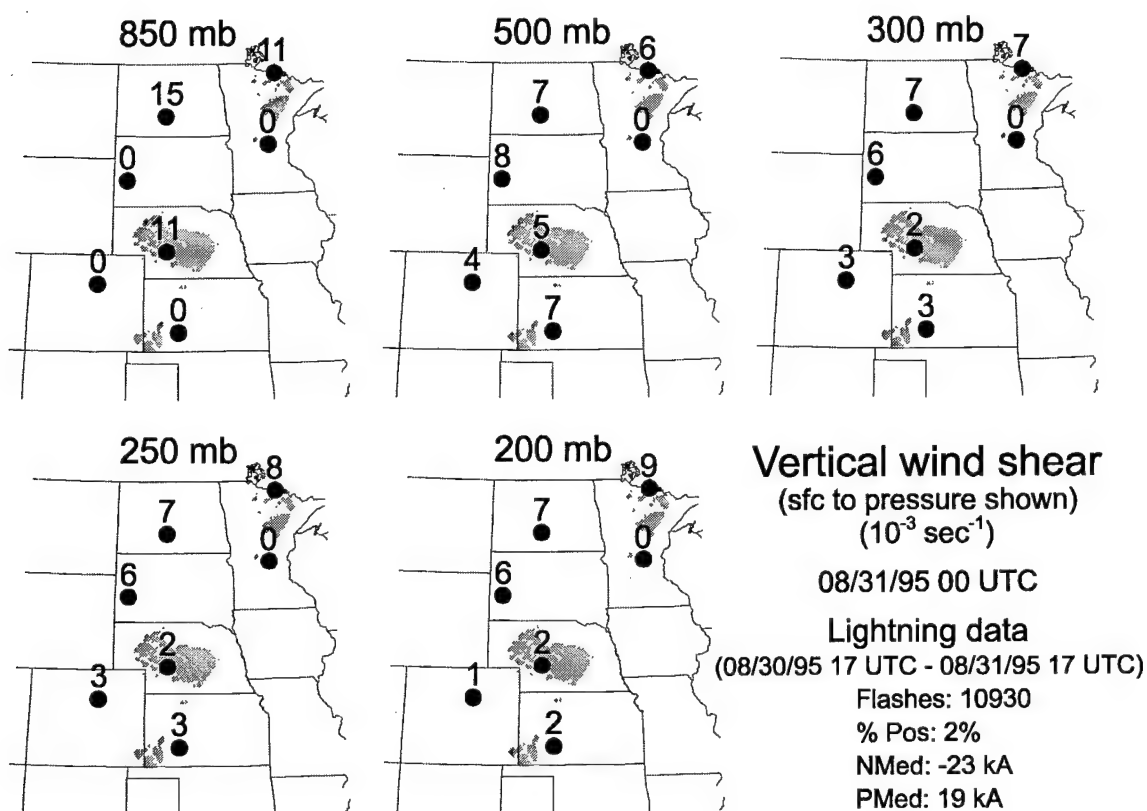


Figure B-7. Vertical wind shear and lightning locations for 31 Aug 95. Lightning locations are shown as gray shaded regions and the vertical wind shear is listed above the circle. Vertical wind shears are calculated from the surface to the pressure levels shown. Missing data are represented as zeroes. The lightning summary information is also provided to include the number of flashes, the percentage of positive flashes, and the median peak currents for negative and positive flashes. Only positive flashes of at least 10 kA were included.

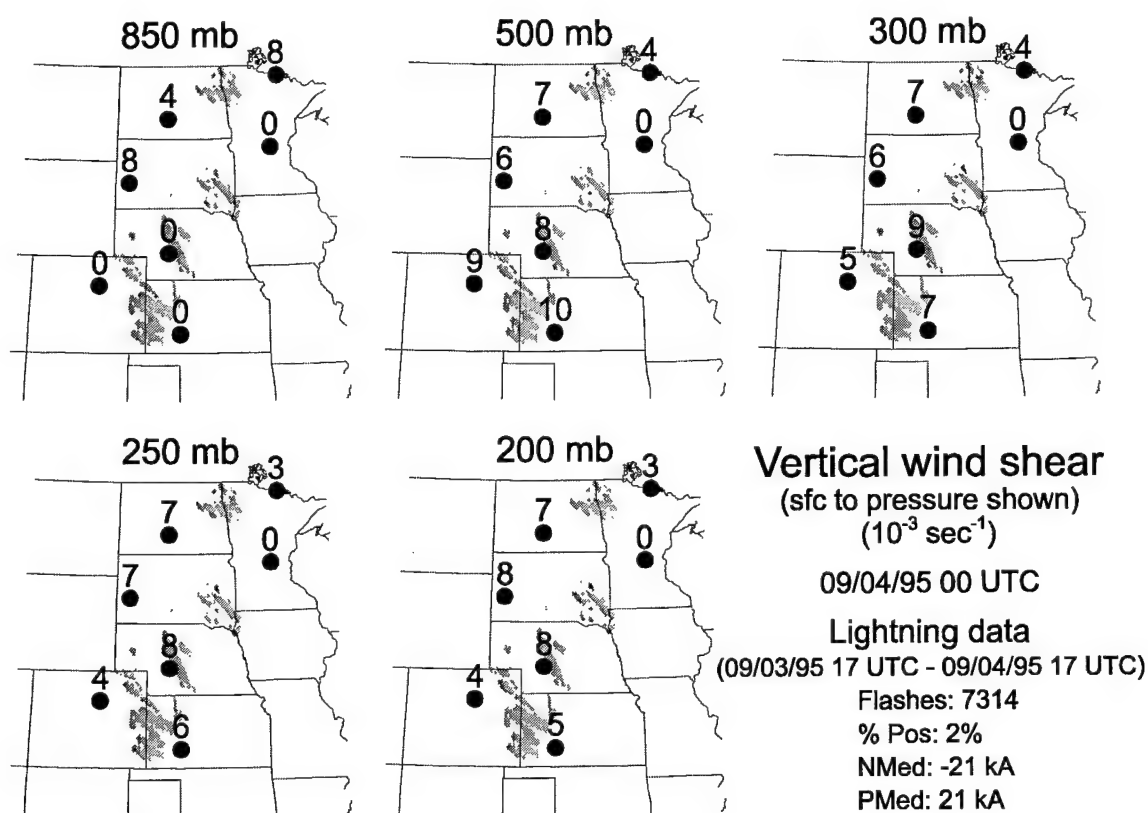


Figure B-8. Vertical wind shear and lightning locations for 4 Sep 95. Lightning locations are shown as gray shaded regions and the vertical wind shear is listed above the circle. Vertical wind shears are calculated from the surface to the pressure levels shown. Missing data are represented as zeroes. The lightning summary information is also provided to include the number of flashes, the percentage of positive flashes, and the median peak currents for negative and positive flashes. Only positive flashes of at least 10 kA were included.

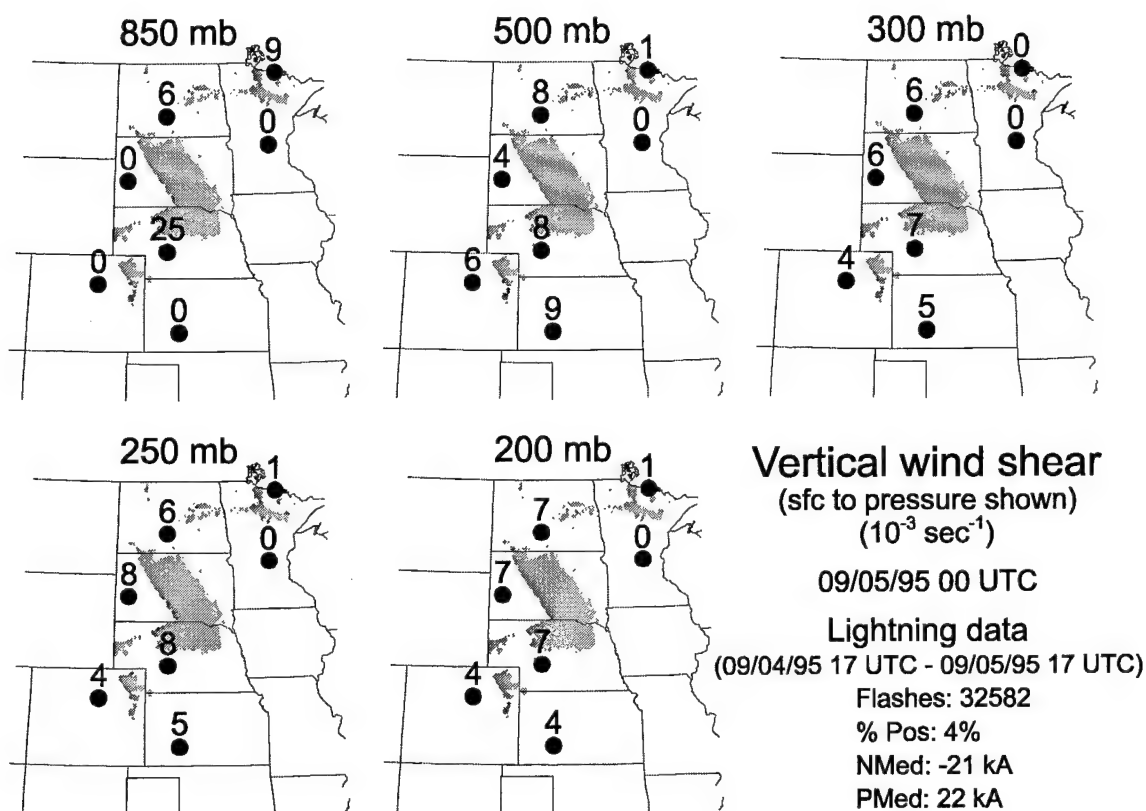


Figure B-9. Vertical wind shear and lightning locations for 5 Sep 95. Lightning locations are shown as gray shaded regions and the vertical wind shear is listed above the circle. Vertical wind shears are calculated from the surface to the pressure levels shown. Missing data are represented as zeroes. The lightning summary information is also provided to include the number of flashes, the percentage of positive flashes, and the median peak currents for negative and positive flashes. Only positive flashes of at least 10 kA were included.

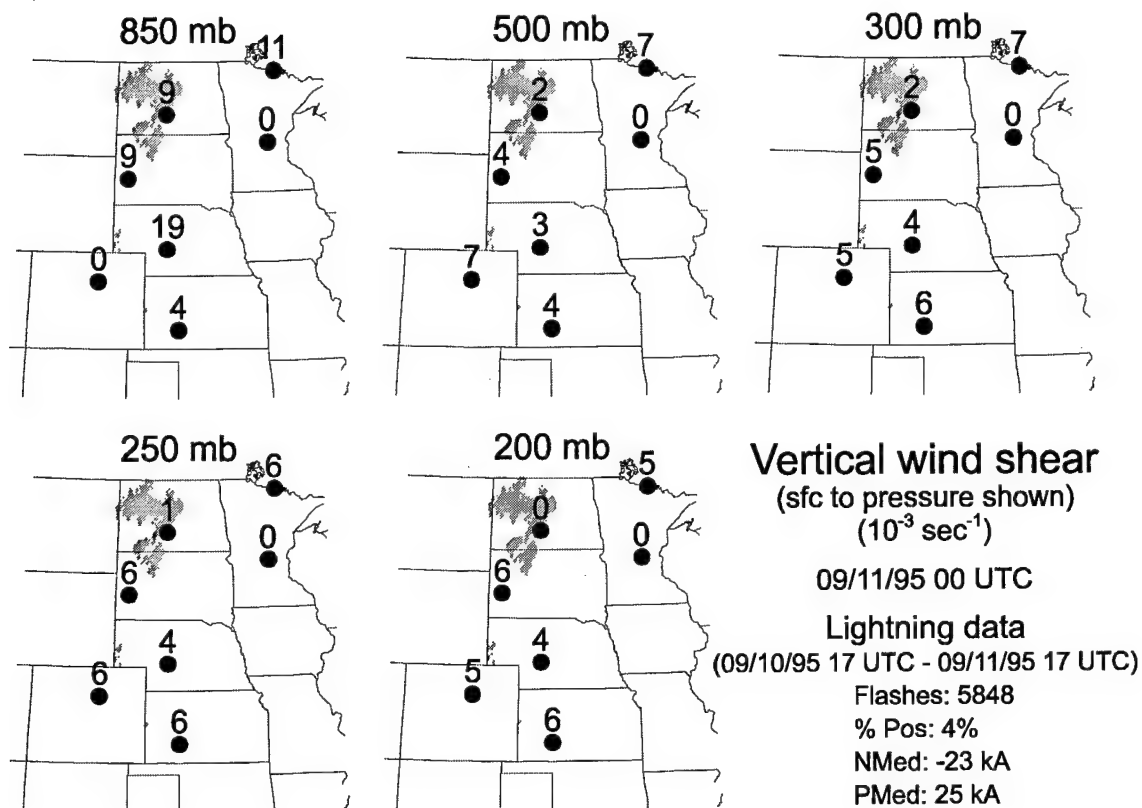


Figure B-10. Vertical wind shear and lightning locations for 11 Sep 95. Lightning locations are shown as gray shaded regions and the vertical wind shear is listed above the circle. Vertical wind shears are calculated from the surface to the pressure levels shown. Missing data are represented as zeroes. The lightning summary information is also provided to include the number of flashes, the percentage of positive flashes, and the median peak currents for negative and positive flashes. Only positive flashes of at least 10 kA were included.

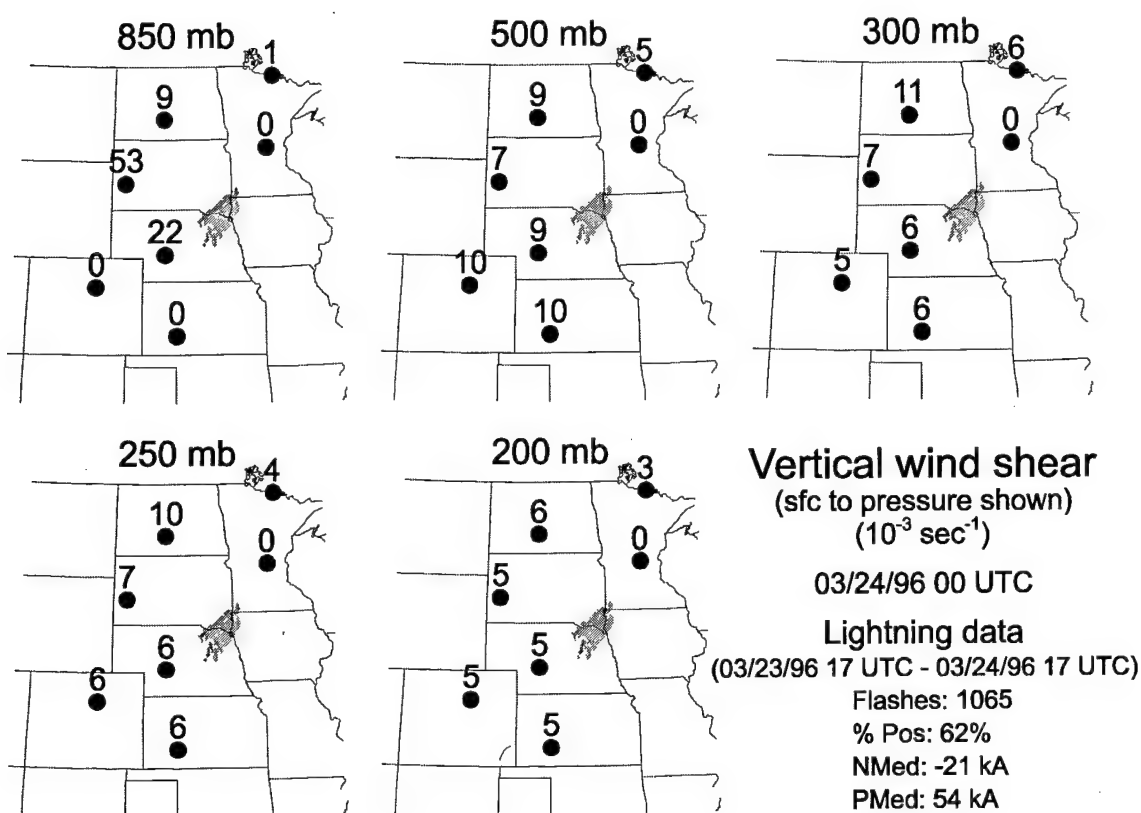


Figure B-11. Vertical wind shear and lightning locations for 24 Mar 96. Lightning locations are shown as gray shaded regions and the vertical wind shear is listed above the circle. Vertical wind shears are calculated from the surface to the pressure levels shown. Missing data are represented as zeroes. The lightning summary information is also provided to include the number of flashes, the percentage of positive flashes, and the median peak currents for negative and positive flashes. Only positive flashes of at least 10 kA were included.

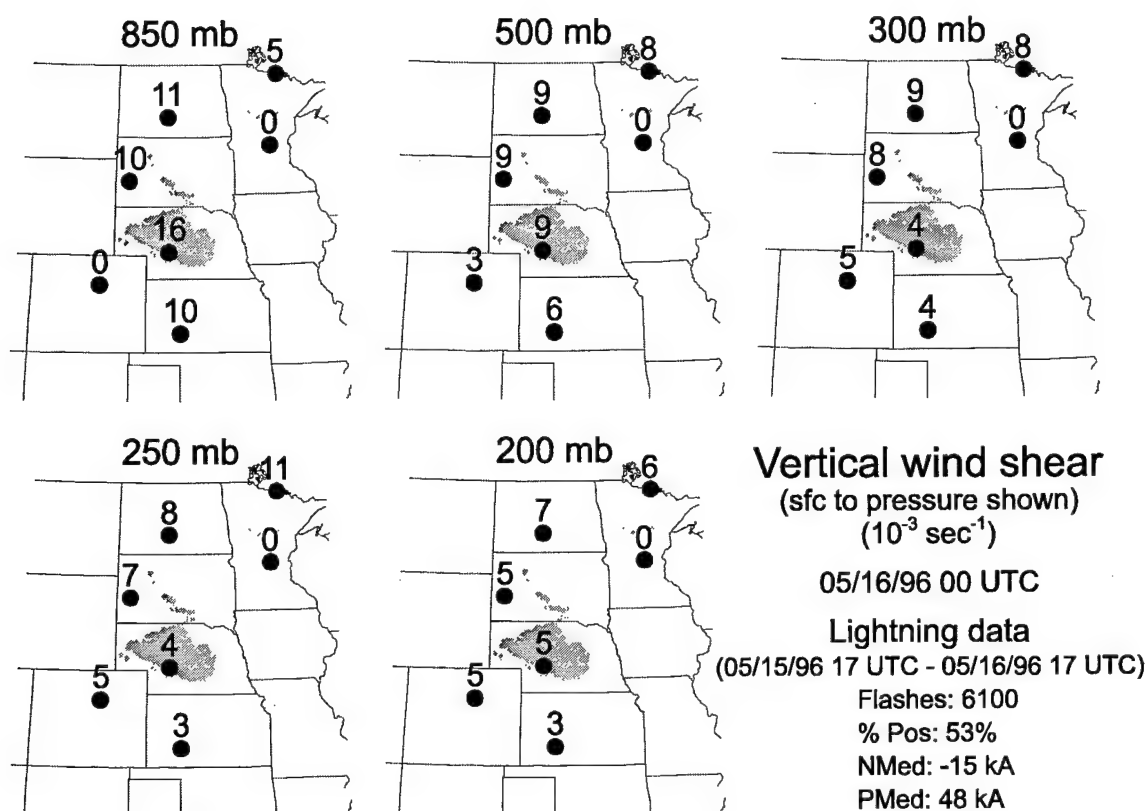


Figure B-12. Vertical wind shear and lightning locations for 16 May 96. Lightning locations are shown as gray shaded regions and the vertical wind shear is listed above the circle. Vertical wind shears are calculated from the surface to the pressure levels shown. Missing data are represented as zeroes. The lightning summary information is also provided to include the number of flashes, the percentage of positive flashes, and the median peak currents for negative and positive flashes. Only positive flashes of at least 10 kA were included.

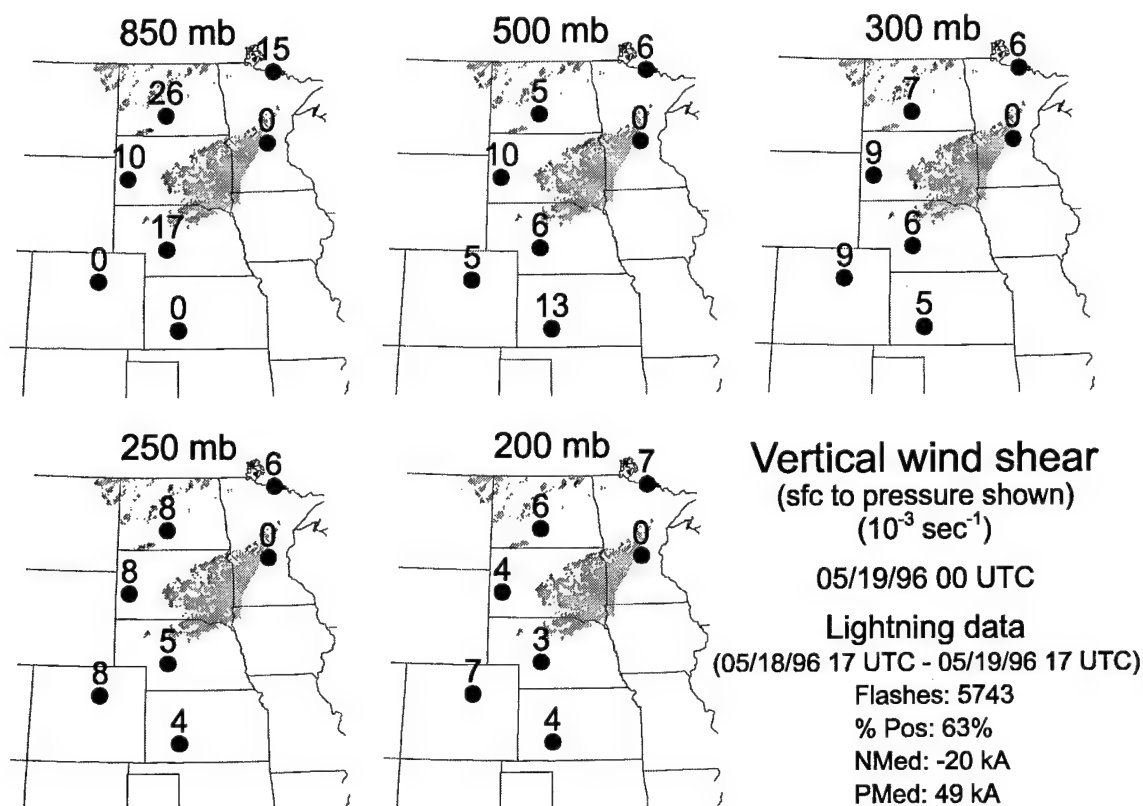


Figure B-13. Vertical wind shear and lightning locations for 19 May 96. Lightning locations are shown as gray shaded regions and the vertical wind shear is listed above the circle. Vertical wind shears are calculated from the surface to the pressure levels shown. Missing data are represented as zeroes. The lightning summary information is also provided to include the number of flashes, the percentage of positive flashes, and the median peak currents for negative and positive flashes. Only positive flashes of at least 10 kA were included.

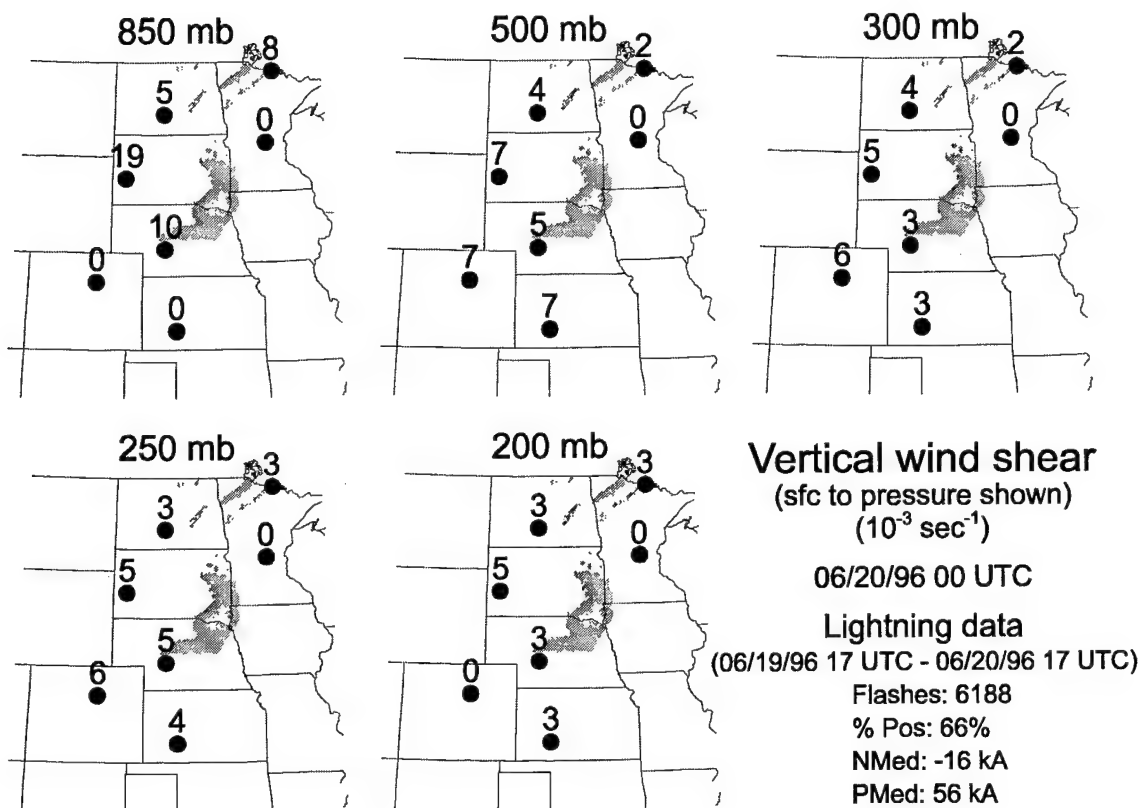


Figure B-14. Vertical wind shear and lightning locations for 20 Jun 96. Lightning locations are shown as gray shaded regions and the vertical wind shear is listed above the circle. Vertical wind shears are calculated from the surface to the pressure levels shown. Missing data are represented as zeroes. The lightning summary information is also provided to include the number of flashes, the percentage of positive flashes, and the median peak currents for negative and positive flashes. Only positive flashes of at least 10 kA were included.

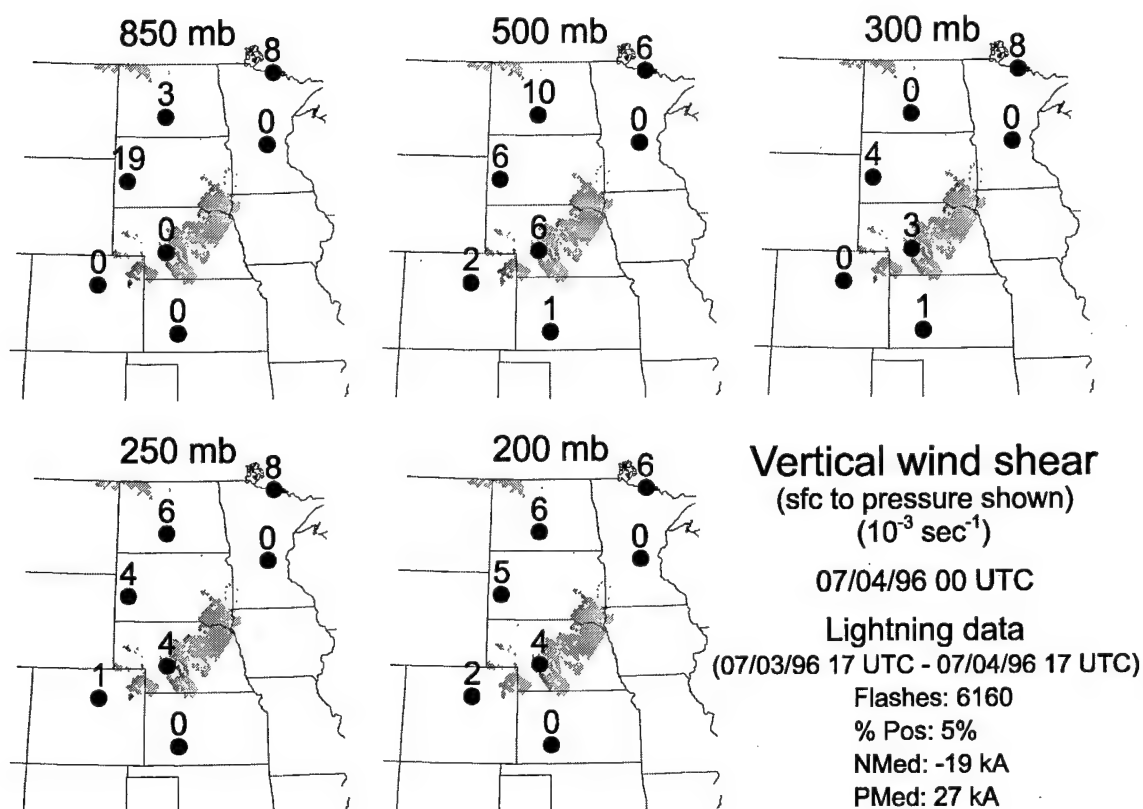


Figure B-15. Vertical wind shear and lightning locations for 4 Jul 96. Lightning locations are shown as gray shaded regions and the vertical wind shear is listed above the circle. Vertical wind shears are calculated from the surface to the pressure levels shown. Missing data are represented as zeroes. The lightning summary information is also provided to include the number of flashes, the percentage of positive flashes, and the median peak currents for negative and positive flashes. Only positive flashes of at least 10 kA were included.

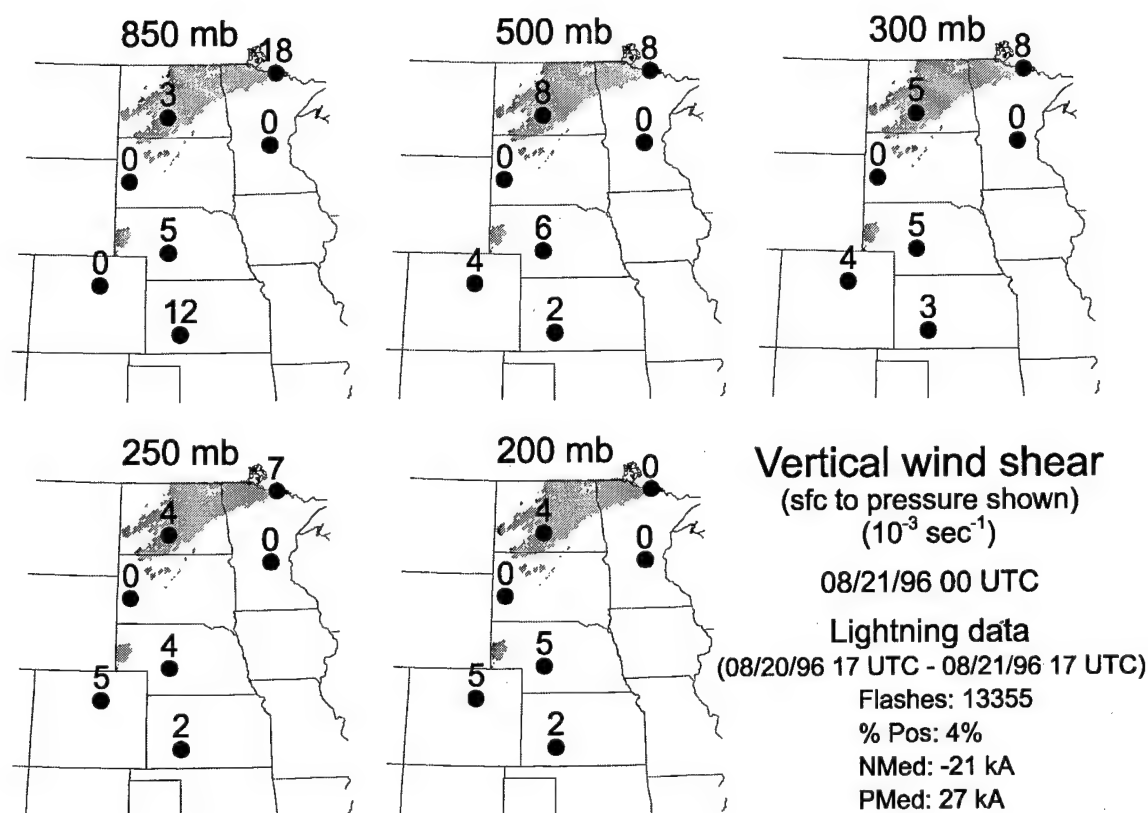


Figure B-16. Vertical wind shear and lightning locations for 21 Aug 96. Lightning locations are shown as gray shaded regions and the vertical wind shear is listed above the circle. Vertical wind shears are calculated from the surface to the pressure levels shown. Missing data are represented as zeroes. The lightning summary information is also provided to include the number of flashes, the percentage of positive flashes, and the median peak currents for negative and positive flashes. Only positive flashes of at least 10 kA were included.

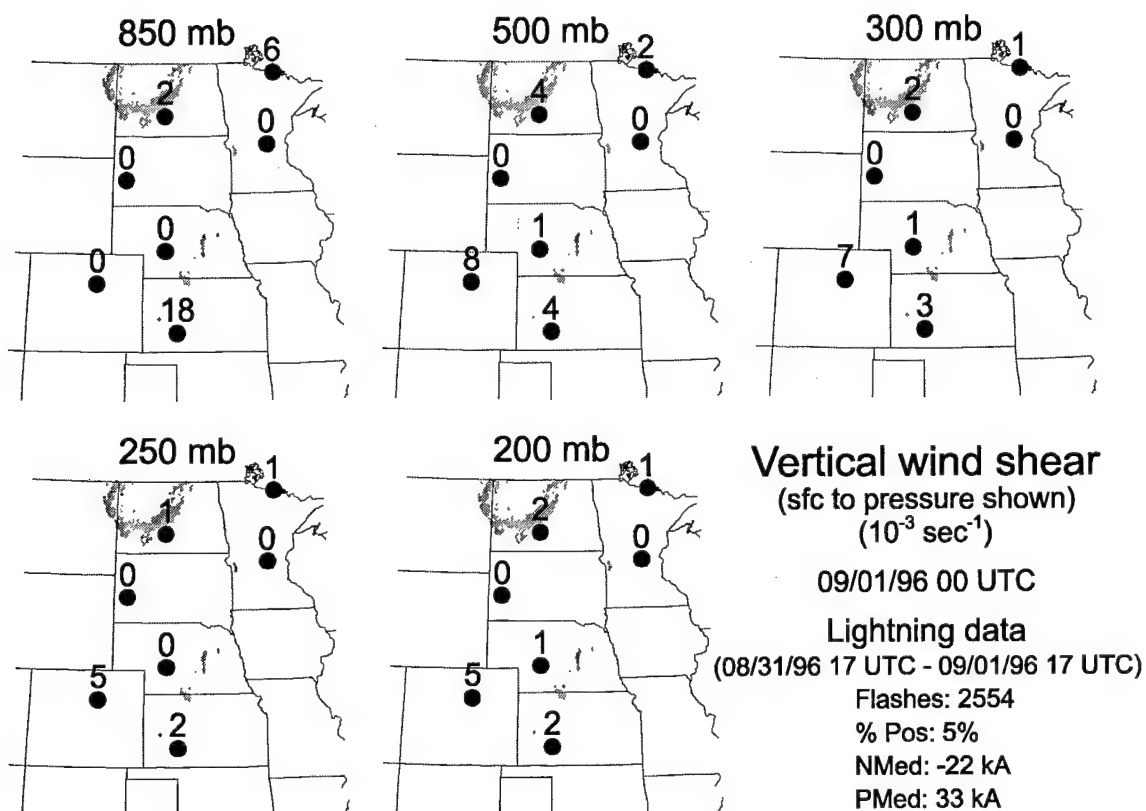


Figure B-17. Vertical wind shear and lightning locations for 1 Sep 96. Lightning locations are shown as gray shaded regions and the vertical wind shear is listed above the circle. Vertical wind shears are calculated from the surface to the pressure levels shown. Missing data are represented as zeroes. The lightning summary information is also provided to include the number of flashes, the percentage of positive flashes, and the median peak currents for negative and positive flashes. Only positive flashes of at least 10 kA were included.

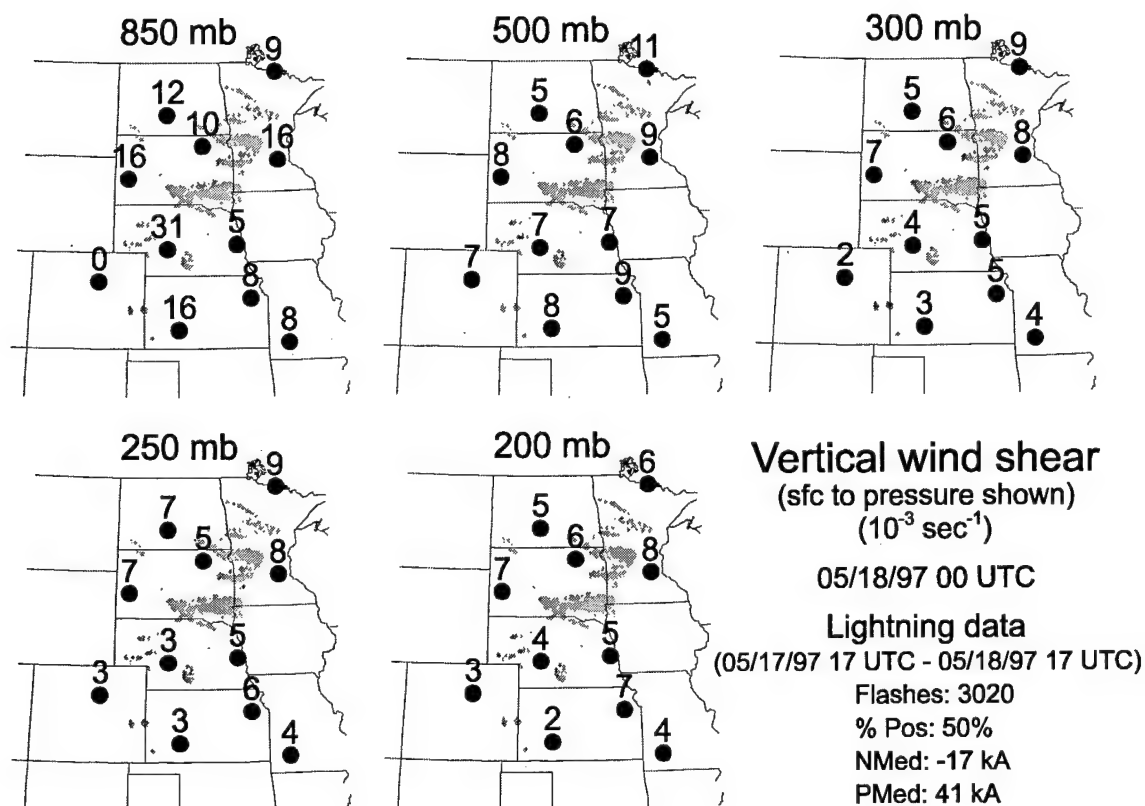


Figure B-18. Vertical wind shear and lightning locations for 18 May 97. Lightning locations are shown as gray shaded regions and the vertical wind shear is listed above the circle. Vertical wind shears are calculated from the surface to the pressure levels shown. Missing data are represented as zeroes. The lightning summary information is also provided to include the number of flashes, the percentage of positive flashes, and the median peak currents for negative and positive flashes. Only positive flashes of at least 10 kA were included.

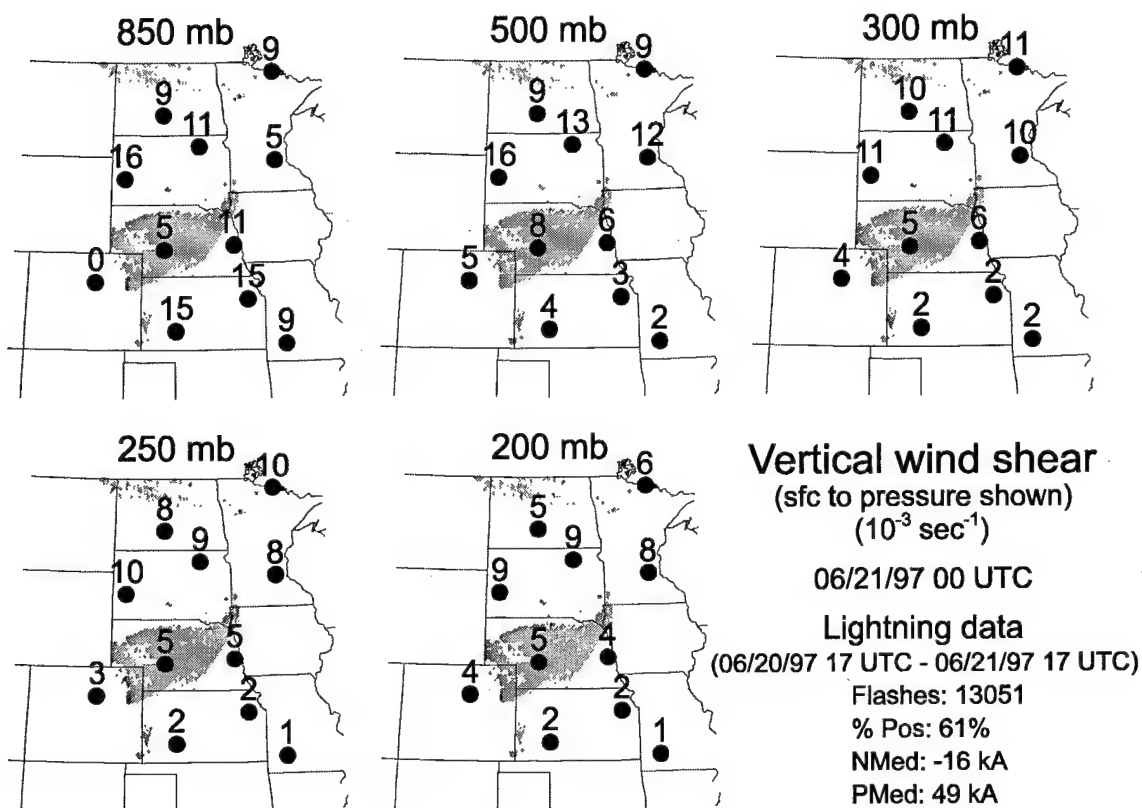


Figure B-19. Vertical wind shear and lightning locations for 21 Jun 97. Lightning locations are shown as gray shaded regions and the vertical wind shear is listed above the circle. Vertical wind shears are calculated from the surface to the pressure levels shown. Missing data are represented as zeroes. The lightning summary information is also provided to include the number of flashes, the percentage of positive flashes, and the median peak currents for negative and positive flashes. Only positive flashes of at least 10 kA were included.

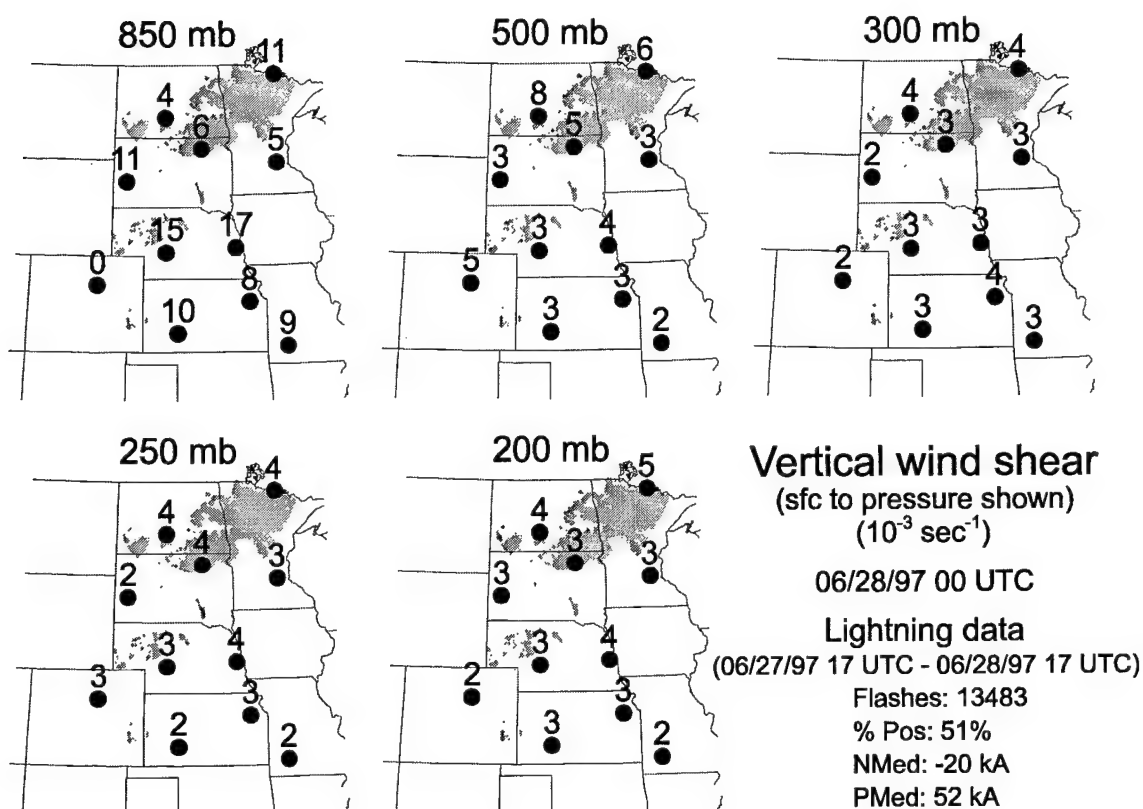


Figure B-20. Vertical wind shear and lightning locations for 28 Jun 97. Lightning locations are shown as gray shaded regions and the vertical wind shear is listed above the circle. Vertical wind shears are calculated from the surface to the pressure levels shown. Missing data are represented as zeroes. The lightning summary information is also provided to include the number of flashes, the percentage of positive flashes, and the median peak currents for negative and positive flashes. Only positive flashes of at least 10 kA were included.

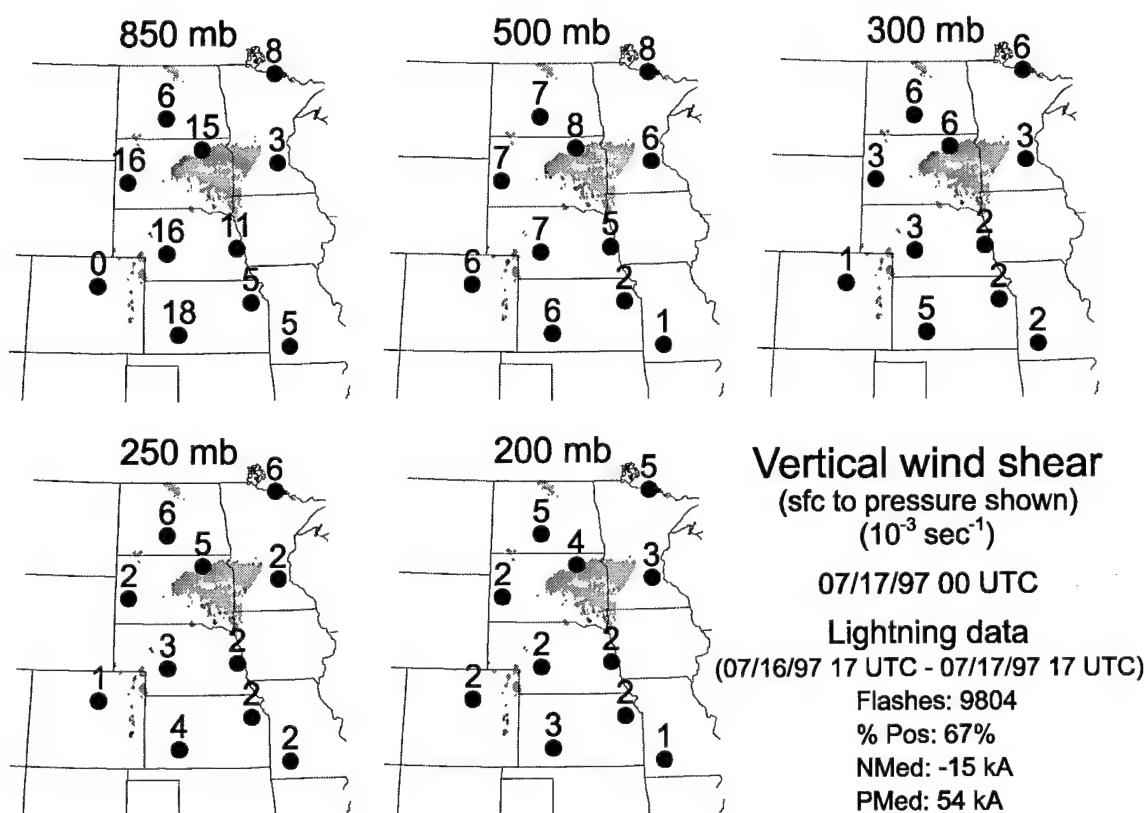


Figure B-21. Vertical wind shear and lightning locations for 17 Jul 97. Lightning locations are shown as gray shaded regions and the vertical wind shear is listed above the circle. Vertical wind shears are calculated from the surface to the pressure levels shown. Missing data are represented as zeroes. The lightning summary information is also provided to include the number of flashes, the percentage of positive flashes, and the median peak currents for negative and positive flashes. Only positive flashes of at least 10 kA were included.

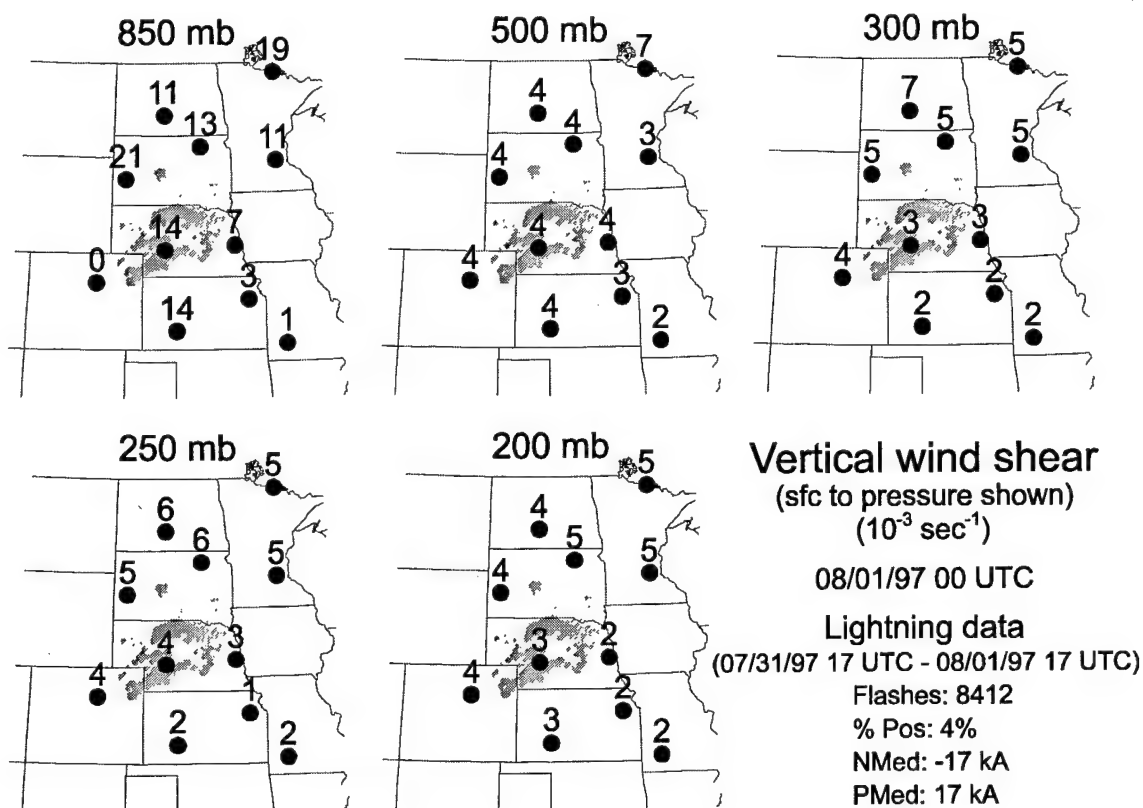


Figure B-22. Vertical wind shear and lightning locations for 1 Aug 97. Lightning locations are shown as gray shaded regions and the vertical wind shear is listed above the circle. Vertical wind shears are calculated from the surface to the pressure levels shown. Missing data are represented as zeroes. The lightning summary information is also provided to include the number of flashes, the percentage of positive flashes, and the median peak currents for negative and positive flashes. Only positive flashes of at least 10 kA were included.

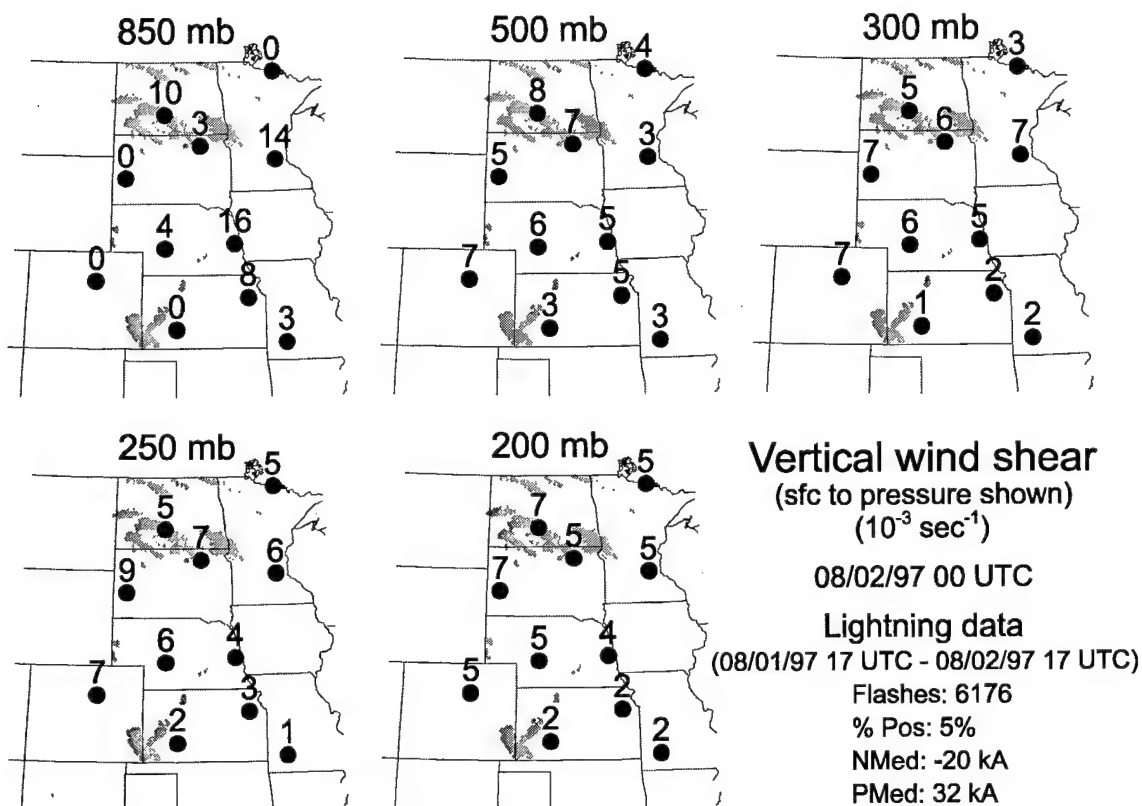


Figure B-23. Vertical wind shear and lightning locations for 2 Aug 97. Lightning locations are shown as gray shaded regions and the vertical wind shear is listed above the circle. Vertical wind shears are calculated from the surface to the pressure levels shown. Missing data are represented as zeroes. The lightning summary information is also provided to include the number of flashes, the percentage of positive flashes, and the median peak currents for negative and positive flashes. Only positive flashes of at least 10 kA were included.

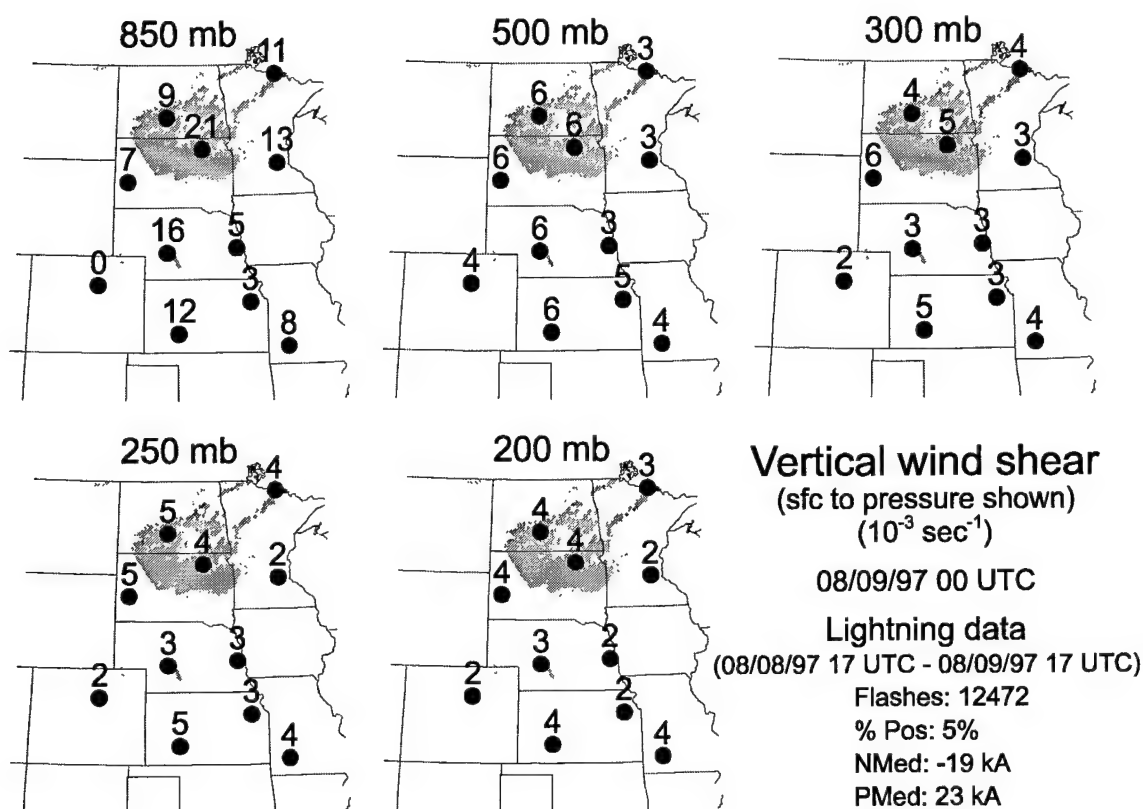


Figure B-24. Vertical wind shear and lightning locations for 9 Aug 97. Lightning locations are shown as gray shaded regions and the vertical wind shear is listed above the circle. Vertical wind shears are calculated from the surface to the pressure levels shown. Missing data are represented as zeroes. The lightning summary information is also provided to include the number of flashes, the percentage of positive flashes, and the median peak currents for negative and positive flashes. Only positive flashes of at least 10 kA were included.

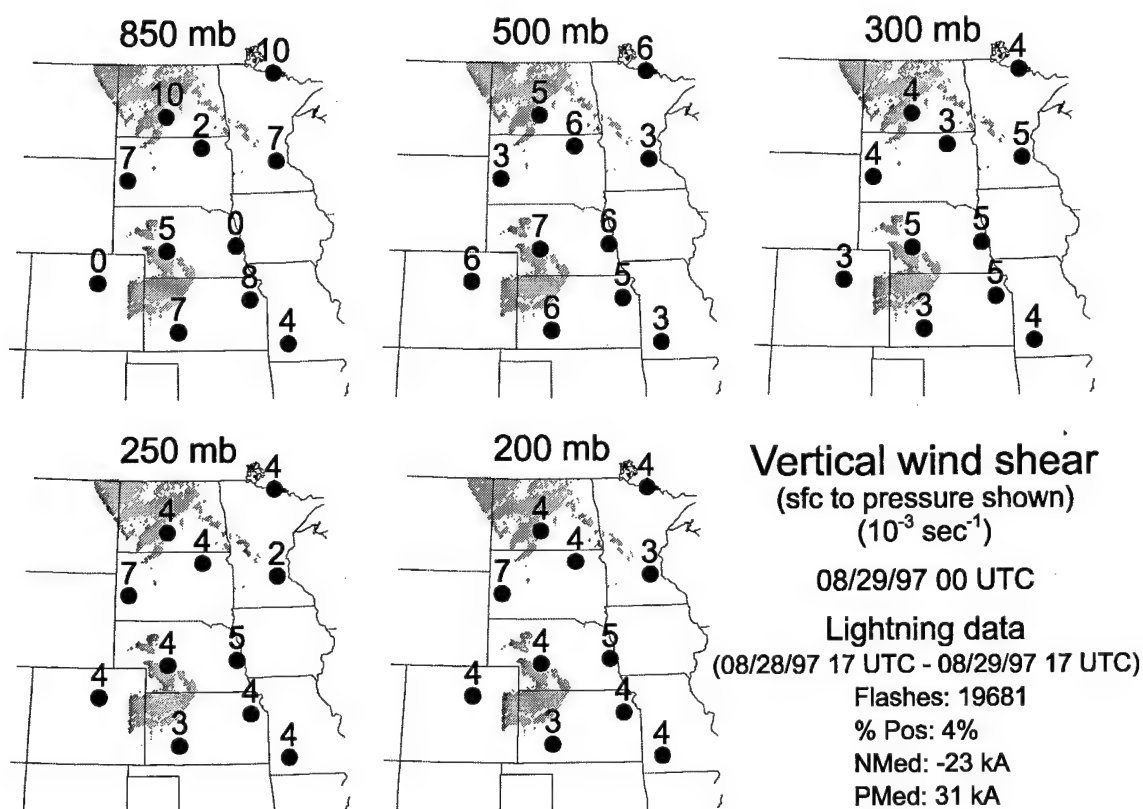


Figure B-25. Vertical wind shear and lightning locations for 29 Aug 97. Lightning locations are shown as gray shaded regions and the vertical wind shear is listed above the circle. Vertical wind shears are calculated from the surface to the pressure levels shown. Missing data are represented as zeroes. The lightning summary information is also provided to include the number of flashes, the percentage of positive flashes, and the median peak currents for negative and positive flashes. Only positive flashes of at least 10 kA were included.

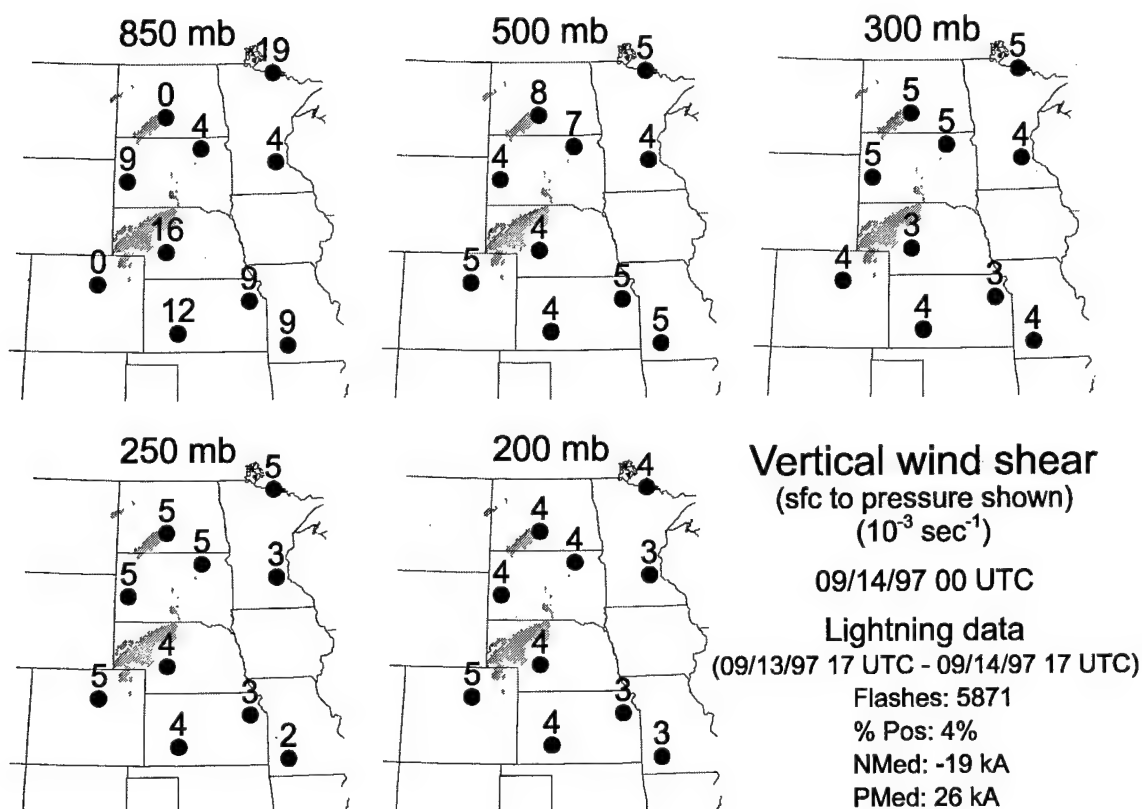


Figure B-26. Vertical wind shear and lightning locations for 14 Sep 97. Lightning locations are shown as gray shaded regions and the vertical wind shear is listed above the circle. Vertical wind shears are calculated from the surface to the pressure levels shown. Missing data are represented as zeroes. The lightning summary information is also provided to include the number of flashes, the percentage of positive flashes, and the median peak currents for negative and positive flashes. Only positive flashes of at least 10 kA were included.

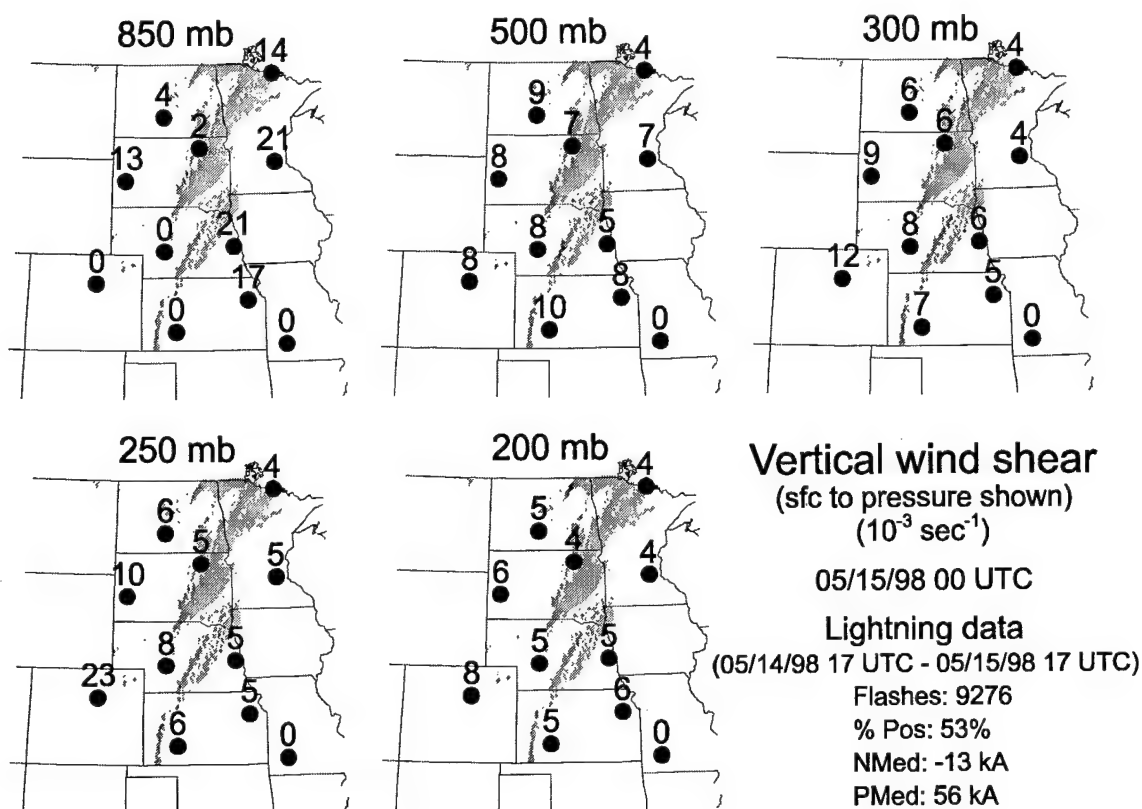


Figure B-27. Vertical wind shear and lightning locations for 15 May 98. Lightning locations are shown as gray shaded regions and the vertical wind shear is listed above the circle. Vertical wind shears are calculated from the surface to the pressure levels shown. Missing data are represented as zeroes. The lightning summary information is also provided to include the number of flashes, the percentage of positive flashes, and the median peak currents for negative and positive flashes. Only positive flashes of at least 10 kA were included.

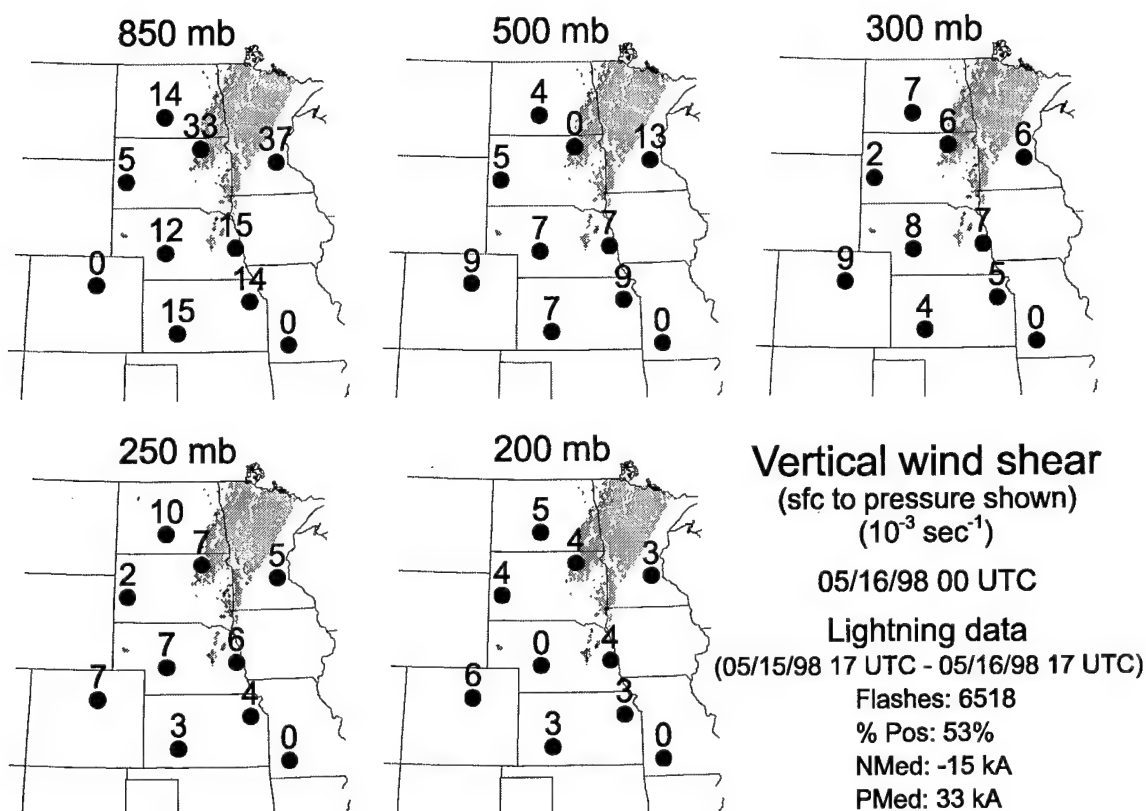


Figure B-28. Vertical wind shear and lightning locations for 16 May 98. Lightning locations are shown as gray shaded regions and the vertical wind shear is listed above the circle. Vertical wind shears are calculated from the surface to the pressure levels shown. Missing data are represented as zeroes. The lightning summary information is also provided to include the number of flashes, the percentage of positive flashes, and the median peak currents for negative and positive flashes. Only positive flashes of at least 10 kA were included.

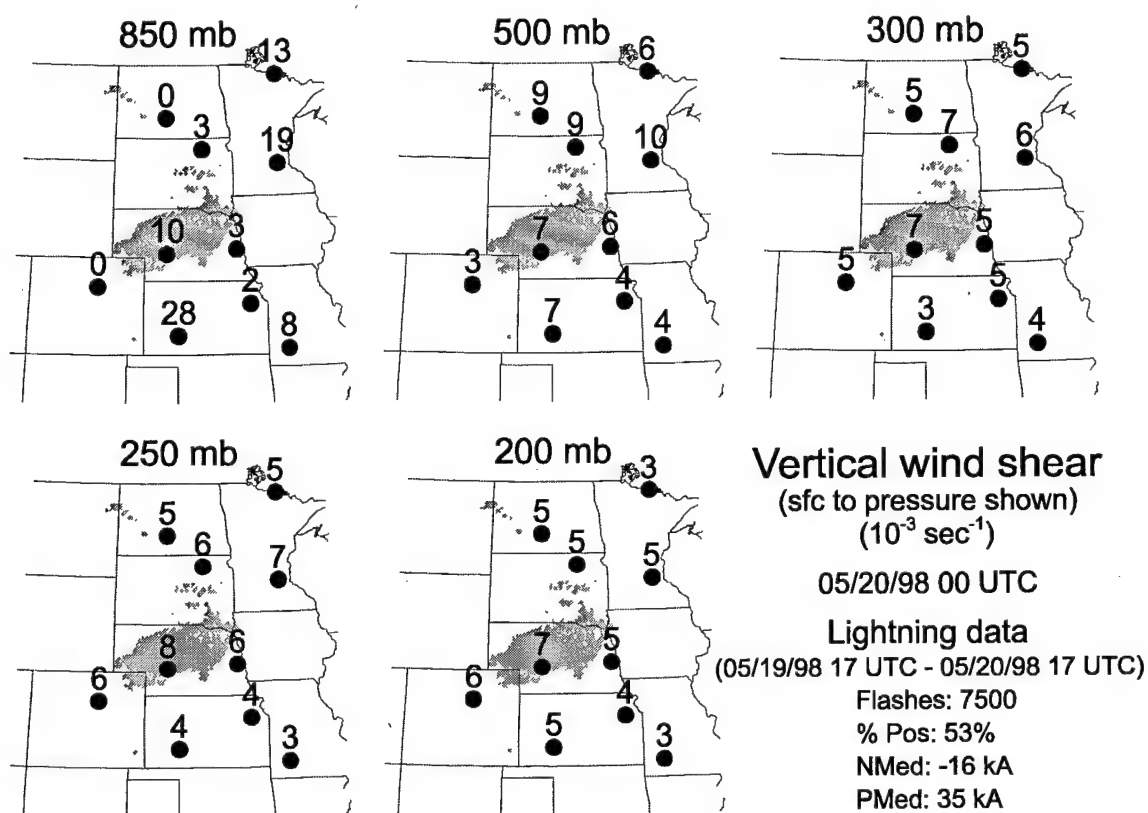


Figure B-29. Vertical wind shear and lightning locations for 20 May 98. Lightning locations are shown as gray shaded regions and the vertical wind shear is listed above the circle. Vertical wind shears are calculated from the surface to the pressure levels shown. Missing data are represented as zeroes. The lightning summary information is also provided to include the number of flashes, the percentage of positive flashes, and the median peak currents for negative and positive flashes. Only positive flashes of at least 10 kA were included.

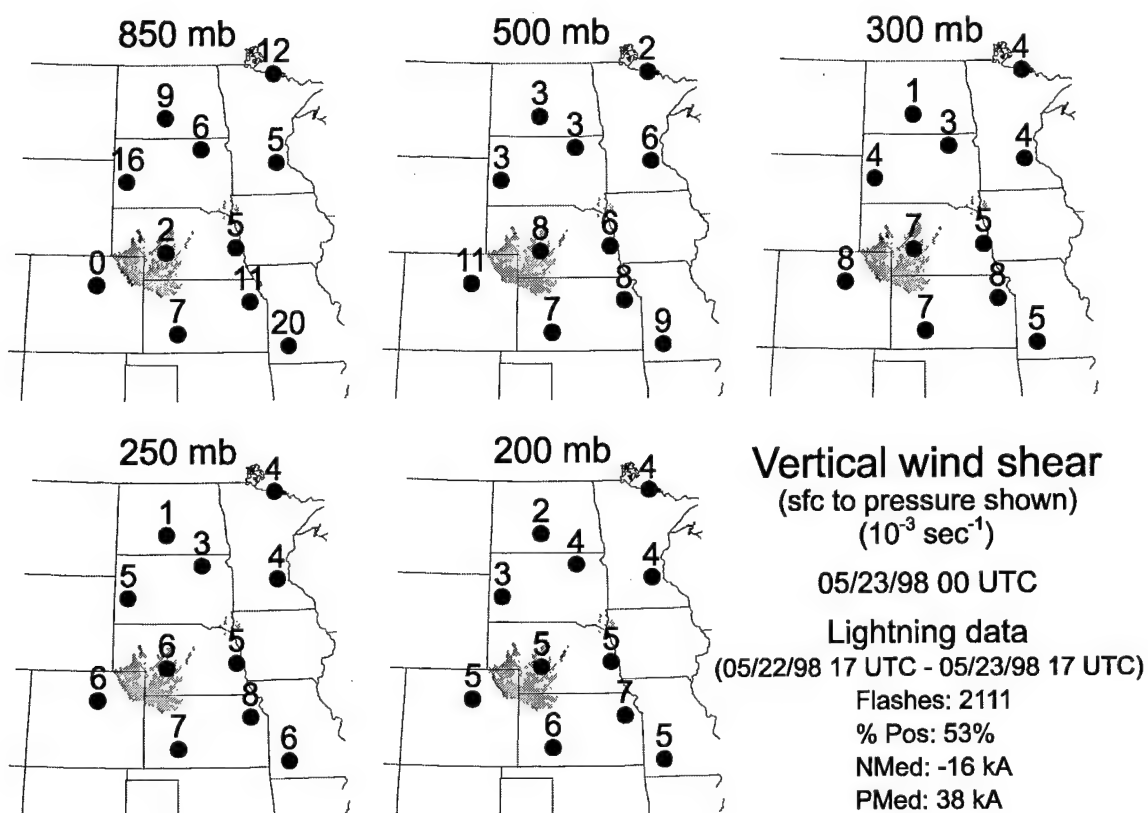


Figure B-30. Vertical wind shear and lightning locations for 23 May 98. Lightning locations are shown as gray shaded regions and the vertical wind shear is listed above the circle. Vertical wind shears are calculated from the surface to the pressure levels shown. Missing data are represented as zeroes. The lightning summary information is also provided to include the number of flashes, the percentage of positive flashes, and the median peak currents for negative and positive flashes. Only positive flashes of at least 10 kA were included.

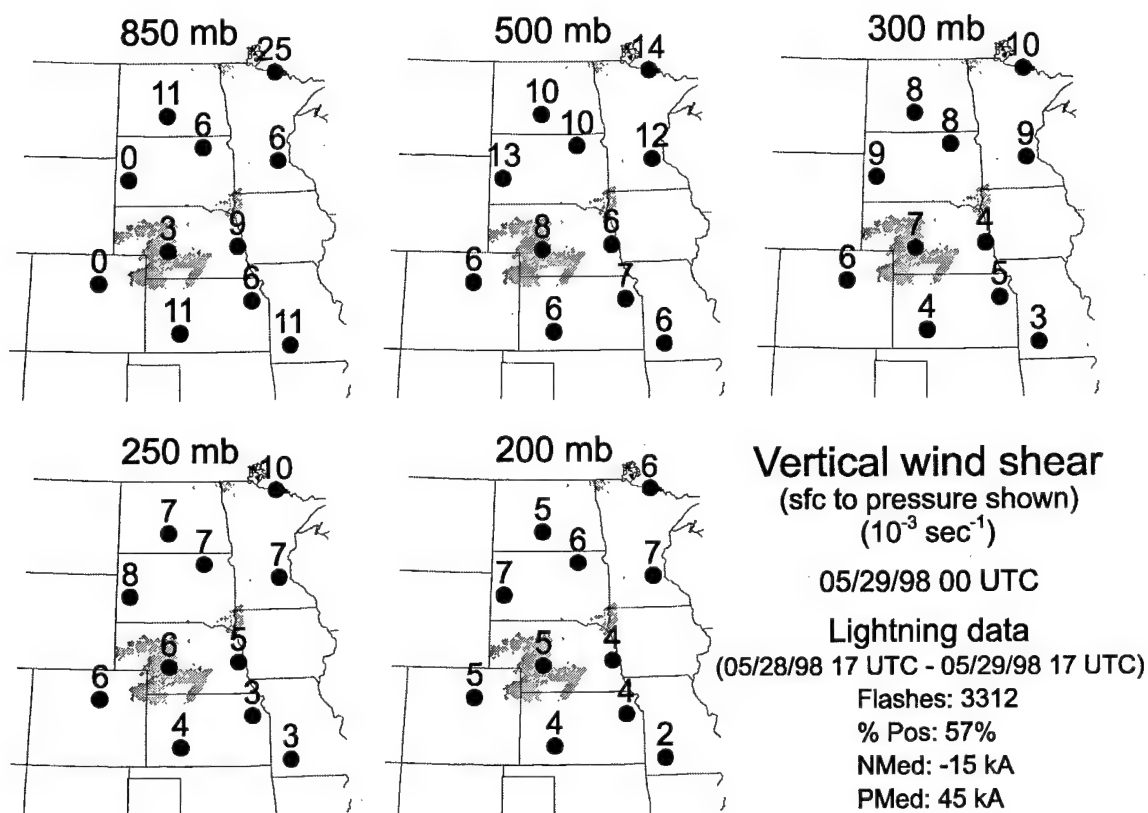


Figure B-31. Vertical wind shear and lightning locations for 29 May 98. Lightning locations are shown as gray shaded regions and the vertical wind shear is listed above the circle. Vertical wind shears are calculated from the surface to the pressure levels shown. Missing data are represented as zeroes. The lightning summary information is also provided to include the number of flashes, the percentage of positive flashes, and the median peak currents for negative and positive flashes. Only positive flashes of at least 10 kA were included.

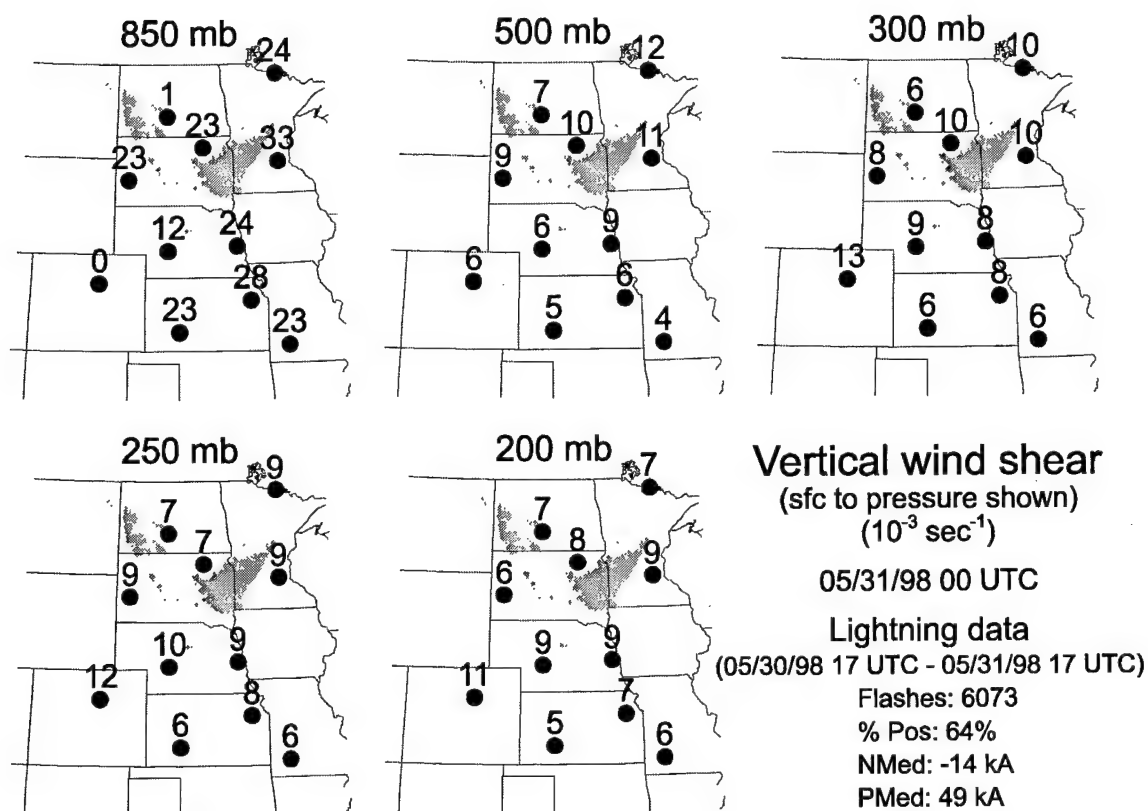


Figure B-32. Vertical wind shear and lightning locations for 31 May98. Lightning locations are shown as gray shaded regions and the vertical wind shear is listed above the circle. Vertical wind shears are calculated from the surface to the pressure levels shown. Missing data are represented as zeroes. The lightning summary information is also provided to include the number of flashes, the percentage of positive flashes, and the median peak currents for negative and positive flashes. Only positive flashes of at least 10 kA were included.

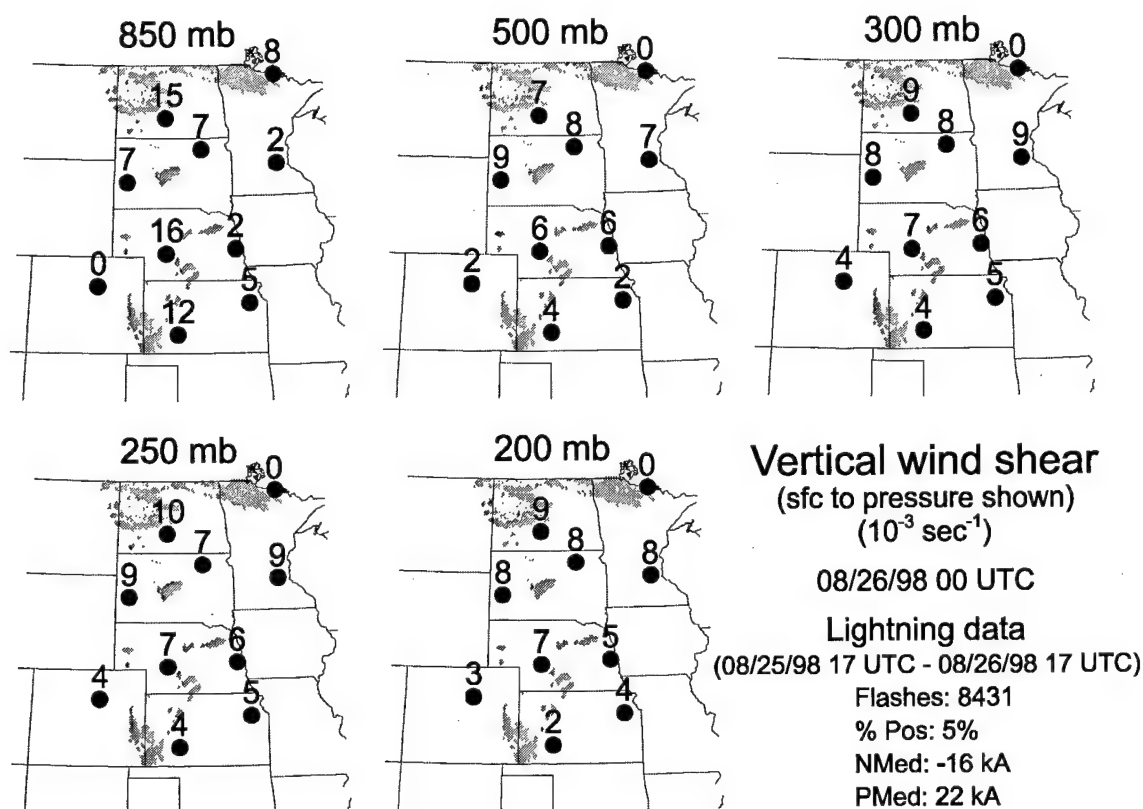


Figure B-33. Vertical wind shear and lightning locations for 26 Aug 98. Lightning locations are shown as gray shaded regions and the vertical wind shear is listed above the circle. Vertical wind shears are calculated from the surface to the pressure levels shown. Missing data are represented as zeroes. The lightning summary information is also provided to include the number of flashes, the percentage of positive flashes, and the median peak currents for negative and positive flashes. Only positive flashes of at least 10 kA were included.

APPENDIX C

APPROXIMATE HEIGHT OF THE MAIN NEGATIVE CHARGE REGION

(-10°C HEIGHT)

The main negative charge region of a thunderstorm occurs near the -10°C level (Stolzenburg et al. 1998). As such, the height of this temperature level is included here. A summary of the heights for each case in the Northern Plains study is included (Table C-1) as a median of the values. The heights for each of the locations used are listed in Table C-2.

Correlation with the temperature levels and the peak currents did not show any connection. Even so, the median peak currents for each of the cases are shown in Table C-1.

The locations of the sites used can be found in Appendix B (Table B-1).

Table C-1. Summary of lightning data and -10°C heights for the Northern Plains cases.

Lightning data covers 24 hours starting at 1700 UTC the previous day				
Date	Median height of -10°C sounding level at 00 UTC (m MSL)	Percentage of positive flashes	Median peak positive current (kA)	Median peak negative current (kA)
06/15/95	4611	54.5	48.2	-17.0
06/19/95	5552	4.0	17.8	-17.0
07/11/95	5066	4.5	28.5	-21.0
08/09/95	5219	4.2	16.3	-20.0
08/26/95	5163	5.0	24.3	-21.0
08/30/95	5460	2.4	25.7	-23.0
08/31/95	5040	1.9	19.4	-22.0
09/04/95	4702	2.0	21.2	-20.0
09/05/95	4990	4.3	22.4	-20.0
09/11/95	4622	3.9	25.3	-23.0
03/24/96	4948	61.4	53.8	-20.0
05/16/96	5636	53.1	48.2	-15.0
05/19/96	5634	63.0	49.3	-19.0
06/20/96	5830	64.8	55.7	-15.0
07/04/96	6370	8.6	30.2	-22.0
08/21/96	6220	4.2	26.4	-21.0
09/01/96	6220	4.7	33.1	-22.0
05/18/97	4165	50.0	41.1	-16.0
06/21/97	4897	60.3	48.9	-16.0
06/28/97	4897	50.4	52.0	-19.0
07/17/97	5124	65.6	54.3	-15.0
08/01/97	5181	4.3	16.9	-17.0
08/02/97	5170	4.8	31.7	-19.0
08/09/97	4733	4.8	22.7	-18.0
08/29/97	5107	3.7	31.1	-22.0
09/14/97	4516	4.2	25.8	-18.0
05/15/98	5700	52.8	56.1	-12.0
05/16/98	5289	51.7	32.7	-14.0
05/20/98	5078	52.5	34.8	-15.0
05/23/98	4786	52.6	37.7	-16.0
05/29/98	4726	56.0	45.2	-15.0
05/31/98	4956	63.9	48.9	-14.0
08/26/98	5033	5.0	21.7	-16.0

Table C-2. Height of the -10C level in the 00 UTC soundings for the Northern Plains cases.

Date	Site (ICAO)	Height of -10°C level (m MSL)	Date	Site (ICAO)	Height of -10°C level (m MSL)
06/15/95	BIS	4376	08/31/95	UNR	5600
06/15/95	DDC	5111	09/04/95	BIS	5695
06/15/95	DEN	5472	09/04/95	DDC	5730
06/15/95	INL	5348	09/04/95	DEN	5702
06/15/95	LBF	5189	09/04/95	INL	5760
06/15/95	UNR	4830	09/04/95	LBF	5696
06/19/95	BIS	5307	09/04/95	UNR	5600
06/19/95	DDC	5600	09/05/95	BIS	5550
06/19/95	DEN	6188	09/05/95	DDC	5612
06/19/95	INL	6098	09/05/95	DEN	5490
06/19/95	LBF	5666	09/05/95	INL	4800
06/19/95	UNR	6052	09/05/95	LBF	4791
07/11/95	BIS	5559	09/05/95	UNR	4486
07/11/95	DDC	5670	09/11/95	BIS	4588
07/11/95	DEN	5566	09/11/95	DDC	5209
07/11/95	INL	4770	09/11/95	DEN	5494
07/11/95	LBF	5539	09/11/95	INL	5622
07/11/95	UNR	5799	09/11/95	LBF	5830
08/09/95	BIS	5719	09/11/95	UNR	5369
08/09/95	DDC	5735	03/24/96	BIS	4662
08/09/95	DEN	6039	03/24/96	DDC	5427
08/09/95	INL	5479	03/24/96	DEN	5152
08/09/95	LBF	5516	03/24/96	INL	4670
08/09/95	UNR	5217	03/24/96	LBF	4948
08/26/95	BIS	5472	03/24/96	UNR	4209
08/26/95	DDC	6163	05/16/96	BIS	5172
08/26/95	DEN	5640	05/16/96	DDC	5820
08/26/95	INL	5798	05/16/96	DEN	5780
08/26/95	LBF	5620	05/16/96	INL	4773
08/26/95	UNR	5552	05/16/96	LBF	5760
08/30/95	BIS	5560	05/16/96	UNR	5636
08/30/95	DDC	5670	05/19/96	BIS	5483
08/30/95	DEN	5718	05/19/96	DDC	5820
08/30/95	INL	4489	05/19/96	DEN	5770
08/30/95	LBF	5460	05/19/96	INL	5487
08/30/95	UNR	5440	05/19/96	LBF	5730
08/31/95	BIS	5540	05/19/96	UNR	5076
08/31/95	DDC	5670	06/20/96	BIS	5634
08/31/95	DEN	5660	06/20/96	DDC	5860
08/31/95	INL	5035	06/20/96	DEN	6250
08/31/95	LBF	5227	06/20/96	INL	5780

Table C-2 (continued)

Date	Site (ICAO)	Height of -10°C level (m MSL)	Date	Site (ICAO)	Height of -10°C level (m MSL)
06/20/96	LBF	5830	06/28/97	TOP	4418
06/20/96	UNR	5739	06/28/97	DEN	5095
07/04/96	BIS	6293	06/28/97	OAX	4788
07/04/96	DDC	7640	06/28/97	LBF	5035
07/04/96	DEN	6370	06/28/97	MPX	4387
07/04/96	INL	4510	06/28/97	ABR	5063
07/04/96	LBF	6489	06/28/97	UNR	5084
07/04/96	UNR	6526	06/28/97	INL	4083
08/21/96	BIS	5790	06/28/97	BIS	4357
08/21/96	DDC	6981	07/17/97	SGF	5146
08/21/96	DEN	5890	07/17/97	DDC	5202
08/21/96	INL	5750	07/17/97	TOP	5182
08/21/96	LBF	6664	07/17/97	FCS	5960
09/01/96	BIS	6220	07/17/97	DEN	5206
09/01/96	DDC	6203	07/17/97	OAX	4911
09/01/96	DEN	6560	07/17/97	LBF	5014
09/01/96	INL	5616	07/17/97	MPX	4530
09/01/96	LBF	6609	07/17/97	ABR	5124
05/18/97	SGF	3883	07/17/97	UNR	4739
05/18/97	DDC	4247	07/17/97	INL	3978
05/18/97	TOP	4346	07/17/97	BIS	4417
05/18/97	DEN	4409	08/01/97	SGF	5191
05/18/97	OAX	3845	08/01/97	DDC	5094
05/18/97	LBF	4372	08/01/97	TOP	5301
05/18/97	MPX	2872	08/01/97	DEN	5348
05/18/97	UNR	4165	08/01/97	OAX	5188
05/18/97	INL	1927	08/01/97	LBF	5181
05/18/97	BIS	3607	08/01/97	MPX	4924
06/21/97	SGF	4814	08/01/97	ABR	4976
06/21/97	DDC	5133	08/01/97	UNR	5172
06/21/97	TOP	5003	08/01/97	INL	5147
06/21/97	DEN	5122	08/01/97	BIS	5145
06/21/97	OAX	5092	08/02/97	SGF	5605
06/21/97	LBF	5024	08/02/97	DDC	5977
06/21/97	MPX	4599	08/02/97	TOP	5691
06/21/97	ABR	4594	08/02/97	DEN	5170
06/21/97	UNR	4882	08/02/97	OAX	5493
06/21/97	INL	3635	08/02/97	LBF	5348
06/21/97	BIS	3634	08/02/97	MPX	5159
06/28/97	SGF	4897	08/02/97	ABR	5033
06/28/97	DDC	4642	08/02/97	UNR	5076

Table C-2 (continued)

Date	Site (ICAO)	Height of -10°C level (m MSL)	Date	Site (ICAO)	Height of -10°C level (m MSL)
08/02/97	INL	4541	05/15/98	UNR	5670
08/02/97	BIS	4804	05/15/98	INL	3281
08/09/97	SGF	4916	05/15/98	BIS	4276
08/09/97	DDC	4692	05/16/98	SGF	5870
08/09/97	TOP	5111	05/16/98	DDC	4623
08/09/97	DEN	4469	05/16/98	TOP	5021
08/09/97	OAX	5115	05/16/98	DEN	5058
08/09/97	LBF	4476	05/16/98	OAX	5387
08/09/97	MPX	4661	05/16/98	LBF	5710
08/09/97	ABR	5088	05/16/98	MPX	5790
08/09/97	UNR	4692	05/16/98	ABR	5720
08/09/97	INL	4726	05/16/98	UNR	4350
08/09/97	BIS	4894	05/16/98	INL	4986
08/29/97	SGF	4733	05/16/98	BIS	3793
08/29/97	DDC	5414	05/20/98	SGF	5289
08/29/97	TOP	5006	05/20/98	TOP	4760
08/29/97	DEN	5163	05/20/98	DEN	5810
08/29/97	OAX	5132	05/20/98	OAX	5085
08/29/97	LBF	5591	05/20/98	LBF	5830
08/29/97	MPX	4571	05/20/98	MPX	5078
08/29/97	ABR	5116	05/20/98	ABR	4048
08/29/97	UNR	5043	05/20/98	UNR	3982
08/29/97	INL	4371	05/20/98	INL	4848
08/29/97	BIS	4785	05/20/98	BIS	4035
09/14/97	SGF	5107	05/23/98	SGF	5260
09/14/97	DDC	5024	05/23/98	DDC	5503
09/14/97	TOP	4620	05/23/98	TOP	4749
09/14/97	DEN	4853	05/23/98	DEN	4670
09/14/97	LBF	4412	05/23/98	OAX	5008
09/14/97	MPX	4372	05/23/98	LBF	4866
09/14/97	ABR	4324	05/23/98	MPX	5740
09/14/97	UNR	3986	05/23/98	ABR	3976
09/14/97	INL	4334	05/23/98	UNR	4786
09/14/97	BIS	4516	05/23/98	BIS	4022
05/15/98	DDC	5790	05/29/98	SGF	4749
05/15/98	TOP	5830	05/29/98	DDC	5850
05/15/98	DEN	5700	05/29/98	TOP	4491
05/15/98	OAX	5800	05/29/98	DEN	5810
05/15/98	LBF	4308	05/29/98	OAX	4584
05/15/98	MPX	5322	05/29/98	LBF	4726
05/15/98	ABR	5710	05/29/98	MPX	4038

Table C-2 (continued)

Date	Site (ICAO)	Height of -10°C level (m MSL)
05/29/98	ABR	4210
05/29/98	UNR	4041
05/29/98	INL	4051
05/29/98	BIS	5244
05/31/98	SGF	5814
05/31/98	DDC	5103
05/31/98	TOP	4860
05/31/98	DEN	5830
05/31/98	OAX	4956
05/31/98	LBF	4923
05/31/98	MPX	4502
05/31/98	ABR	4504
05/31/98	UNR	5494
05/31/98	INL	3179
05/31/98	BIS	4413
08/26/98	SGF	5910
08/26/98	DDC	5910
08/26/98	DEN	5390
08/26/98	OAX	5033
08/26/98	LBF	5199
08/26/98	MPX	4226
08/26/98	ABR	4078
08/26/98	UNR	4574
08/26/98	INL	3834
08/26/98	BIS	4942

APPENDIX D

CAPE VALUES FOR THE CASES STUDIED

The values of Convective Available Potential Energy (CAPE) were found for soundings during each of the cases listed in Table 2. There was no connection between the CAPE and the peak current strength.

There were occasions where the data from a particular site on a given day were not available. These are listed in Table D-2 as N/A. It is unknown if these data would have made a difference in the comparisons of CAPE and peak currents.

Table D-1. Maximum CAPE and median peak currents for Northern Plains cases.

Lightning data covers 24 hours starting at 1700 UTC the previous day				
Date	Maximum CAPE for sites in Northern Plains (00 UTC) (J/kg)	Percentage of positive flashes	Median peak positive current (kA)	Median peak negative current (kA)
06/15/95	5470	54.5	48.2	-17.0
06/19/95	1977	4.0	17.8	-17.0
07/11/95	3375	4.5	28.5	-21.0
08/09/95	4877	4.2	16.3	-20.0
08/26/95	1536	5.0	24.3	-21.0
08/30/95	3594	2.4	25.7	-23.0
08/31/95	1891	1.9	19.4	-22.0
09/04/95	2067	2.0	21.2	-20.0
09/05/95	5136	4.3	22.4	-20.0
09/11/95	1004	3.9	25.3	-23.0
03/24/96	754	61.4	53.8	-20.0
05/16/96	589	53.1	48.2	-15.0
05/19/96	715	63.0	49.3	-19.0
06/20/96	3560	64.8	55.7	-15.0
07/04/96	2772	8.6	30.2	-22.0
08/21/96	2271	4.2	26.4	-21.0
09/01/96	1172	4.7	33.1	-22.0
05/18/97	1257	50.0	41.1	-16.0
06/21/97	7960	60.3	48.9	-16.0
06/28/97	2990	50.4	52.0	-19.0
07/17/97	4218	65.6	54.3	-15.0
08/01/97	2233	4.3	16.9	-17.0
08/02/97	3874	4.8	31.7	-19.0
08/09/97	3352	4.8	22.7	-18.0
08/29/97	5444	3.7	31.1	-22.0
09/14/97	2050	4.2	25.8	-18.0
05/15/98	3857	52.8	56.1	-12.0
05/16/98	2959	51.7	32.7	-14.0
05/20/98	3519	52.5	34.8	-15.0
05/23/98	2700	52.6	37.7	-16.0
05/29/98	3410	56.0	45.2	-15.0
05/31/98	1829	63.9	48.9	-14.0
08/26/98	2566	5.0	21.7	-16.0

Table D-2. Values of CAPE (J/kg) for individual sites.

Date	Time	Site	Pos. CAPE	Neg. CAPE	Date	Time	Site	Pos. CAPE	Neg. CAPE
06/15/95	00 UTC	BIS	N/A	N/A	09/04/95	00 UTC	DDC	3	375
06/15/95	00 UTC	DDC	1809	264	09/04/95	00 UTC	DEN	214	75
06/15/95	00 UTC	DEN	396	123	09/04/95	00 UTC	INL	0	0
06/15/95	00 UTC	INL	693	0	09/04/95	00 UTC	LBF	1210	100
06/15/95	00 UTC	LBF	5470	51	09/04/95	00 UTC	RAP	0	0
06/15/95	00 UTC	RAP	N/A	N/A	09/05/95	00 UTC	BIS	4496	26
06/19/95	00 UTC	BIS	1977	0	09/05/95	00 UTC	DDC	372	382
06/19/95	00 UTC	DDC	65	441	09/05/95	00 UTC	DEN	0	0
06/19/95	00 UTC	DEN	13	13	09/05/95	00 UTC	INL	1712	47
06/19/95	00 UTC	INL	470	188	09/05/95	00 UTC	LBF	5136	29
06/19/95	00 UTC	LBF	1879	5	09/05/95	00 UTC	RAP	0	0
06/19/95	00 UTC	RAP	360	1	09/11/95	00 UTC	BIS	86	235
07/11/95	00 UTC	BIS	3375	28	09/11/95	00 UTC	DDC	0	0
07/11/95	00 UTC	DDC	3014	94	09/11/95	00 UTC	DEN	1004	61
07/11/95	00 UTC	DEN	0	0	09/11/95	00 UTC	INL	24	34
07/11/95	00 UTC	INL	209	119	09/11/95	00 UTC	LBF	0	0
07/11/95	00 UTC	LBF	2674	47	09/11/95	00 UTC	RAP	1000	92
07/11/95	00 UTC	RAP	3176	116	03/24/96	00 UTC	BIS	0	0
08/09/95	00 UTC	BIS	145	11	03/24/96	00 UTC	DDC	754	468
08/09/95	00 UTC	DDC	N/A	N/A	03/24/96	00 UTC	DEN	0	0
08/09/95	00 UTC	DEN	N/A	N/A	03/24/96	00 UTC	INL	0	0
08/09/95	00 UTC	INL	1101	161	03/24/96	00 UTC	LBF	0	0
08/09/95	00 UTC	LBF	4877	105	03/24/96	00 UTC	RAP	0	0
08/09/95	00 UTC	RAP	0	0	05/16/96	00 UTC	BIS	117	0
08/26/95	00 UTC	BIS	1208	4	05/16/96	00 UTC	DDC	N/A	N/A
08/26/95	00 UTC	DDC	211	442	05/16/96	00 UTC	DEN	589	0
08/26/95	00 UTC	DEN	N/A	N/A	05/16/96	00 UTC	INL	3	3
08/26/95	00 UTC	INL	0	0	05/16/96	00 UTC	LBF	N/A	N/A
08/26/95	00 UTC	LBF	1536	21	05/16/96	00 UTC	RAP	555	103
08/26/95	00 UTC	RAP	1354	17	05/19/96	00 UTC	BIS	742	72
08/30/95	00 UTC	BIS	3594	10	05/19/96	00 UTC	DDC	715	353
08/30/95	00 UTC	DDC	N/A	N/A	05/19/96	00 UTC	DEN	0	0
08/30/95	00 UTC	DEN	1122	60	05/19/96	00 UTC	INL	324	12
08/30/95	00 UTC	INL	563	45	05/19/96	00 UTC	LBF	N/A	N/A
08/30/95	00 UTC	LBF	N/A	N/A	05/19/96	00 UTC	RAP	11	184
08/30/95	00 UTC	RAP	1891	0	06/20/96	00 UTC	BIS	0	0
08/31/95	00 UTC	BIS	19	0	06/20/96	00 UTC	DDC	3560	170
08/31/95	00 UTC	DDC	1046	104	06/20/96	00 UTC	DEN	74	179
08/31/95	00 UTC	DEN	0	0	06/20/96	00 UTC	INL	630	59
08/31/95	00 UTC	INL	298	83	06/20/96	00 UTC	LBF	2707	20
08/31/95	00 UTC	LBF	N/A	N/A	06/20/96	00 UTC	RAP	0	0
08/31/95	00 UTC	RAP	0	0	07/04/96	00 UTC	BIS	N/A	N/A
09/04/95	00 UTC	BIS	2067	100	07/04/96	00 UTC	DDC	905	356

Table D-2 (continued)

Date	Time	Site	Pos. CAPE	Neg. CAPE	Date	Time	Site	Pos. CAPE	Neg. CAPE
07/04/96	00 UTC	DEN	292	85	08/01/97	00 UTC	LBF	2107	19
07/04/96	00 UTC	INL	723	2	08/01/97	00 UTC	RAP	865	8
07/04/96	00 UTC	LBF	N/A	N/A	08/02/97	00 UTC	BIS	850	65
07/04/96	00 UTC	RAP	2772	114	08/02/97	00 UTC	DDC	2768	19
08/21/96	00 UTC	BIS	1260	176	08/02/97	00 UTC	DEN	1613	1
08/21/96	00 UTC	DDC	1038	159	08/02/97	00 UTC	INL	155	0
08/21/96	00 UTC	DEN	298	76	08/02/97	00 UTC	LBF	3874	0
08/21/96	00 UTC	INL	120	199	08/02/97	00 UTC	RAP	N/A	N/A
08/21/96	00 UTC	LBF	2271	8	08/09/97	00 UTC	BIS	610	48
09/01/96	00 UTC	BIS	N/A	N/A	08/09/97	00 UTC	DDC	555	257
09/01/96	00 UTC	DDC	847	255	08/09/97	00 UTC	DEN	1754	14
09/01/96	00 UTC	DEN	1172	64	08/09/97	00 UTC	INL	1422	39
09/01/96	00 UTC	INL	N/A	N/A	08/09/97	00 UTC	LBF	1556	57
09/01/96	00 UTC	LBF	N/A	N/A	08/09/97	00 UTC	RAP	3352	78
05/18/97	00 UTC	BIS	656	0	08/29/97	00 UTC	BIS	N/A	N/A
05/18/97	00 UTC	DDC	715	369	08/29/97	00 UTC	DDC	1310	231
05/18/97	00 UTC	DEN	1172	64	08/29/97	00 UTC	DEN	N/A	N/A
05/18/97	00 UTC	INL	0	0	08/29/97	00 UTC	INL	N/A	N/A
05/18/97	00 UTC	LBF	80	182	08/29/97	00 UTC	LBF	5444	49
05/18/97	00 UTC	RAP	1257	85	08/29/97	00 UTC	RAP	5070	27
06/21/97	00 UTC	BIS	235	0	09/14/97	00 UTC	BIS	N/A	N/A
06/21/97	00 UTC	DDC	7960	21	09/14/97	00 UTC	DDC	2050	139
06/21/97	00 UTC	DEN	1097	29	09/14/97	00 UTC	DEN	764	23
06/21/97	00 UTC	INL	N/A	N/A	09/14/97	00 UTC	INL	N/A	N/A
06/21/97	00 UTC	LBF	5397	36	09/14/97	00 UTC	LBF	1343	70
06/21/97	00 UTC	RAP	N/A	N/A	09/14/97	00 UTC	RAP	784	70
06/28/97	00 UTC	BIS	2739	60	05/15/98	00 UTC	BIS	319	54
06/28/97	00 UTC	DDC	1709	92	05/15/98	00 UTC	DDC	0	0
06/28/97	00 UTC	DEN	785	0	05/15/98	00 UTC	INL	1684	32
06/28/97	00 UTC	INL	N/A	N/A	05/15/98	00 UTC	LBF	1740	13
06/28/97	00 UTC	LBF	2990	72	05/15/98	00 UTC	LCH	2849	155
06/28/97	00 UTC	RAP	2007	145	05/15/98	00 UTC	OUN	3857	17
07/17/97	00 UTC	BIS	N/A	N/A	05/15/98	00 UTC	SIL	1049	110
07/17/97	00 UTC	DDC	4218	73	05/15/98	00 UTC	TOP	2644	178
07/17/97	00 UTC	DEN	512	131	05/15/98	00 UTC	BIS	0	0
07/17/97	00 UTC	INL	2350	15	05/15/98	00 UTC	DDC	75	29
07/17/97	00 UTC	LBF	3257	112	05/15/98	00 UTC	GRB	922	40
07/17/97	00 UTC	RAP	2783	46	05/15/98	00 UTC	LBF	0	0
07/31/97	00 UTC	RAP	2227	15	05/15/98	00 UTC	LCH	2475	493
08/01/97	00 UTC	BIS	2233	32	05/15/98	00 UTC	SIL	1296	0
08/01/97	00 UTC	DDC	827	161	05/15/98	00 UTC	TOP	2432	158
08/01/97	00 UTC	DEN	743	9	05/16/98	00 UTC	BIS	53	7
08/01/97	00 UTC	INL	23	18	05/16/98	00 UTC	DDC	23	0

Table D-2 (continued)

Date	Time	Site	Pos. CAPE	Neg. CAPE
05/16/98	00 UTC	FTD	1281	35
05/16/98	00 UTC	JAN	2581	14
05/16/98	00 UTC	LBF	54	18
05/16/98	00 UTC	LCH	2959	158
05/16/98	00 UTC	SIL	2753	37
05/16/98	00 UTC	TOP	0	0
05/20/98	00 UTC	BIS	0	0
05/20/98	00 UTC	DDC	3519	191
05/20/98	00 UTC	DEN	N/A	N/A
05/20/98	00 UTC	INL	41	13
05/20/98	00 UTC	LBF	2854	11
05/20/98	00 UTC	RAP	N/A	N/A
05/23/98	00 UTC	BIS	20	0
05/23/98	00 UTC	DDC	2700	58
05/23/98	00 UTC	DEN	N/A	N/A
05/23/98	00 UTC	INL	0	0
05/23/98	00 UTC	LBF	373	2
05/23/98	00 UTC	RAP	816	2
05/29/98	00 UTC	BIS	0	0
05/29/98	00 UTC	DDC	2965	171
05/29/98	00 UTC	DEN	N/A	N/A
05/29/98	00 UTC	INL	54	67
05/29/98	00 UTC	LBF	3410	39
05/29/98	00 UTC	RAP	9	0
05/31/98	00 UTC	BIS	936	0
05/31/98	00 UTC	DDC	13	0
05/31/98	00 UTC	DEN	N/A	N/A
05/31/98	00 UTC	INL	0	0
05/31/98	00 UTC	LBF	1829	88
05/31/98	00 UTC	RAP	639	133
08/26/98	00 UTC	BIS	1351	0
08/26/98	00 UTC	DDC	1114	187
08/26/98	00 UTC	DEN	N/A	N/A
08/26/98	00 UTC	INL	N/A	N/A
08/26/98	00 UTC	LBF	770	216
08/26/98	00 UTC	RAP	2566	0

APPENDIX E

TIME SERIES AND PERIODICITY OF PEAK CURRENTS FOR INDIVIDUAL CASES

Time series plots of flash counts and peak currents for the cases studied (Table 2) are included for the peak currents in each case. The periodicity was found in each case by applying a narrow width band-pass filter to the average of the top three peak currents in each 5 minute interval during the storm. This was accomplished for positive and negative flashes. The frequency, or period, of the band-pass filter that provided the smallest least-squared error when comparing the filtered time series to the original data was selected as the most appropriate (Table 12). The periodicity for positive flashes is within a few minutes of the periodicity for negative flashes. Calculations for negative and positive peak currents were conducted separately.

Each of the plots contains a panel that shows the average of the highest three peak currents within the 5 minute window. The filtered time series is plotted over the actual time series. There is a separate panel for both positive and negative flashes. Likewise, there is an additional panel in each plot for the number of positive and negative flashes in each time interval.

Additional discussion of these results may be found in Chapter 6.

Data summary for case 95022712

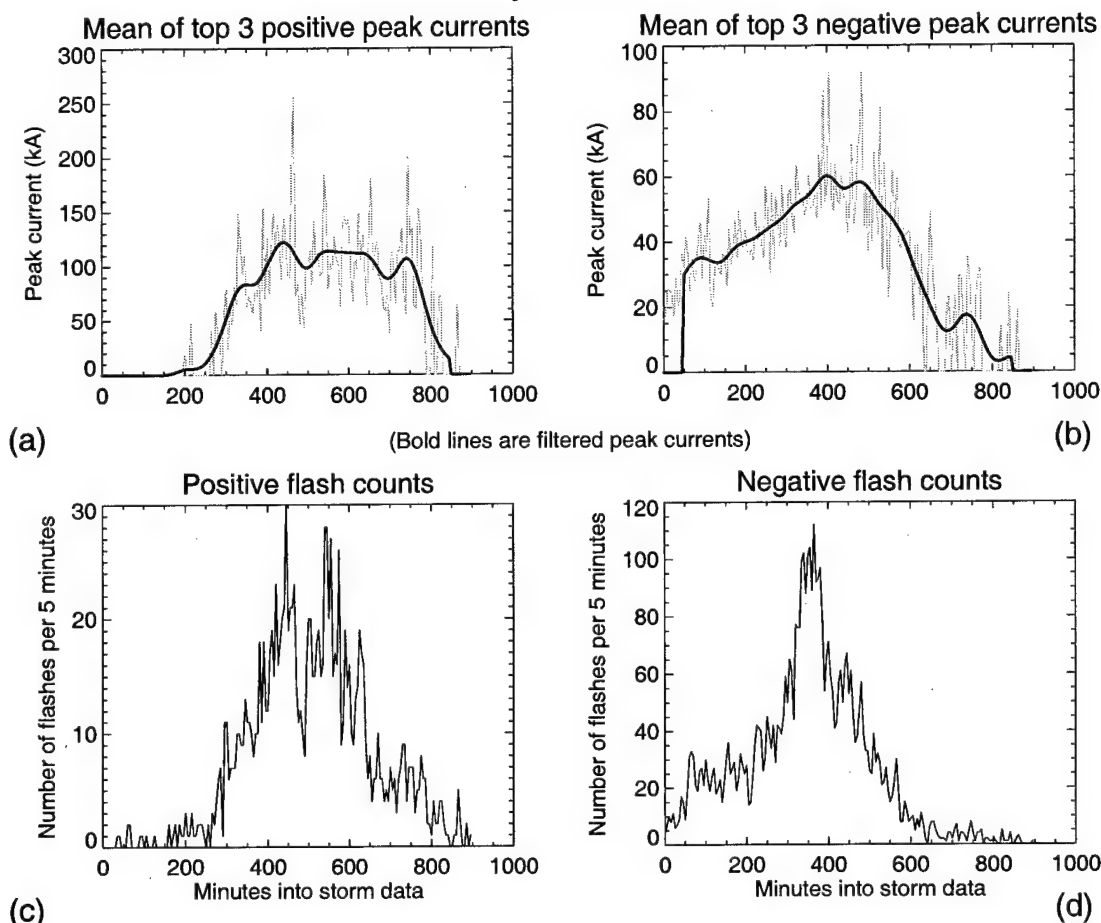


Figure E-1. Time series of peak currents and flash counts for 27 Feb 95. The three extreme peak currents were found for each 5 minute interval and plotted in light gray for positive (a) and negative (b) flashes. A band-pass filter was applied to the peak currents using a 45.0 minute period for positive flashes and a 46.0 minute window for negatives with the resulting wave shown as a dark curve in (a) and (b). The number of positive and negative flashes in each 5 minute window are shown in (c) and (d), respectively.

Data summary for case 95032420

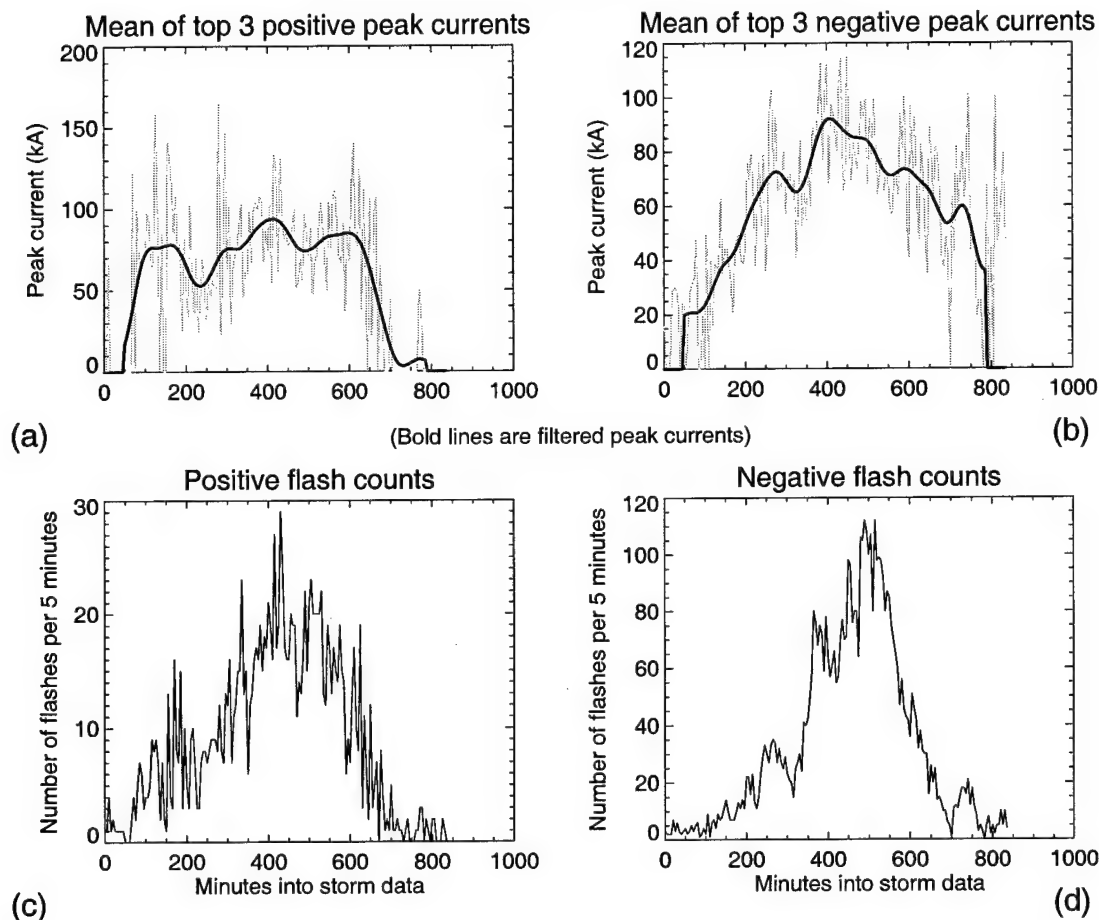


Figure E-2. Time series of peak currents and flash counts for 25 Mar 95. The three extreme peak currents were found for each 5 minute interval and plotted in light gray for positive (a) and negative (b) flashes. A band-pass filter was applied to the peak currents using a 44.5 minute period for positive flashes and a 40.5 minute window for negatives with the resulting wave shown as a dark curve in (a) and (b). The number of positive and negative flashes in each 5 minute window are shown in (c) and (d), respectively.

Data summary for case 95052112

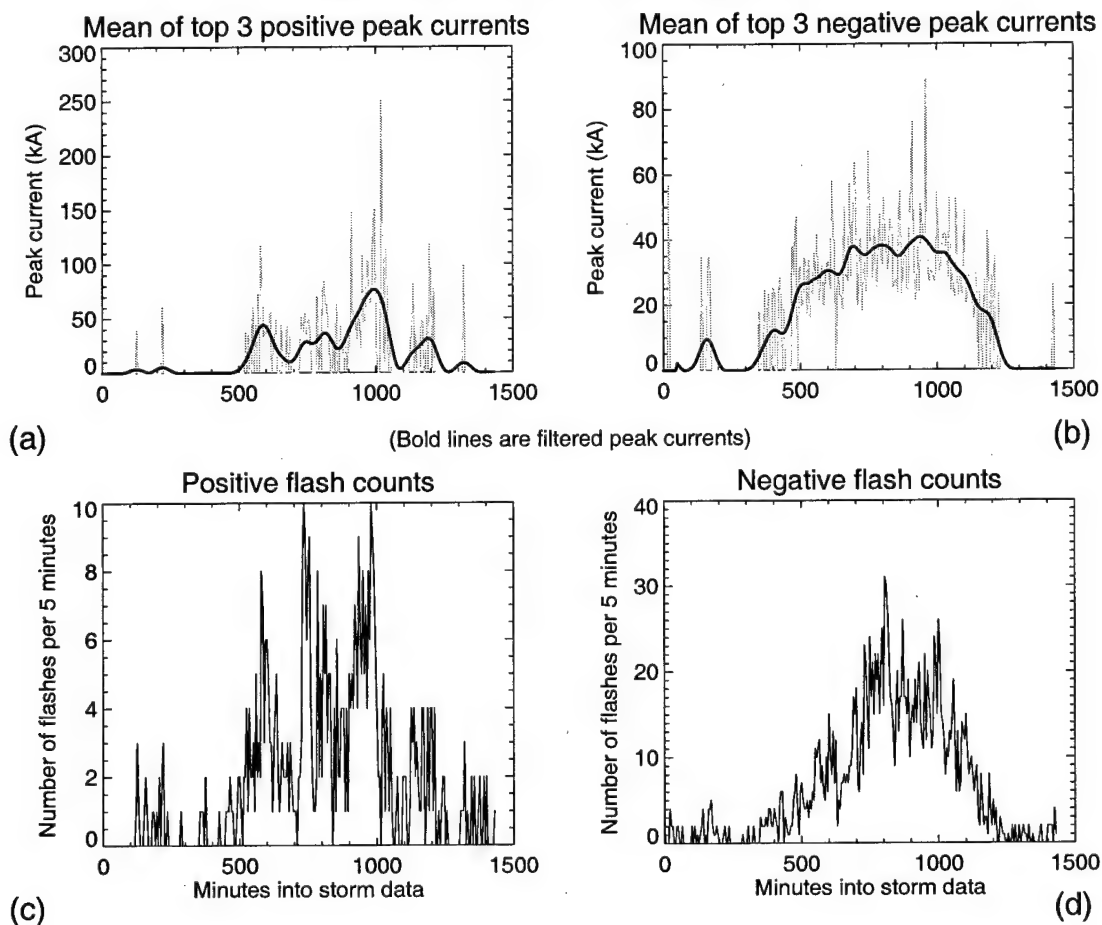


Figure E-3. Time series of peak currents and flash counts for 21 May 95. The three extreme peak currents were found for each 5 minute interval and plotted in light gray for positive (a) and negative (b) flashes. A band-pass filter was applied to the peak currents using a 72.5 minute period for positive flashes and a 74.5 minute window for negatives with the resulting wave shown as a dark curve in (a) and (b). The number of positive and negative flashes in each 5 minute window are shown in (c) and (d), respectively.

Data summary for case 95060612

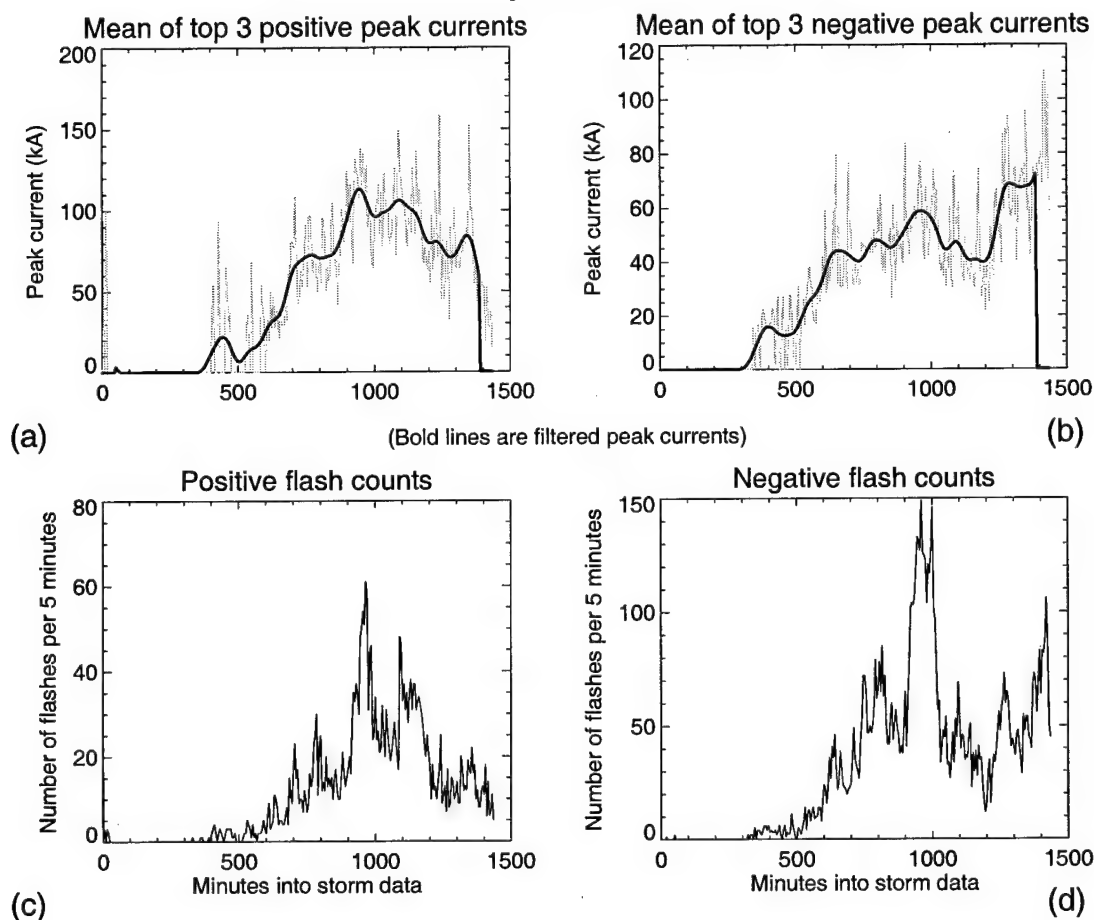


Figure E-4. Time series of peak currents and flash counts for 6 Jun 95. The three extreme peak currents were found for each 5 minute interval and plotted in light gray for positive (a) and negative (b) flashes. A band-pass filter was applied to the peak currents using a 72.0 minute period for positive flashes and a 73.5 minute window for negatives with the resulting wave shown as a dark curve in (a) and (b). The number of positive and negative flashes in each 5 minute window are shown in (c) and (d), respectively.

Data summary for case 95070212

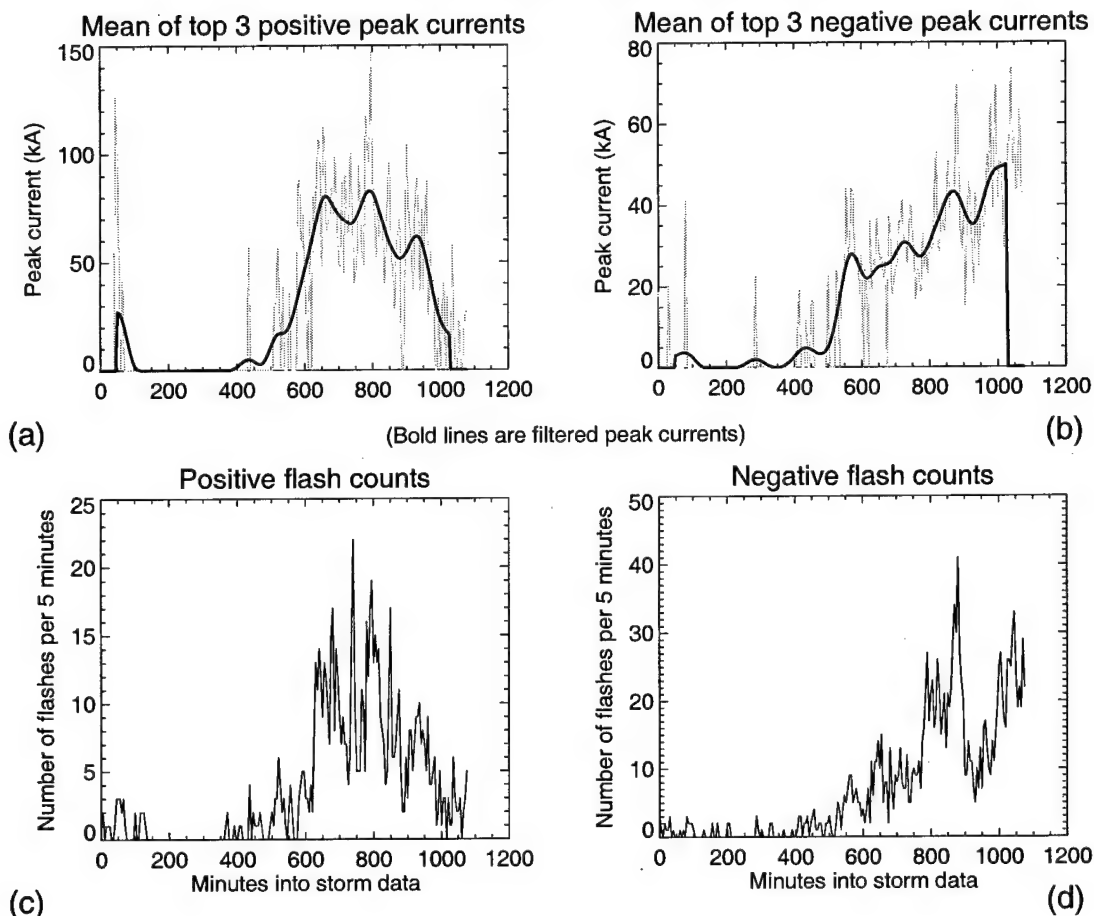


Figure E-5. Time series of peak currents and flash counts for 2 Jul 95. The three extreme peak currents were found for each 5 minute interval and plotted in light gray for positive (a) and negative (b) flashes. A band-pass filter was applied to the peak currents using a 54.0 minute period for positive flashes and a 52.0 minute window for negatives with the resulting wave shown as a dark curve in (a) and (b). The number of positive and negative flashes in each 5 minute window are shown in (c) and (d), respectively.

Data summary for case 95070803

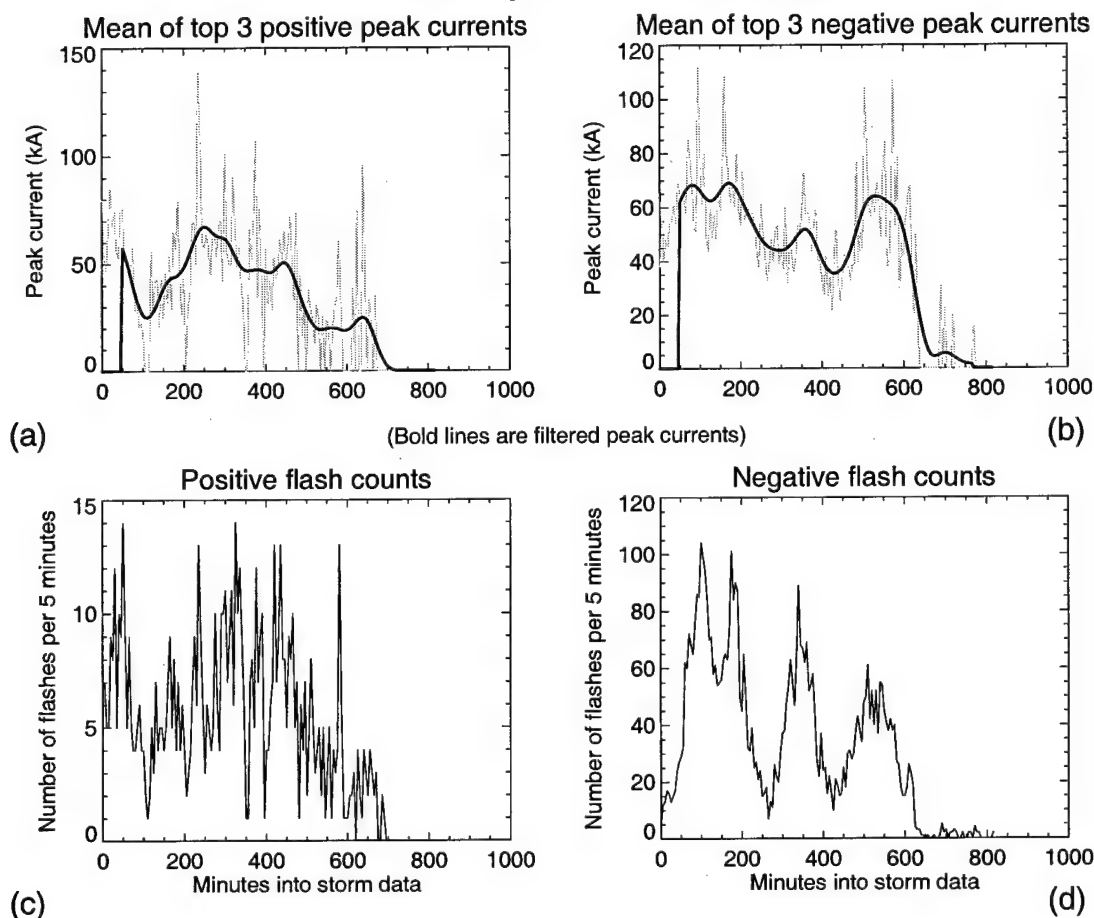


Figure E-6. Time series of peak currents and flash counts for 8 Jul 95. The three extreme peak currents were found for each 5 minute interval and plotted in light gray for positive (a) and negative (b) flashes. A band-pass filter was applied to the peak currents using a 42.0 minute period for positive flashes and a 39.0 minute window for negatives with the resulting wave shown as a dark curve in (a) and (b). The number of positive and negative flashes in each 5 minute window are shown in (c) and (d), respectively.

Data summary for case 95071115

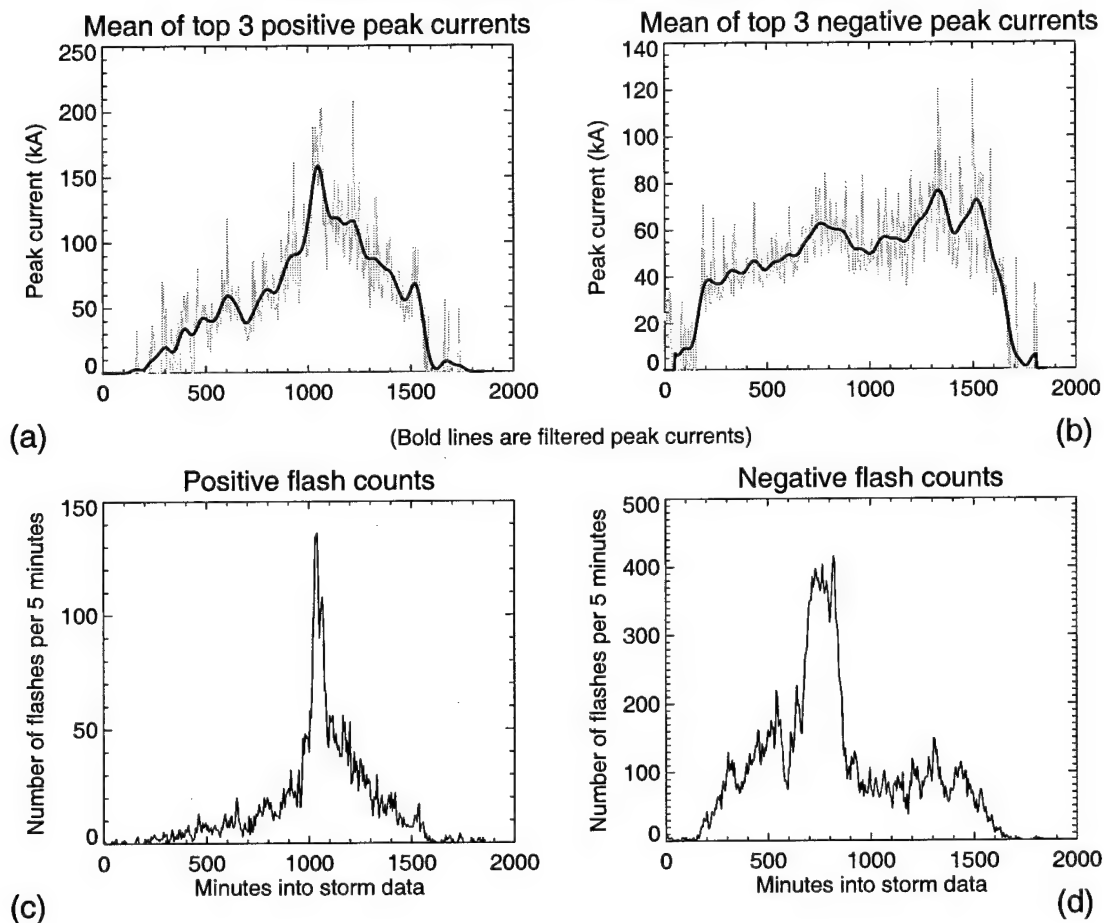


Figure E-7. Time series of peak currents and flash counts for 11 Jul 95. The three extreme peak currents were found for each 5 minute interval and plotted in light gray for positive (a) and negative (b) flashes. A band-pass filter was applied to the peak currents using a 91.5 minute period for positive flashes and a 96.0 minute window for negatives with the resulting wave shown as a dark curve in (a) and (b). The number of positive and negative flashes in each 5 minute window are shown in (c) and (d), respectively.

Data summary for case 95071400

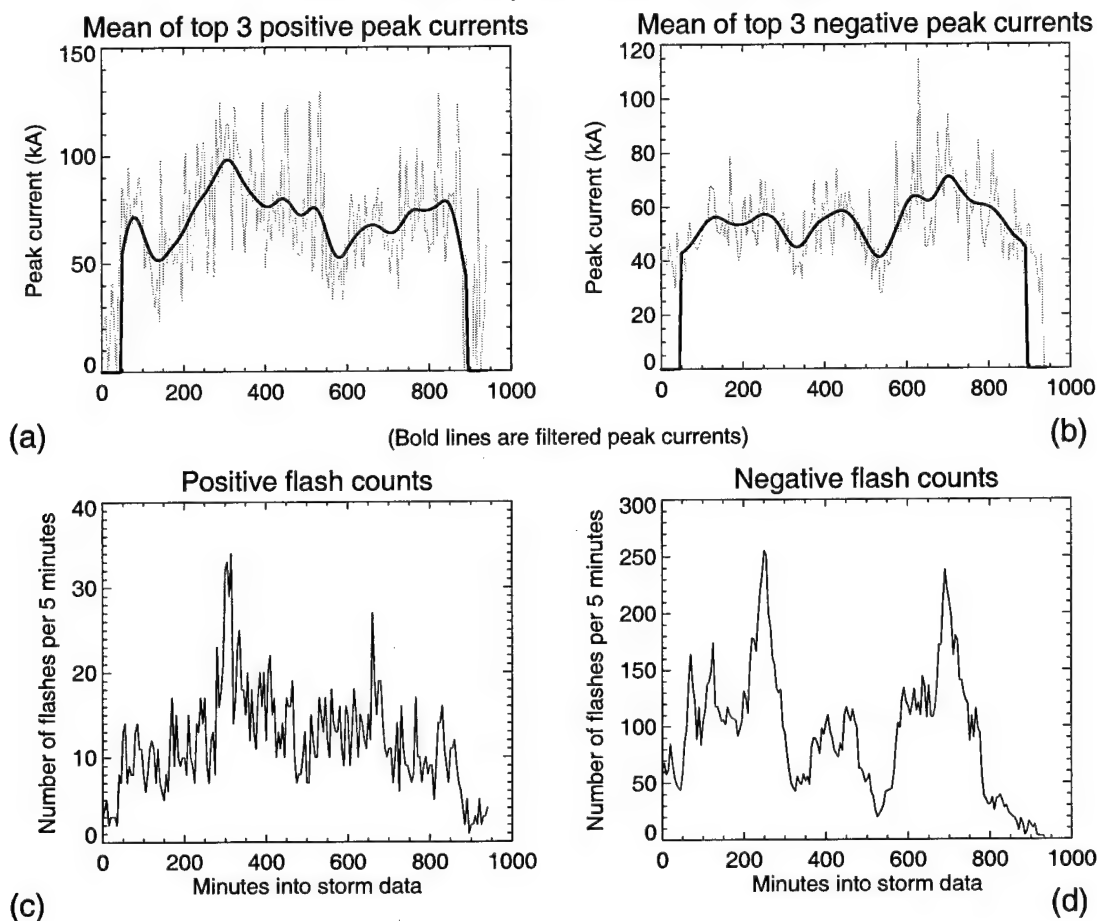


Figure E-8. Time series of peak currents and flash counts for 14 Jul 95. The three extreme peak currents were found for each 5 minute interval and plotted in light gray for positive (a) and negative (b) flashes. A band-pass filter was applied to the peak currents using a 46.5 minute period for positive flashes and a 47.5 minute window for negatives with the resulting wave shown as a dark curve in (a) and (b). The number of positive and negative flashes in each 5 minute window are shown in (c) and (d), respectively.

Data summary for case 95071822

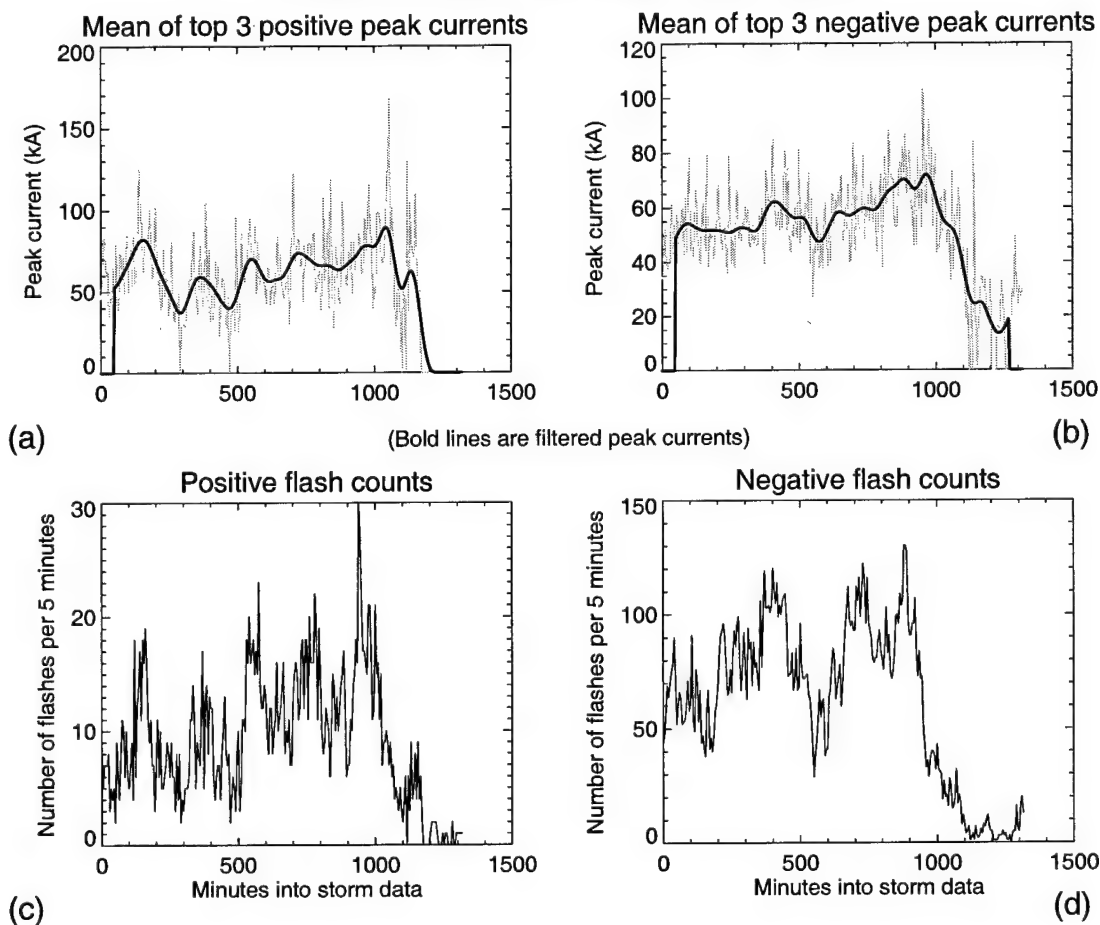


Figure E-9. Time series of peak currents and flash counts for 18 Jul 95. The three extreme peak currents were found for each 5 minute interval and plotted in light gray for positive (a) and negative (b) flashes. A band-pass filter was applied to the peak currents using a 63.0 minute period for positive flashes and a 66.0 minute window for negatives with the resulting wave shown as a dark curve in (a) and (b). The number of positive and negative flashes in each 5 minute window are shown in (c) and (d), respectively.

Data summary for case 95072422

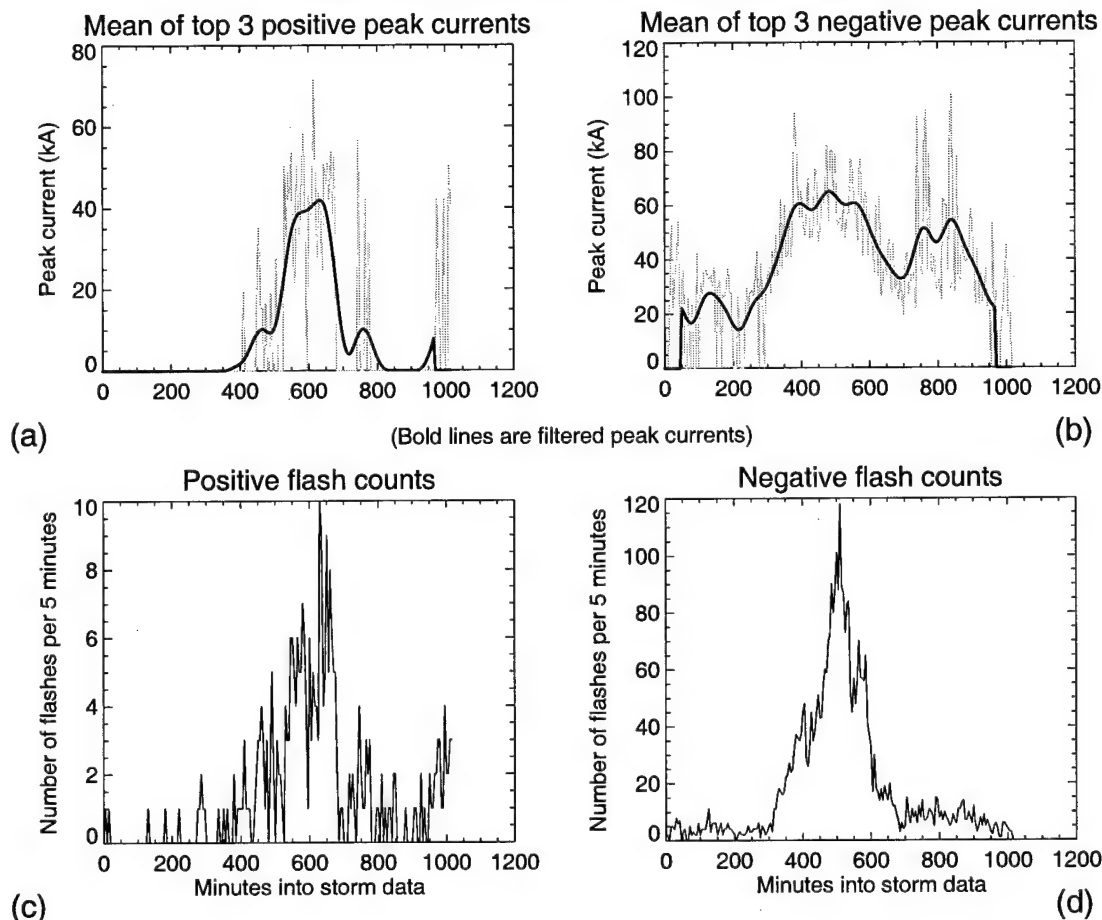


Figure E-10. Time series of peak currents and flash counts for 24 Jul 95. The three extreme peak currents were found for each 5 minute interval and plotted in light gray for positive (a) and negative (b) flashes. A band-pass filter was applied to the peak currents using a 49.5 minute period for positive flashes and a 49.0 minute window for negatives with the resulting wave shown as a dark curve in (a) and (b). The number of positive and negative flashes in each 5 minute window are shown in (c) and (d), respectively.

Data summary for case 95072612

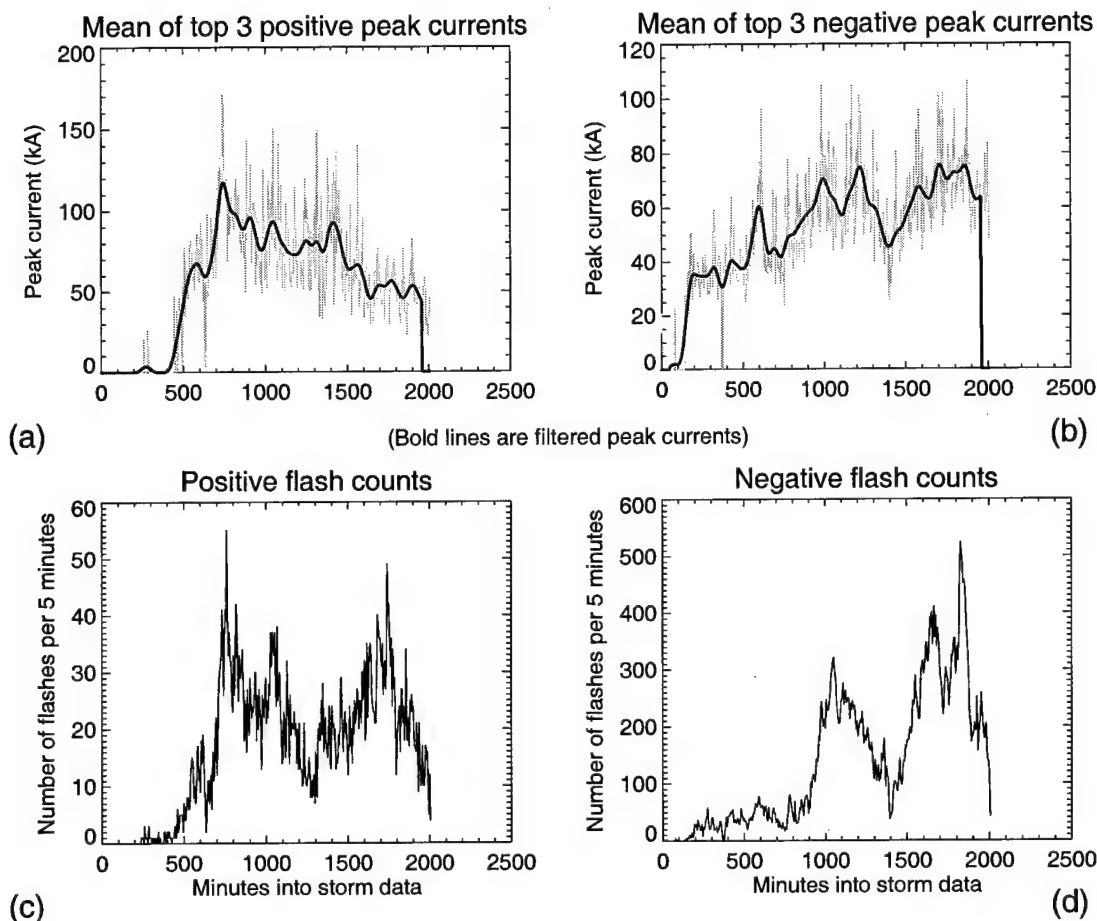


Figure E-11. Time series of peak currents and flash counts for 26 Jul 95. The three extreme peak currents were found for each 5 minute interval and plotted in light gray for positive (a) and negative (b) flashes. A band-pass filter was applied to the peak currents using a 99.5 minute period for positive flashes and a 98.5 minute window for negatives with the resulting wave shown as a dark curve in (a) and (b). The number of positive and negative flashes in each 5 minute window are shown in (c) and (d), respectively.

Data summary for case 95080212

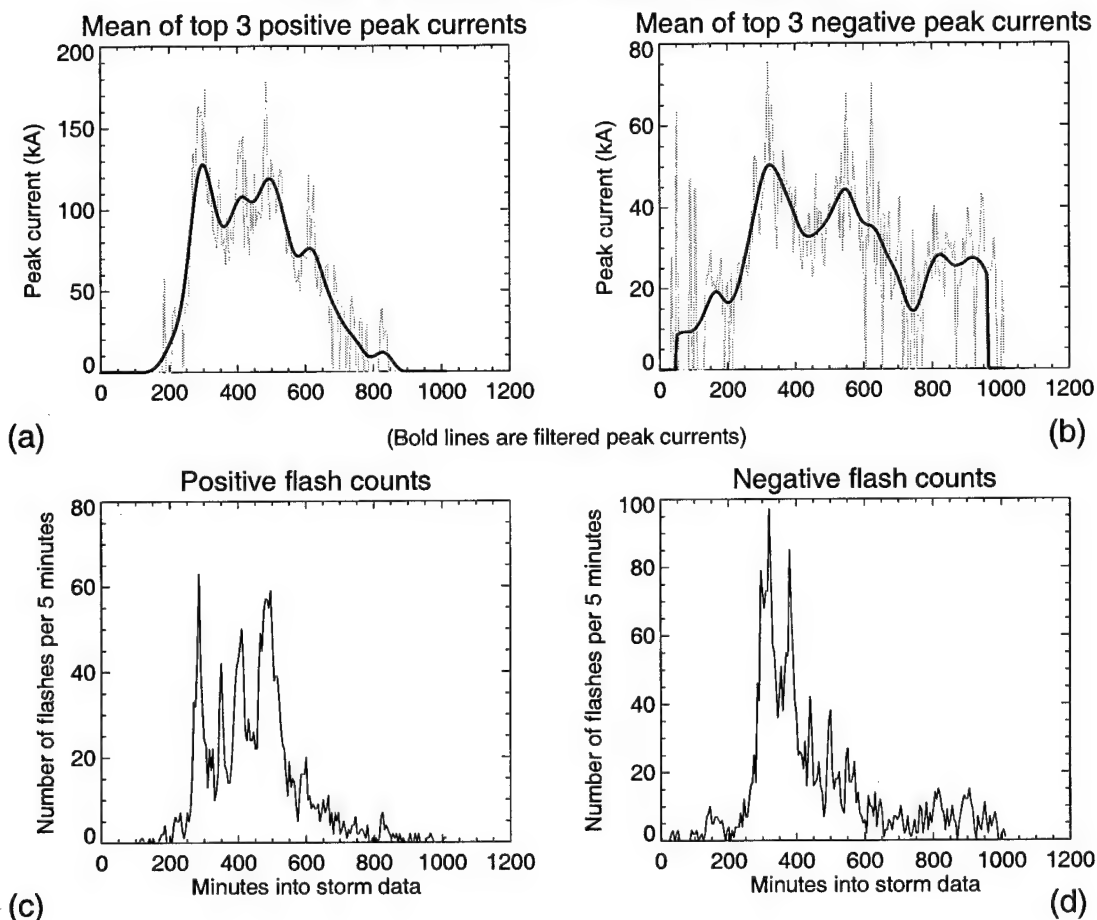


Figure E-12. Time series of peak currents and flash counts for 2 Aug 95. The three extreme peak currents were found for each 5 minute interval and plotted in light gray for positive (a) and negative (b) flashes. A band-pass filter was applied to the peak currents using a 47.0 minute period for positive flashes and a 54.5 minute window for negatives with the resulting wave shown as a dark curve in (a) and (b). The number of positive and negative flashes in each 5 minute window are shown in (c) and (d), respectively.

Data summary for case 95080400

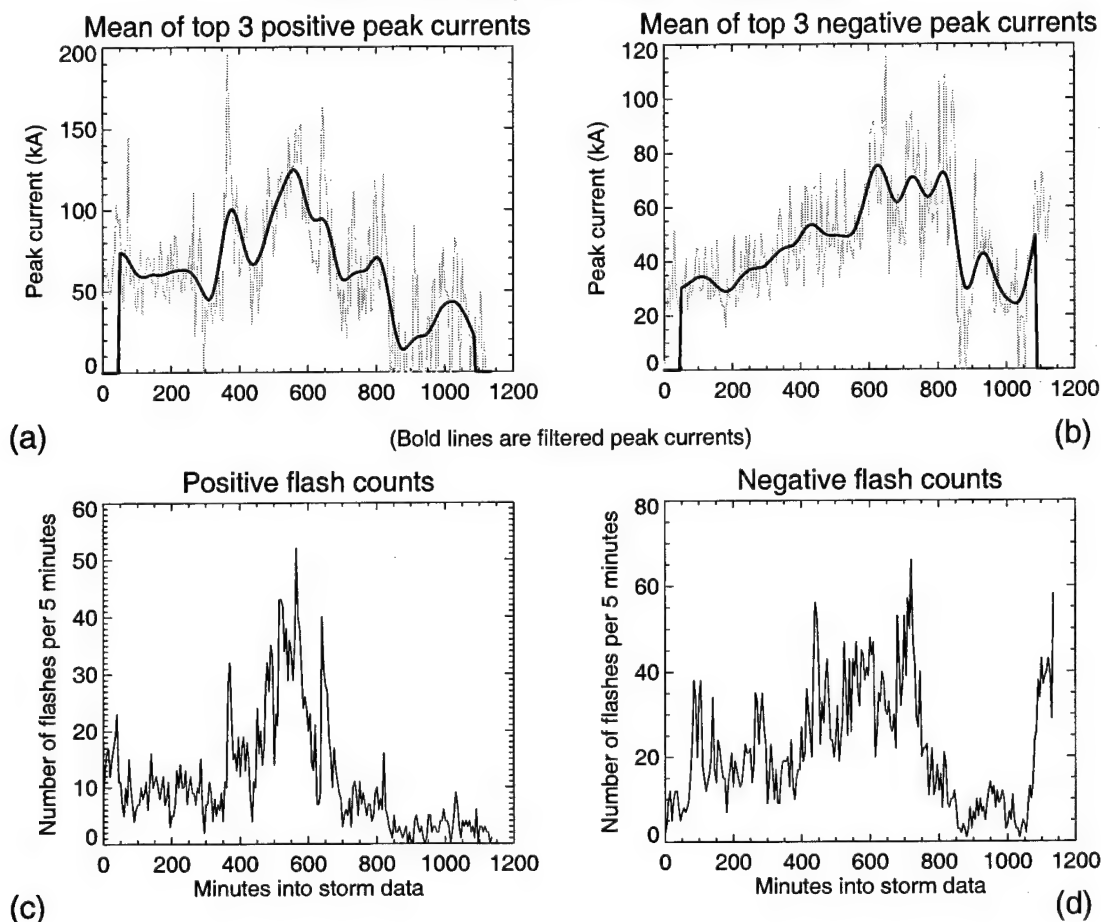


Figure E-13. Time series of peak currents and flash counts for 4 Aug 95. The three extreme peak currents were found for each 5 minute interval and plotted in light gray for positive (a) and negative (b) flashes. A band-pass filter was applied to the peak currents using a 55.5 minute period for positive flashes and a 53.0 minute window for negatives with the resulting wave shown as a dark curve in (a) and (b). The number of positive and negative flashes in each 5 minute window are shown in (c) and (d), respectively.

Data summary for case 95091806

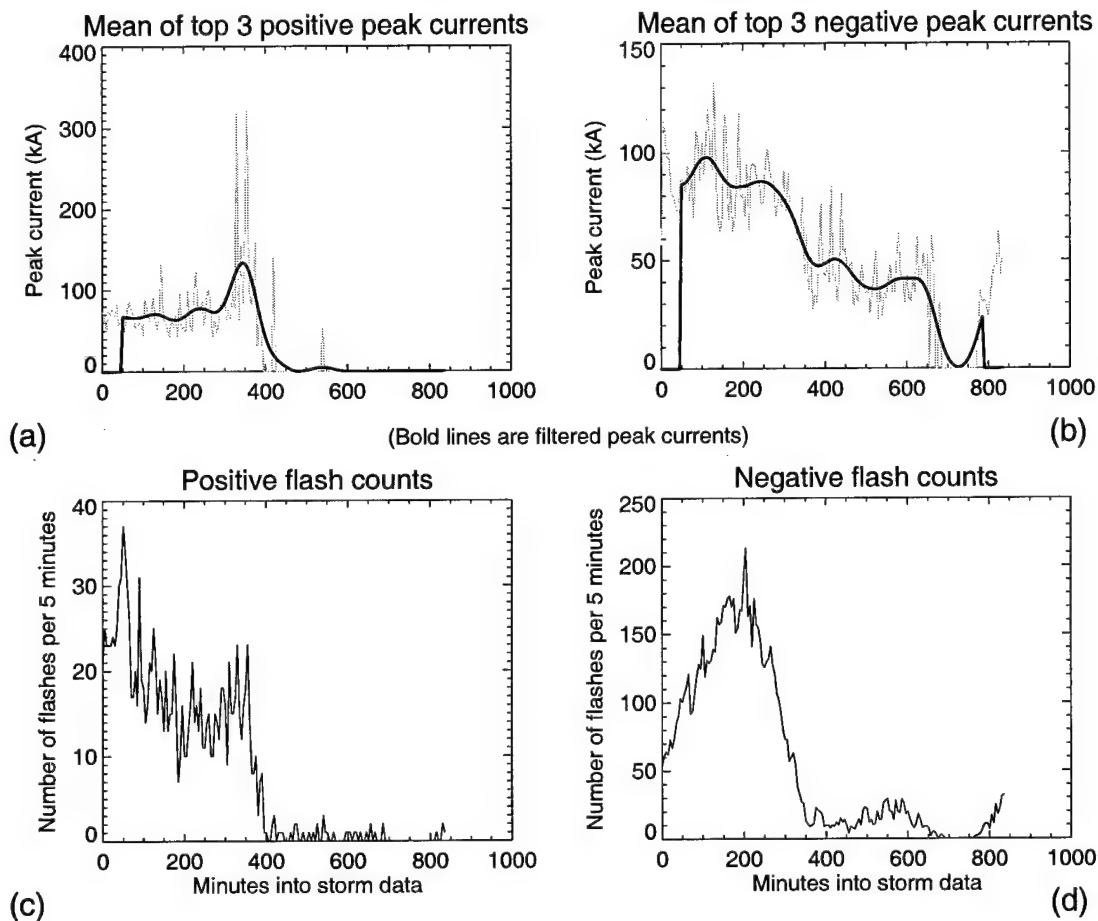


Figure E-14. Time series of peak currents and flash counts for 18 Sep 95. The three extreme peak currents were found for each 5 minute interval and plotted in light gray for positive (a) and negative (b) flashes. A band-pass filter was applied to the peak currents using a 38.0 minute period for positive flashes and a 40.0 minute window for negatives with the resulting wave shown as a dark curve in (a) and (b). The number of positive and negative flashes in each 5 minute window are shown in (c) and (d), respectively.

Data summary for case 96011800

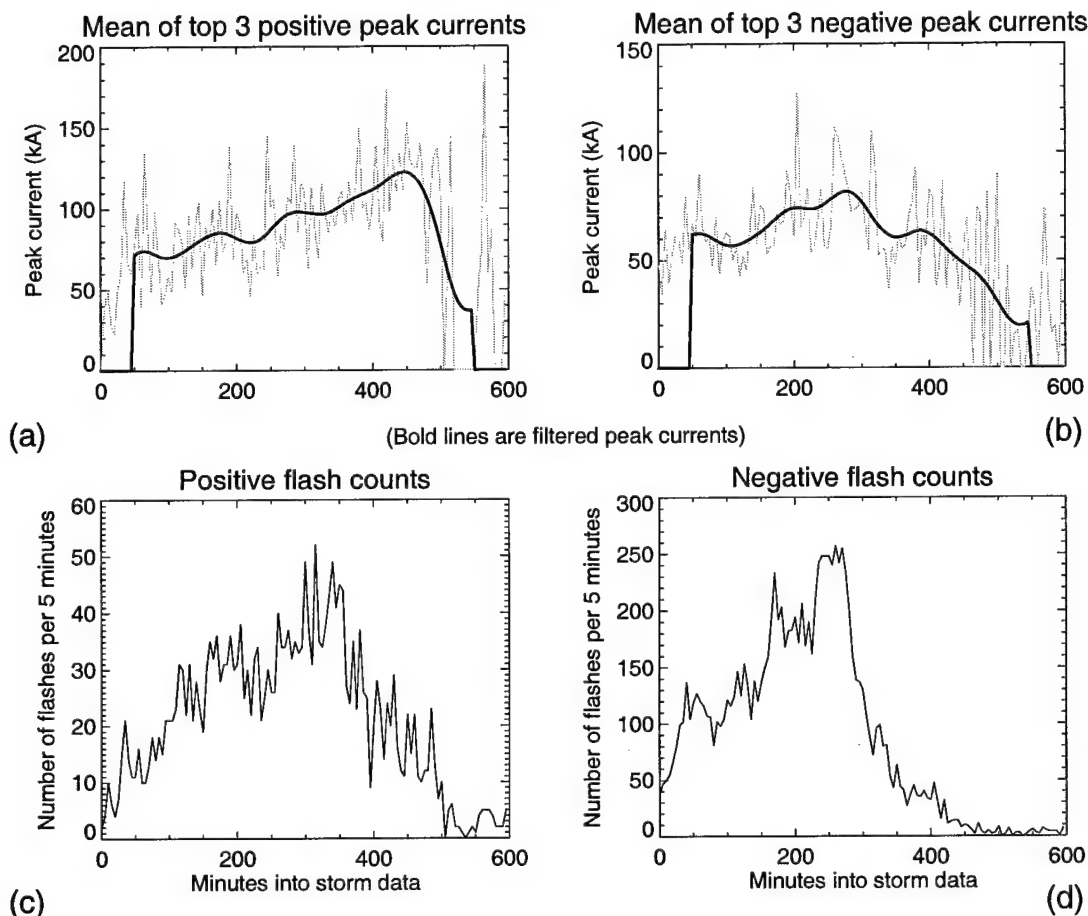


Figure E-15. Time series of peak currents and flash counts for 18 Jan 96. The three extreme peak currents were found for each 5 minute interval and plotted in light gray for positive (a) and negative (b) flashes. A band-pass filter was applied to the peak currents using a 28.5 minute period for positive flashes and a 30.0 minute window for negatives with the resulting wave shown as a dark curve in (a) and (b). The number of positive and negative flashes in each 5 minute window are shown in (c) and (d), respectively.

Data summary for case 96050900

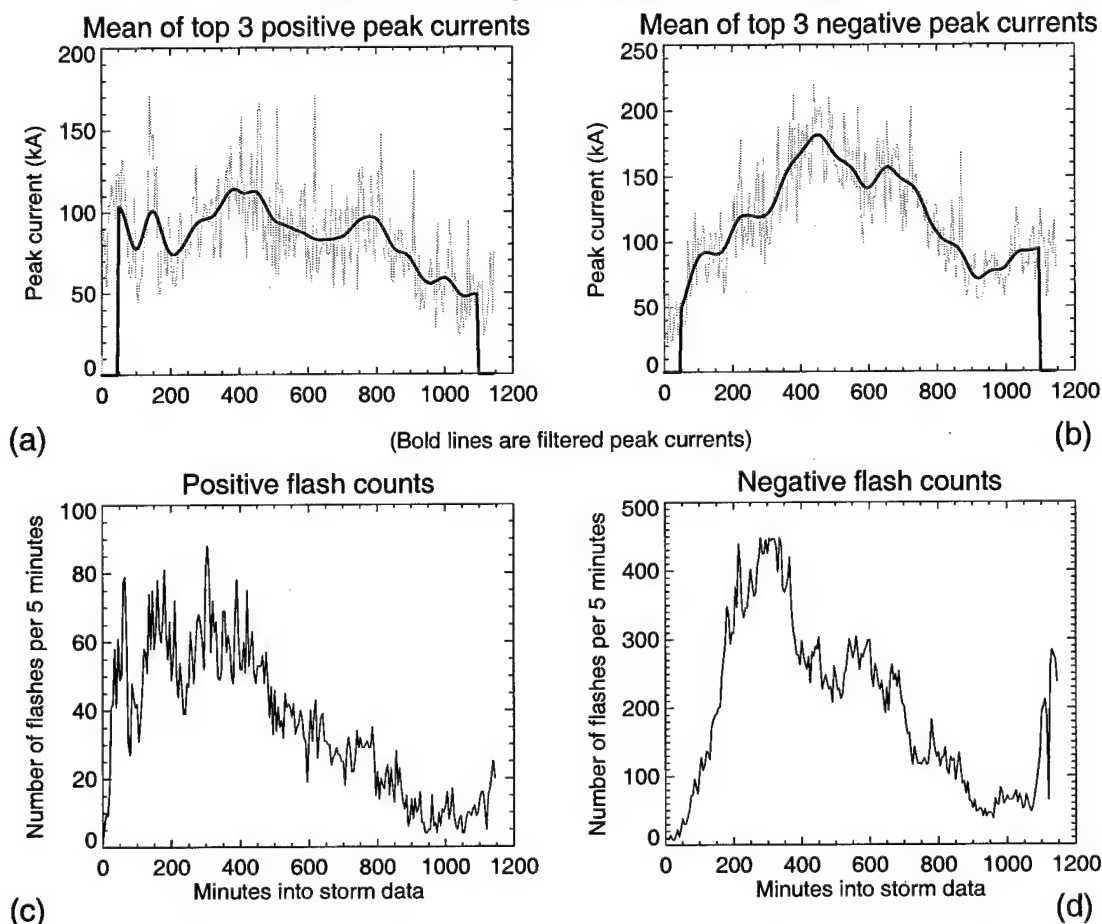


Figure E-16. Time series of peak currents and flash counts for 9 May 96. The three extreme peak currents were found for each 5 minute interval and plotted in light gray for positive (a) and negative (b) flashes. A band-pass filter was applied to the peak currents using a 57.0 minute period for positive flashes and a 59.0 minute window for negatives with the resulting wave shown as a dark curve in (a) and (b). The number of positive and negative flashes in each 5 minute window are shown in (c) and (d), respectively.

Data summary for case 96051518

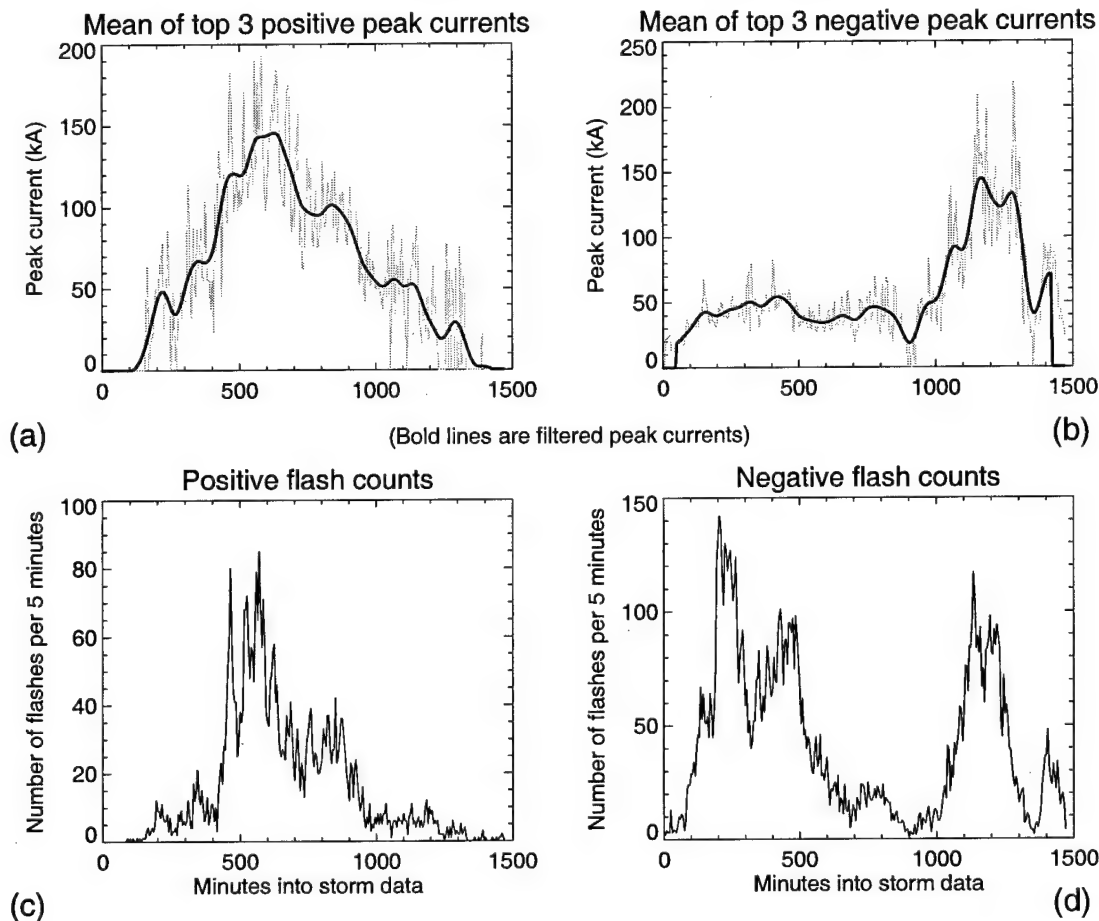


Figure E-17. Time series of peak currents and flash counts for 15 May 96. The three extreme peak currents were found for each 5 minute interval and plotted in light gray for positive (a) and negative (b) flashes. A band-pass filter was applied to the peak currents using a 76.5 minute period for positive flashes and a 67.0 minute window for negatives with the resulting wave shown as a dark curve in (a) and (b). The number of positive and negative flashes in each 5 minute window are shown in (c) and (d), respectively.

Data summary for case 96051812

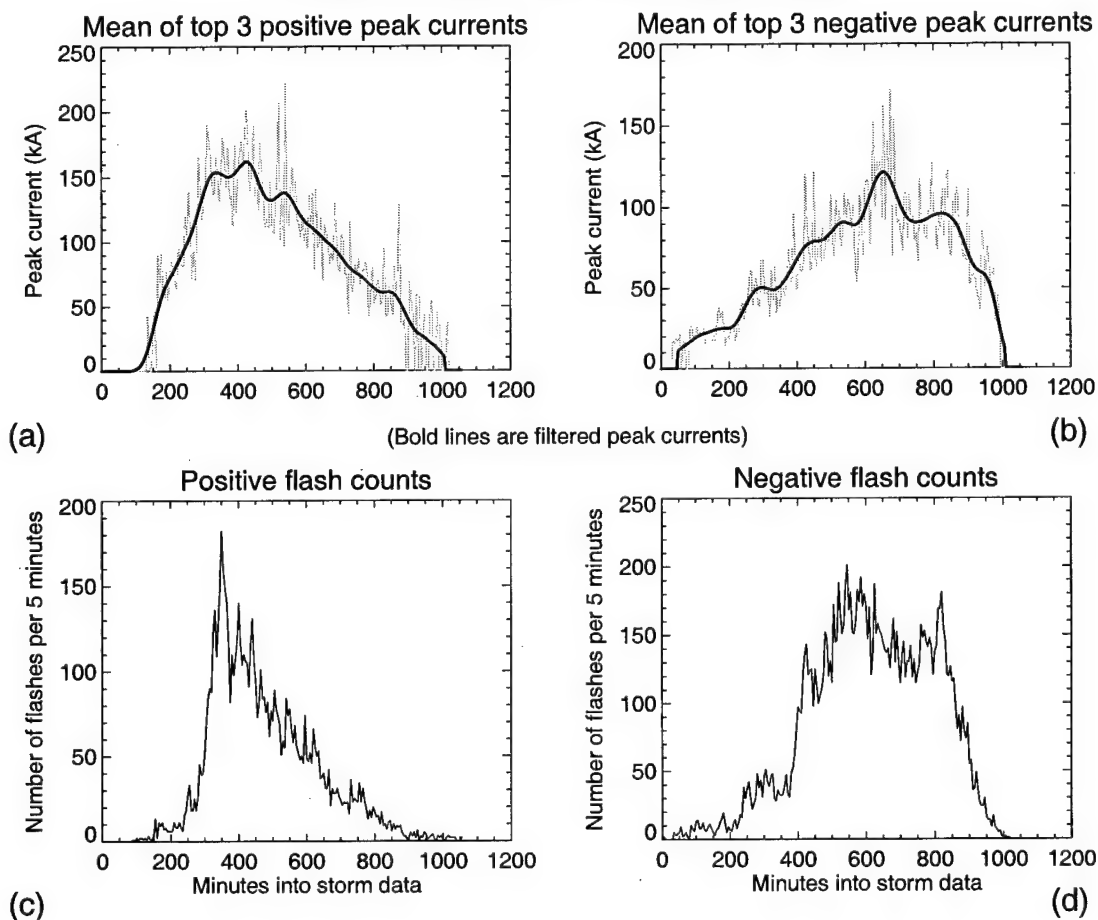


Figure E-18. Time series of peak currents and flash counts for 18 May 96. The three extreme peak currents were found for each 5 minute interval and plotted in light gray for positive (a) and negative (b) flashes. A band-pass filter was applied to the peak currents using a 53.0 minute period for positive flashes and a 51.5 minute window for negatives with the resulting wave shown as a dark curve in (a) and (b). The number of positive and negative flashes in each 5 minute window are shown in (c) and (d), respectively.

Data summary for case 96061904

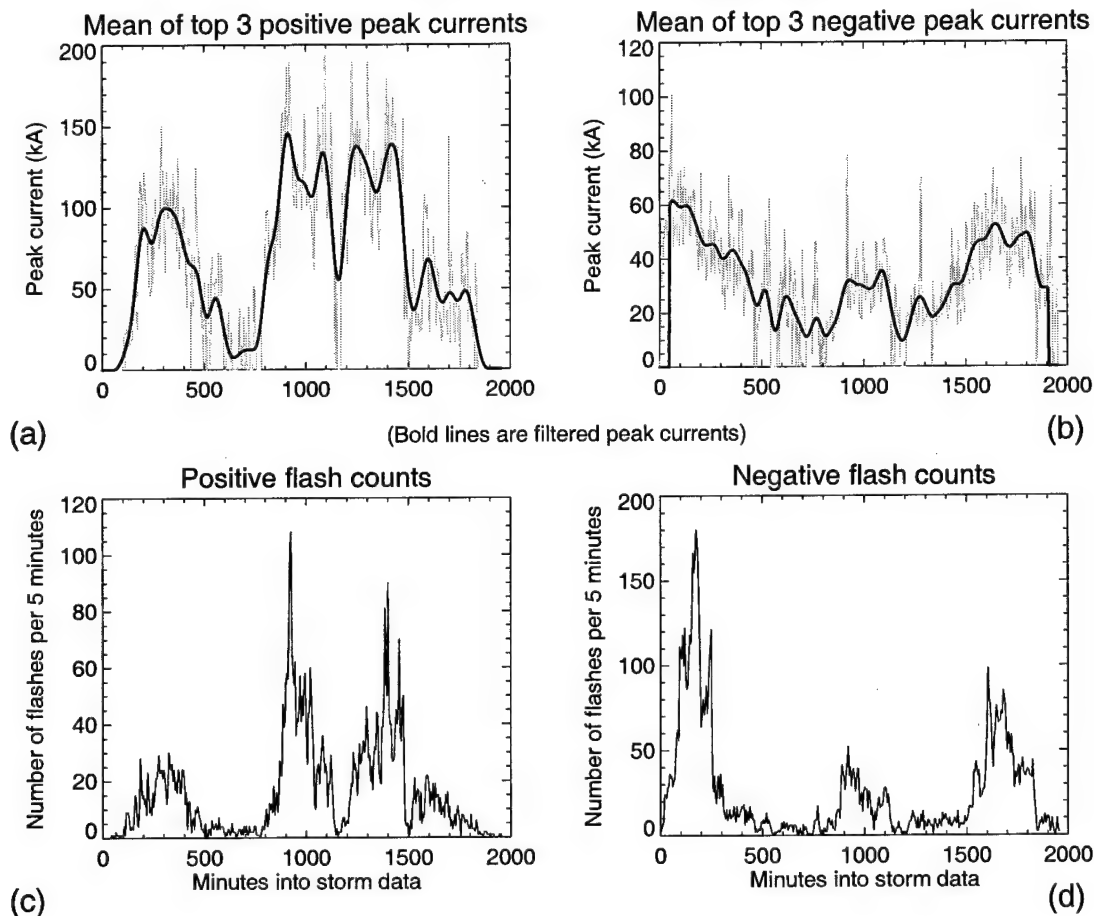


Figure E-19. Time series of peak currents and flash counts for 19 Jun 96. The three extreme peak currents were found for each 5 minute interval and plotted in light gray for positive (a) and negative (b) flashes. A band-pass filter was applied to the peak currents using a 94.0 minute period for positive flashes and a 99.0 minute window for negatives with the resulting wave shown as a dark curve in (a) and (b). The number of positive and negative flashes in each 5 minute window are shown in (c) and (d), respectively.

Data summary for case 96071512

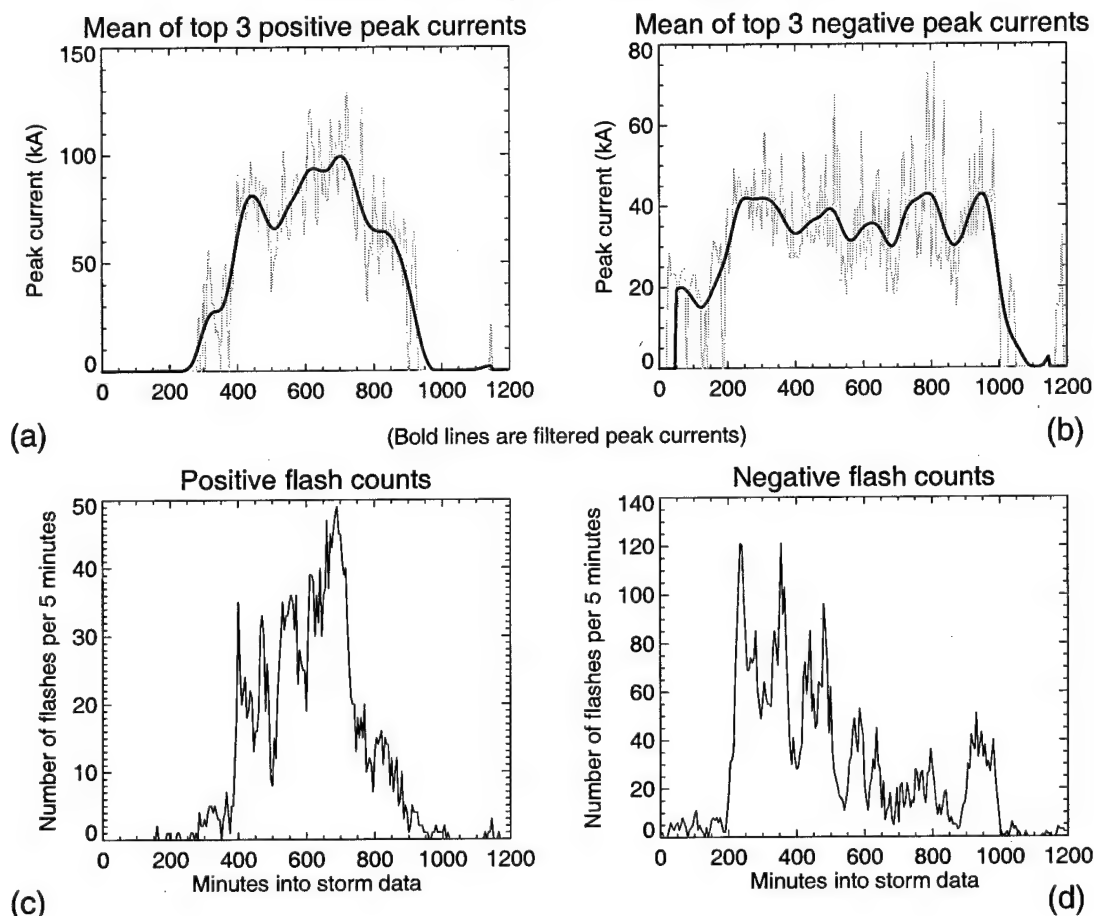


Figure E-20. Time series of peak currents and flash counts for 15 Jul 96. The three extreme peak currents were found for each 5 minute interval and plotted in light gray for positive (a) and negative (b) flashes. A band-pass filter was applied to the peak currents using a 62.5 minute period for positive flashes and a 60.5 minute window for negatives with the resulting wave shown as a dark curve in (a) and (b). The number of positive and negative flashes in each 5 minute window are shown in (c) and (d), respectively.

Data summary for case 96072712

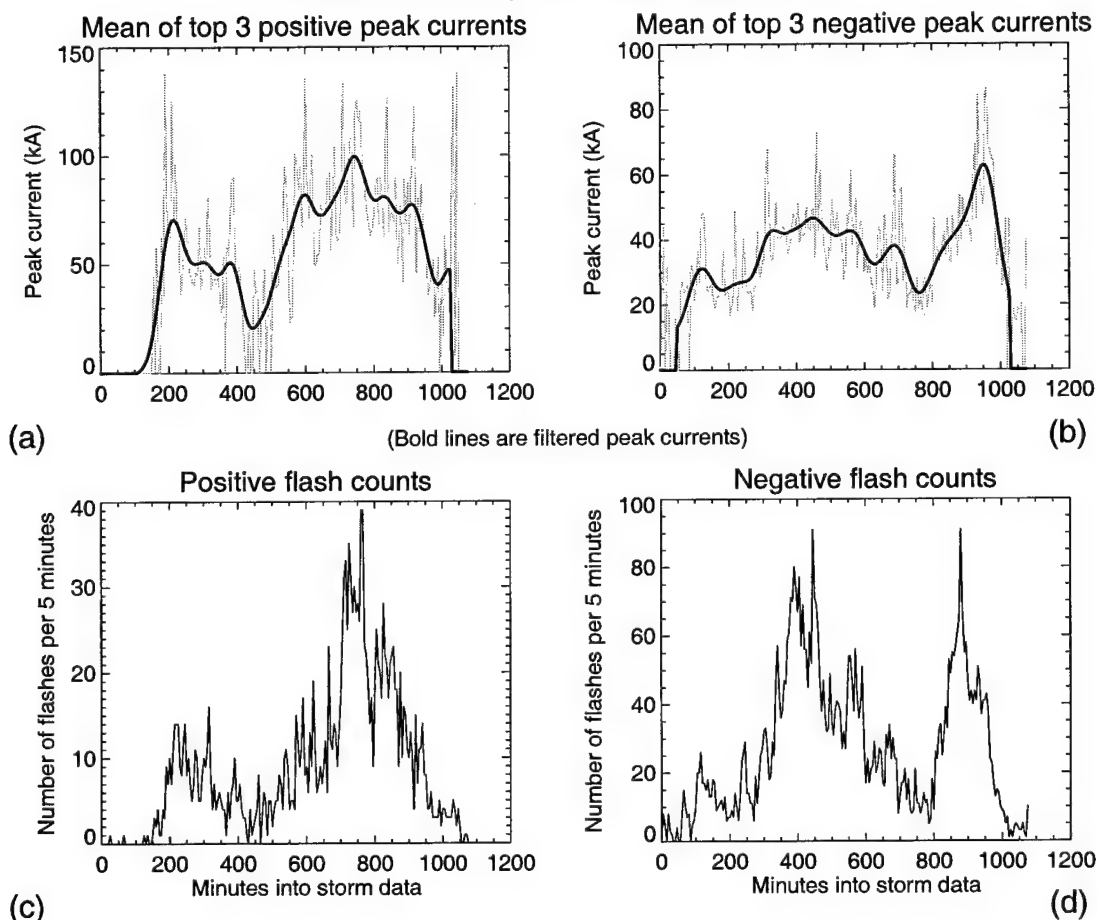


Figure E-21. Time series of peak currents and flash counts for 27 Jul 96. The three extreme peak currents were found for each 5 minute interval and plotted in light gray for positive (a) and negative (b) flashes. A band-pass filter was applied to the peak currents using a 49.5 minute period for positive flashes and a 52.5 minute window for negatives with the resulting wave shown as a dark curve in (a) and (b). The number of positive and negative flashes in each 5 minute window are shown in (c) and (d), respectively.

Data summary for case 96080212

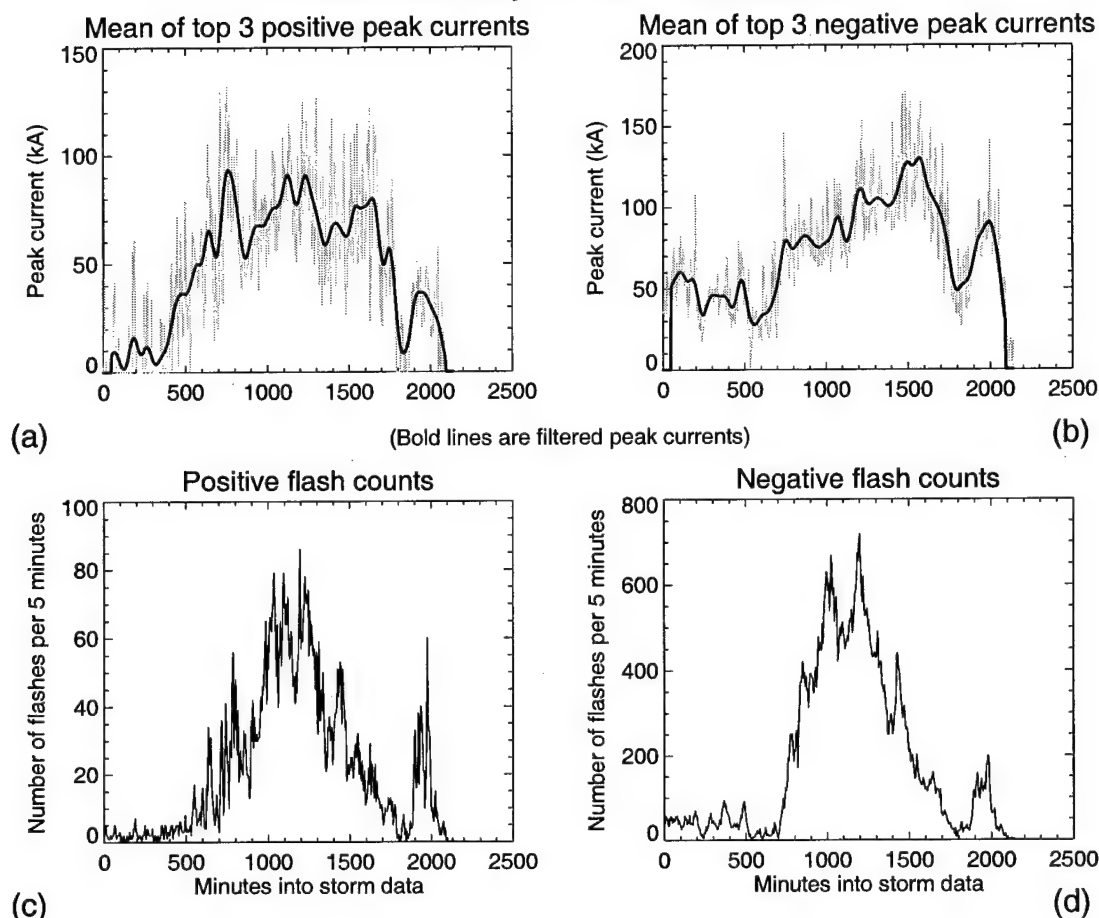


Figure E-22. Time series of peak currents and flash counts for 2 Aug 96. The three extreme peak currents were found for each 5 minute interval and plotted in light gray for positive (a) and negative (b) flashes. A band-pass filter was applied to the peak currents using a 108.0 minute period for positive flashes and a 104.5 minute window for negatives with the resulting wave shown as a dark curve in (a) and (b). The number of positive and negative flashes in each 5 minute window are shown in (c) and (d), respectively.

Data summary for case 96080621

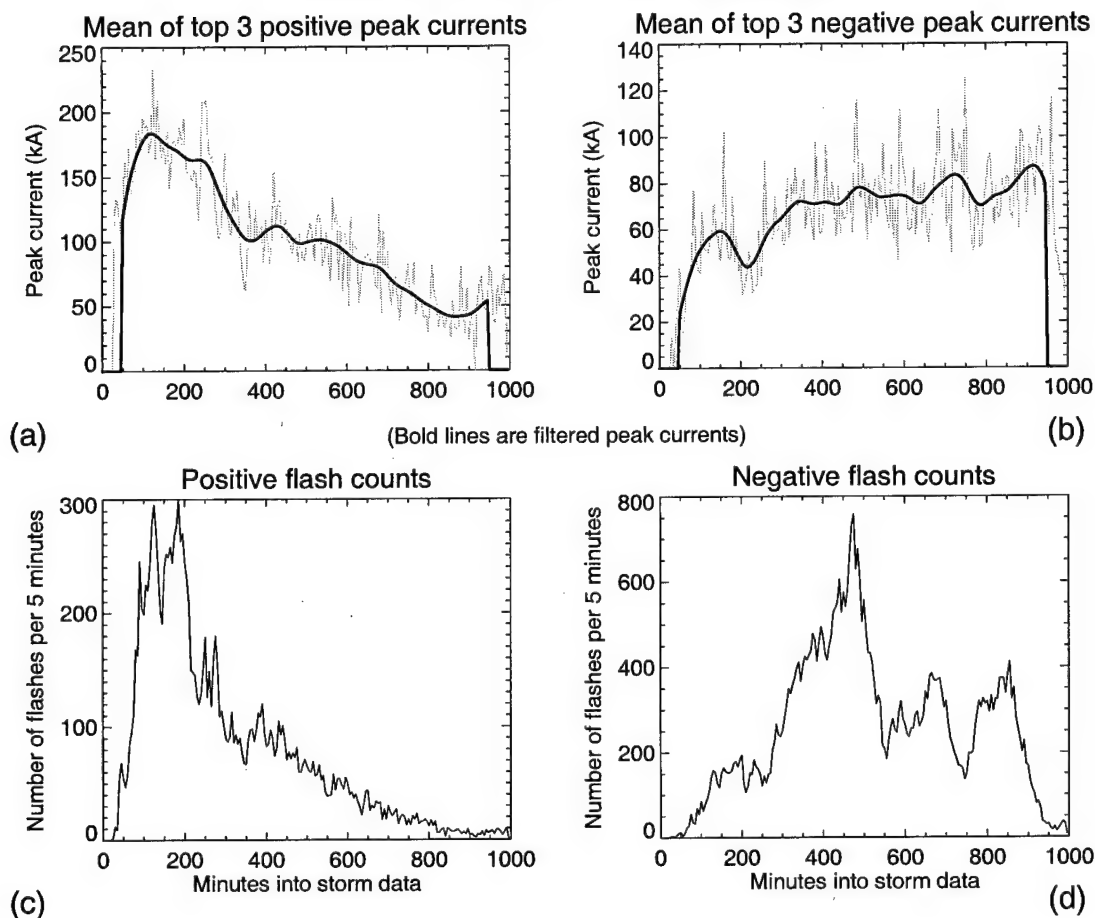


Figure E-23. Time series of peak currents and flash counts for 6 Aug 96. The three extreme peak currents were found for each 5 minute interval and plotted in light gray for positive (a) and negative (b) flashes. A band-pass filter was applied to the peak currents using a 50.0 minute period for positive flashes and a 50.5 minute window for negatives with the resulting wave shown as a dark curve in (a) and (b). The number of positive and negative flashes in each 5 minute window are shown in (c) and (d), respectively.

Data summary for case 96082123

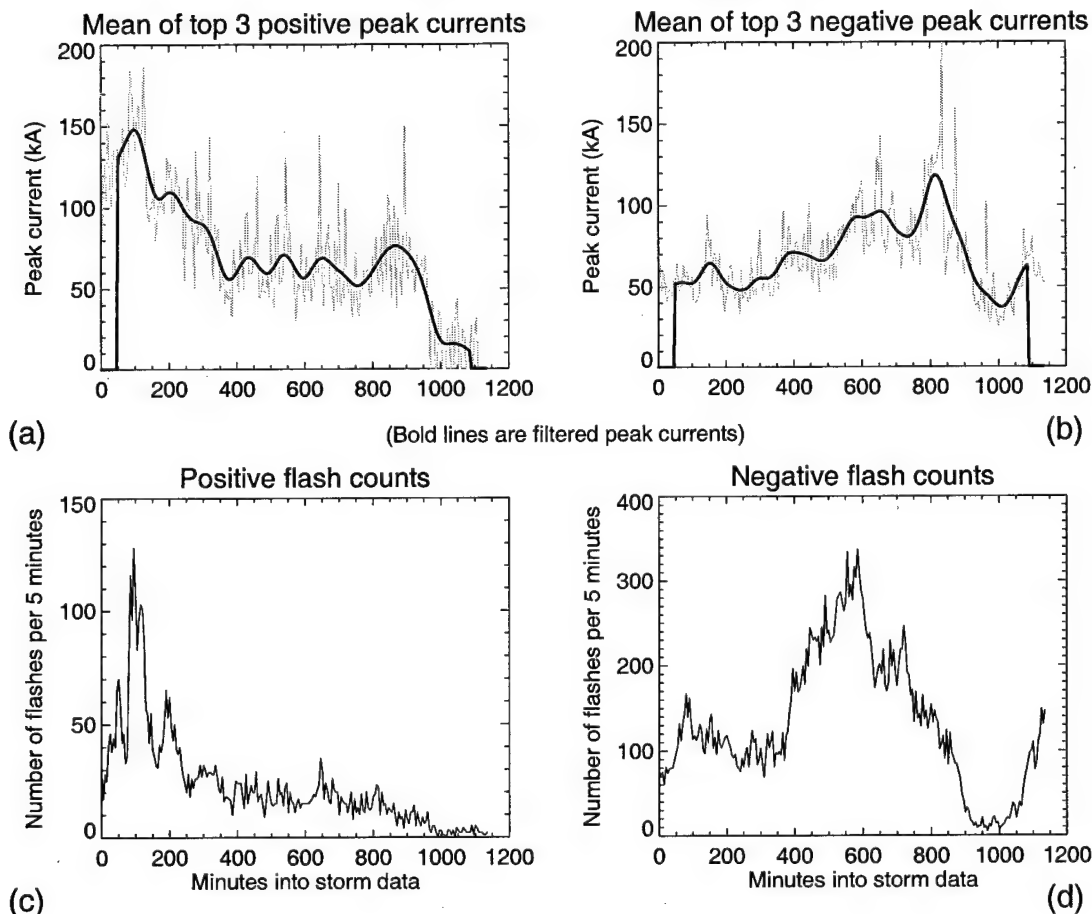


Figure E-24. Time series of peak currents and flash counts for 21 Aug 96. The three extreme peak currents were found for each 5 minute interval and plotted in light gray for positive (a) and negative (b) flashes. A band-pass filter was applied to the peak currents using a 54.0 minute period for positive flashes and a 58.5 minute window for negatives with the resulting wave shown as a dark curve in (a) and (b). The number of positive and negative flashes in each 5 minute window are shown in (c) and (d), respectively.

Data summary for case 96102412

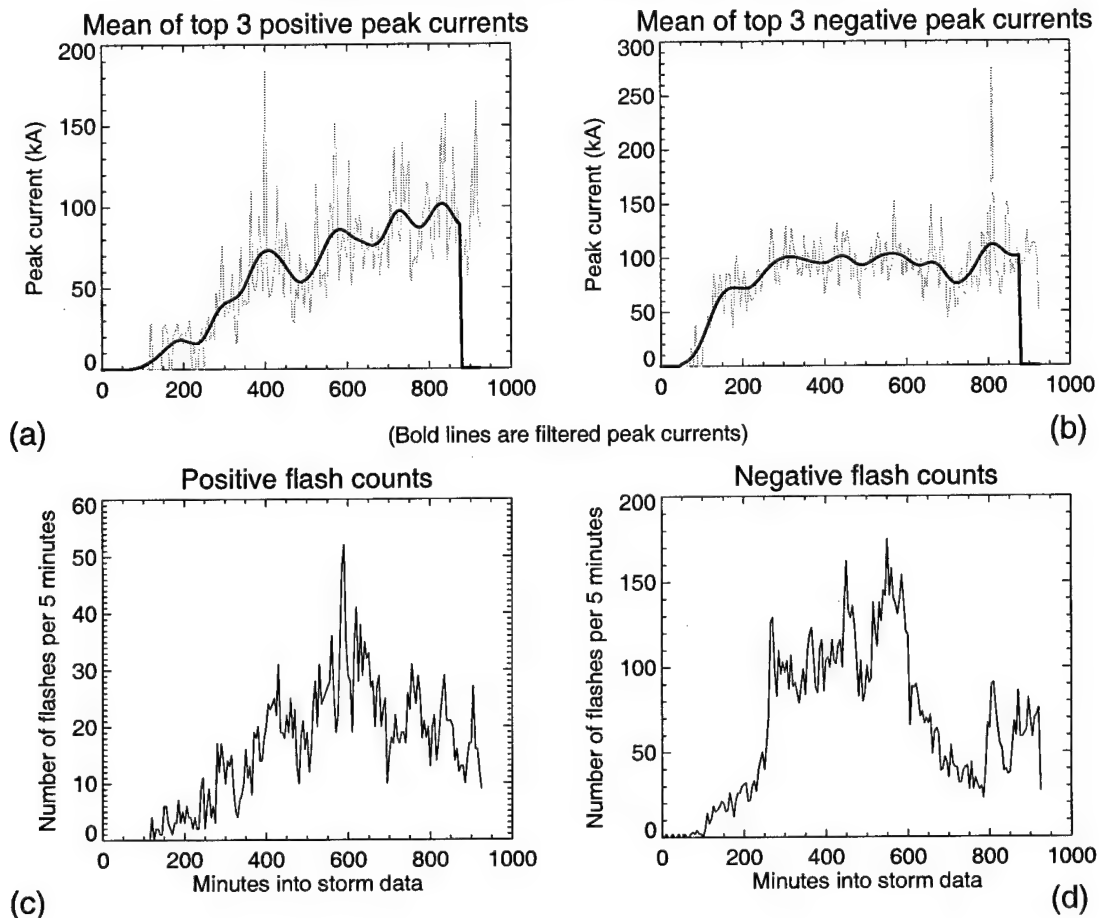


Figure E-25. Time series of peak currents and flash counts for 24 Oct 96. The three extreme peak currents were found for each 5 minute interval and plotted in light gray for positive (a) and negative (b) flashes. A band-pass filter was applied to the peak currents using a 47.0 minute period for positive flashes and a 47.0 minute window for negatives with the resulting wave shown as a dark curve in (a) and (b). The number of positive and negative flashes in each 5 minute window are shown in (c) and (d), respectively.

Data summary for case 96112321

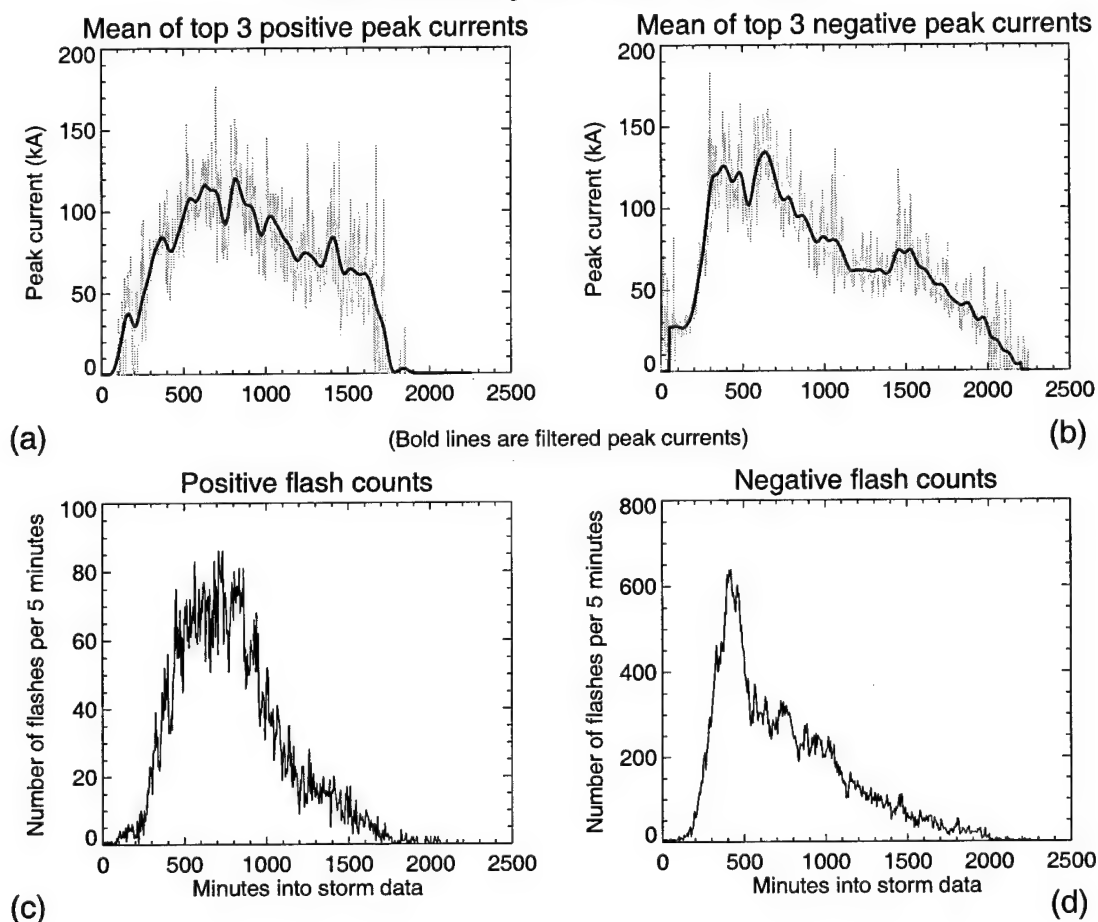


Figure E-26. Time series of peak currents and flash counts for 23 Nov 96. The three extreme peak currents were found for each 5 minute interval and plotted in light gray for positive (a) and negative (b) flashes. A band-pass filter was applied to the peak currents using a 113.0 minute period for positive flashes and a 114.0 minute window for negatives with the resulting wave shown as a dark curve in (a) and (b). The number of positive and negative flashes in each 5 minute window are shown in (c) and (d), respectively.

Data summary for case 97020317

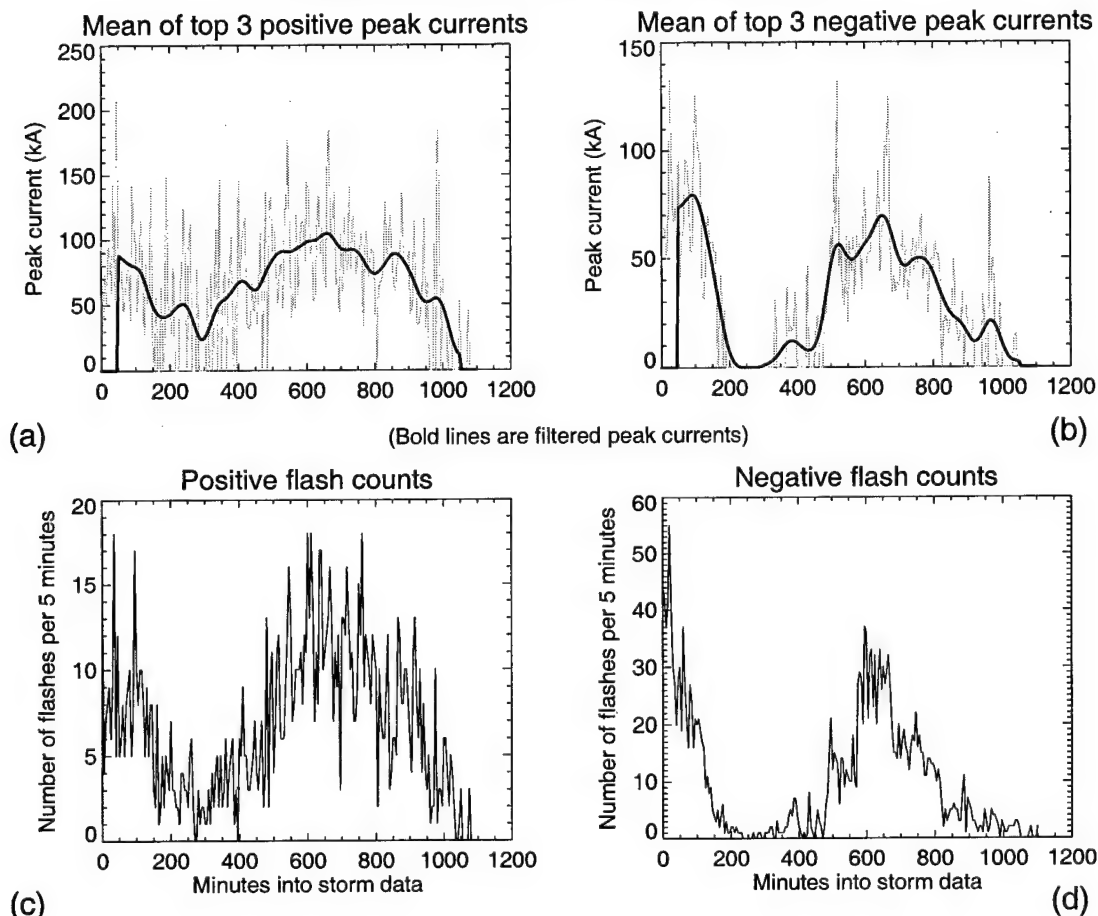


Figure E-27. Time series of peak currents and flash counts for 3 Feb 97. The three extreme peak currents were found for each 5 minute interval and plotted in light gray for positive (a) and negative (b) flashes. A band-pass filter was applied to the peak currents using a 57.5 minute period for positive flashes and a 54.0 minute window for negatives with the resulting wave shown as a dark curve in (a) and (b). The number of positive and negative flashes in each 5 minute window are shown in (c) and (d), respectively.

Data summary for case 97030912

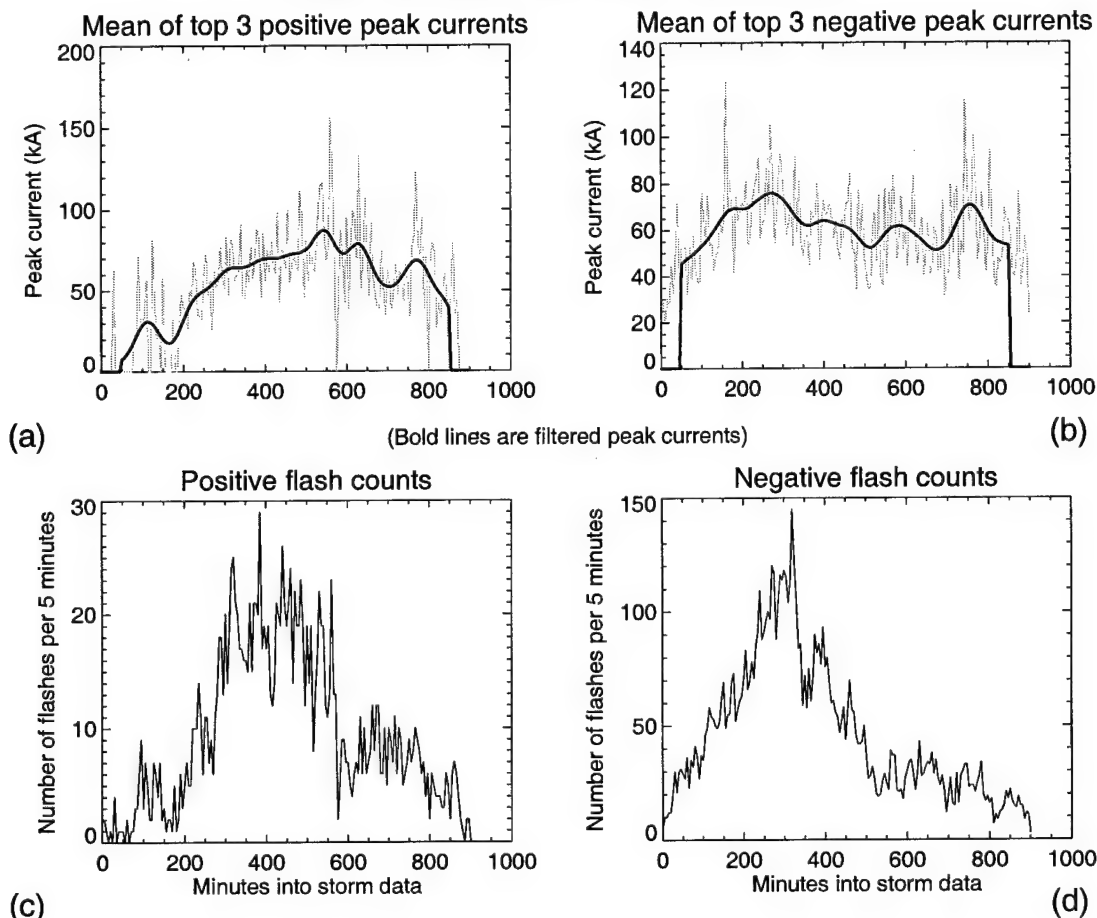


Figure E-28. Time series of peak currents and flash counts for 9 Mar 97. The three extreme peak currents were found for each 5 minute interval and plotted in light gray for positive (a) and negative (b) flashes. A band-pass filter was applied to the peak currents using a 42.5 minute period for positive flashes and a 48.5 minute window for negatives with the resulting wave shown as a dark curve in (a) and (b). The number of positive and negative flashes in each 5 minute window are shown in (c) and (d), respectively.

Data summary for case 97032422

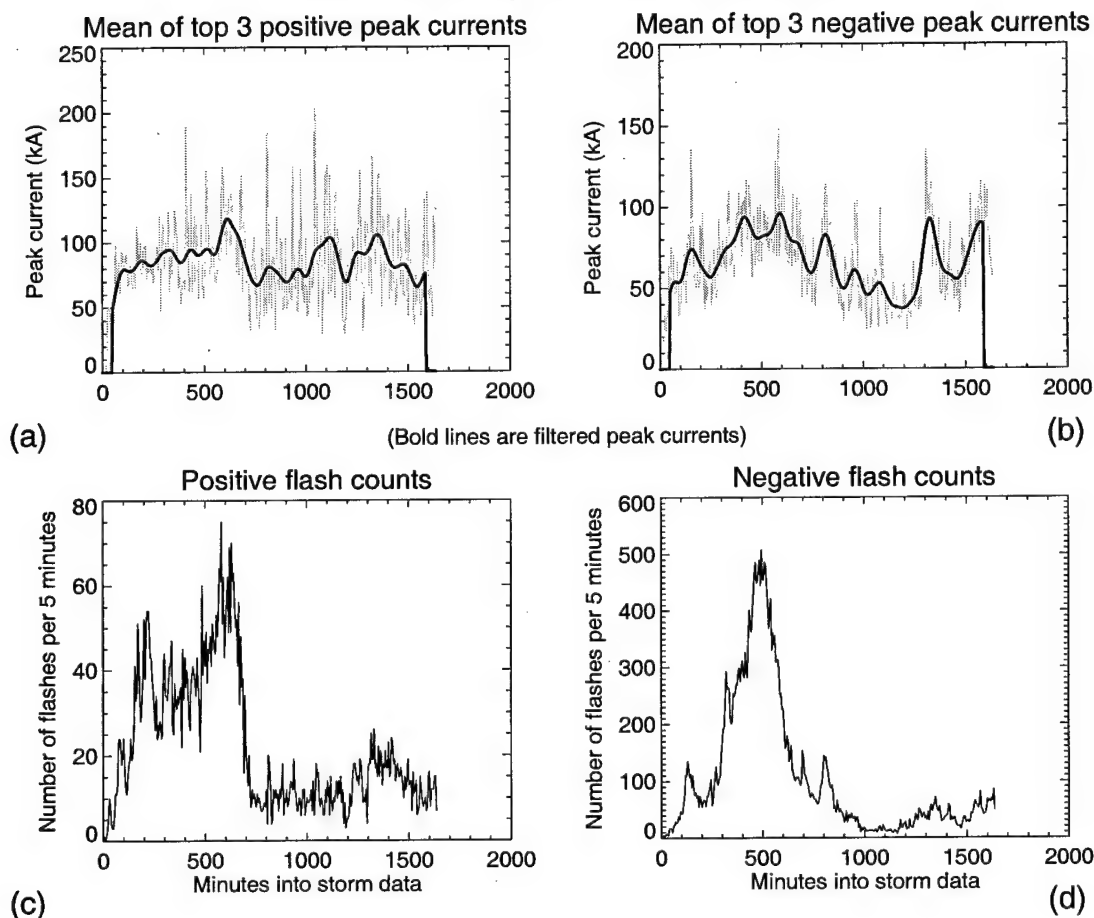


Figure E-29. Time series of peak currents and flash counts for 24 Mar 97. The three extreme peak currents were found for each 5 minute interval and plotted in light gray for positive (a) and negative (b) flashes. A band-pass filter was applied to the peak currents using a 84.5 minute period for positive flashes and a 80.5 minute window for negatives with the resulting wave shown as a dark curve in (a) and (b). The number of positive and negative flashes in each 5 minute window are shown in (c) and (d), respectively.

Data summary for case 97061120

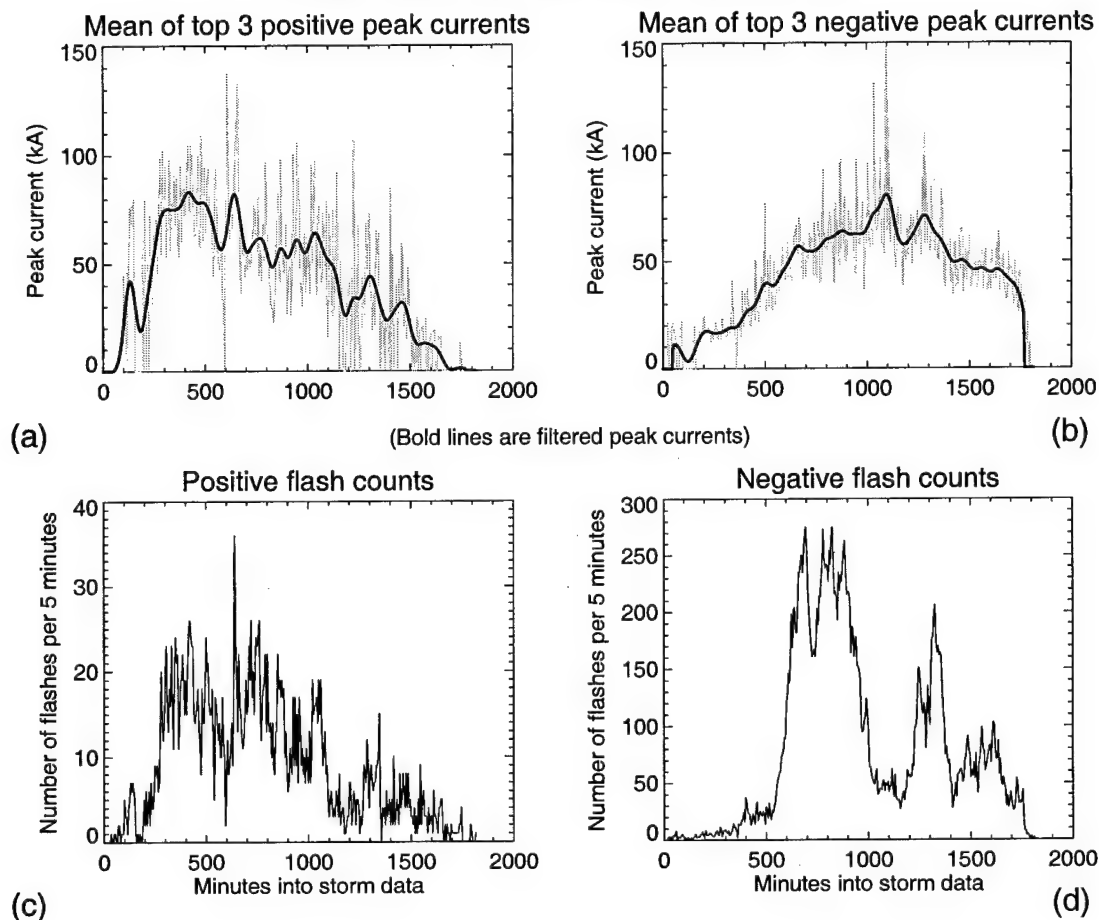


Figure E-30. Time series of peak currents and flash counts for 11 Jun 97. The three extreme peak currents were found for each 5 minute interval and plotted in light gray for positive (a) and negative (b) flashes. A band-pass filter was applied to the peak currents using a 89.5 minute period for positive flashes and a 91.5 minute window for negatives with the resulting wave shown as a dark curve in (a) and (b). The number of positive and negative flashes in each 5 minute window are shown in (c) and (d), respectively.

Data summary for case 97061412

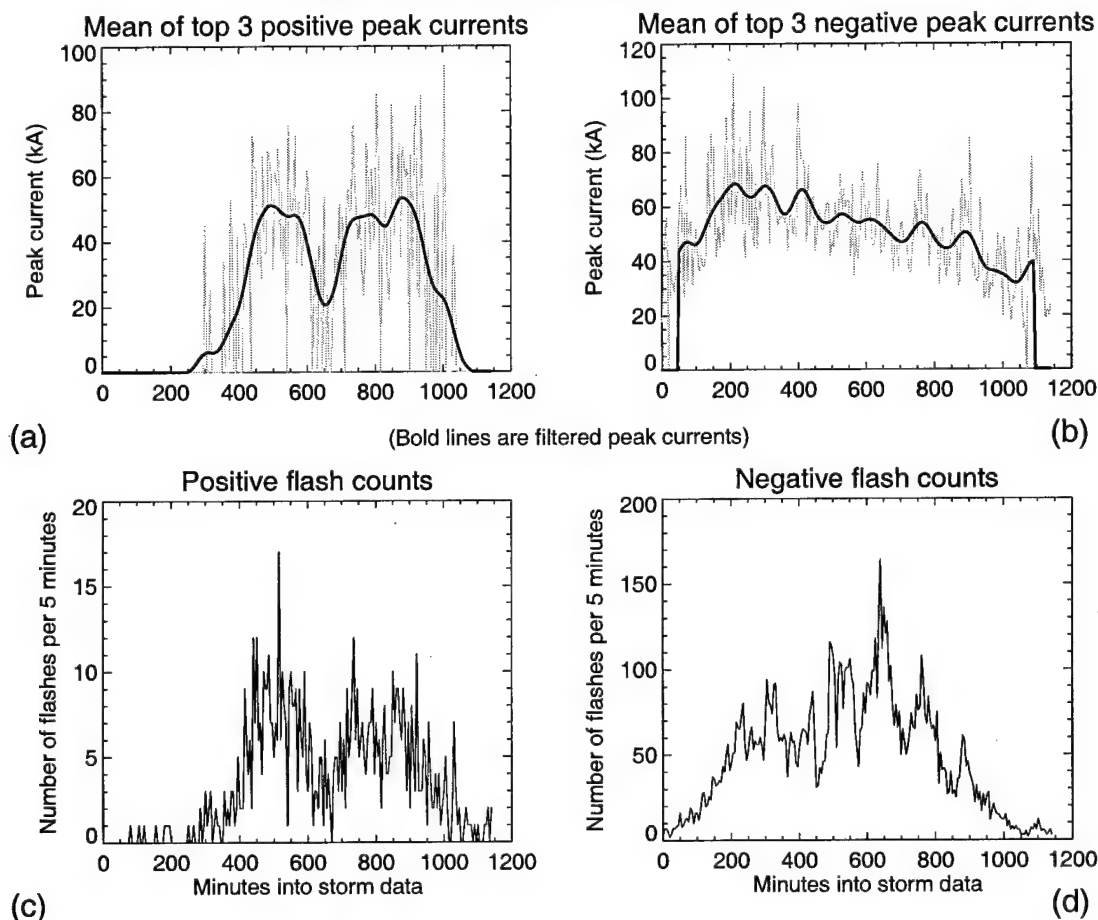


Figure E-31. Time series of peak currents and flash counts for 14 Jun 97. The three extreme peak currents were found for each 5 minute interval and plotted in light gray for positive (a) and negative (b) flashes. A band-pass filter was applied to the peak currents using a 57.5 minute period for positive flashes and a 59.0 minute window for negatives with the resulting wave shown as a dark curve in (a) and (b). The number of positive and negative flashes in each 5 minute window are shown in (c) and (d), respectively.

Data summary for case 97062018

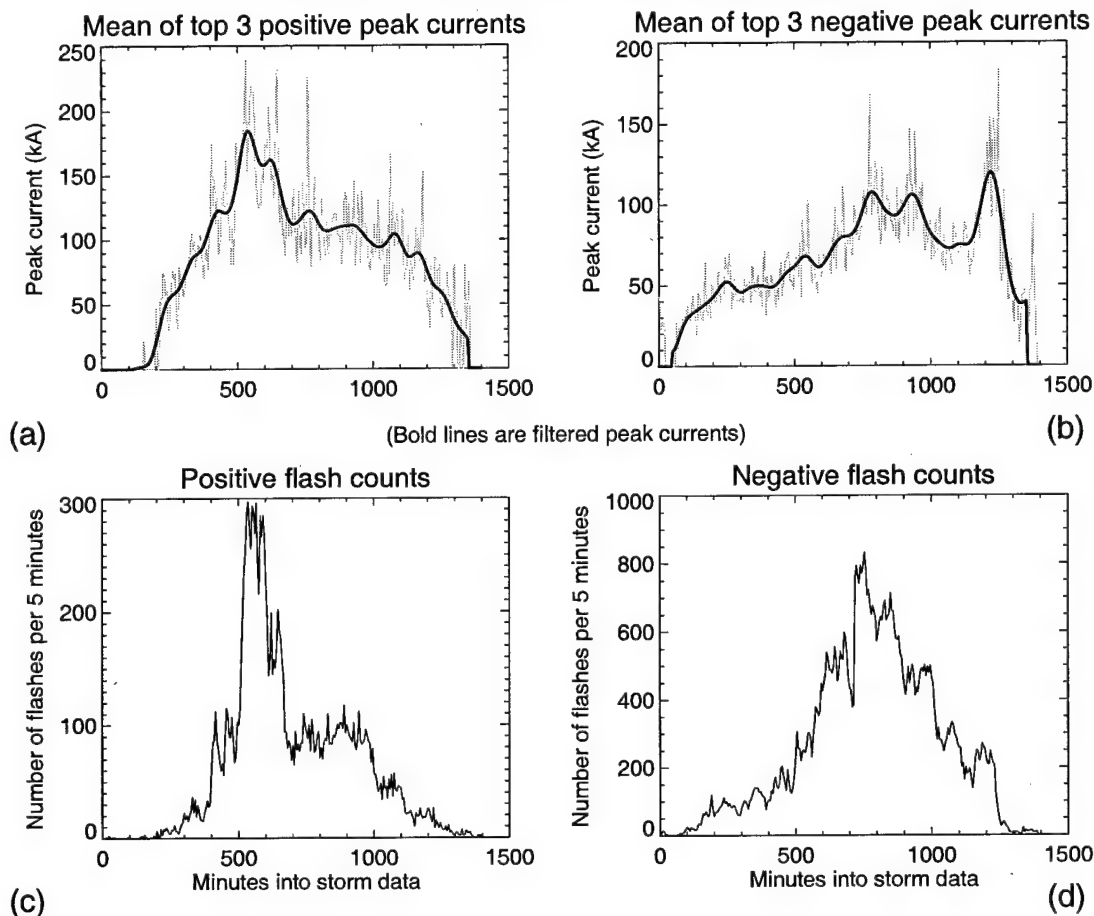


Figure E-32. Time series of peak currents and flash counts for 20 Jun 97. The three extreme peak currents were found for each 5 minute interval and plotted in light gray for positive (a) and negative (b) flashes. A band-pass filter was applied to the peak currents using a 70.0 minute period for positive flashes and a 63.5 minute window for negatives with the resulting wave shown as a dark curve in (a) and (b). The number of positive and negative flashes in each 5 minute window are shown in (c) and (d), respectively.

Data summary for case 97062200

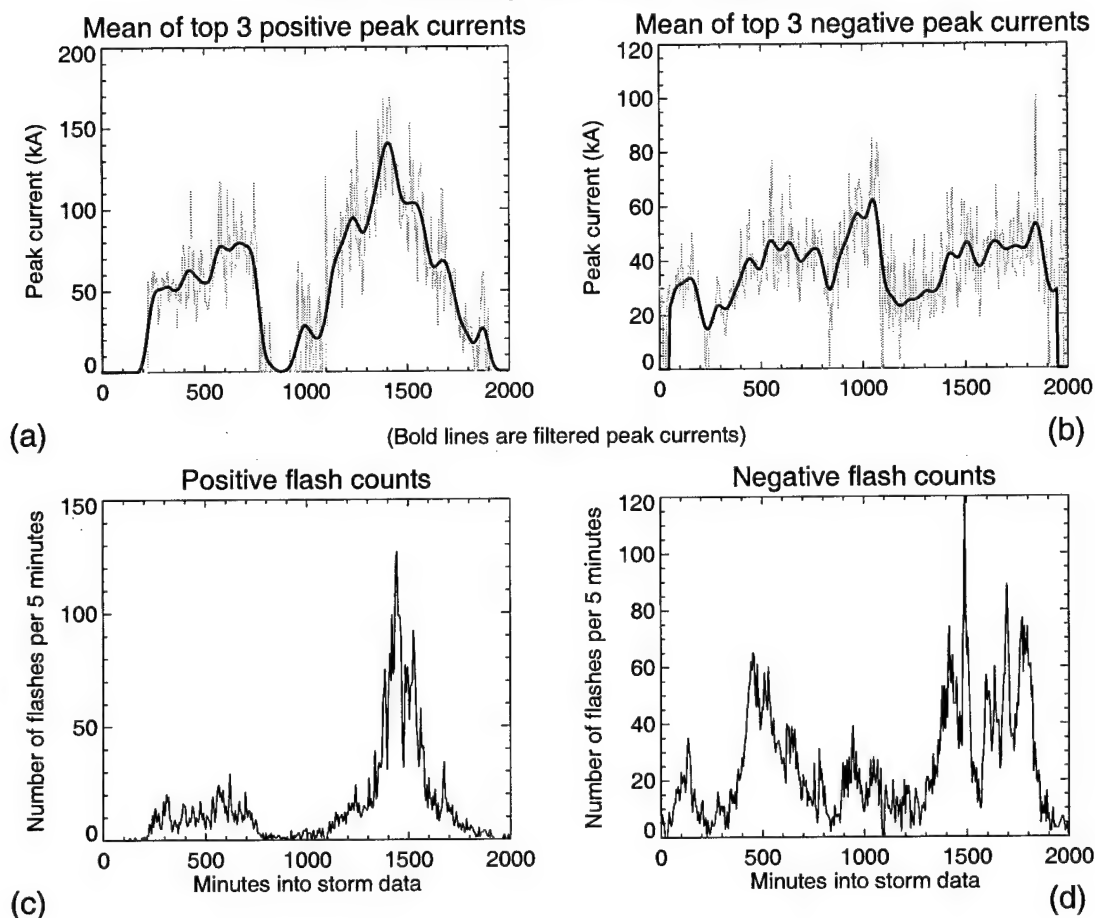


Figure E-33. Time series of peak currents and flash counts for 22 Jun 97. The three extreme peak currents were found for each 5 minute interval and plotted in light gray for positive (a) and negative (b) flashes. A band-pass filter was applied to the peak currents using a 102.0 minute period for positive flashes and a 99.0 minute window for negatives with the resulting wave shown as a dark curve in (a) and (b). The number of positive and negative flashes in each 5 minute window are shown in (c) and (d), respectively.

Data summary for case 97062418

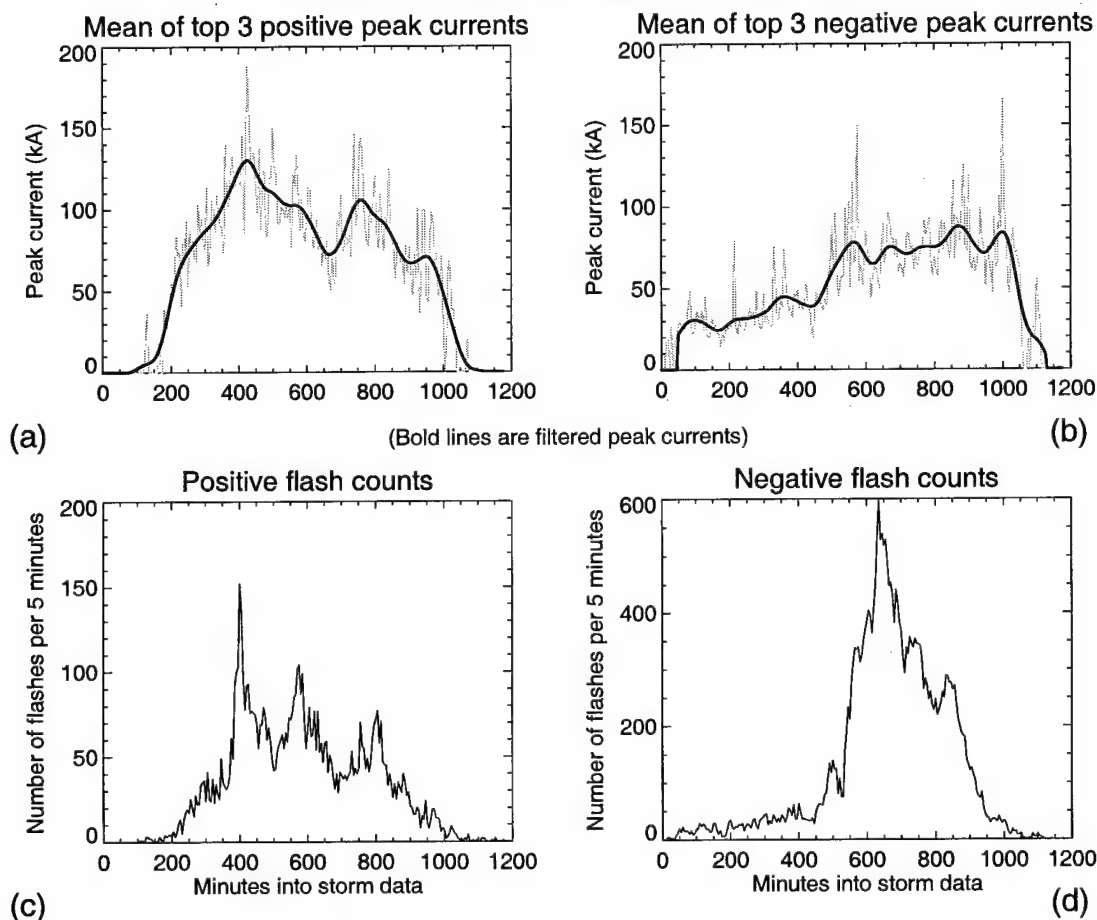


Figure E-34. Time series of peak currents and flash counts for 24 Jun 97. The three extreme peak currents were found for each 5 minute interval and plotted in light gray for positive (a) and negative (b) flashes. A band-pass filter was applied to the peak currents using a 60.0 minute period for positive flashes and a 60.5 minute window for negatives with the resulting wave shown as a dark curve in (a) and (b). The number of positive and negative flashes in each 5 minute window are shown in (c) and (d), respectively.

Data summary for case 97062800

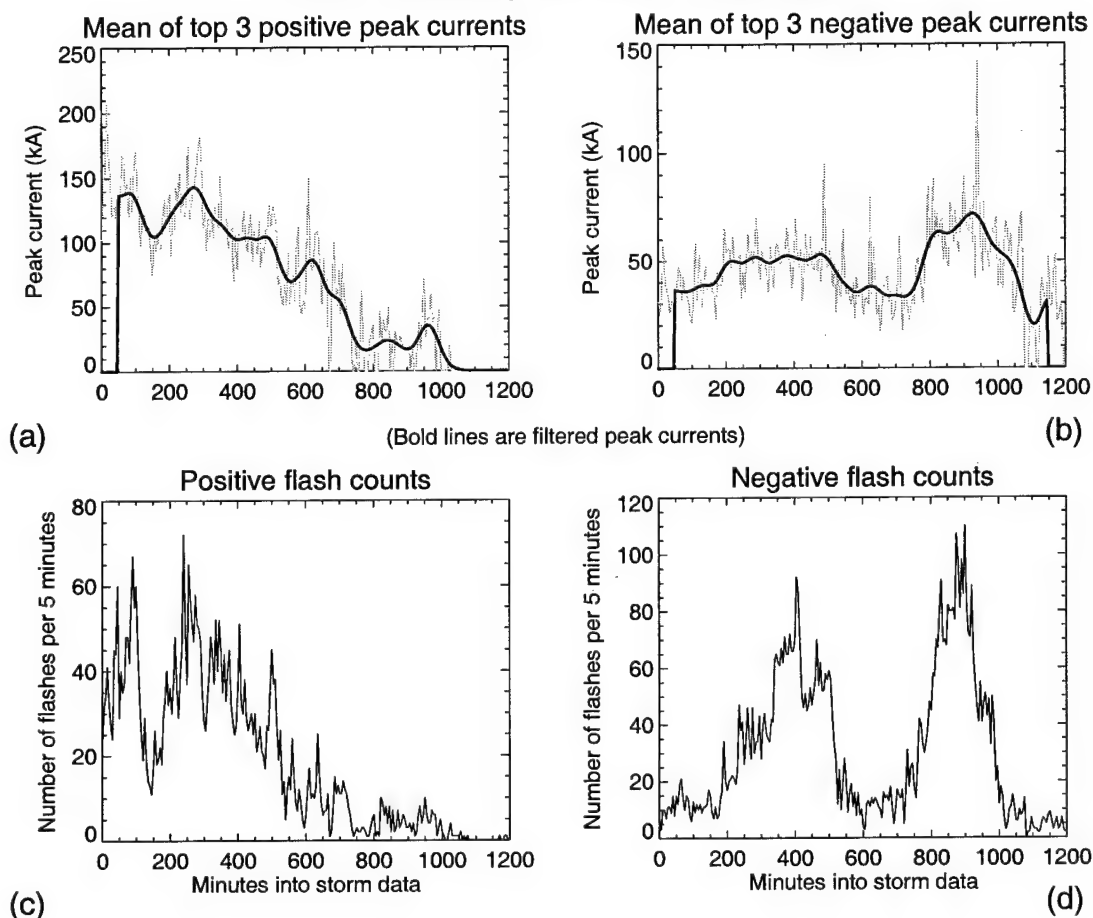


Figure E-35. Time series of peak currents and flash counts for 28 Jun 97. The three extreme peak currents were found for each 5 minute interval and plotted in light gray for positive (a) and negative (b) flashes. A band-pass filter was applied to the peak currents using a 57.5 minute period for positive flashes and a 61.5 minute window for negatives with the resulting wave shown as a dark curve in (a) and (b). The number of positive and negative flashes in each 5 minute window are shown in (c) and (d), respectively.

Data summary for case 97070817

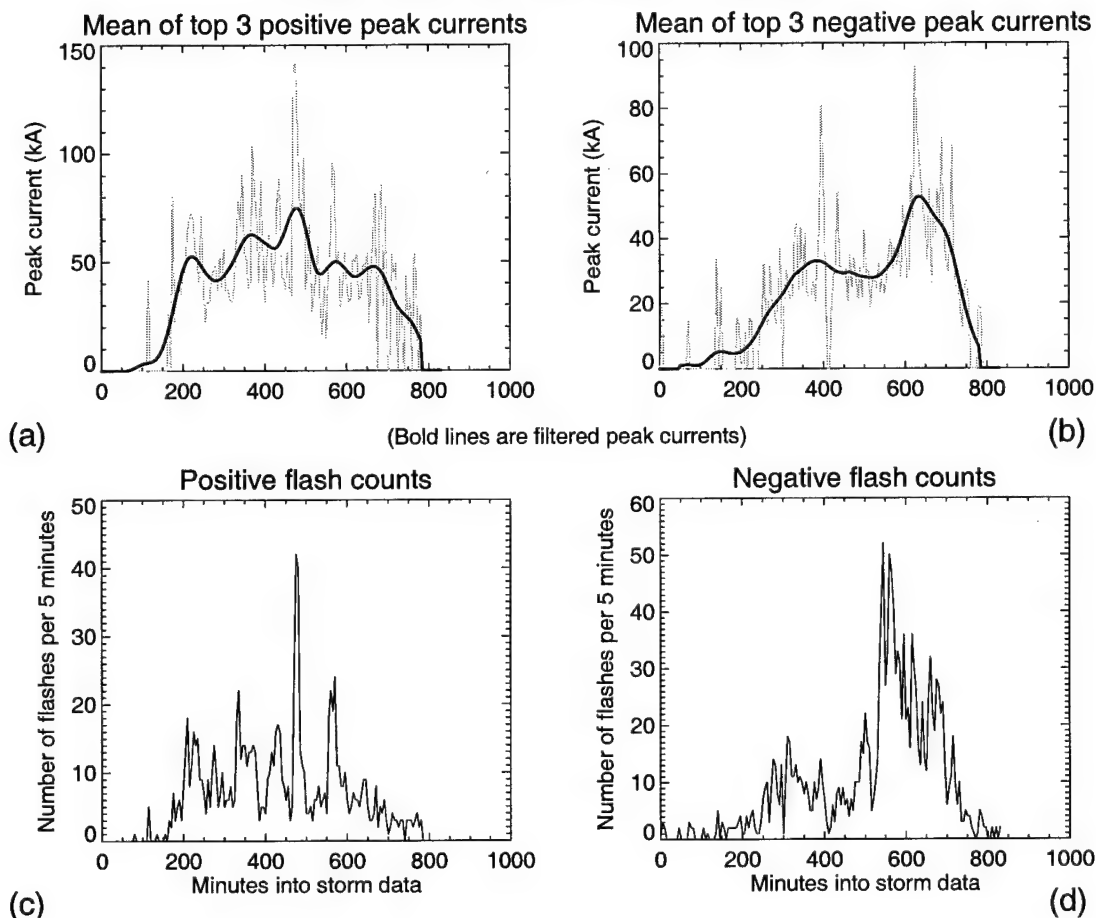


Figure E-36. Time series of peak currents and flash counts for 8 Jul 97. The three extreme peak currents were found for each 5 minute interval and plotted in light gray for positive (a) and negative (b) flashes. A band-pass filter was applied to the peak currents using a 42.0 minute period for positive flashes and a 44.0 minute window for negatives with the resulting wave shown as a dark curve in (a) and (b). The number of positive and negative flashes in each 5 minute window are shown in (c) and (d), respectively.

Data summary for case 97071623

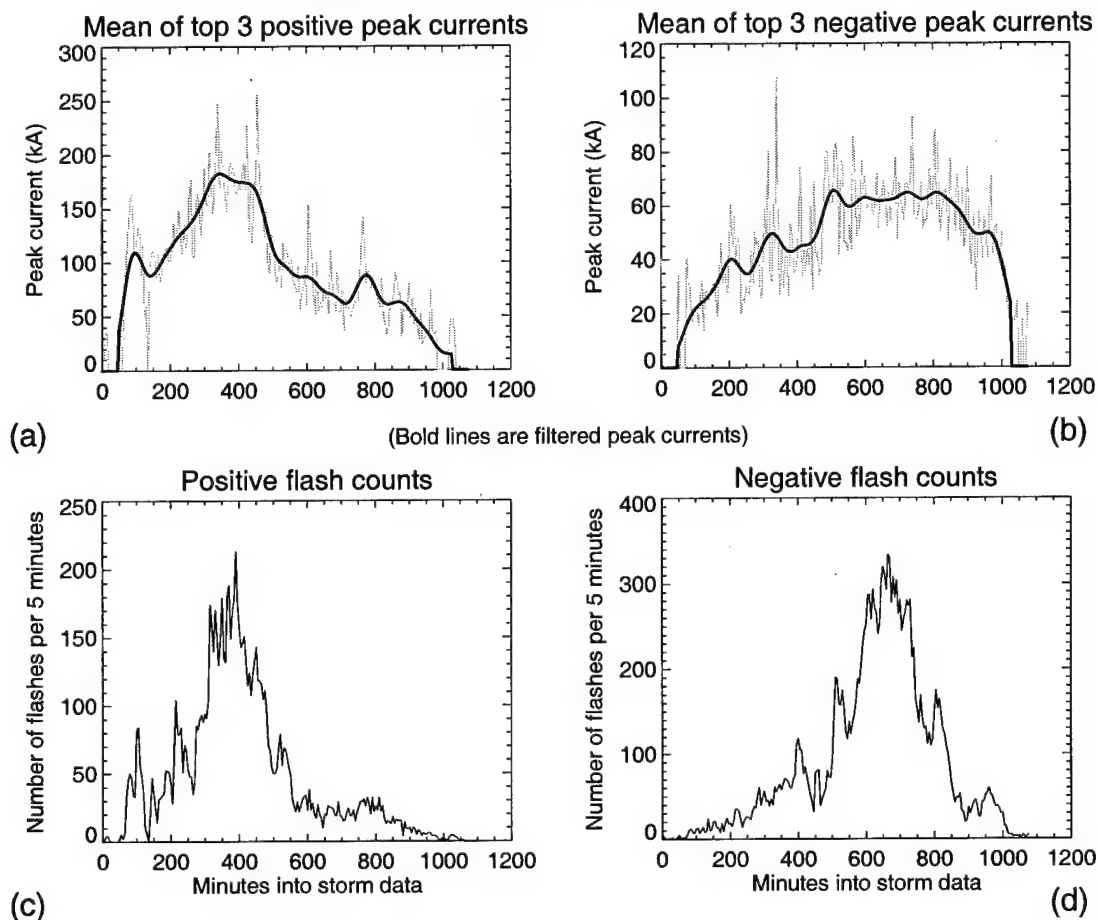


Figure E-37. Time series of peak currents and flash counts for 16 Jul 97. The three extreme peak currents were found for each 5 minute interval and plotted in light gray for positive (a) and negative (b) flashes. A band-pass filter was applied to the peak currents using a 52.0 minute period for positive flashes and a 52.0 minute window for negatives with the resulting wave shown as a dark curve in (a) and (b). The number of positive and negative flashes in each 5 minute window are shown in (c) and (d), respectively.

Data summary for case 97071717

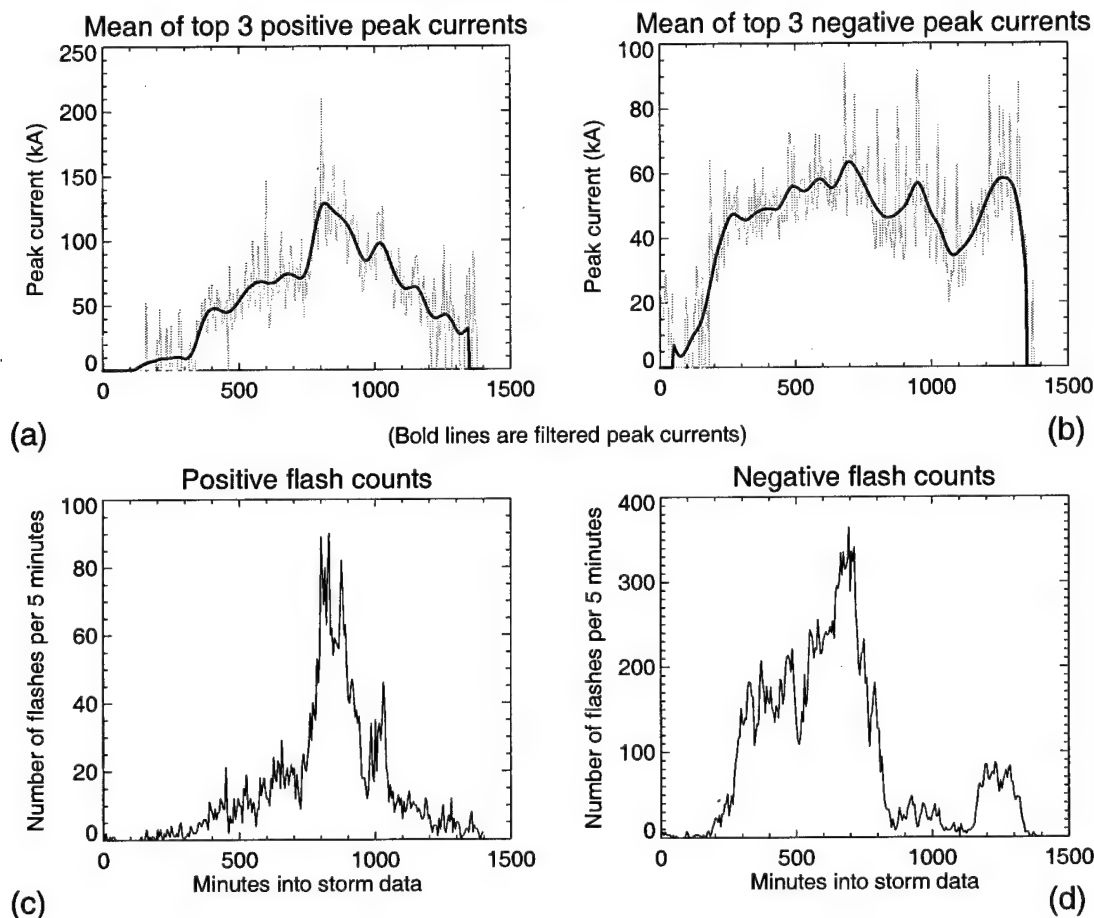


Figure E-38. Time series of peak currents and flash counts for 17 Jul 97. The three extreme peak currents were found for each 5 minute interval and plotted in light gray for positive (a) and negative (b) flashes. A band-pass filter was applied to the peak currents using a 68.5 minute period for positive flashes and a 72.5 minute window for negatives with the resulting wave shown as a dark curve in (a) and (b). The number of positive and negative flashes in each 5 minute window are shown in (c) and (d), respectively.

Data summary for case 97081312

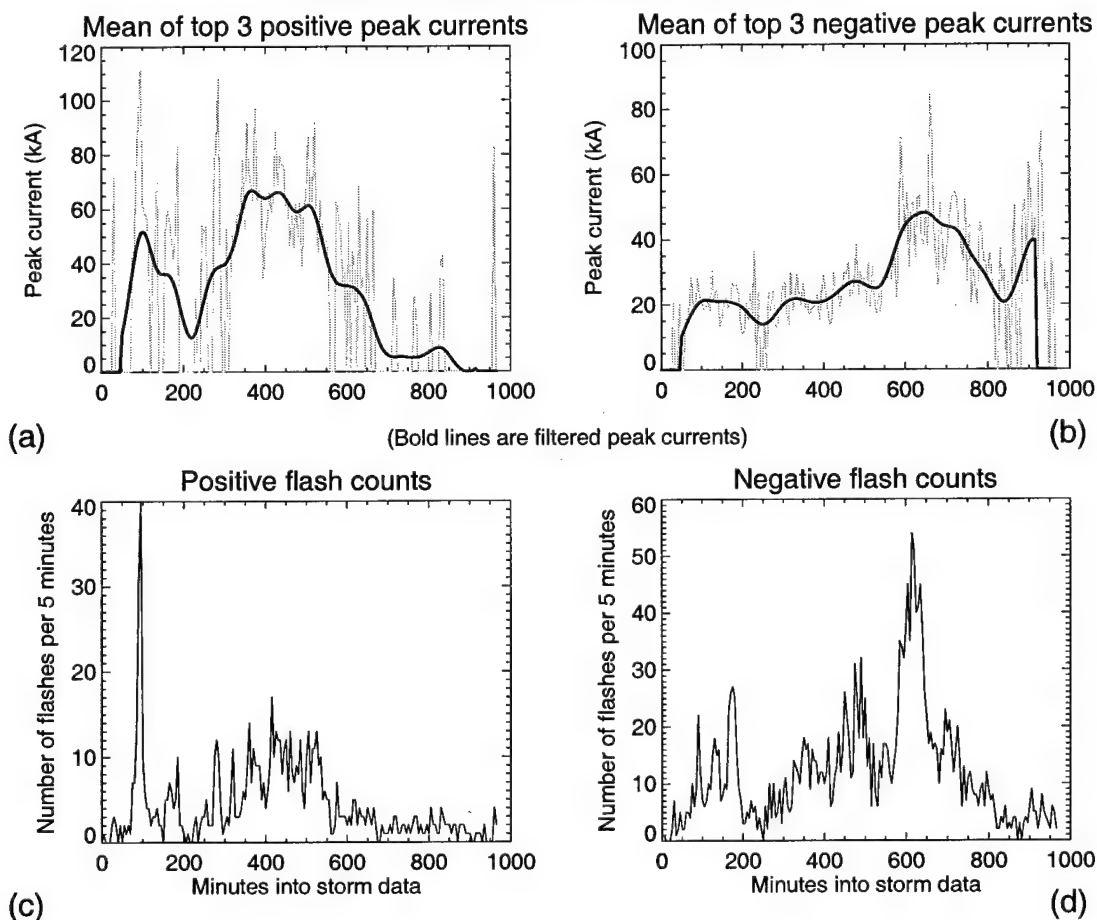


Figure E-39. Time series of peak currents and flash counts for 13 Aug 97. The three extreme peak currents were found for each 5 minute interval and plotted in light gray for positive (a) and negative (b) flashes. A band-pass filter was applied to the peak currents using a 47.5 minute period for positive flashes and a 49.0 minute window for negatives with the resulting wave shown as a dark curve in (a) and (b). The number of positive and negative flashes in each 5 minute window are shown in (c) and (d), respectively.

Data summary for case 97082612

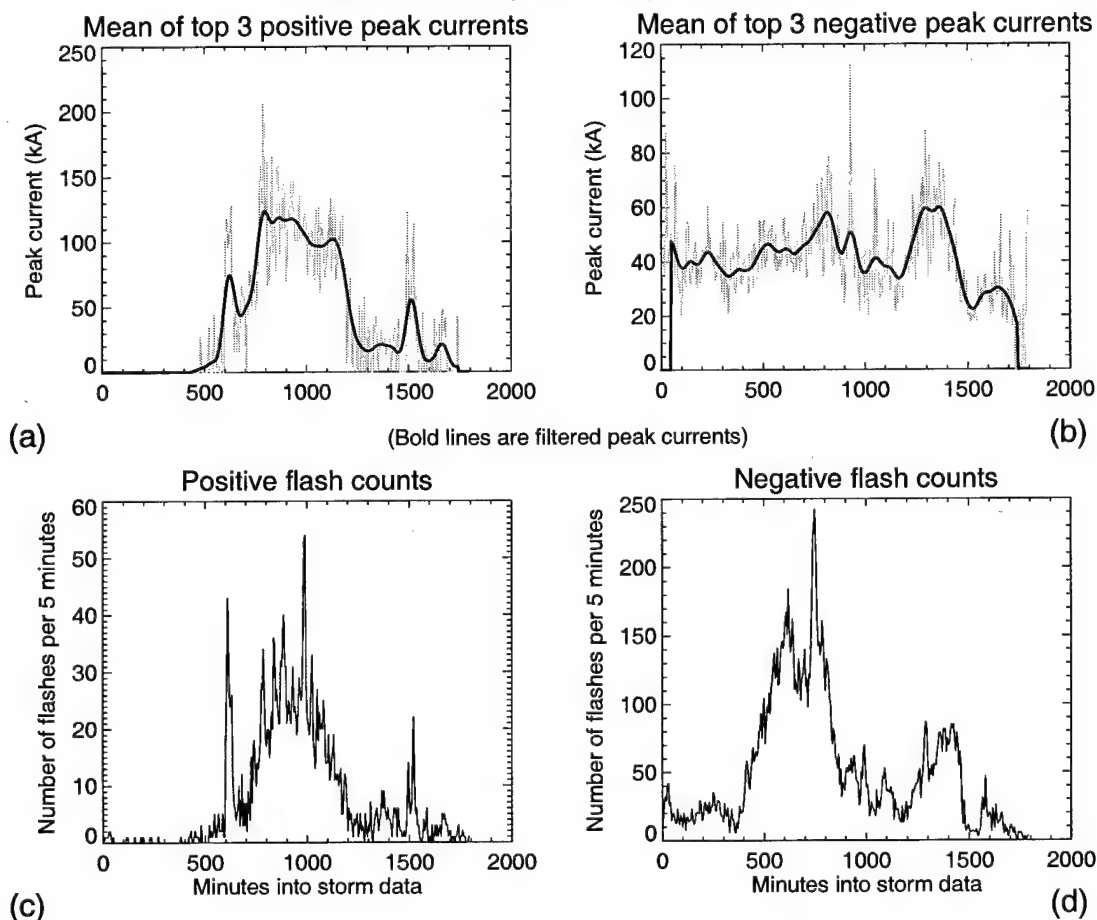


Figure E-40. Time series of peak currents and flash counts for 26 Aug 97. The three extreme peak currents were found for each 5 minute interval and plotted in light gray for positive (a) and negative (b) flashes. A band-pass filter was applied to the peak currents using a 85.5 minute period for positive flashes and a 90.5 minute window for negatives with the resulting wave shown as a dark curve in (a) and (b). The number of positive and negative flashes in each 5 minute window are shown in (c) and (d), respectively.

Data summary for case 97082912

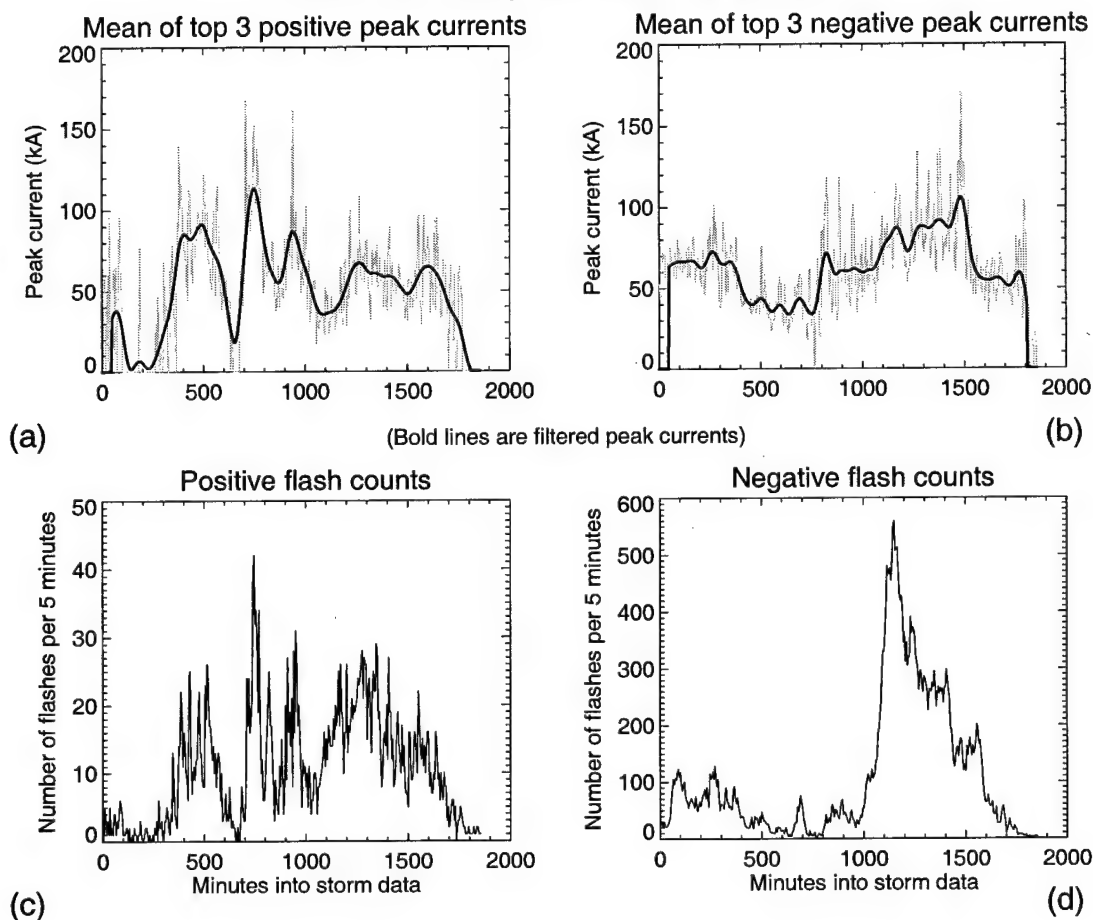


Figure E-41. Time series of peak currents and flash counts for 29 Aug 97. The three extreme peak currents were found for each 5 minute interval and plotted in light gray for positive (a) and negative (b) flashes. A band-pass filter was applied to the peak currents using a 93.0 minute period for positive flashes and a 91.0 minute window for negatives with the resulting wave shown as a dark curve in (a) and (b). The number of positive and negative flashes in each 5 minute window are shown in (c) and (d), respectively.

Data summary for case 97083121

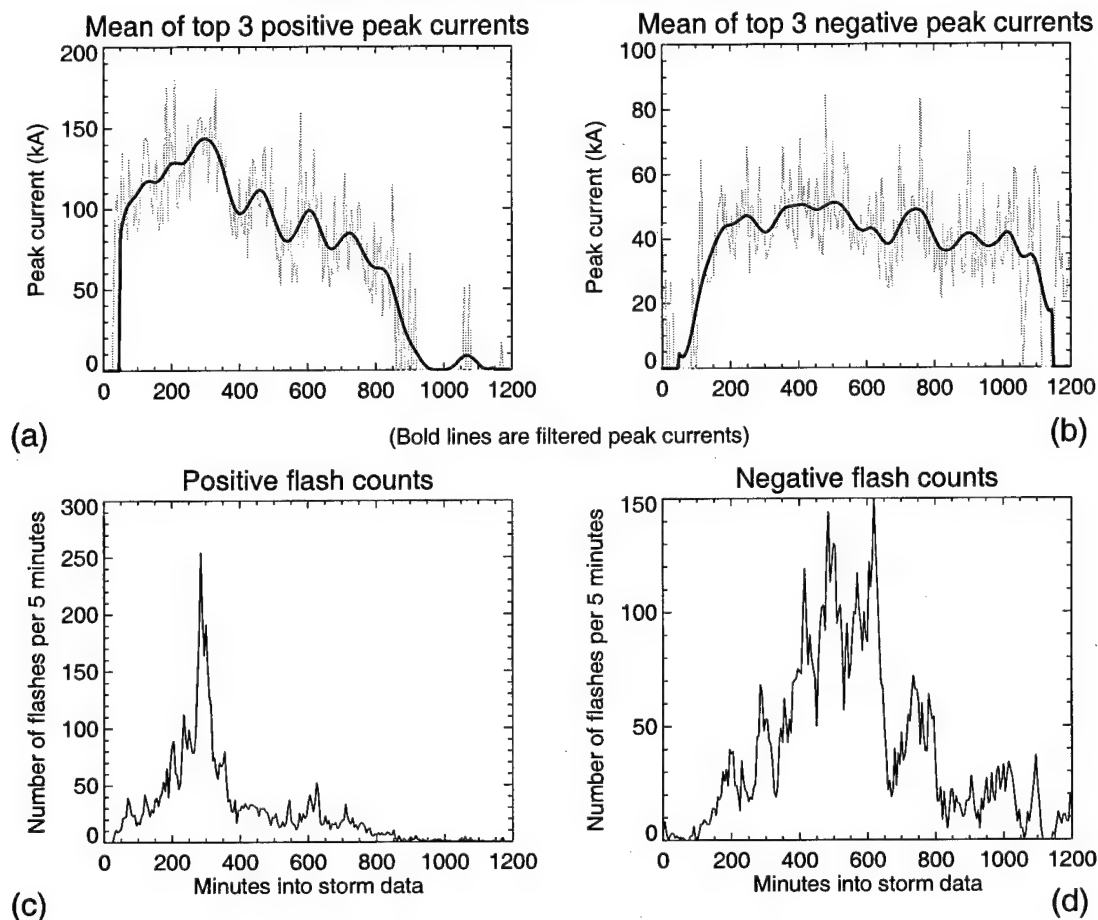


Figure E-42. Time series of peak currents and flash counts for 31 Aug 97. The three extreme peak currents were found for each 5 minute interval and plotted in light gray for positive (a) and negative (b) flashes. A band-pass filter was applied to the peak currents using a 57.5 minute period for positive flashes and a 59.0 minute window for negatives with the resulting wave shown as a dark curve in (a) and (b). The number of positive and negative flashes in each 5 minute window are shown in (c) and (d), respectively.

Data summary for case 97090500

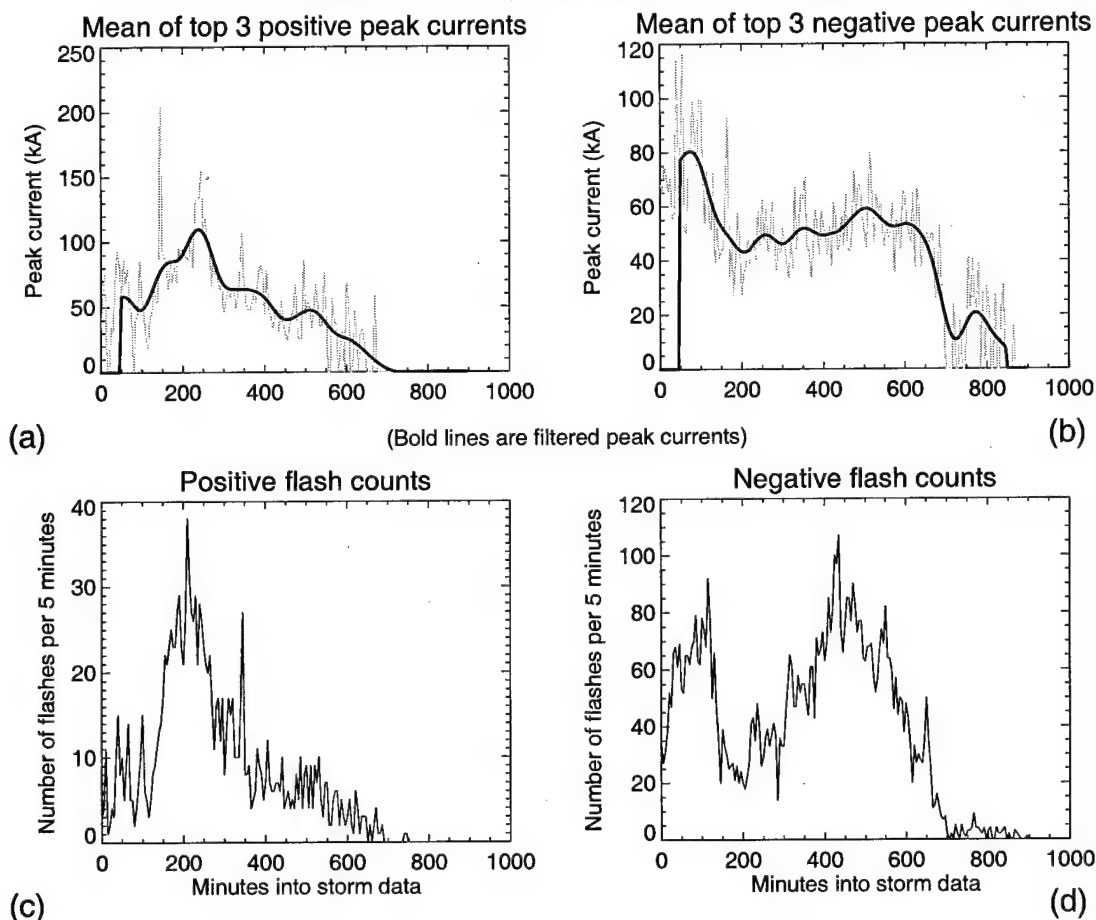


Figure E-43. Time series of peak currents and flash counts for 5 Sep 97. The three extreme peak currents were found for each 5 minute interval and plotted in light gray for positive (a) and negative (b) flashes. A band-pass filter was applied to the peak currents using a 44.5 minute period for positive flashes and a 43.0 minute window for negatives with the resulting wave shown as a dark curve in (a) and (b). The number of positive and negative flashes in each 5 minute window are shown in (c) and (d), respectively.

Data summary for case 97090501

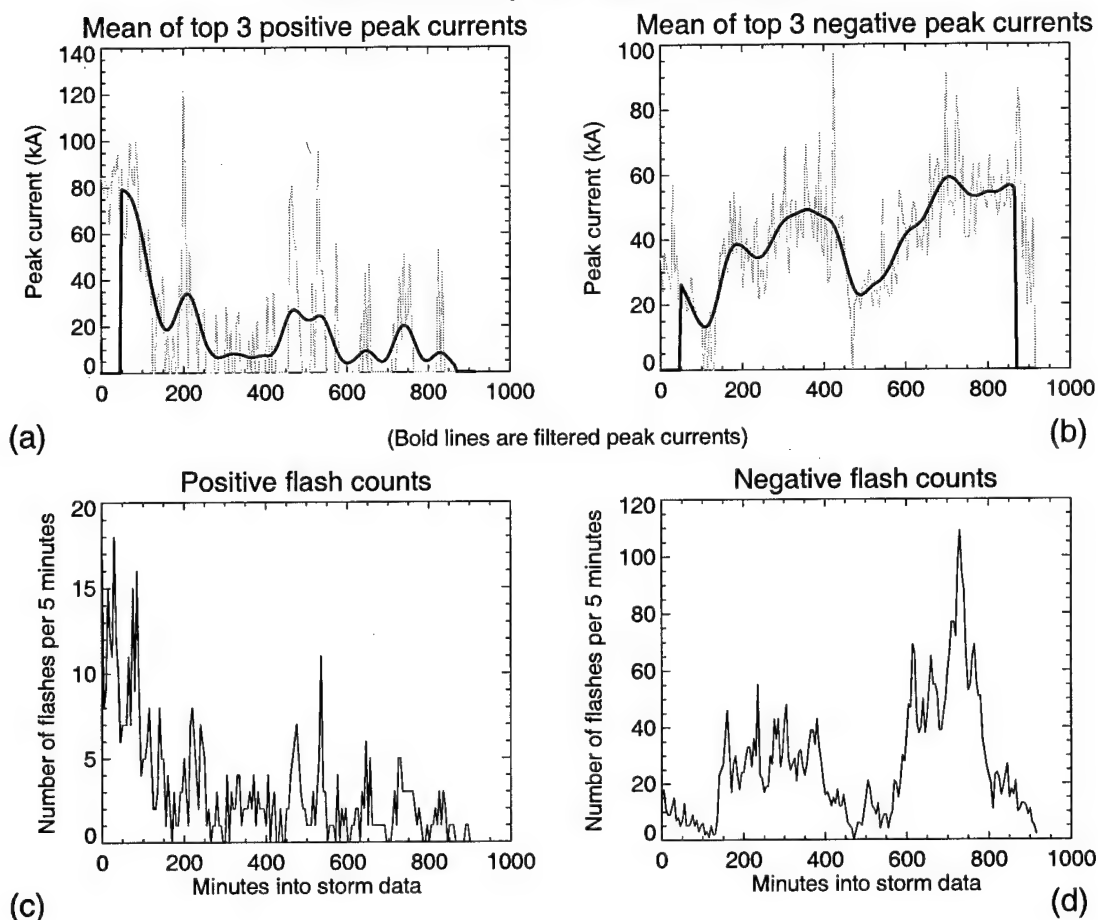


Figure E-44. Time series of peak currents and flash counts for 5 Sep 97. The three extreme peak currents were found for each 5 minute interval and plotted in light gray for positive (a) and negative (b) flashes. A band-pass filter was applied to the peak currents using a 46.0 minute period for positive flashes and a 42.5 minute window for negatives with the resulting wave shown as a dark curve in (a) and (b). The number of positive and negative flashes in each 5 minute window are shown in (c) and (d), respectively.

Data summary for case 97090820

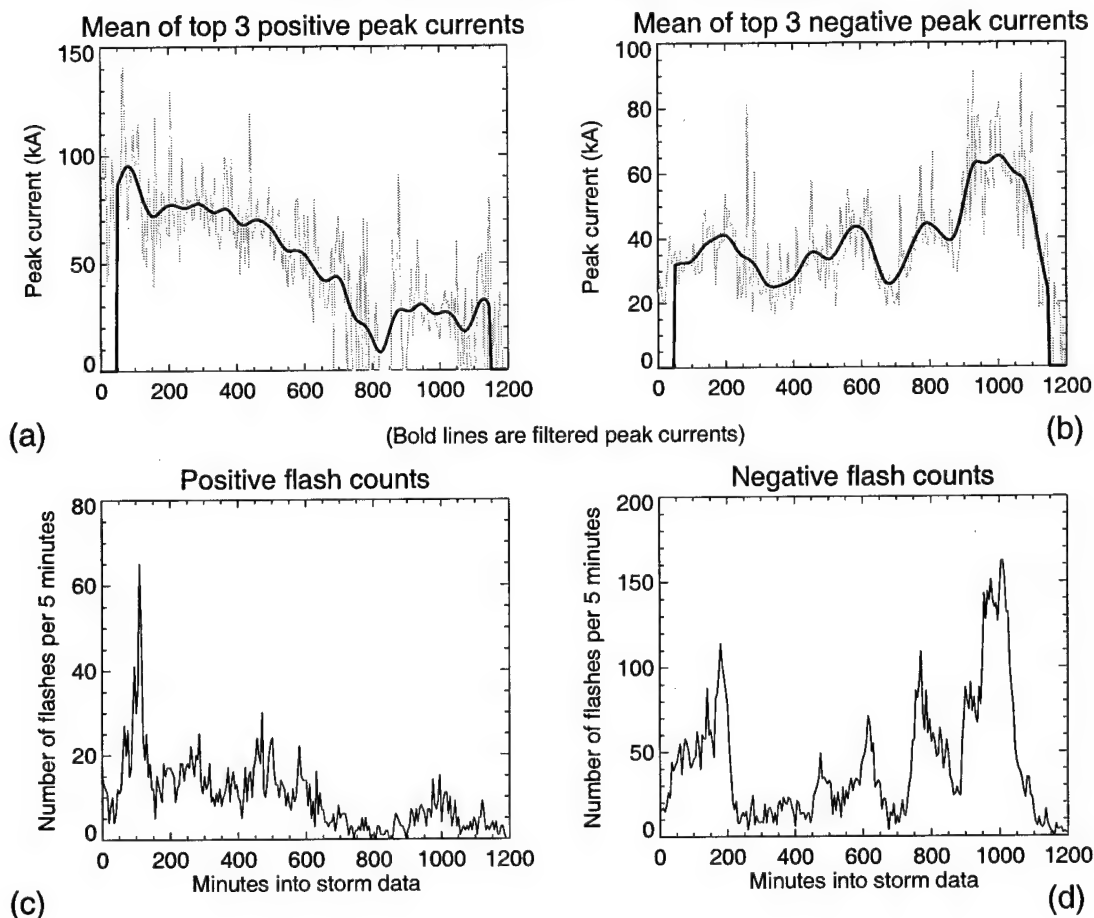


Figure E-45. Time series of peak currents and flash counts for 8 Sep 97. The three extreme peak currents were found for each 5 minute interval and plotted in light gray for positive (a) and negative (b) flashes. A band-pass filter was applied to the peak currents using a 59.5 minute period for positive flashes and a 59.5 minute window for negatives with the resulting wave shown as a dark curve in (a) and (b). The number of positive and negative flashes in each 5 minute window are shown in (c) and (d), respectively.

Data summary for case 97102020

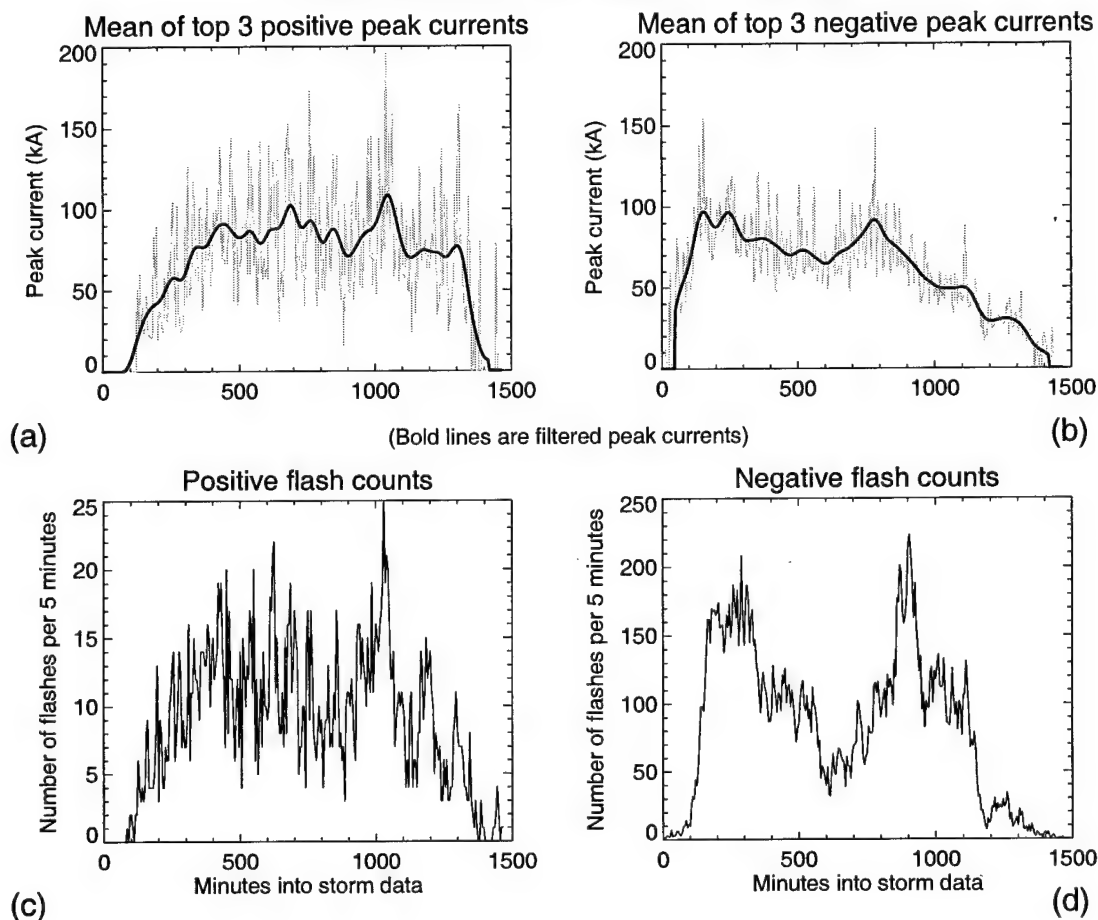


Figure E-46. Time series of peak currents and flash counts for 21 Oct 97. The three extreme peak currents were found for each 5 minute interval and plotted in light gray for positive (a) and negative (b) flashes. A band-pass filter was applied to the peak currents using a 75.5 minute period for positive flashes and a 72.5 minute window for negatives with the resulting wave shown as a dark curve in (a) and (b). The number of positive and negative flashes in each 5 minute window are shown in (c) and (d), respectively.

Data summary for case 97122015

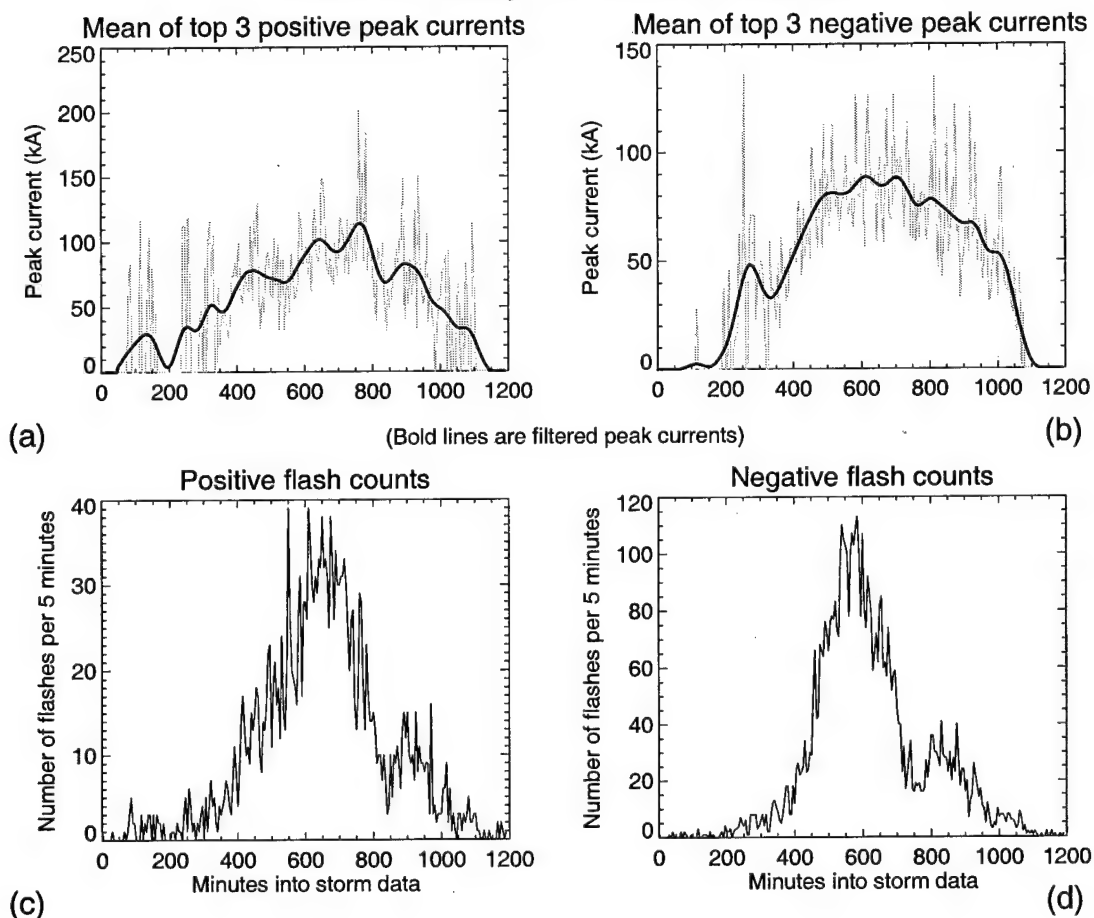


Figure E-47. Time series of peak currents and flash counts for 20 Dec 97. The three extreme peak currents were found for each 5 minute interval and plotted in light gray for positive (a) and negative (b) flashes. A band-pass filter was applied to the peak currents using a 59.5 minute period for positive flashes and a 59.5 minute window for negatives with the resulting wave shown as a dark curve in (a) and (b). The number of positive and negative flashes in each 5 minute window are shown in (c) and (d), respectively.

Data summary for case 98051504

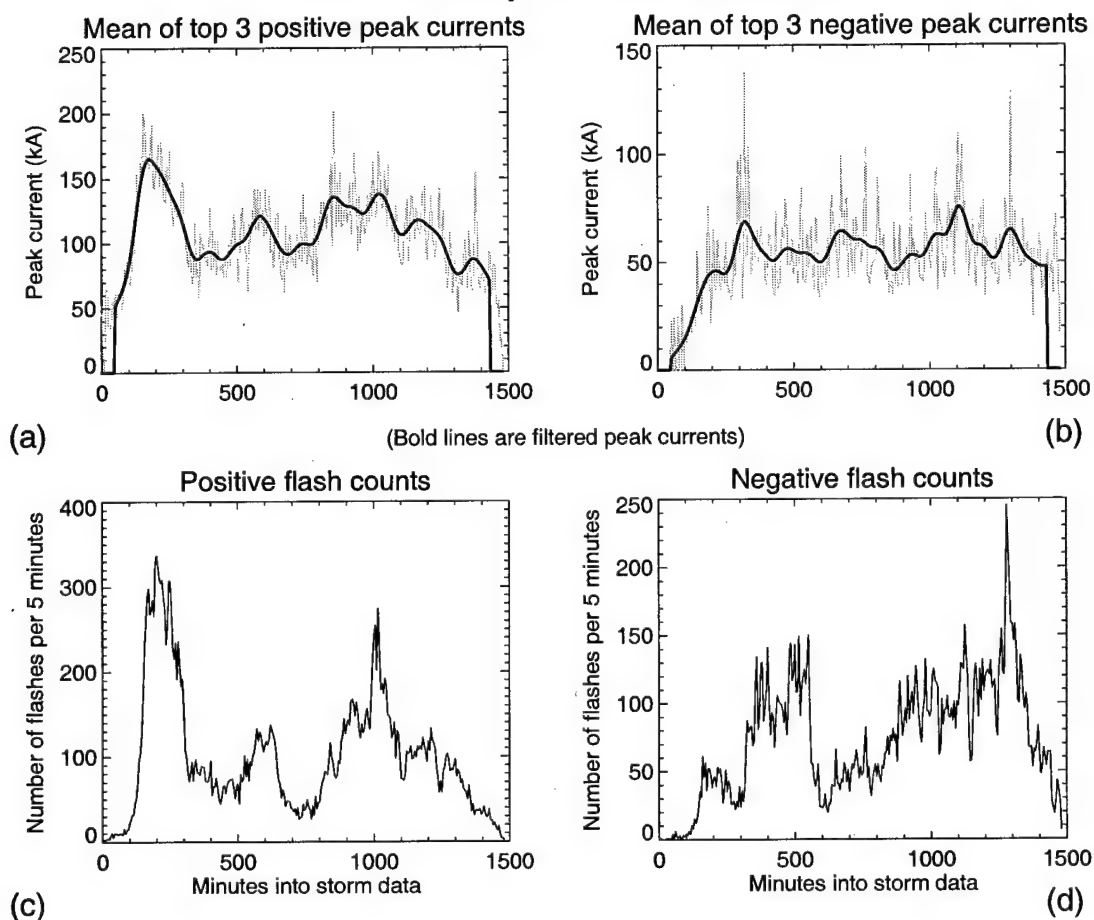


Figure E-48. Time series of peak currents and flash counts for 15 May 98. The three extreme peak currents were found for each 5 minute interval and plotted in light gray for positive (a) and negative (b) flashes. A band-pass filter was applied to the peak currents using a 72.0 minute period for positive flashes and a 73.5 minute window for negatives with the resulting wave shown as a dark curve in (a) and (b). The number of positive and negative flashes in each 5 minute window are shown in (c) and (d), respectively.

APPENDIX F
CLOUD-TOP BRIGHTNESS TEMPERATURES AND LIGHTNING DATA FOR
15 MAY 1998

The satellite brightness temperatures are contoured with the lightning locations in the following figures. The lightning flashes are plotted with the symbol size proportional to the peak current of the flash. No correlation could be made between the peak currents and the cloud top temperatures, as the time between available satellite images was 1 hour, which corresponded to the average time of the peak current periodicity.

The lightning data were plotted here using a 10 minute time window. While that may show too many flashes to be able to distinguish individual characteristics, any shorter time frame may miss some of the stronger flashes that occurred during the satellite pass. A shorter time window was also used, but this did not provided any useful correlation between the peak currents and cloud top temperatures.

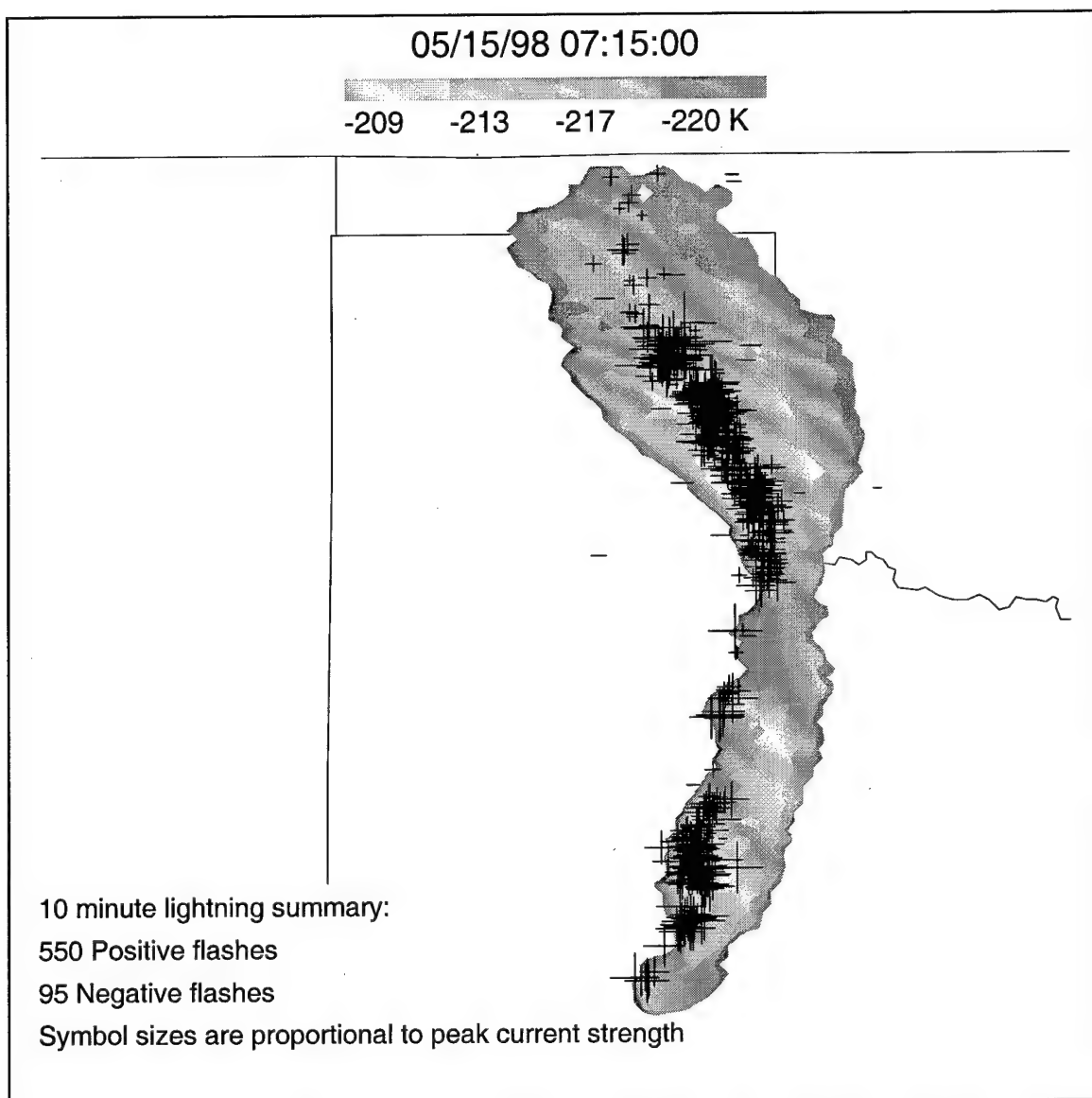


Figure F-1. Brightness temperatures and lightning data for 15 May 98 at 0715 UTC. The lightning data are plotted on the contour of the brightness temperatures with the symbol size proportional to the peak current.

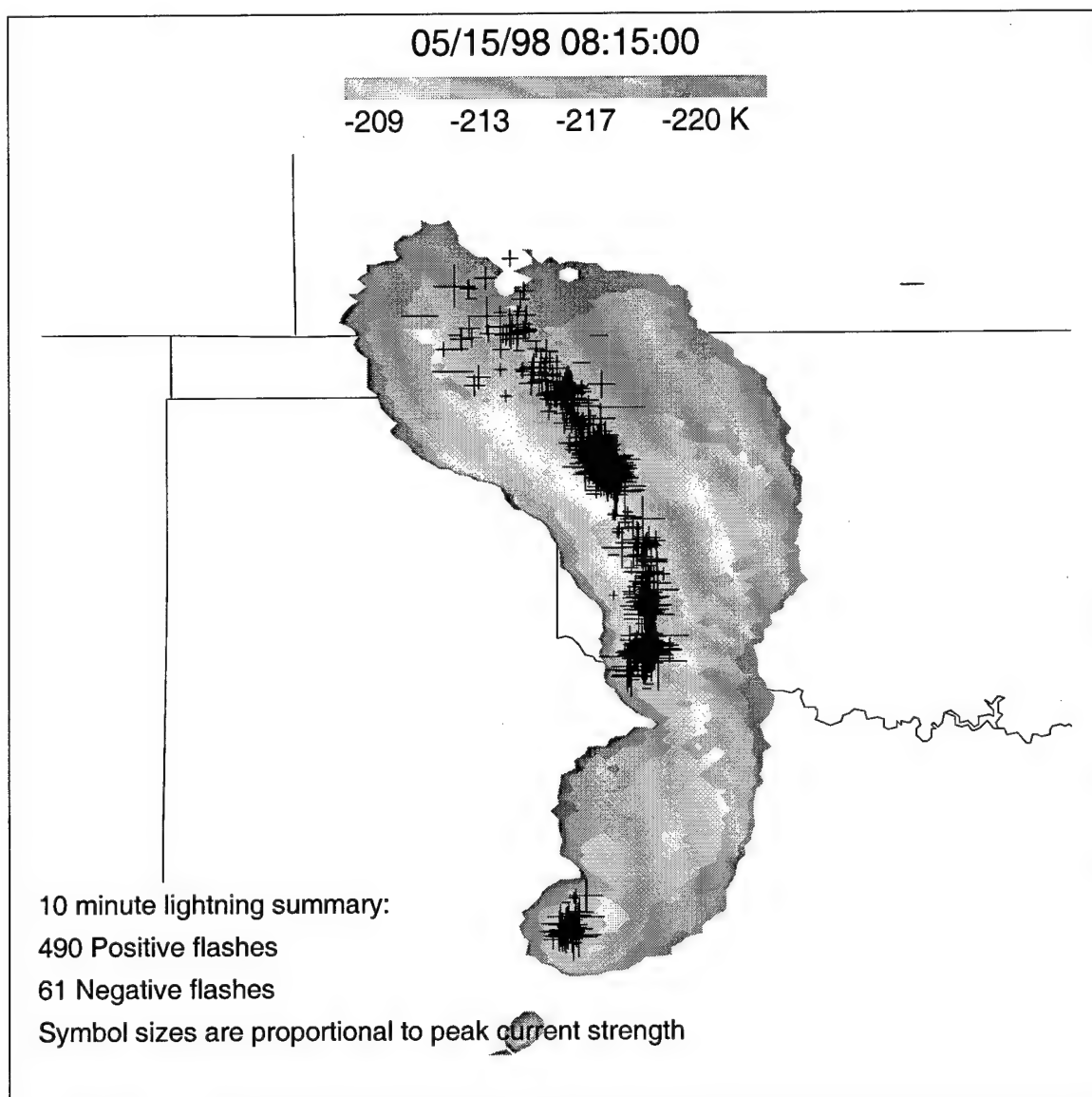


Figure F-2. Brightness temperatures and lightning data for 15 May 98 at 0815 UTC. The lightning data are plotted on the contour of the brightness temperatures with the symbol size proportional to the peak current.

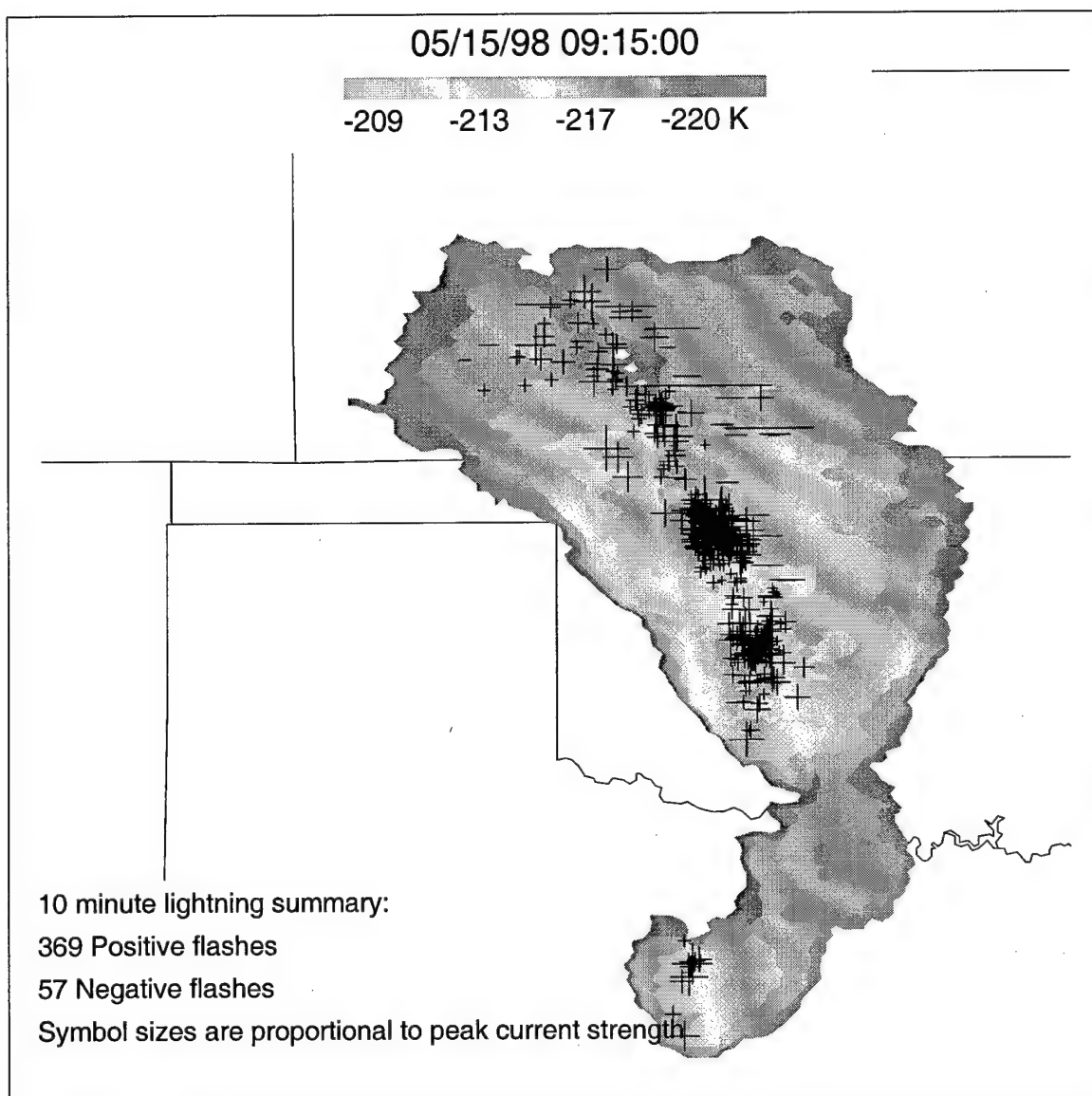


Figure F-3. Brightness temperatures and lightning data for 15 May 98 at 0915 UTC. The lightning data are plotted on the contour of the brightness temperatures with the symbol size proportional to the peak current.

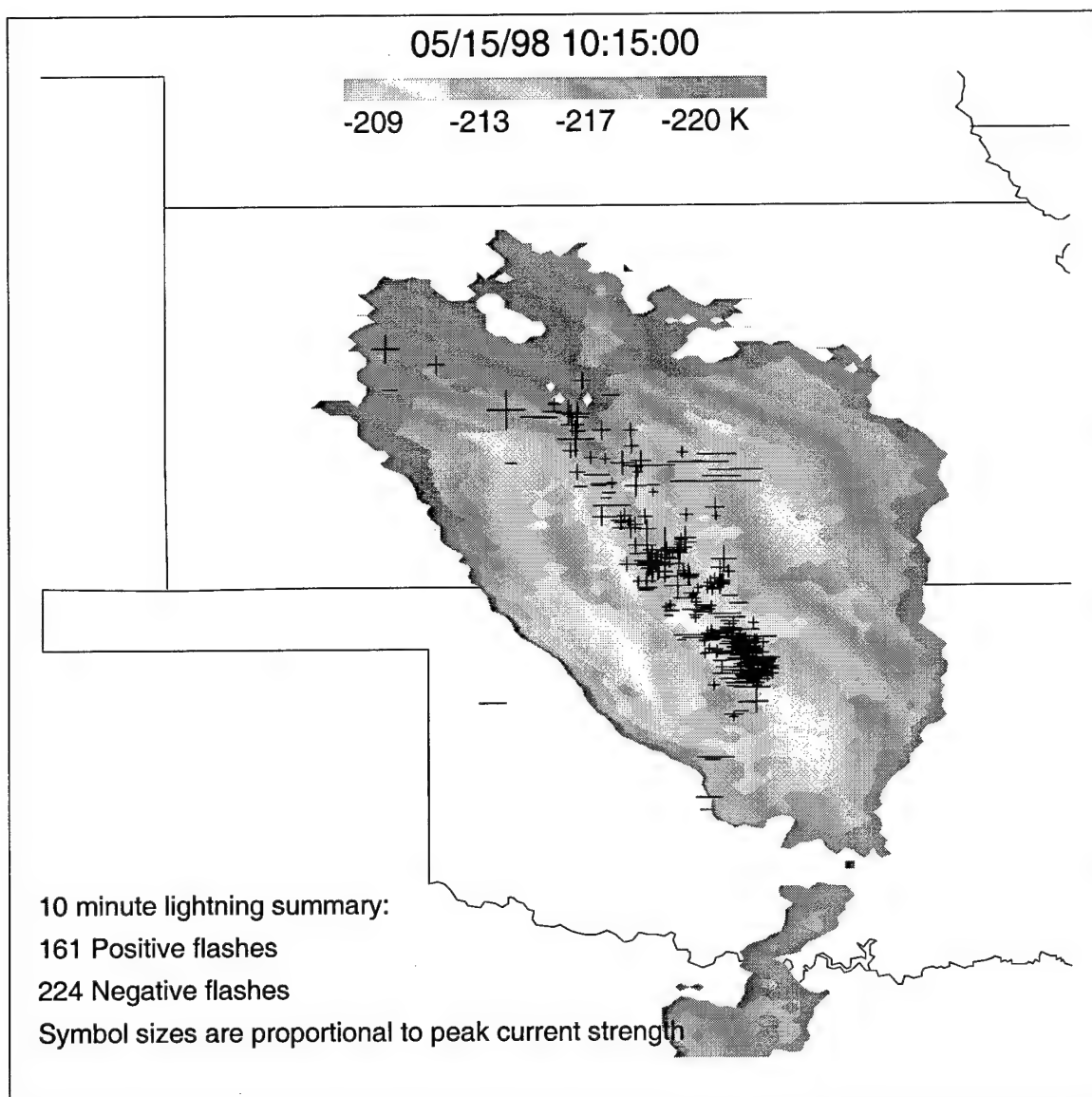


Figure F-4. Brightness temperatures and lightning data for 15 May 98 at 1015 UTC. The lightning data are plotted on the contour of the brightness temperatures with the symbol size proportional to the peak current.

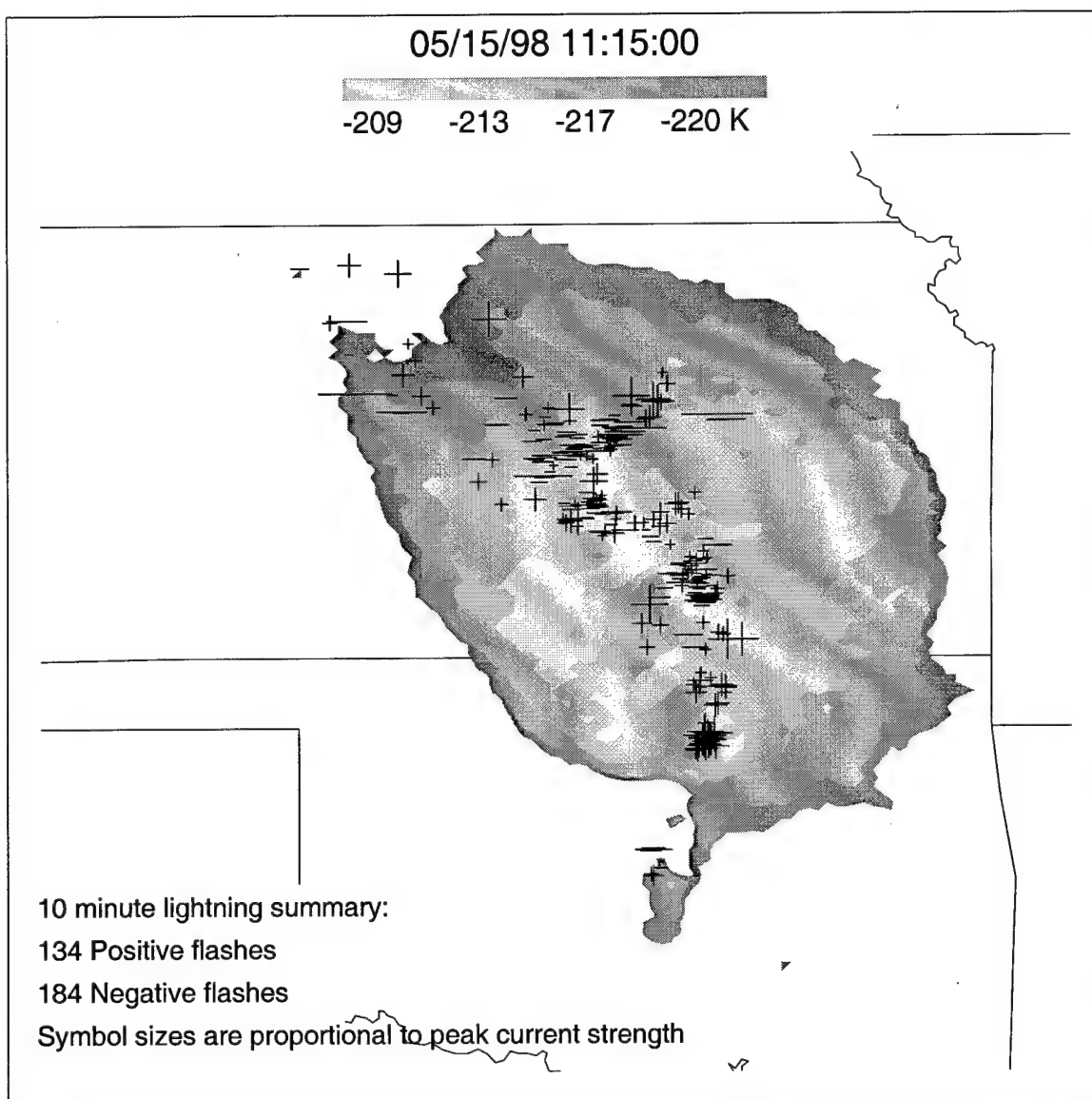


Figure F-5. Brightness temperatures and lightning data for 15 May 98 at 1115 UTC. The lightning data are plotted on the contour of the brightness temperatures with the symbol size proportional to the peak current.

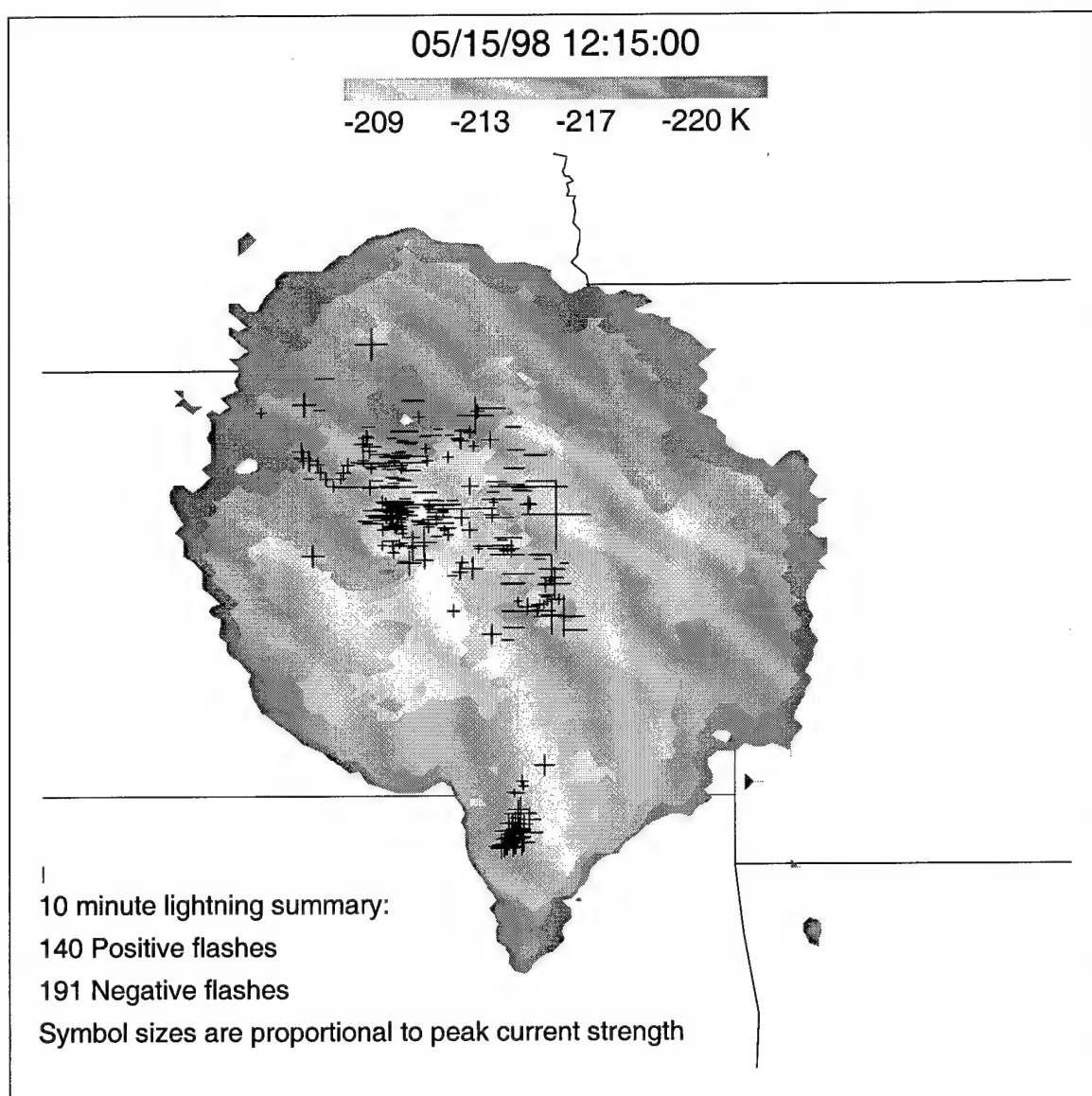


Figure F-6. Brightness temperatures and lightning data for 15 May 98 at 1215 UTC. The lightning data are plotted on the contour of the brightness temperatures with the symbol size proportional to the peak current.

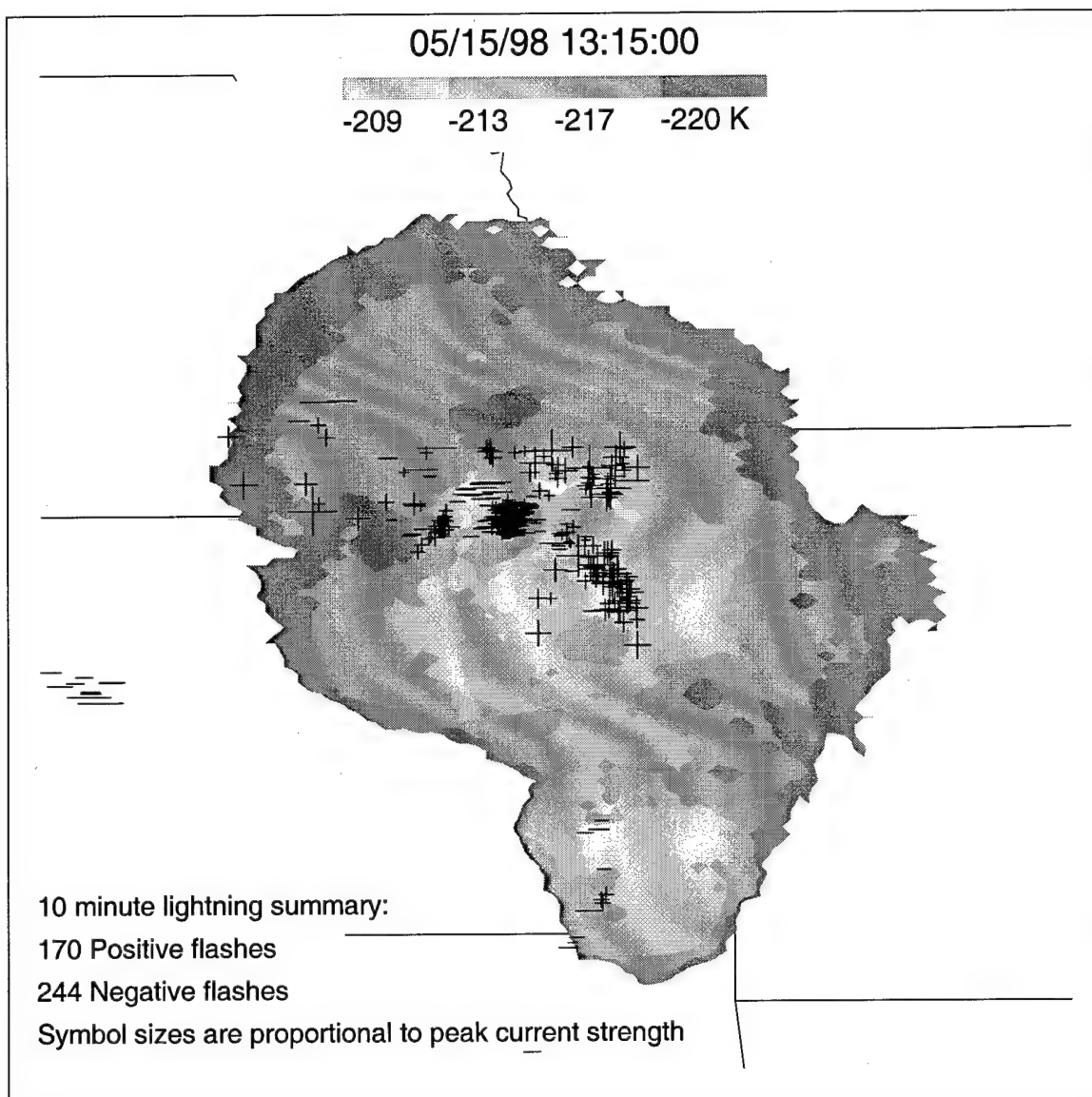


Figure F-7. Brightness temperatures and lightning data for 15 May 98 at 1315 UTC. The lightning data are plotted on the contour of the brightness temperatures with the symbol size proportional to the peak current.

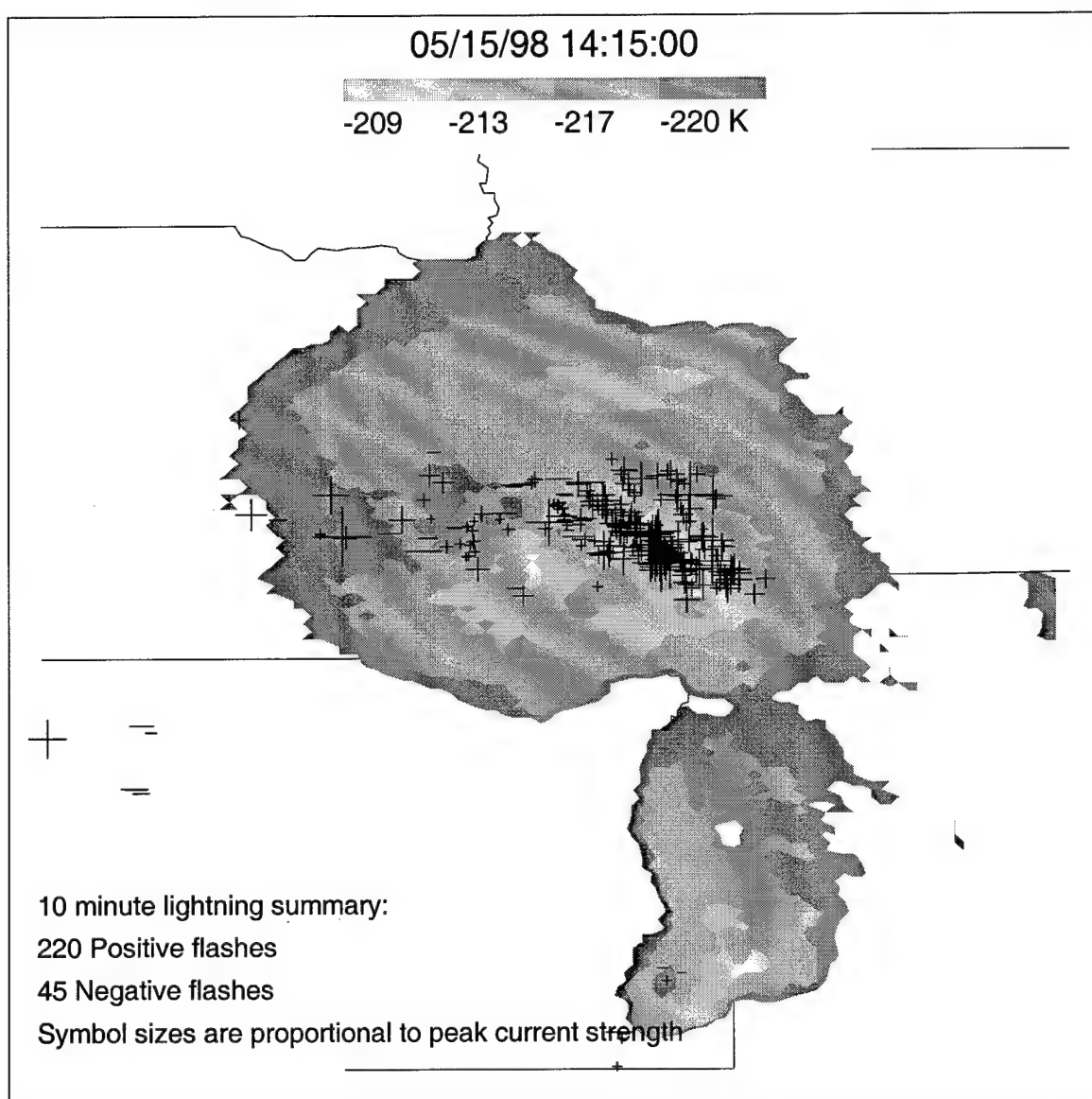


Figure F-8. Brightness temperatures and lightning data for 15 May 98 at 1415 UTC. The lightning data are plotted on the contour of the brightness temperatures with the symbol size proportional to the peak current.

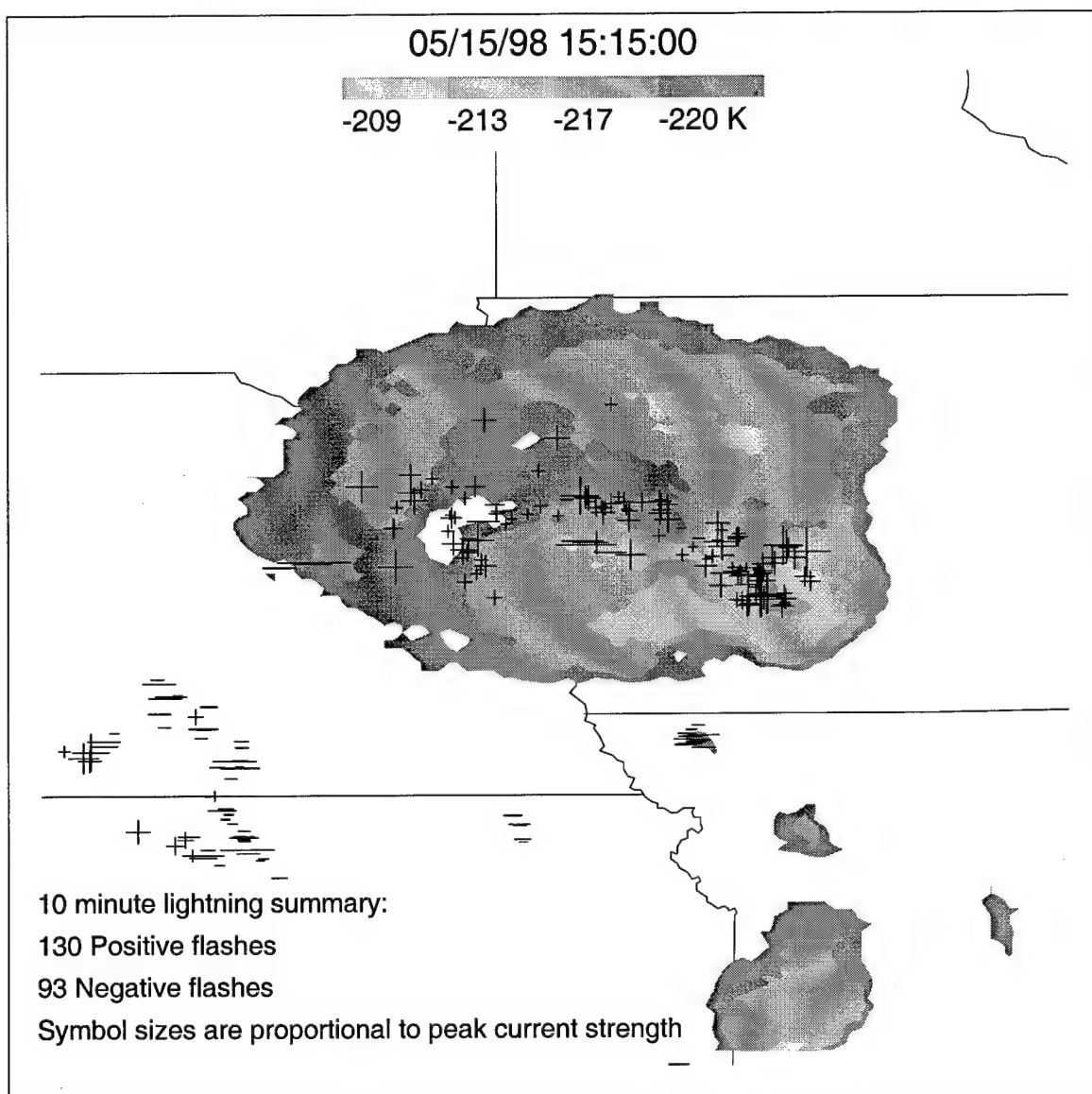


Figure F-9. Brightness temperatures and lightning data for 15 May 98 at 1515 UTC. The lightning data are plotted on the contour of the brightness temperatures with the symbol size proportional to the peak current.

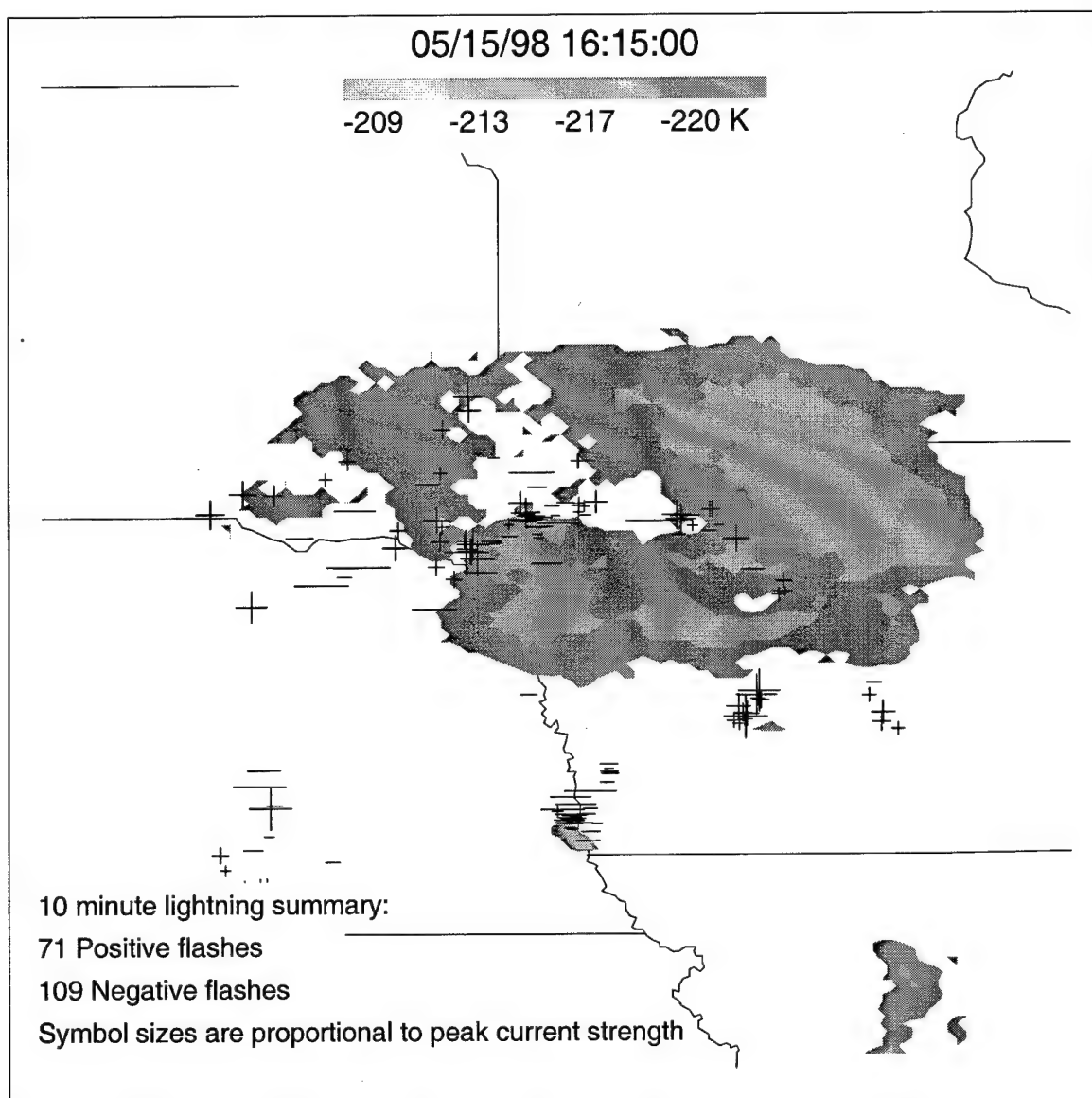


Figure F-10. Brightness temperatures and lightning data for 15 May 98 at 1615 UTC. The lightning data are plotted on the contour of the brightness temperatures with the symbol size proportional to the peak current.

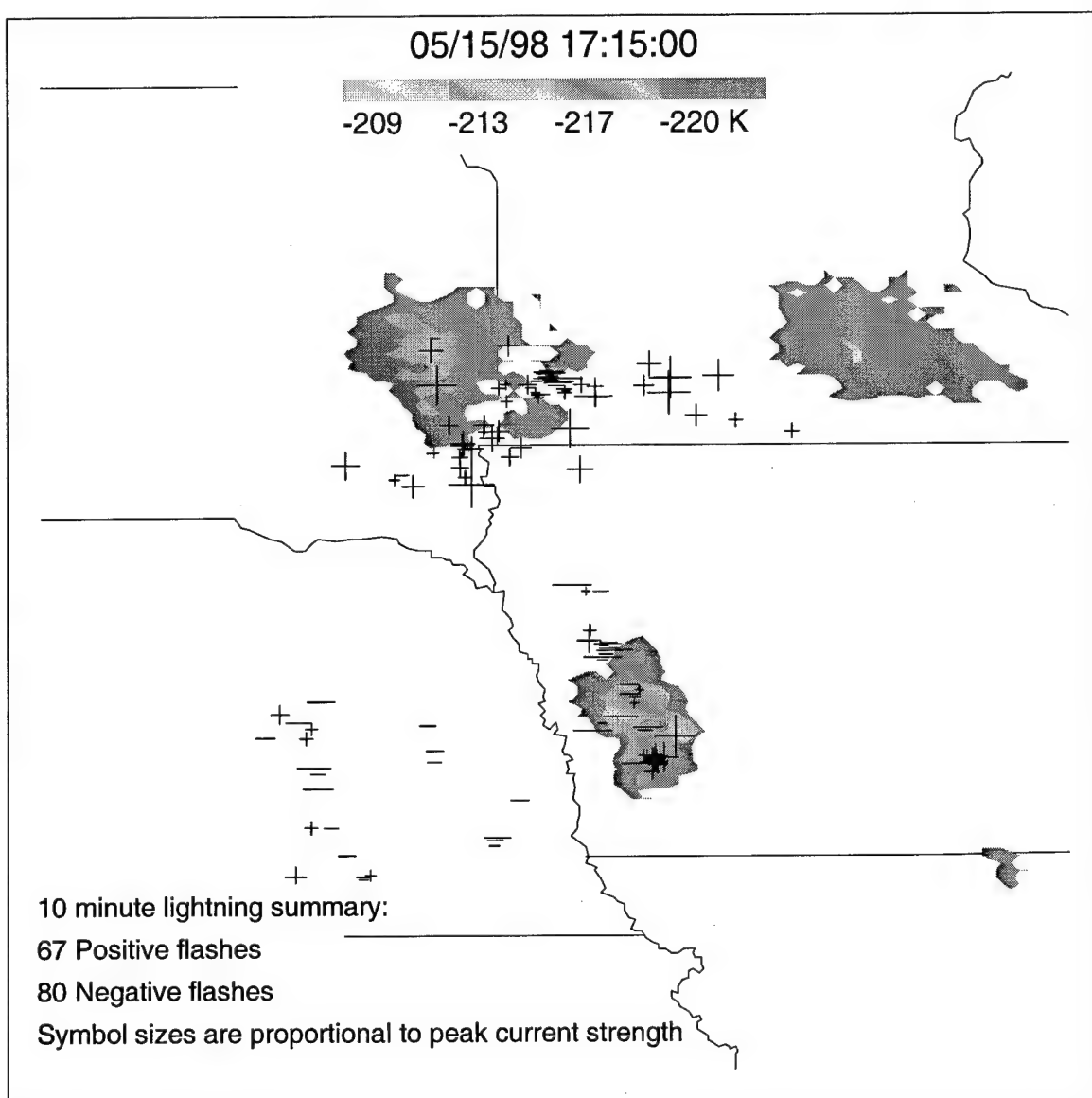


Figure F-11. Brightness temperatures and lightning data for 15 May 98 at 1715 UTC. The lightning data are plotted on the contour of the brightness temperatures with the symbol size proportional to the peak current.

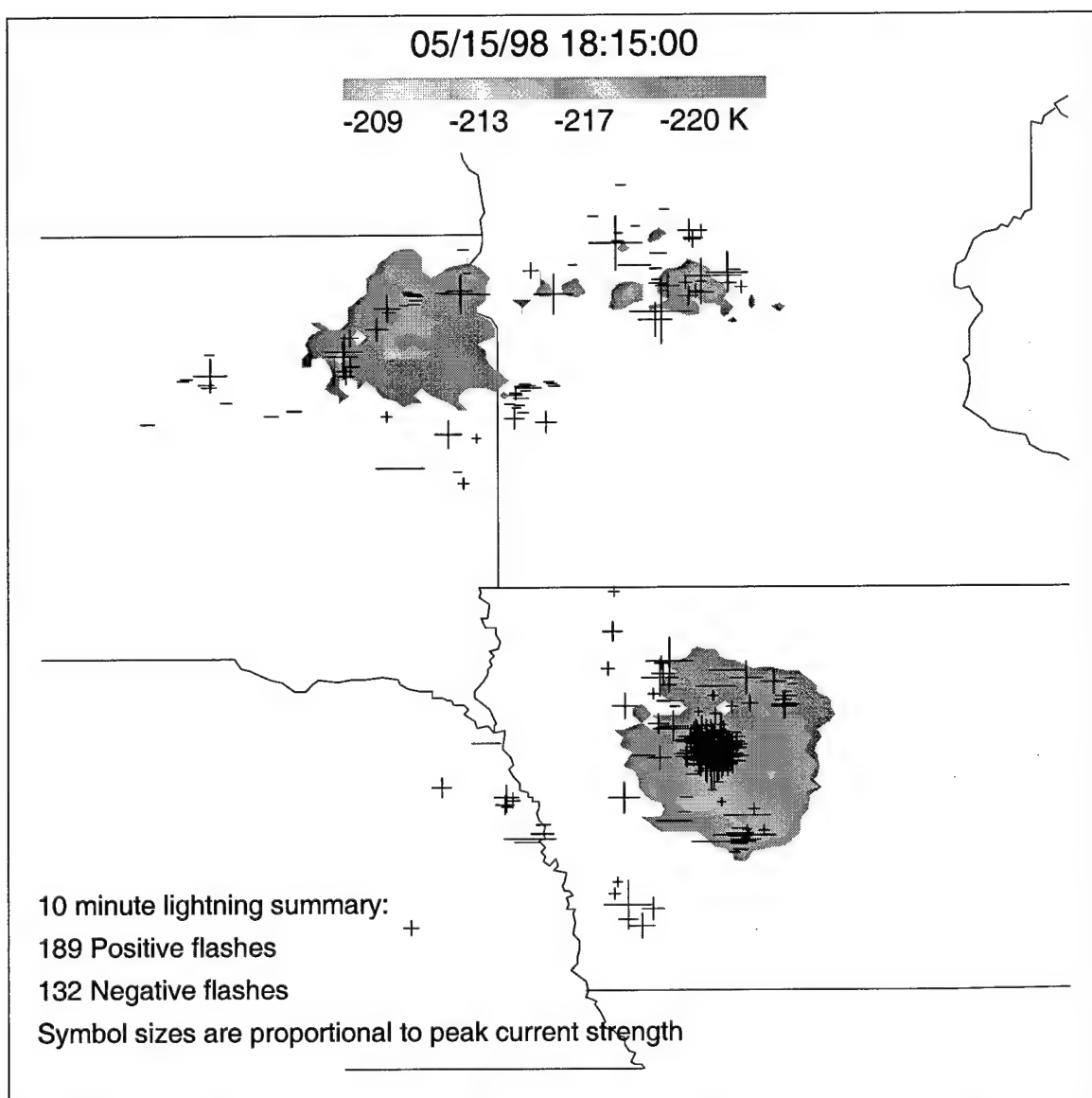


Figure F-12. Brightness temperatures and lightning data for 15 May 98 at 1815 UTC. The lightning data are plotted on the contour of the brightness temperatures with the symbol size proportional to the peak current.

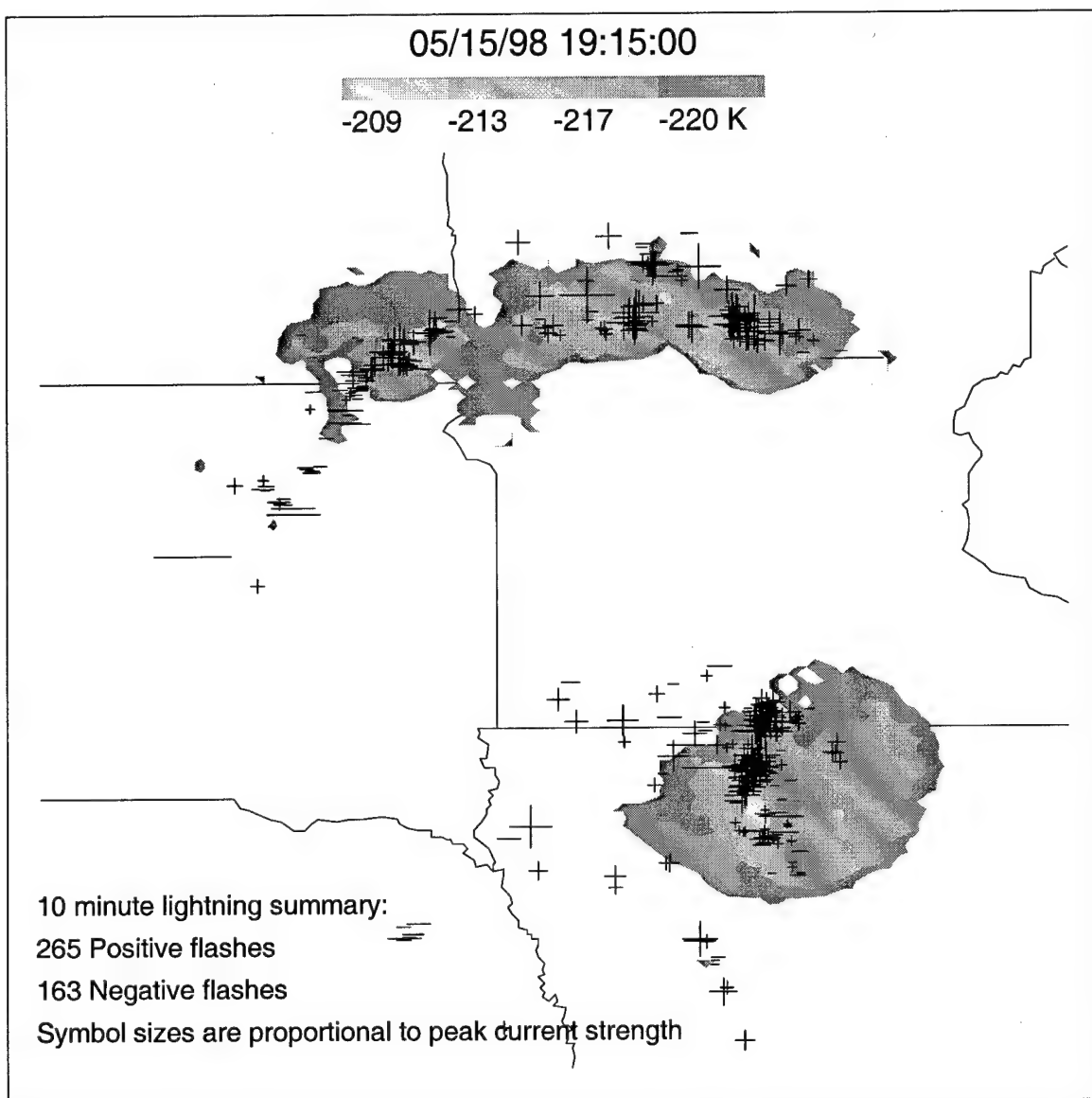


Figure F-13. Brightness temperatures and lightning data for 15 May 98 at 1915 UTC. The lightning data are plotted on the contour of the brightness temperatures with the symbol size proportional to the peak current.

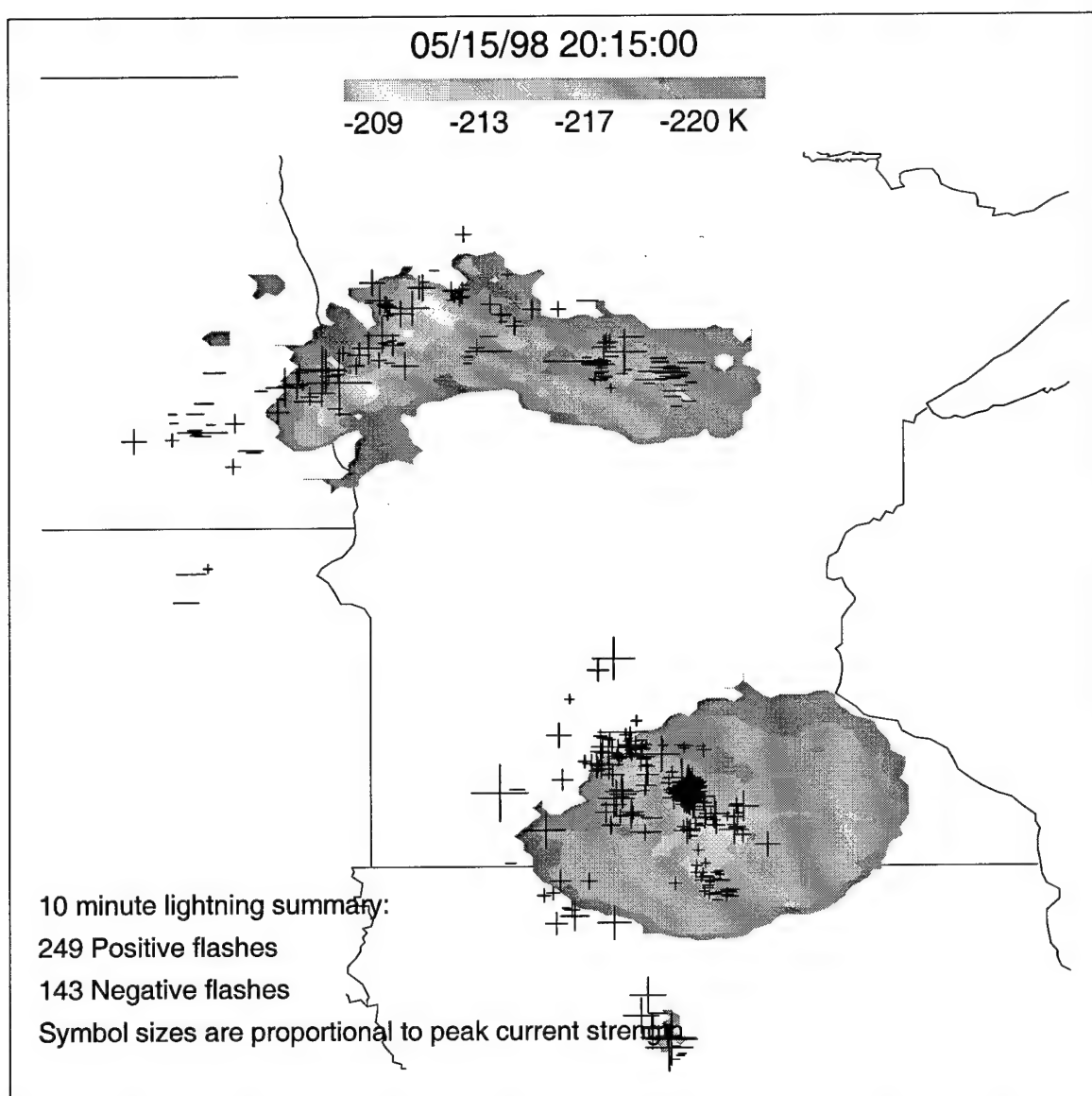


Figure F-14. Brightness temperatures and lightning data for 15 May 98 at 2015 UTC. The lightning data are plotted on the contour of the brightness temperatures with the symbol size proportional to the peak current.

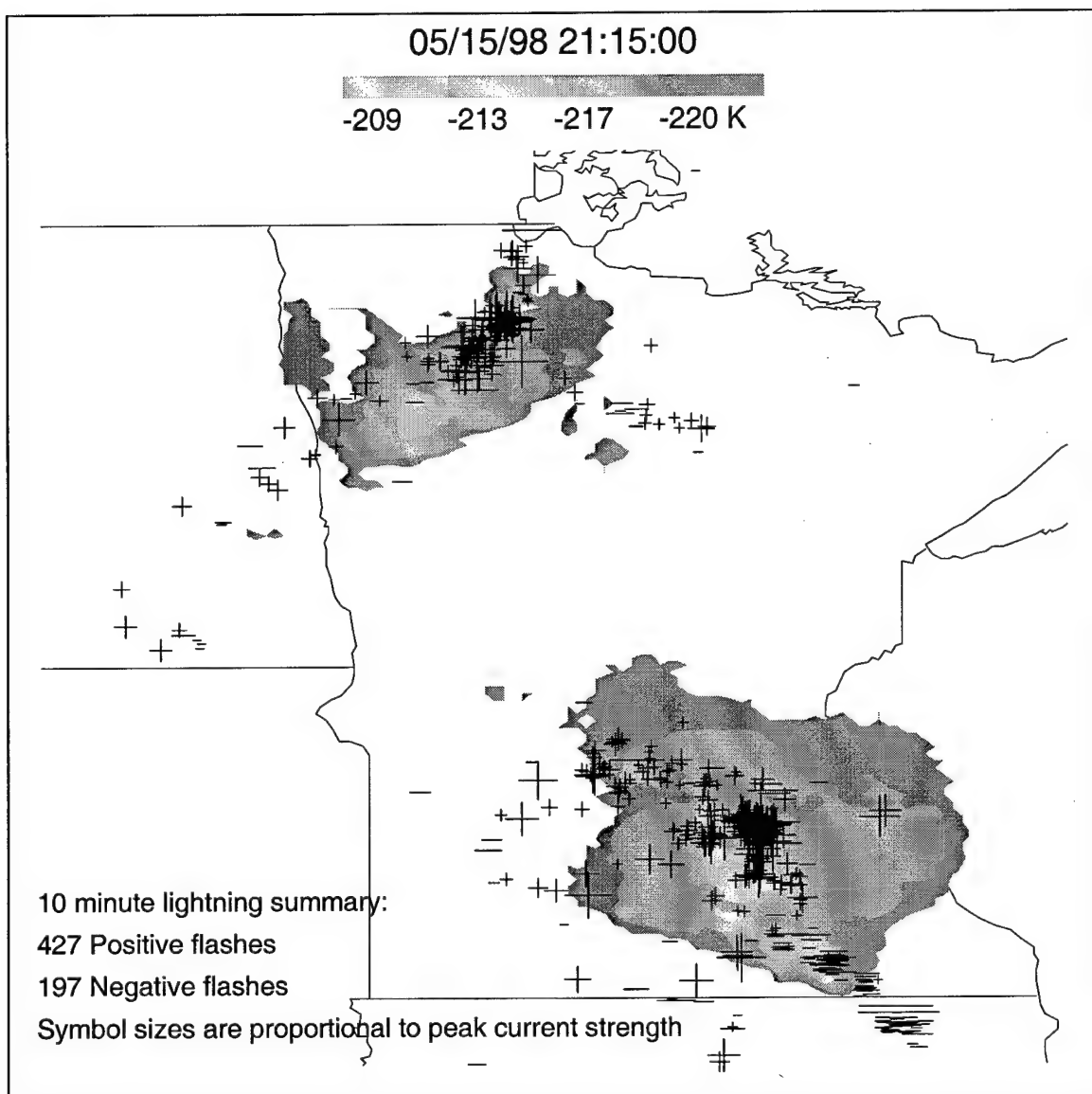


Figure F-15. Brightness temperatures and lightning data for 15 May 98 at 2115 UTC. The lightning data are plotted on the contour of the brightness temperatures with the symbol size proportional to the peak current.

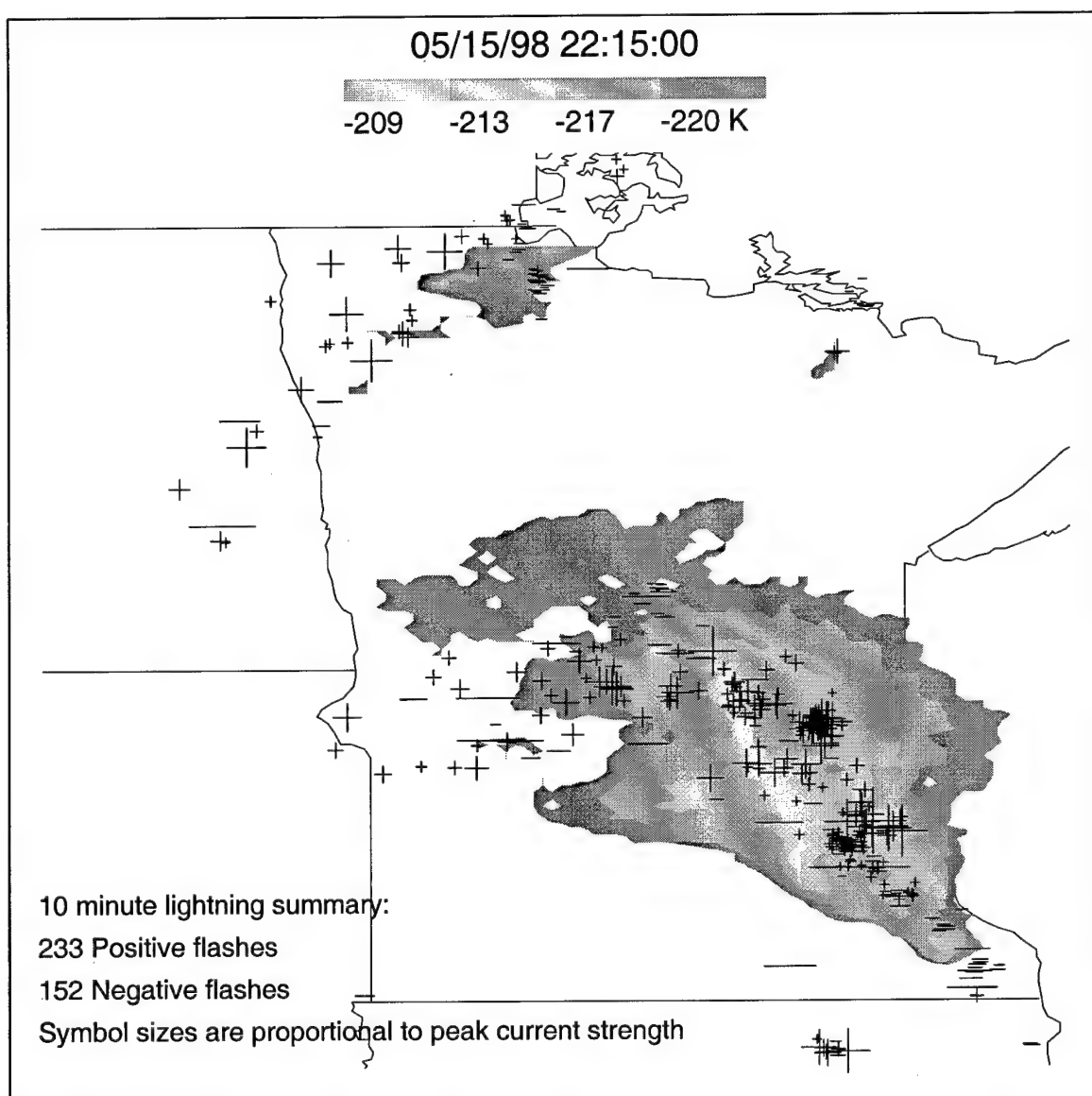


Figure F-16. Brightness temperatures and lightning data for 15 May 98 at 2215 UTC. The lightning data are plotted on the contour of the brightness temperatures with the symbol size proportional to the peak current.

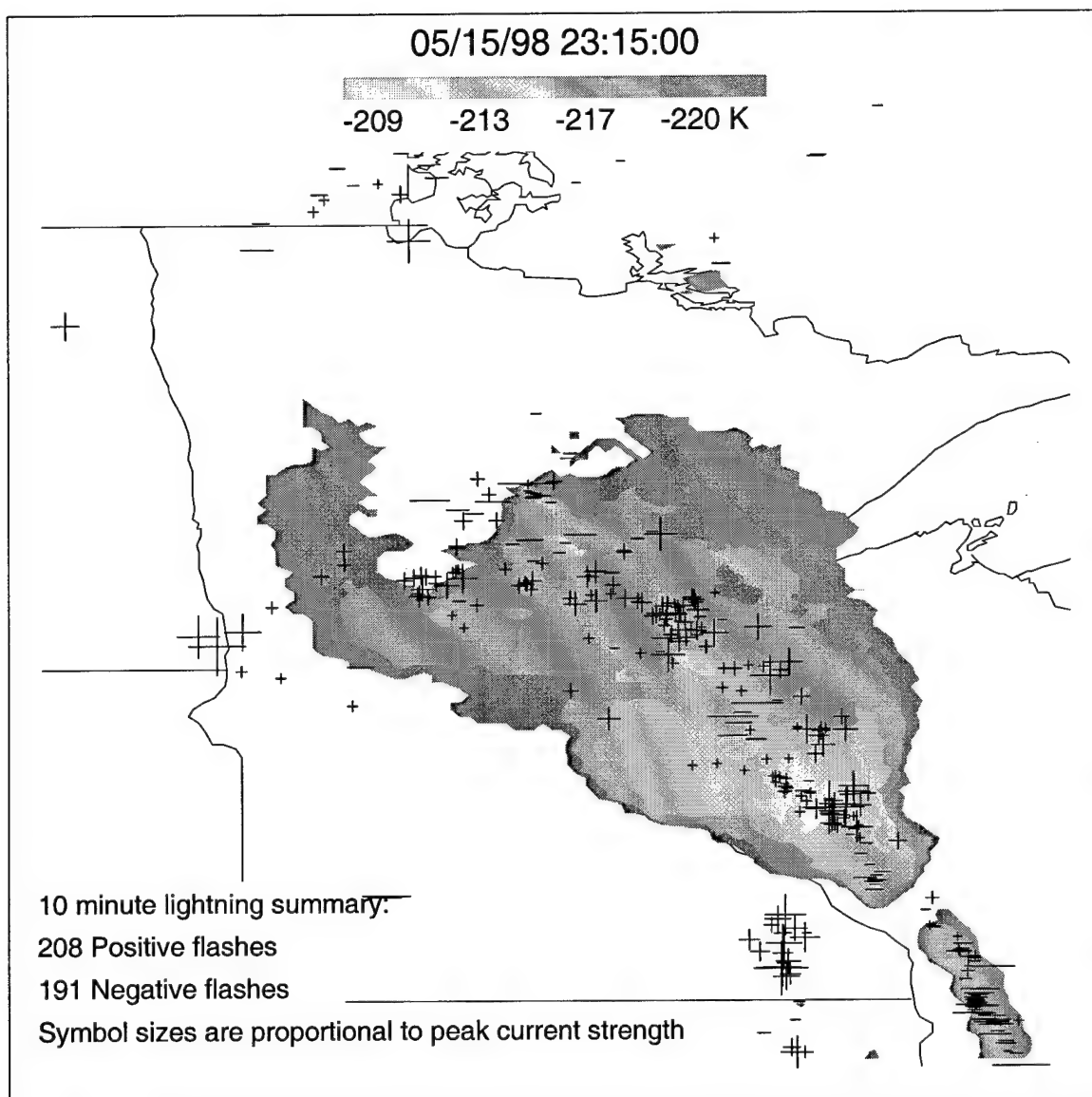


Figure F-17. Brightness temperatures and lightning data for 15 May 98 at 2315 UTC. The lightning data are plotted on the contour of the brightness temperatures with the symbol size proportional to the peak current.

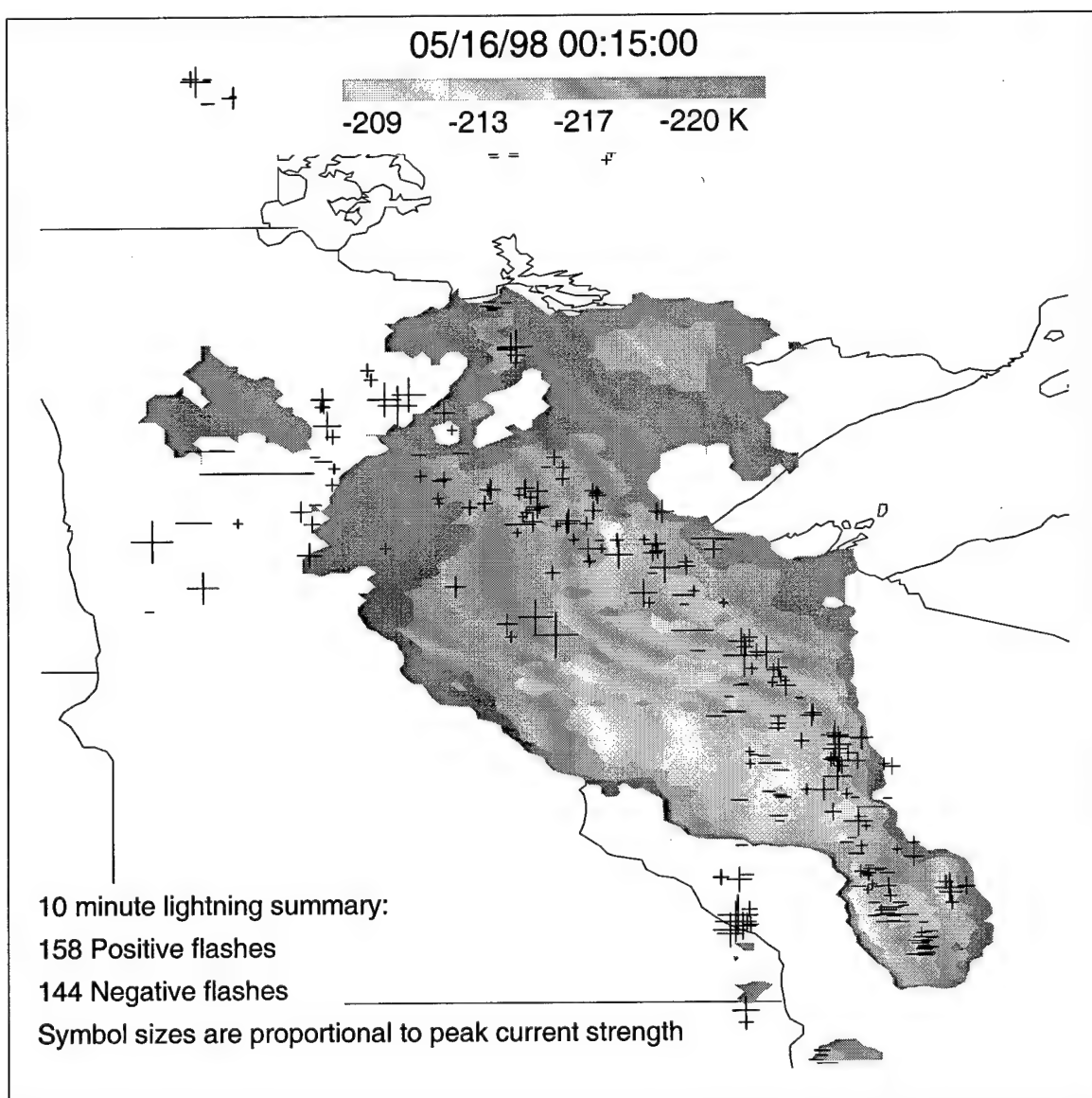


Figure F-18. Brightness temperatures and lightning data for 16 May 98 at 0015 UTC. The lightning data are plotted on the contour of the brightness temperatures with the symbol size proportional to the peak current.

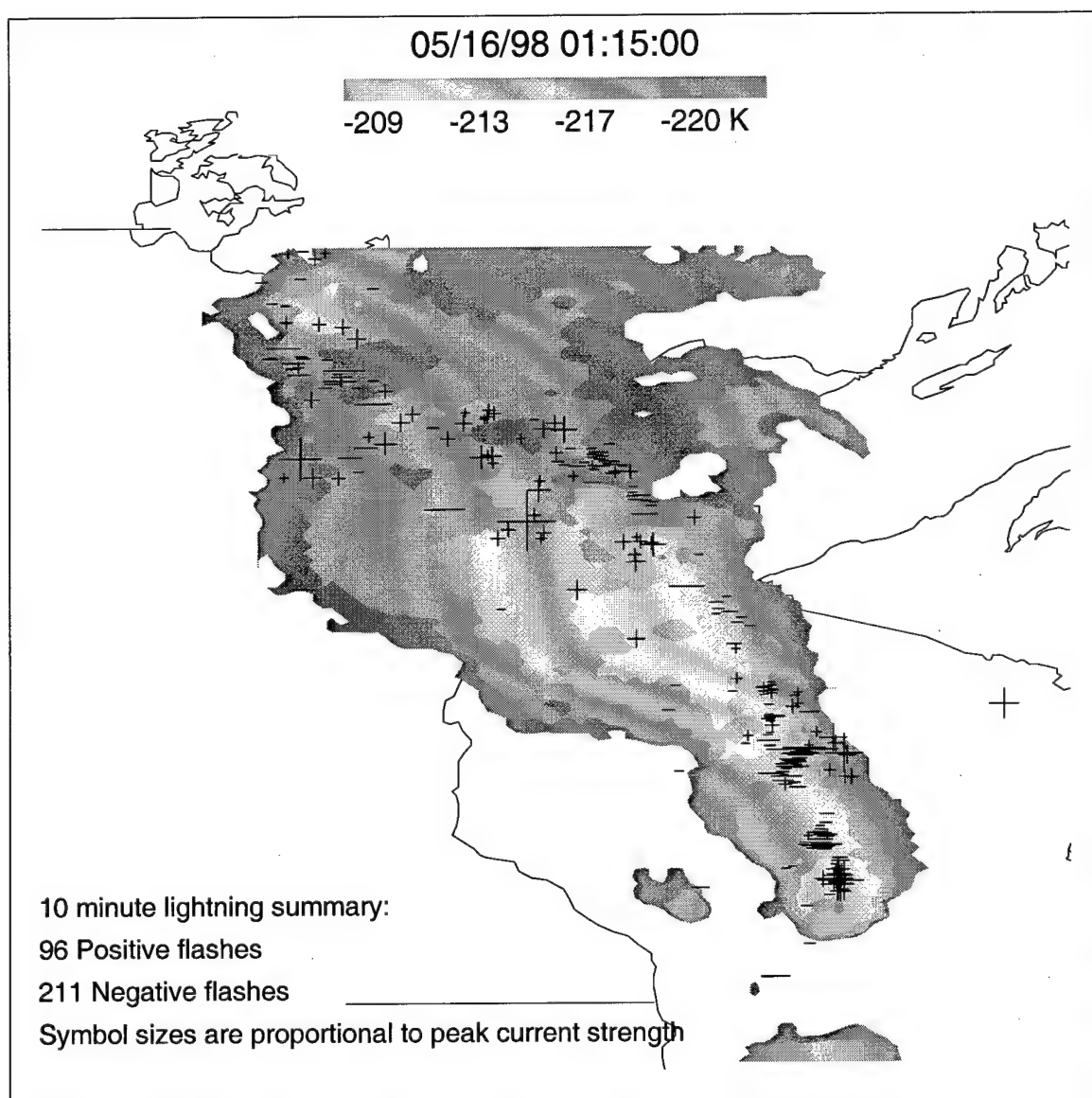


Figure F-19. Brightness temperatures and lightning data for 16 May 98 at 0115 UTC. The lightning data are plotted on the contour of the brightness temperatures with the symbol size proportional to the peak current.

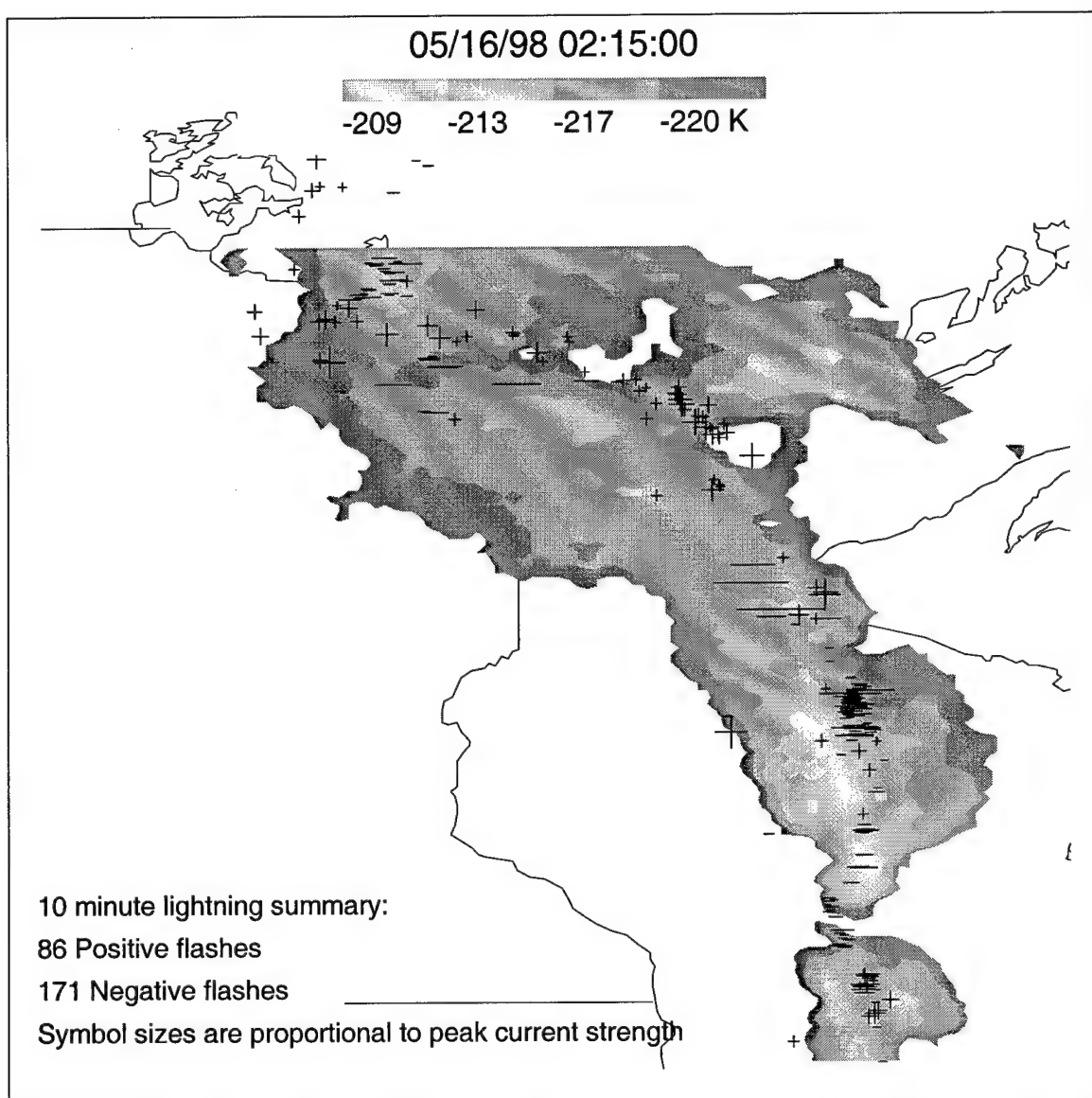


Figure F-20. Brightness temperatures and lightning data for 16 May 98 at 0215 UTC. The lightning data are plotted on the contour of the brightness temperatures with the symbol size proportional to the peak current.

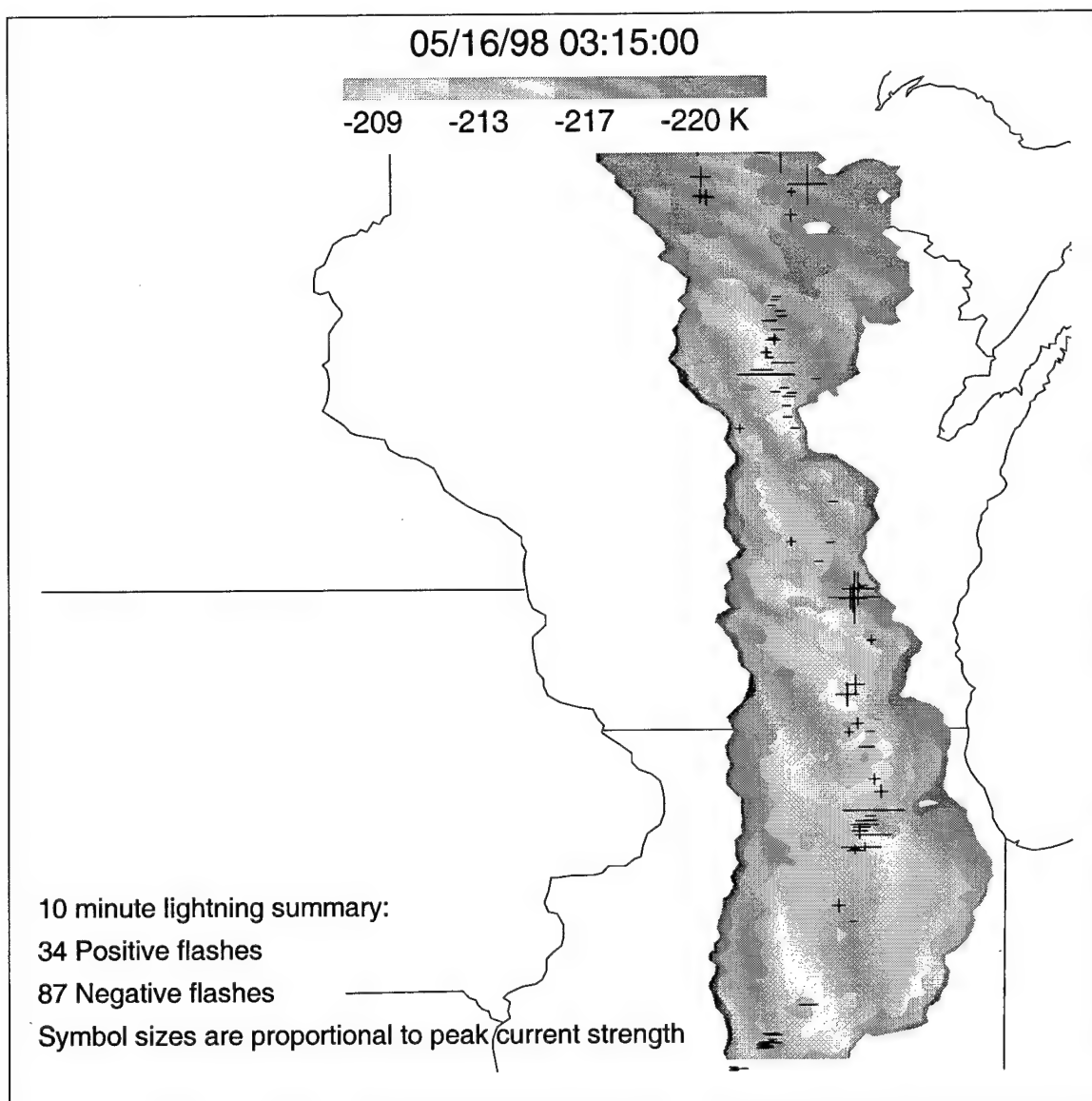


Figure F-21. Brightness temperatures and lightning data for 16 May 98 at 0315 UTC. The lightning data are plotted on the contour of the brightness temperatures with the symbol size proportional to the peak current.

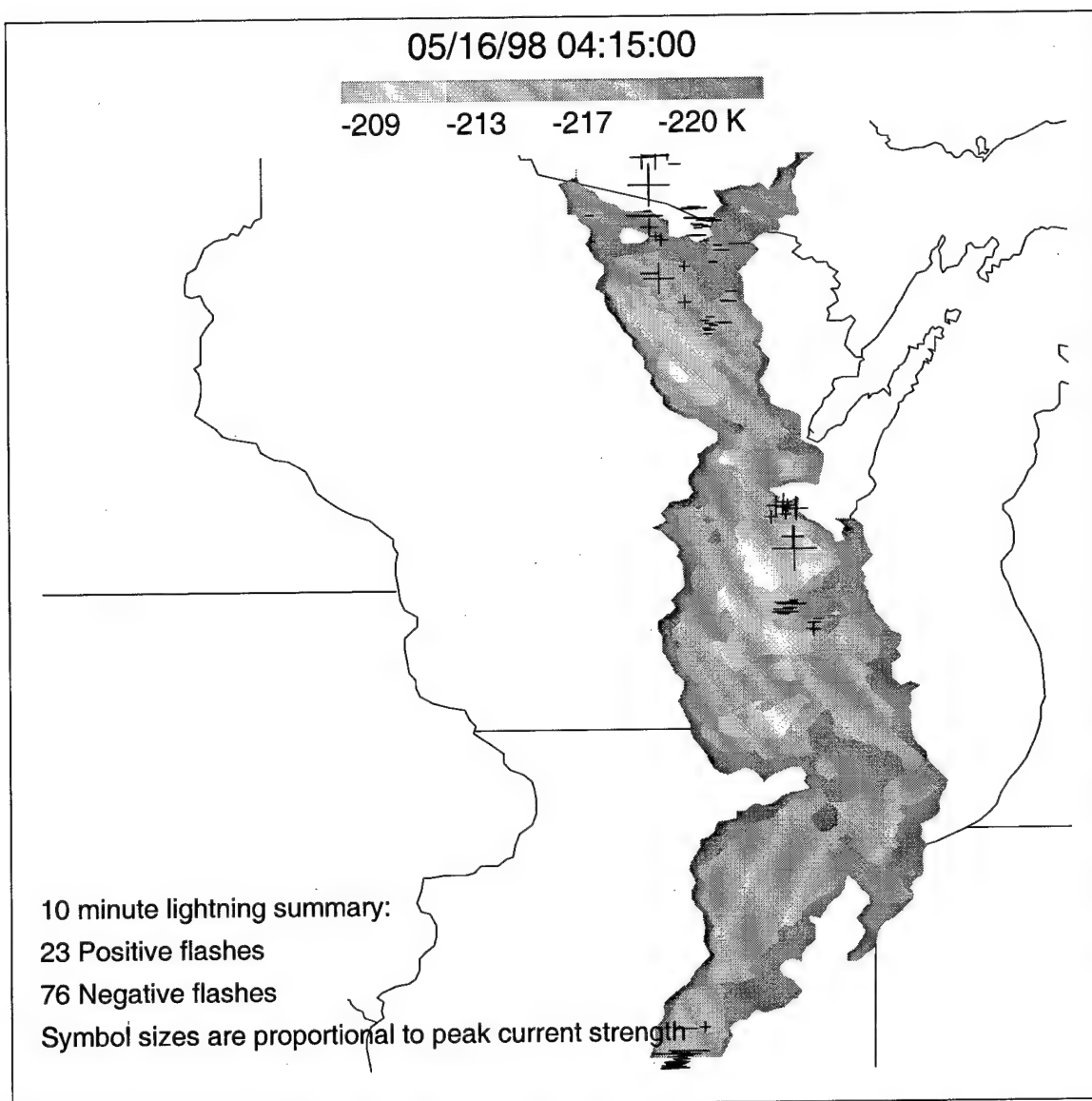


Figure F-22. Brightness temperatures and lightning data for 16 May 98 at 0415 UTC. The lightning data are plotted on the contour of the brightness temperatures with the symbol size proportional to the peak current.

APPENDIX G

IDL PROGRAMS USED TO ANALYZE LIGHTNING DATA

The main IDL programs used to analyze the lightning data are provided here for those who may be interested in using them. There are two functions that are not provided that convert the binary version of the lightning data into a format that is easier to work with and the program that filters the lightning data for the US landmass only. The general algorithms involved with the lightning analysis are contained in the four programs included here.

The conversion program that changes the lightning data from binary to structured values is not included as the format of the binary data is proprietary and was available by permission from Global Atmospheric, Inc. Providing the program would also provide the format of the data structure. The function that filters the data for the US works in the same fashion as the program that finds data for the Northern Plains region. Latitude and longitudes were found manually from a map and used for the US and the Northern Plains filters. This process could be duplicated using latitude and longitude coordinates for any given region.

To make the programs easier to locate, the page numbers of each program are listed in Table G-1.

Table G-1. Program list with brief description and page numbers.

Program	Description	Starting page
Density.pro	Finds the flash density, percent positive flashes, and positive flash density for a grid given a region.	266
Med_cur.pro	Calculates the median peak positive and negative currents for a grid given a region.	269
Nplains.pro	Separate data for the Northern Plains region from the rest of the lightning data. Process works for an irregular shape.	272
Med_dist.pro	Finds the median peak currents for given increments in sensor separation. Allows the direct comparison of peak currents and other parameters.	274

pro density

```
; Finds the flash density for each year listed in the
; years array and save the results to a file named
; densyear.txt where year is 1989, 1990, etc.

; Programmer: Gary Huffines
; Last Update: 8 Sep 98

; set up the region, resolution, years, months, and filenames
region = [21.0, 53.0, -129.0, -61.0]
res = 0.5
years = ['95', '96', '97', '98']
nyears = n_elements(years)
if (!d.name EQ 'WIN') then begin
    slash = '\'
    outpath = 'd:\huffines\us_0_2\us_land\'
    dirs = replicate('d:\us\' , nyears) + 'lgh19'
endif else begin
    slash = '/'
    outpath = ''
    dirs = replicate('/blitz1/lgh_flash/lgh19', nyears)
endelse
months = ['jan', 'feb', 'mar', 'apr', 'may', 'jun', $
    'jul', 'aug', 'sep', 'oct', 'nov', 'dec']
files = strarr(nyears*12)
for y = 0, nyears-1 do $
    for m = 0, 11 do $
        files(y*12+m) = dirs(y)+years(y)+slash+months(m)+years(y)+'.lgh'

; set up the sizes of the arrays
nlon = long((region(3)-region(2))/res)
nlat = long((region(1)-region(0))/res)

; set up area array
lat = findgen(nlat)*res+region(0)
area = 6340.0^2.0*((cos(lat)*!dton)+cos((lat+res)*!dton))/2.0*$
    (res*!dton)^2.0

; set the number of passes to make through the data file
npasses = 4

; pass through the data for each year
for y = 0, nyears-1 do begin
    dens = lonarr(nlon, nlat)
    dens = reform(dens, nlon*nlat)
    pdens = dens
    for m = 0, 11 do begin
        ; check to see if file is there
        dum = findfile(files(y*12+m), count = okay)
        if (count GT 0) then begin
            openr, 2, files(y*12+m)
            ; determine the number of flashes in the file
            a = fstat(2)
```

```

npass = a.size/(11*npasses)
for pass = 0, npasses-1 do begin
    ; get the binary form of the data
    f = bytarr(11, npass)
    readu, 2, f
    ; convert the binary data to an array of structures
    f = exp_lgh(f)
    ; make sure the data is within the region
    within = where((f.lat GE region(0)) AND (f.lat LT region(1)) $
        AND (f.lon GE region(2)) AND (f.lon LT region(3)), count)
    if (count GT 1) then begin
        ; limit the data to the region
        f = f(within)
        ; find the index for the density array
        index = long((f.lat-region(0))/res)*nlon + $
            long((f.lon-region(2))/res)
        ; count the flashes in each grid element
        dens = histogram(index, min = 0, max = nlon*nlat-1, $
            binsize = 1, input = dens)
        ; find the positive flash counts
        pos = where(f.peak GT 0.0, pcount)
        if (pcount GT 1) then $
            pdens = histogram(index(pos), min = 0, $
                max = nlon*nlat-1, binsize = 1, input = pdens)
        endif
        print, 'Pass ', strcompress(string(pass+1), /remove_all), ' $
            of ', strcompress(string(npasses), /remove_all), $
            ' finished for ', months(m), years(y)
    endif
endfor ; pass
close, 2
endif
endfor ; months
; reformat the variables
dens = float(reform(dens, nlon, nlat))
pdens = float(reform(pdens, nlon, nlat))
; find the percent positive flashes
ppos = 0.0*dens
non_zero = where(dens NE 0.0, count)
if (count GT 0) then $
    ppos(non_zero) = 100.0*pdens(non_zero)/dens(non_zero)
; find the flash density
for i = 0, nlat-1 do begin
    dens(*,i) = dens(*,i)/area(i)
    pdens(*,i) = pdens(*,i)/area(i)
endfor
; save result to file
openw, 2, outpath+'dens19'+years(y)+' .txt'
printf, 2, region
printf, 2, nlat, nlon, res, 0
printf, 2, dens
close, 2
openw, 2, outpath+'pos_19'+years(y)+' .txt'
printf, 2, region
printf, 2, nlat, nlon, res, 0

```

```
printf, 2, pdens
close, 2
openw, 2, outpath+'ppos19'+years(y)+'.txt'
printf, 2, region
printf, 2, nlat, nlon, res, 0
printf, 2, ppos
close, 2

; reset the counters to zero
dens = dens * 0.0
pdens = pdens * 0.0
endfor ; years

end
```

```

pro med_cur, res, outpath, suffix, us_only = us_only, region = region, $
  cutoff = cutoff

; Calculate the median peak currents on a grid with
; a resolution defined by res. The results go to
; files in the outpath directory designated by
; nmedsuffix.txt or pmedsuffix.txt where suffix is
; provided.

; Programmer: Gary Huffines
; Last Update: 4 Sep 98

; start the timer
time = systime(1)

; define the years and data path
years = ['95','96', '97','98']
nyears = float(n_elements(years))
if (!d.name = 'WIN') then begin
  inpath = 'd:\us\lgh19'
  slash = '\'
endif else begin
  inpath = '/stroke1/lgh19'
  slash = '/'
endelse

; set up file names for input
months = ['jan','feb','mar','apr','may','jun',$
          'jul','aug','sep','oct','nov','dec']
nmonths = n_elements(months)
files = strarr(nyears*nmonths)
for y = 0, nyears-1 do $
  for m = 0, nmonths-1 do $
    files(y*nmonths+m) = inpath+years(y)+slash+months(m)+$
      years(y)+'.lgh'

; set up array based on region and peak current range
if (n_elements(region) EQ 0) then region = [21.0, 53.0, -129.0, -61.0]
nx = fix((region(3)-region(2))/res)
ny = fix((region(1)-region(0))/res)
nmed = fltarr(nx,ny)
pmed = fltarr(nx,ny)

; the maximum number of flashes to be processed
nf = 50000L

; the array for the "cumulative histograms"
curr = lonarr(nx, ny, 201)
nn = 0L
np = 0L
tt = 0L
neg = 99-indgen(100) ; indicates the negative current bins
pos = indgen(100)+100 ; indicates the positive bins

```

```

; set the cutoff value to 0.0 if not supplied (positive flashes)
if (n_elements(cutoff) EQ 0) then cutoff = 0.0

; start passes through data years first
for yr = 0, nyears-1 do begin
  for m = 0, nmonths-1 do begin
    ; check to see if the file is there
    dum = findfile(files(y*nmonths+m), count = okay)
    if (okay GT 0) then begin
      openr, 2, files(yr*nmonths+m)
      a = fstat(2)
      tf = 0L
      while (tf LT a.size/11) do begin
        ; determine the number of flashes to process
        n = (nf < (a.size/11 - tf))
        tf = tf + n
        f = bytarr(11, n)
        readu, 2, f
        ; convert data and filter if selected
        if keyword_set(us_only) then $
          f = usfilter(f) $
        else $
          f = exp_lgh(f)
        within = where((f.lat GE region(0)) AND $
                      (f.lat LT region(1)) AND (f.lon GE region(2)) $
                      AND (f.lon LT region(3)), count)
        if (count GT 0) then begin
          ; limit the data to the region specified
          f = f(within)
          tt = tt + count
          ; find flashes with peak current magnitude GT cutoff
          okay = where((f.peak GE cutoff) OR (f.peak LT 0.0), count)
          if (count GT 0) then begin
            f = f(okay)
            ; find the geographic indices
            xind = fix((f.lon - region(2))/res)
            yind = fix((f.lat - region(0))/res)
            ; set extreme currents to +/- 100 kA for array limit
            f.peak = (f.peak > (-100.0))
            f.peak = (f.peak < 100.0)
            ; ind the peak current index
            pind = ((fix(floor(f.peak + 100.0)) < 200) > 0)
            ; count the flashes in the appropriate bins
            for j = 0L, count-1 do begin
              curr(xind(j), yind(j), pind(j)) = $
                curr(xind(j), yind(j), pind(j)) + 1
            endfor
          endif ; above cutoff
        endif ; within boundary
        print, months(m)+years(yr), ',', tf, ' of',$
          a.size/11, ' flashes done', $
          format = "(a5,a1,i8,a3,i8,a13)"
      endwhile
    endfor
  close, 2

```

```

endif
print, '    Used ', strcompress(string(long(total(curr))), $
    /remove_all), ' of ', strcompress(string(tt), /remove_all), $
    ' flashes thus far.'
endfor ; months
print, 'Processed 19', years(yr), ', ', $
    'US_only = ', keyword_set(usonly)
endfor ; years

; calculate the median from the histogram
; pass through the grid for positive and negative values
cum = lonarr(100)
for y = 0, ny-1 do begin
    for x = 0, nx-1 do begin
        ; check for sufficient flashes
        ptot = total(curr(x, y, pos))
        ntot = total(curr(x, y, neg))
        if (ptot GE 2L) then begin ; find median positive value
            for i = 0, 99 do $
                cum(i) = total(curr(x, y, pos(0:i)))
            pmed(x, y) = float(min(where(cum GT ptot/2)))
        endif else pmed(x, y) = 0.0
        if (ntot GE 2L) then begin ; find median negative value
            for i = 0, 99 do $
                cum(i) = total(curr(x, y, neg(0:i)))
            nmed(x,y) = -1.0*float(min(where(cum GT ntot/2)))
        endif else nmed(x, y) = 0.0
    endfor ; x
    print, 'Finished with ', y+1, ' of ', ny, ' latitudes'
endfor ; y

; save information to files
openw, 2, outpath + 'nmed'+suffix+'.txt'
printf, 2, region
printf, 2, ny, nx, res, 0
printf, 2, nmed
close, 2

openw, 2, outpath + 'pmed'+suffix+'.txt'
printf, 2, region
printf, 2, ny, nx, res, 0
printf, 2, pmed
close, 2

; end the timer and print elapsed run time
time = systime(1) - time
hr = fix(time/3600.0)
time = time - hr * 3600.0
minut = fix(time / 60.0)
time = time - minut * 60.0
print, 'Elapsed time was ', hr, ':', minut, ':', time, $
    format = "(a17,i2,a1,i2,a1,f6.3)"
end

```


Pro nplains

```

; Finds the data for the Northern Plains and saves it to a file

; Programmer: Gary Huffines
; Last Update: 15 January 1999

; define the output file
outfile = 'nplains.lgh'

; set up the overall region for the data
region = [37.0, 49.0, -106.0, -91.0]

; set up the fine tuned regional information
lat = findgen(13)+region(0)
lon1 = [102, 103, 104, 104, 100, 101, 102, 103, 104, 105, 106]
lon2 = [101, 101, 100, 99, 98, 97, 96, 96, 95, 94, 93, 92, 91]
lon1 = -1.0*float(lon1)
lon2 = -1.0*float(lon2)

; set up data files
years = ['95','96','97']
nyears = n_elements(years)
months = ['jan','feb','mar','apr','may','jun','$
          'jul','aug','sep','oct','nov','dec']
nmonths = n_elements(months)
inpath = '/stroke1/lgh19'
files = strarr(nyears*nmonths)
for y = 0, nyears-1 do $
  for m = 0, nmonths-1 do $
    files(y*nmonths+m)=inpath+years(y)+'/'+months(m)+years(y)+'.lgh'

; set up the number of passes through each data file
npasses = 30

; erase output file
openw, 2, outfile
close, 2

; run through the data set
for y = 0, nyears-1 do begin
  for m = 0, nmonths-1 do begin
    ; check to see if file exists
    dum = findfile(files(y*nmonths+m), count = count)
    if (count GT 0) then begin
      ; open file and run through passes
      openr, 2, files(y*nmonths+m)
      a = fstat(2)
      npass = a.size/npasses/11L
      for pass = 1, npasses do begin
        ; get data
        d = bytarr(11, npass)
        readu, 2, d
        ; convert data

```

```

f = exp_lgh(d)
; find flashes in general region
within=where((f.lat GE region(0)) AND (f.lat LT region(1)) $
AND (f.lon GE region(2)) AND (f.lon LT region(3)), count)
If (count GT 0) then begin
  F = f(within)
  D = d(*,within)
  ; find the limits for the fine tuned region
  latind = fix(f.lat - region(0))
  west = lon1(latind)+(f.lat mod 1.0)* $
        (lon1(latind+1)-lon1(latind))
  east = lon2(latind)+(f.lat mod 1.0)* $
        (lon2(latind+1)-lon2(latind))
  ; find the flashes inside the fine tuned region
  within = where((f.lon GE west) AND (f.lon LT east), count)
  if (count GT 0) then begin
    ; restrict data and save
    d = d(*,within)
    openu, 3, outfile, append
    writeu, 3, d
    close, 3
  endif ; data in fine tuned region
endif ; data in larger region
print, 'Finished with pass', pass, ' of', npasses, 'for ', $
      months(m), years(y)
endfor ; passes
close, 2
endif ; file exists
endfor ; months
endfor ; years

end

```

```

pro med_dist, outfile, years = years, impact = impact

; Finds the median peak current for all flashes in the
; files list by classifying the peak currents according
; to the distance associated with the NDLN sensors.
; The keyword impact uses the IMPACT separation
; versus the distance from the grid to the furthest
; required sensor.

; Programmer: Gary Huffines
; Last Update: 24 Feb 99

; check to see that the output file is available (path okay)
openw, 2, outfile
close, 2

; define the files used
if (n_elements(years) EQ 0) then years = ['95','96','97','98']
months = ['jan','feb','mar','apr','may','jun',$
          'jul','aug','sep','oct','nov','dec']
nyears = n_elements(years)
dirs = 'd:\us\lgh19'
files = strarr(nyears*12)
for y = 0, nyears-1 do $
  for m = 0, 11 do $
    files(y*12+m) = dirs+years(y)+'\'+months(m)+years(y)+'_lgh'

; set up the array to hold the peak current counts
d_alt = 10.0 ; 5.0 ; kilometers
min_alt = 1.0 ; meter
max_alt = 901.0 ; meters
n_alt = fix((max_alt-min_alt)/d_alt)
d_cur = 0.1 ; kA
min_cur = -600.0
max_cur = 600.0
n_cur = long((max_cur-min_cur)/d_cur)+1L
tally = lonarr(n_alt, n_cur)

; read in the distance data
if keyword_set(impact) then $
  openr, 2, 'd:\huffines\us_0_2\us_land2\dfdistr.txt' $
else $
  openr, 2, 'd:\huffines\us_0_2\us_land2\sen4dist.txt'
region = fltarr(4)
info = fltarr(4)
readf, 2, region, info
elev = fltarr(info(1), info(0))
res = info(2)
readf, 2, elev
close, 2

; pass through data and put the values in bin
npasses = 6L
snpasses = strcompress(string(npasses), /remove_all)

```

```

for y = 0, nyears-1 do begin
  for m = 0, 11 do begin
    openr, 2, files(y*12+m)
    a = fstat(2)
    npass = a.size/11L/npasses
    for pass = 0, npasses-1 do begin
      ; read data
      f = bytarr(11, npass)
      readu, 2, f
      ; convert data and filter for US only
      f = usfilter(f)
      ; find flashes within region
      within = where((f.lat GE region(0)) AND (f.lat LT region(1)) $
        AND (f.lon GE region(2)) AND (f.lon LT region(3))), count)
      if (count GT 0) then begin
        ; make sure data is within bounds
        f = f(within)
        within = 0B
        ; find the elevation for each flash from the elevation array
        ht = elev(fix((f.lon - region(2))/res), $
          fix((f.lat - region(0))/res))
        ; find those flashes within the elevation bounds
        inside = where((ht GE min_alt) AND (ht LT max_alt), hcount)
        if (hcount GT 0) then begin
          f = f(inside)
          ht = ht(inside)
          inside = 0B
          ; set any peak current outside the extreme to the min or max
          lo = where(f.peak LT min_cur, lcount)
          if (lcount GT 0) then f(lo).peak = min_cur
          lo = 0B
          hi = where(f.peak GT max_cur, hcount)
          if (hcount GT 0) then f(hi).peak = max_cur
          hi = 0B
          ; increment the counting array by one for each flash
          for i = 0L, hcount-1L do $
            tally(fix((ht(i) - min_alt)/d_alt), $
              long((f(i).peak - min_cur)/d_cur)) = $
              tally(fix((ht(i) - min_alt)/d_alt), $
                long((f(i).peak - min_cur)/d_cur)) + 1L
          endif ; inside elevation bounds
        endif ; inside region
        print, 'Pass ', strcompress(string(pass+1), /remove_all), $
          ' of ', snpasses, ' for ', months(m), years(y), ' is done.'
      endif
    endfor ; pass
    close, 2
  endfor ; months
endfor ; years

; calculate the median peak current for each distance level
nmed = fltarr(n_alt)
pmed = fltarr(n_alt)
for lev = 0, n_alt-1 do begin
  c_count = lonarr(n_cur/2)

```

```

; do positive currents first
if (max(tally(lev, n_cur/2+1:*)) GT 0) then begin
  for i = 10L, n_cur/2-1 do $
    c_count(i) = total(tally(lev, n_cur/2+11:n_cur/2+11+i))
    ; find the median of this array
    pmed(lev) = float(min(where(c_count GT $
      total(tally(lev, n_cur/2+11:*)) / 2))) * d_cur + 10.0
  endif else pmed(lev) = 0.0
; now do the negatives
if (max(tally(lev, 0:n_cur/2)) GT 0) then begin
  for i = 0, n_cur/2-1 do $
    c_count(i) = total(tally(lev, n_cur/2-i:n_cur/2))
    ; find the median of this array
    nmed(lev) = -1.0 * float(max(where(c_count LT total(tally(lev,
0:n_cur/2)) / 2))) * d_cur
  endif else nmed(lev) = 0.0
  print, lev+1, ' of ', n_alt
endifor

; print the min and max of the negative and positive median currents
print, min(nmed), max(nmed)
print, min(pmed), max(pmed)

; send the results to the output file
dataform = "(f7.1,2x,f7.2,2x,f7.2,2x,i9,2x,i9)"
headform = "(a4,5x,a7,2x,a7,2x,a9,2x,a9)"
openw, 2, outfile
printf, 2, 'DIST', 'NMED', 'PMED', 'NCOUNT', 'PCOUNT', format = headform
for i = 0, n_alt-1 do $
  printf, 2, float(i)*d_alt+min_alt, nmed(i), pmed(i), $
    total(tally(i,0:n_cur/2)), $
    total(tally(i,n_cur/2+11:)), format = dataform
close, 2

end

```

VITA

Gary Russell Huffines was born in Logan, Ohio on 21 January 1961 and was the only child of John and Mona Huffines. He graduated from Logan High School in 1979 and received his Bachelor of Arts in Physics from Ohio Northern University in 1983. Immediately after graduating from undergraduate studies, he joined the Air Force and was commissioned as a second lieutenant on 9 September 1983. He attended a year of Basic Meteorology Training at the Naval Postgraduate School in Monterey, California.

After serving at Offutt Air Force Base in Omaha, Nebraska and Kunsan Air Base, Republic of Korea, the Air Force sponsored him for a Master of Science degree in Plant and Soil Science and Biometeorology at Utah State University in Logan, Utah. It was there that he married Ann Swain and gained an instant family of four children. He was then assigned to Cheyenne Mountain Air Force Base in Colorado Springs, Colorado to provide weather and space environmental support to the North American Aerospace Defense command (NORAD). Later, he was given the duties of a staff meteorologist at Wright Patterson Air Force Base in Dayton, Ohio supporting emerging technologies for the Department of Defense.

Gary is currently assigned at Wright Patterson Air Force Base, again, where he is an instructor of atmospheric physics for the Air Force's graduate school, the Air Force Institute of Technology. His permanent address is:

307 Randy Drive

West Carrollton, Ohio 45449